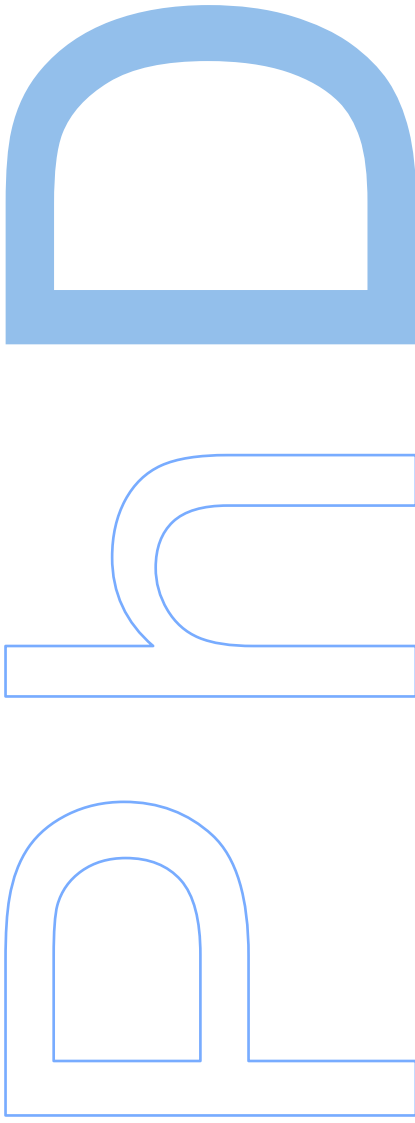
Nanopartículas para a Deteção Luminescente em Fibra Ótica de Espécies Químicas Reativas de Oxigénio e Azoto

Eliana Filipa Carrinho Simões

Tese de Doutoramento apresentada à
Faculdade de Ciências de Universidade do Porto, Química
2016

Orientador
Joaquim Carlos Gomes Esteves da Silva, Professor Associado com Agregação,
Faculdade de Ciências da Universidade do Porto

João Manuel Martins Leitão, Professor Auxiliar,
Faculdade de farmácia da Universidade de Coimbra



This work was supported by a Ph.D. scholarship with the reference SFRH/BD/81074/2011, co-funded by the European Social Fund (Fundo Social Europeu, FSE), through Programa Operacional Potencial Humano – Quadro de Referência Estratégico Nacional (POPH – QREN), and by national funds from the Ministry of Education and Science through the Portuguese Fundação para a Ciência e a Tecnologia, I.P. (FCT). Also, this work was made in part under project PTDC/QEQ-QFI/0289/2014 and PTDC/QEQ-QAN/5955/2014 and it was supported within Project 3599 – "Promover a Produção Científica e Desenvolvimento Tecnológico e a Constituição de Redes Temáticas (3599-PPCDT) e comparticipado pelo Fundo Comunitário Europeu FEDER".









Agradecimentos

O trabalho desenvolvido surge ao fim de um período de tempo marcado por alegrias e fadigas, dúvidas e certezas… momentos bons e menos bons… Não é só meu… é de todos os que comigo partilharam as certezas de uma caminhada nem sempre fácil.

Os meus agradecimentos vão, em geral, para aqueles que me apoiaram e estiveram sempre presentes ao longo deste percurso.

Agradeço em primeiro lugar aos meus orientadores Prof. Dr. João Manuel Martins Leitão, da Faculdade de Farmácia da Universidade de Coimbra e Prof. Dr. Joaquim Carlos Gomes Esteves da Siva, do Departamento de Química e Bioquímica da Faculdade de Ciências da Universidade do Porto por todo apoio prestado, por toda a dedicação no desenvolvimento de todos os trabalhos práticos efetuados bem como na revisão dos diferentes trabalhos de pesquisa publicados. Agradeço a atenção, dedicação, compreensão e disponibilidade dispensados sem os quais não teria conseguido desenvolver este trabalho.

Aos meus pais, um muito obrigado pela vida que me destes e pelo sonho que me ajudaste a realizar!

À minha irmã, pelo auxílio nas horas mais difíceis e pelo amor de “mana” que sinto sempre presente, como uma força. Um beijo Flor.

Ao Ricardo, pela compreensão, paciência e atenção que sempre me ofereceu.

A todos os meus amigos pelo apoio em todos os momentos. Um agradecimento especial à Sra. D. Celeste Lucas pela amizade, ajuda e apoio que me ofereceu em todos os dias de trabalho.

Jamais chegaria ao fim sem o vosso apoio e sem a presença inigualável de Deus.

Com amizade, um muito obrigado a todos!

Resumo

A síntese, caracterização e aplicação de nanopartículas, tem sido alvo de muitos estudos e tem tido uma enorme evolução nestes últimos anos. Uma das suas principais aplicações é como sensores ou biossensores. As nanopartículas fluorescentes apresentam características interessantes e atrativas, o que permite que sejam usadas como sensores óticos.

Neste trabalho são usadas nanopartículas fluorescentes para a deteção de espécies químicas reativas de oxigénio (ROS) e azoto (RNS). O estudo de nanopartículas fluorescentes de carbono, vulgarmente conhecidas por carbon dots (CDs) é utilizado devido ao facto de os CDs possuírem caraterísticas semelhantes às dos quantum dots (QDs) mas com as vantagens de não colocarem problemas de toxicidade e serem biocompatíveis.

A deteção ROS e RNS é de extrema relevância para o conhecimento de diversos processos patológicos e fisiológicos, e representa um desafio permanente, devido à sua grande reatividade, tempos de vida curtos, baixas concentrações, mecanismos antioxidantes e interferências. Os resultados mostraram que foi possível a deteção de algumas ROS/RNS usando CDs preparados e funcionalizados de diferentes formas utilizando diferentes percursores.

Neste trabalho foram sintetizados QDs e CDs. Foram estudados diferentes métodos de síntese e funcionalização de CDs. Dos métodos estudados, foi escolhido para a síntese das nanopartículas, o método de síntese por pirólise em microondas. Após a síntese, as nanopartículas foram avaliadas na deteção de ROS/RNS.

Palavras-chave:

Nanopartículas fluorescentes, quantum dots, carbon dots, espécies reativas de azoto e oxigénio

Abstract

The synthesis, characterization and application of nanoparticles, has been the subject of many studies and has been a great development in recent years. One of its main applications is as sensors and biosensors. Fluorescent nanoparticles present interesting and attractive features, which allows them to be used as optical sensors.

In this work, fluorescent nanoparticles for detection of reactive oxygen (ROS) and nitrogen species (RNS) are used. The study of fluorescent carbon nanoparticles, usually known as carbon dots (CDs) is privileged due to the fact that CDs have features similar to those of the quantum dots (QDs) but with the advantages of not putting toxicity problems and be biocompatible.

The detection of ROS and RNS is of highest importance for the knowledge of pathological and physiological processes and represents a permanent challenge due to its great reactivity, short lifetimes, low concentrations, antioxidant mechanisms and interferences. The results showed that it was possible the detection of some ROS/RNS using CDs prepared and functionalized with different methods and from different precursors.

In this work QDs and CDs were synthesized. Different methods of synthesis and functionalization of CDs were studied. The methods studied were chosen for synthesis of nanoparticles, the synthesis method by microwave pyrolysis. After synthesis the nanoparticles were used for detection of ROS/RNS.

Keywords:

Fluorescent nanoparticles, quantum dots, carbon dots, reactive oxygen and nitrogen species

Publications and presentations of the author containing work related with this thesis

This work was published in book chapters, reviewed scientific journals and presented in scientific conferences.

Book Chapters

Chapter: "Fluorescence Sensing by Functionalized Carbon Dots Nanoparticles"
João M.M. Leitão, Eliana F. C. Simões, Joaquim C.G. Esteves da Silva
Book: Chemical Functionalization of Carbon Nanomaterials: Chemistry and Applications, Chapter 11, pp. 292-309, Vijav Kumar Thakur and Manju Kumari Thakur Eds., CRC Press Taylor & Francis Group, Boca Raton, United States of America (2015) ISBN: 978-1-4822-5394-8, EBOOK ISBN: 987-1-4822-5396-2, DOI: 10.120/B187247-13.

Chapter: "Synthesis and Applications of Carbon Dots Nanocomposites"
João M.M. Leitão, Eliana F. C. Simões, Joaquim C.G. Esteves da Silva
Book: Nanocomposites: Synthesis, Characterization and Applications, Chapter 6, pp. 121-138, Xiaoying Wang Ed., Nova Science Publishers, Inc., New York, United States of America (2013) Print ISBN-10: 1629482269, Print ISBN-13:978-1629482262, eBook ISBN:978-1-62948-227-9.

Chapter:" Carbon Nanomaterials for Tumor Targeting Theranostics"
João M.M. Leitão, Eliana F. C. Simões, Joaquim C.G. Esteves da Silva
Book: Nanomaterials for Tumor Targeting Theranostics, Chapter 8, Mingqian Tan and Aiguo Wu Eds., Higher Education Press Limited Company and World Scientific Publishing Company, Inc (2016) ISBN-10 9814635413, ISBN 13 978-9814635417, PRINT ISBN:978-981-4635-41-7.

Chapter: "Nanomaterials For in Vivo NO Sensing"
João M.M. Leitão, Eliana F. C. Simões, Joaquim C.G. Esteves da Silva

Book: Nitric Oxide: Emerging Developments, Therapeutic Role in Disease States and Health Effects, Chapter 4, Dominic M. Evans Ed., Nova Science Publishers Inc., New York. United States of America (2015) PRINT ISBN 10 1634829611, ISBN 13 978-1634829618, EBOOK ISBN 978-1-63483-016-4.

Chapter: "Reactive Oxygen/Nitrogen Species Nanoprobes"
Eliana F. C. Simões, João M.M. Leitão, Joaquim C.G. Esteves da Silva
Book: Advances in Nanotechnology. Volume 16, Chapter 3, Zacharie Bartul and Jérôme Trenor, Nova Science Publishers Inc., New York. United States of America (2016) ISBN: 978-1-63485-961-5.

Publications in Peer Reviewed Journals

"NO Fluorescence Sensing by Europium Tetracyclines Complexes in the Presence of H_2O_2"
Eliana F. C. Simões, João M.M. Leitão, Joaquim C.G. Esteves da Silva
Journal of Fluorescence, 2013, 23 (4), 681–688. DOI 10.1007/s10895-013-1207-9.

"NO Fluorescence Quantification by CdSe Quantum Dots Chitosan Nanocomposites"
Eliana F. C. Simões, João M.M. Leitão, Joaquim C.G. Esteves da Silva
Journal of Fluorescence, 2014, 24 (2), 639–648. DOI 10.1007/s10895-013-1337-0.

"Carbon Dots from Tryptophan Doped Glucose for Peroxynitrite Sensing"
Eliana F. C. Simões, Joaquim C.G. Esteves da Silva, João M.M. Leitão
Analytica Chimica Acta, 2014, 10, 852, 174–80. DOI: 10.1016/j.aca.2014.08.050.

"Peroxynitrite and Nitric Oxide Fluorescence Sensing by Ethylenediamnine Doped Carbon Dots"
Eliana F. C. Simões, Joaquim C.G. Esteves da Silva, João M.M. Leitão
Sensors and Actuators B: Chemical, 2015, 220, 1043–1049. DOI: 10.1016/j.snb.2015.06.072.

"Carbon Dots Prepared from Citric Acid and Urea as Fluorescent Probes for Hypochlorite and Peroxynitrite"
Eliana F. C. Simões, Joaquim C.G. Esteves da Silva, João M.M. Leitão
Microchimica Acta, 2016, 183 (5), 1769–1777. DOI 10.1007/s00604-016-1807-6.

"Sulphur and nitrogen co-doped carbon dots sensors for nitric oxide fluorescence quantification"
Eliana F. C. Simões, Joaquim C.G. Esteves da Silva, João M.M. Leitão
Submitted to Analytica Chimica Acta in September 2016.

Oral Communications

Carbon Dots from Tryptophan Doped Glucose for Peroxynitrite Sensing
Eliana F. C. Simões, Abel J. Duarte, João M.M. Leitão, Joaquim C.G. Esteves da Silva
Oral Communication QA6, XX Encontro Luso-Galego de Química (XXLGQ), 26 - 28 Novembro 2014, Complexo FFUP/ICBAS, Porto, Portugal.

Poster Communications

"ROS and RNS Fluorescence Sensing by the Europium- Tetracyclines Complex"
E. F. C. Simões, J. M. M. Leitão, J. C.G. Esteves da Silva
VI CIE - XXII RNE (VI Congresso Ibérico de Espectroscopia OP-15), 8 - 10 Setembro 2010, Porto, Portugal.

"Nanopartículas Fluorescentes Baseadas em Carbono"
Eliana F. C. Simões, João M.M. Leitão, Joaquim C.G. Esteves da Silva,
E2N 2013 (Encontro Nacional de Nanotoxicologia P-21 Toxicidade Humana), 2, 3 Abril 2013, Instituto Superior Técnico, Lisboa, Portugal.

"NO Fluorescence Quantification by CdSe Quantum Dots Chitosan Nanocomposites"
Eliana F. C. Simões, João M.M. Leitão, Joaquim C.G. Esteves da Silva

XXIII ENCONTRO NACIONAL DA SPQ P-3.13 Novas Tecnologias, 12 - 14 Junho 2013, Complexo Pedagógico (edifício 23), Universidade de Aveiro, Aveiro, Portugal.

Organization of the thesis

For a correct appreciation of the work developed, a report of the experimental work and bibliographic research done was described in this thesis.

This report shows the main results obtained in the four years as a PhD student with the grant SFRH/BD/81074/2011, on the Linha de Quimiometria de Sistemas Ambientais, Forenses e Biológicos of Centro de Investigação em Química of Universidade do Porto and on the Laboratory of Métodos Instrumentais de Análise of Faculdade de Farmácia of Universidade de Coimbra. The theme of the work developed is "Nanopartículas para a deteção luminescente em fibra ótica de espécies químicas reativas de oxigénio e azoto". Some of the experimental results obtained were not conclusive. On the other hand, were also obtained successful works that are published in international journals and some of them were presented in scientific meetings in the form of oral presentations or panel presentations (poster).

This thesis is organized and separated in different chapters. Firstly a brief introduction is done where is done the framework of the main issues presented in this thesis. In the introduction a reference to nanoparticles and their main synthesis and functionalization processes was made. A reference to the several determination methods of determination of ROS/RNS is also presented.

Then the bibliographic and the experimental research made in this thesis are presented divided in two main chapters, where is showed the papers and book chapters written along the work. In the bibliographic research, the main topics covered in this thesis are presented in the form of book chapters. In the experimental research the experimental results obtained along these four years are presented the form of papers.

The bibliographic research of the main focuses of this thesis was made when the opportunity of written book chapters appears. Themes involving the ROS/RNS determination, the methods of CDs nanocomposites synthesis and the different carbon nanomaterials used in theranostic applications, the fluorescence sensing functionalized CDs were addressed. In these chapters where specifically presented the main nanoprobes used in the determination of the main ROS/RNS; the different nanomaterials used for *in vivo* NO sensing; methods of the synthesis and applications

of CDs nanocomposites; carbon nanomaterials that can be used for tumor targeting theranostics; the fluorescence sensing by functionalized CDs nanoparticles.

Besides of this bibliographic research, the experimental work that was done along the doctoral project is presented. The determination of NO in the presence of H_2O_2 by fluorescence sensing using Europium Tetracyclines Complexes; a work showing a fluorescence quantification of NO using Chitosan CdSe QDs nanocomposites; the synthesis of CDs from tryptophan and glucose for peroxynitrite sensing; the synthesis of ethylenediamine doped CDs for peroxynitrite and NO fluorescence sensing; the synthesis of CDs prepared from citric acid and urea as fluorescent probes for hypochlorite and peroxynitrite; the synthesis of CDs sulfur and nitrogen co-doped for NO detection was also presented.

Finally general conclusions about the work performed as well the futures perspectives are presented.

Table of Contents

Agradecimentos ..... **iii**

Resumo ..... **v**

Abstract ..... **vii**

Publications and presentations of the author containing work related with this thesis ..... **ix**

Organization of the thesis ..... **xiii**

Table of Contents ..... **xv**

List of Abbreviations ..... **xvii**

Introduction 1

Objectives of this Thesis 9

Bibliographic Research 11

Chapter 1 - Carbon Nanomaterials For Tumor Targeting Theranostics 13

Chapter 2 - Synthesis and Applications of Carbon Dots Nanocomposites 35

Chapter 3 - Fluorescence Sensing By Functionalized Carbon Dots Nanoparticles 55

Chapter 4 - Nanomaterials for in vivo NO Sensing 75

Chapter 5 - Reactive Oxygen/Nitrogen Species Nanoprobes 95

Experimental Research 147

Chapter 6 - Nitric Oxide Fluorescence Sensing by Europium Tetracyclines Complexes in the Presence of Hydrogen Peroxide 149

Chapter 7 - Nitric Oxide Fluorescence Quantification by Chitosan CdSe Quantum Dots Nanocomposites 159

Chapter 8 - Carbon Dots from Tryptophan Doped Glucose for Peroxynitrite Sensing …..… 171
Chapter 9 - Peroxynitrite and Nitric Oxide Fluorescence Sensing by Ethylenediamine Doped Carbon Dots …….. 207
Chapter 10 - Carbon Dots Prepared from Citric Acid and Urea as Fluorescent Probes for Hypochlorite and Peroxynitrite ……..…….... 231
Chapter 11 - Sulphur and nitrogen co-doped carbon dots sensors for nitric oxide fluorescence quantification ……..…….. 255
Conclusions and Future Perspectives ……..... 271

List of Abbreviations

AF	Alexa-fluor
Ag	silver
AEAPMS	3-(2-aminoethylamino)propyltrimethoxysilane
APS	3-Aminopropyltrimethoxysilane
APTES	3-Aminopropyltriethoxysilane
Au	gold
AUA	11-aminoundecaoic acid
BDA	1,4-butanediamine
BPA	Bisphenol A
BPEI	Branched Polyethylenimine
BSA	Bovine serum albumin
CA	Citric Acid
CDs	Carbon Dots
ClO^-	Hypochlorite
CNT	Carbon Nanotube
CS	Chitosan
CTAB	Cetyl trimethylammonium bromide
Cu	Copper
DAB	diaminebenzene
DEA	Diethylamine
DLS	Dynamic Light Scattering
DNA	Deoxyribonucleic acid
DOX	Doxorubicin
EDA	Ethylenediamine
EDC	1-Ethyl-3-[3-dimethylaminopropyl]carbodiimide hydrochloride
EMFL	Endohedral metallofullerenes
EPR	Paramagnetic Ressonance
ESR	Electron spin resonance
Eu	Europium
FA	Folic acid
Fe	Iron
FITC	Fluorescein isothiocyanate

FL	Fullerene
FRET	Förster resonance energy transfer
GCE	Glassy carbon electrode
Gd	Gadolinium
Glc	Glucose
GMA	Glycidyl methacrylate
GO	Graphene oxide
GP	Graphene
GPTMS	3-Glycidoxypropyl)methyldiethoxysilane
GSH	Glutathione
HA	Hyaluronic acid
HB	Hemoglobin
HClO	Hypoclorous acid
HDA	1-hexadecylamine
Hg	Mercury
H_2O_2	Hydrogen peroxide
HRP	Horseradish peroxidase
LOD	Limit of detection
LRET	Luminescence resonance energy transfer
MCD	Mesoporous carbon dots
MEF	Metal Enhanced Fluorescence
MMA	Methyl methacrylate
MPA	3-Mercaptopropionic acid
MRI	Magnetic resonance imaging
MSA	Mercaptosuccinic acid
MTX	Methotrexate
MWCNT	Multi-walled carbon nanotubes
NAC	N-Acetyl-L-Cysteine
ND	Nanodiamond
NHS	N-hydroxysulfosuccinimide
NIPAM	N-Isopropylacrylamide
NIR	Near-infrared spectroscopy
NPs	Nanoparticles
NO	Nitric oxide
NOPD	o-phenylenediamine

$O_2^{\bullet-}$	Superoxide ion
$OONO^-$	Peroxynitrite
PAA	Polyallylamine
PAH	Polyallylamine hydrochloride
PDMAA	Poly N,N-dimethylacrylamide
PEG	Polyethylene glycol
PEI	Polyethylenimine
PET	Positron emission tomography
Pd	Palladium
PHA	Phenanthroline
PHFL	Polyhydroxy fullerenes
PMMA	Polymethyl methacrylate
PNIPAM	Poly(N-isopropylacrylamide)
PPEI	polypropionylethyleneimine
PPy	Polypyrrole
PSS	Polysodium 4-styrenesulfonate
PTX	Paclitaxel
PVA	Polyvinyl alcohol
PY	Pyrene
QDs	Quantum Dots
QY	Quantum Yield
RBC	Red blood cell
RGO	Reduced Graphene oxide
RNA	Ribonucleic acid
RNS	Reactive nitrogen species
ROS	Reactive oxygen species
SCE	Satured calomel electrode
Si	Silicon
SOD	Superoxide dismutase
SPECT	Single photon emission computed tomography
ST	Sodium thiosulfate
SWCNT	Single-walled carbon nanotubes
Tc	Tetracycline
TC	Thiocarbamide
TEA	Triethylamine

TEM	Transmission electron microscopy
TEOS	Tetraethyl orthosilicate
TEPA	N,N,N′-tris(pyridin-2-ylmethyl)ethane-1,2-diamine
TMB	1,3,5-trimethylbenzene
TF	Transferrin
TGA	Thioglycolic acid
TMR	Tetramethylrhodamine
Trp	Tryptophan
TTDDA	4, 7.10-Trioxo-1.13-tridecanediamina
UR	Urea
UV	UltraViolet
Zn	Zinc

Introduction

Nanomaterials, namely nanoparticles (NPs) have become a priority for the scientific research and technological development, in particular in the areas of health sciences, as a vehicle for transport of drugs and as a means of diagnosis. The potential for the use of nanotechnology in medicine, in the particular case of the carbon dots (CDs), non-toxic, especially in the area of cancer, is very wide. As an example, the targeted NPs for tumor cells will allow to apply selective therapies with fewer side effects. The fluorescent features would show its location easily by monitoring the treatment. Fluorescent NPs emerge as an alternative with great development potential for use in image analysis and as chemical sensors or biosensors. The advantages of these nanomaterials are the high molar extinction coefficients, high quantum yields, great photostability, relatively high life times and their optical properties vary with the size [1]. The most common fluorescent nanomaterials are crystalline semiconductor NPs, commonly called quantum dots (QDs). However, the QDs contains potentially toxic metals, have given increase problems of cytotoxic and biocompatibility. To resolve these problems a new carbon-based nanomaterial appeared known as CDs [2, 3]. The QDs, of different materials or, more recently, the CDs have been target of an intense research with regard to its synthesis and functionalization. The QDs are semiconductor NPs that exhibit fluorescence but comparing to CDs, only their functionalization allows obtaining fluorescent NPs.

Some examples appear in the literature on detection by functionalized NPs [4-7]. The majority is developed for detection of ionic species [6]. Also some of these systems have been developed for the detection of small molecules [6] and biomolecules [5, 6]. Have also been described the participation of NPs as donors in chemical systems of luminescence resonance energy transfer (LRET) [5-7]. Some sensors based on, LRET systems of fluorescence or bioluminescence, have been developed [6].

Carbon is an element that exists in abundance in nature and can present itself in different shapes and sizes [8]. These different forms, which may include, in addition to CDs, other forms of carbon as the fullerenes, the nanodiamonds, the graphene and carbon nanotubes have been used in various analytical and bioanalytical applications

and have been target of an intensive study for use in biomedicine and in theranostic applications [9]. Have had relevance in the treatment of cancer and other diseases, finding the place treating and releasing controlled in time and space the therapeutic drug.

CDs are a fluorescent carbon class of NPs discovery casually in 2004 [10]. The CDs are photoluminescent NPs with properties similar to QDs but are nontoxic and biocompatible alternatives. The CDs are spherical or almost spherical. Typically have dimensions under 10 nm but can reach up to 100 nm [2, 11]. The CDs are interest due their optical properties, solubility in aqueous medium, chemical stability, low toxicity and facility of functionalization. Carbon is a nontoxic element. The nontoxic response of carbon combined with interesting optical properties and high solubility of the CDs, motivated the study of various means for their synthesis. Although the CDs applications still are reduced; the potential of these fluorescent NPs is immense and bioimage applications, nanosensors and optoelectronics applications have been demonstrated [10, 12].

Several methodologies for the CDs synthesis have been presented. CDs synthesis strategies can be divided into two types: “top-down” and “bottom-up” methods. Top-down procedures consist in producing CDs by breaking large carbon structures [13]. The main methods top-down include the laser ablation [14, 15] and electrochemical techniques, electrochemical oxidation, chemical oxidation [16] and electric discharge [17]. With bottom-up methods, the CDs are created from rich carbon precursors. The bottom-up synthesis procedures consist of carbonizations [18], solvothermic methods [3, 11], microwave radiation [19] and ultrasonic synthesis [20]. The top-down methods require difficult production conditions and costly materials. For this reason, bottom-up procedures, more simple and economic, have been the subject of growing interest and have shown promising results. The procedures are complemented with purification methods such as filtration, centrifuging, dialysis and electrophoresis [13]. Some CDs produced by top-down methods have weak fluorescence and weak colloidal stability. In these cases there is a need to carry out a procedure for passivating the surface of NPs. The passivation can be accomplished by chemical oxidation with highly oxidizing agents, such as nitric acid, to create hydroxyl, carboxyl and carbonyl groups in the CDs surface, or by attachment of organic, as the polyethylene glycol (PEG) polymers in the surface [10, 13]. The passivation procedure not only enhances the fluorescence intensity as by decreasing the aggregation, increases the stability of the NPs in solution [21]. In bottom-up procedures, the CDs

doesn't need any additional passivation step because the process itself induces synthesis of surface passivation with functional groups [13]. The passivated CDs may be subject to functionalization of its surface to the providing of specificity in chemical bonding. The functionalization can be made with small organic molecules such as peptides and small oligomers or polymers or macromolecules such as proteins to allow the combination of CDs with specific biomolecules. Generally the passivation procedures and functionalization of the CDs are simple [2, 22].

Different types of nanocomposites of CDs can be synthesized. Many nanocomposites are synthesized by binding of polymers to passivate the CDs making them fluorescent or increasing their fluorescence. One of the most used polymers for the passivation of CDs is the PEG. Many organic molecules are used in the synthesis of nanocomposites of CDs. Most of these organic molecules have amine groups in its structure, which will allow the connection to the carboxylic groups of CDs through an amidation reaction. Some of the organic molecules used for the synthesis of nanocomposites of CDs are the ethylenediamine (EDA), diethylamine (DEA), triethylamine (TEA). There are also some examples of nanocomposites of CDs with biomolecules or derivatives. Examples of biomolecules used in the synthesis of CDs are the trimetilglicine, antibody GAM and single stranded DNA. Some inorganic compounds such as iron and iron oxides, gold and silver, platinum, palladium, copper, silicon, silicon dioxide and titanium were used in the synthesis of CDs nanocomposites.

The CDs exhibit great solubility in aqueous medium than other fluorescent NPs giving to the CDs a great versatility. The presence of charged groups on the surface of passivated NPs controls the aggregation and is at the origin of the solubility [13]. The solubility in aqueous medium allows the application of CDs in physiological medium [10] and functionalization surface procedures make it possible conjugations with biomolecules. Additionally the chemical composition on the surface of NPs is of great importance for their internalisation through interactions with charged groups on the membrane [36]. The solubilization of CDs in various organic solvents is also possible giving to these NPs great versatility.

Although there are few studies related to cytotoxicity, the rare mention of significant decrease in cell viability are only for extremely high concentrations of CDs. In case of functionalization of the surface of NPs toxicity becomes dependent on the molecule used [23]. Low cytotoxicity to the CDs feature donates these NPs of excellent biocompatibility and therefore ideal candidates for use *in vitro* and *in vivo*.

The emission spectra of the CDs are wide and asymmetric stretch for the red, unlike the high symmetry and small half-width) displayed in the spectra of emission of QDs. However the CDs share with the QDs the dependency of the emission with the excitation wavelength and size of NPs [2, 10, 13]. The quantum yield (QY) of the CDs can vary widely. The synthesis methods and precursors used strongly influence this spectroscopic parameter [10]. In most cases the QY of CDs is less than 15% [23]. The surface passivation of CDs, whether made directly or indirectly in the synthesis procedure, whether obtained by an additional step, appears to be a necessary requirement for obtaining fluorescent NPs and therefore is directly related to the CDs QY. Reports in the literature report QY of these NPs as high as 78% [23].

The extraordinary optical properties and biocompatibility thus submitted by the CDs make these NPs promising candidates for fluorescent biological studies *in vitro* and *in vivo*. Nevertheless, biological studies that make use of these fluorescent NPs are still reduced.

The objective of this study is also the determination of chemical reactive oxygen (ROS) and nitrogen species (RNS) and a development of a sensor to their detection and quantification. The ROS/RNS are very important and are known to play a dual role in biological systems, they can be harmful but they can also be helpful to biological systems. The ROS/RNS are often associated with physiological and pathological processes and thus their detection is of utmost importance for the detection and prevention of diseases, as well as for the understanding of many pathological processes [24]. They are present in neuronal transmission, phagocytose and signal transduction processes [25]. In stress conditions their concentration is higher and can origin numerous damages to the organism. The determination is difficult because these species are found in low concentrations, have high reactivity, and very short lifetimes, possible antioxidant mechanisms and potential interferences. The main ROS/RNS hydrogen peroxide (H_2O_2), superoxide ion ($O_2^{\bullet -}$), nitric oxide (NO) and peroxynitrite ($OONO^-$). The determination methods used are based in electron spin resonance (ESR), fluorescence, chemiluminescence, colorimetric and electrochemical analytical techniques [26-29].

Due to its high QY, the CDs are particularly interesting and with great potential for use in optical fiber-based methodologies. Some applications employed QDs in immobilization membrane and fiber optic detection [30]. Few applications meet CDs in fiber optic detection applications [1, 31]. In the literature were not found references with immobilization of LRET systems and fiber optic detection. A way to increase the

sensitivity based on the use of optimization techniques and/or multivariate calibration [32] and Metal Enhanced Fluorescence (MEF) [3].

References

1. Gonçalves, H.M.R., A.J. Duarte, and Joaquim C. G. Esteves da Silva, *Optical fiber sensor for Hg(II) based on carbon dots.* Biosensors and Bioelectronics, 2010. **26**: p. 1302–1306.
2. Silva, Joaquim C. G. Esteves da and H.M.R. Gonçalves, *Analytical and bioanalytical applications of carbon dots.* TrAC Trends in Analytical Chemistry, 2011. **30**(8): p. 1327–1336.
3. Yongxia Zhang, H.G., Joaquim C. G. Esteves da Silva and Chris D. Geddes, *Metal-enhanced photoluminescence from carbon nanodots.* Chem. Comm., 2011. **47**: p. 5313–5315.
4. Kristin A. Fletcher, S.O.F., Mark Lowry, Sheryl A. Tucker, Sharon L. Neal, Irene W. Kimaru, Matthew E. McCarroll, Gabor Patonay, Philip B. Oldham, Oleksandr Rusin, Robert M. Strongin, and Isiah M. Warner, *Molecular Fluorescence, Phosphorescence, and Chemiluminescence Spectrometry.* Anal Chem. , 2006. **78**(12): p. 4047–4068.
5. Ute Resch-Genger, M.G., Sara Cavaliere-Jaricot, Roland Nitschke & Thomas Nann, *Quantum dots versus organic dyes as fluorescent labels.* Nat. Methods, 2008. **5**(9).
6. Alejandro Simón de Dios, M.E.D.-G., *Review Multifunctional nanoparticles: Analytical prospects.* Analytica Chimica Acta 2010. **666**: p. 1–22.
7. Sheng-Tao Yang, X.W., Haifang Wang, Fushen Lu, Pengju G. Luo, Li Cao, Mohammed J. Meziani, Jia-Hui Liu,‡ Yuanfang Liu, Min Chen, Yipu Huang, and Ya-Ping Sun, *Carbon Dots as Nontoxic and High-Performance Fluorescence Imaging Agents.* J. Phys. Chem. C 2009. **113**: p. 18110–18114.
8. Terrones, M. and H. Terrones, *The carbon nanocosmos: novel materials for the twenty-first century.* Philos Trans A Math Phys Eng Sci, 2003. **361**(1813): p. 2789–806.
9. Liu, Z. and X.J. Liang, *Nano-carbons as theranostics.* Theranostics, 2012. **2**(3): p. 235–7.

10. Li, H., et al., *Carbon nanodots: synthesis, properties and applications.* Journal of Materials Chemistry, 2012. **22**(46): p. 24230–24253.
11. Yan, H., et al., *Development of multicolor carbon nanoparticles for cell imaging.* Talanta, 2013. **108**: p. 59–65.
12. Ruedas-Rama, M.J., et al., *Fluorescent nanoparticles for intracellular sensing: A review.* Analytica Chimica Acta, 2012. **751**: p. 1–23.
13. Baker, S.N. and G.A. Baker, *Luminescent carbon nanodots: emergent nanolights.* Angew Chem Int Ed, 2010. **49**(38): p. 6726–44.
14. Gonçalves, H., et al., *Hg(II) sensing based on functionalized carbon dots obtained by direct laser ablation.* Sensors and Actuators B: Chemical, 2010. **145**(2): p. 702–707.
15. Zhao, Q.-L., et al., *Facile preparation of low cytotoxicity fluorescent carbon nanocrystals by electrooxidation of graphite.* Chemical Communications, 2008(41): p. 5116–5118.
16. Ye, R., et al., *Coal as an abundant source of graphene quantum dots.* Nat Commun, 2013. 4.
17. Xu, X., et al., *Electrophoretic Analysis and Purification of Fluorescent Single-Walled Carbon Nanotube Fragments.* Journal of the American Chemical Society, 2004. **126**(40): p. 12736–12737.
18. Zhou, J., et al., *Facile synthesis of fluorescent carbon dots using watermelon peel as a carbon source.* Materials Letters, 2012. **66**(1): p. 222–224.
19. Zhu, H., et al., *Microwave synthesis of fluorescent carbon nanoparticles with electrochemiluminescence properties.* Chemical Communications, 2009 (34): p. 5118–5120.
20. Li, H., et al., *One-step ultrasonic synthesis of water-soluble carbon nanoparticles with excellent photoluminescent properties.* Carbon, 2011. **49**(2): p. 605–609.
21. Ray, S.C., et al., *Fluorescent Carbon Nanoparticles: Synthesis, Characterization, and Bioimaging Application.* The Journal of Physical Chemistry C, 2009. **113**(43): p. 18546–18551.
22. Sun, Y.-P., et al., *Quantum-Sized Carbon Dots for Bright and Colorful Photoluminescence.* Journal of the American Chemical Society, 2006. **128**(24): p. 7756–7757.

23. Ding, C., A. Zhu, and Y. Tian, *Functional Surface Engineering of C-Dots for Fluorescent Biosensing and in Vivo Bioimaging.* Accounts of Chemical Research, 2014. **47**(1): p. 20–30.
24. Valko, M., et al., *Free radicals and antioxidants in normal physiological functions and human disease.* Int J Biochem Cell Biol, 2007. **39**(1): p. 44–84.
25. Bergendi, L., et al., *Chemistry, physiology and pathology of free radicals.* Life Sciences, 1999. **65**(18–19): p. 1865–1874.
26. Halliwell, B. and M. Whiteman, *Measuring reactive species and oxidative damage in vivo and in cell culture: how should you do it and what do the results mean?* Br J Pharmacol, 2004. **142**(2): p. 231–55.
27. Borgmann, S., *Electrochemical quantification of reactive oxygen and nitrogen: challenges and opportunities.* Anal Bioanal Chem, 2009. **394**(1): p. 95–105.
28. Chen, X., et al., *Fluorescent and luminescent probes for detection of reactive oxygen and nitrogen species.* Chemical Society Reviews, 2011. **40**(9): p. 4783–4804.
29. Tarpey, M.M. and I. Fridovich, *Methods of detection of vascular reactive species: nitric oxide, superoxide, hydrogen peroxide, and peroxynitrite.* Circ Res, 2001. **89**(3): p. 224–36.
30. Pedro Jorge, M.A.M., Tito Trindade, José Luís Santos and Faramarz Farahi, *Review Optical Fiber Sensing Using Quantum Dots.* Sensors 2007. **7**: p. 3489–3534.
31. Gonçalves, H.M.R., et al., *Layer-by-layer immobilization of carbon dots fluorescent nanomaterials on single optical fiber.* Analytica Chimica Acta, 2012. **735**: p. 90–95.
32. Leitão, J.M.M., H. Gonçalves, and Joaquim C. G. Esteves da Silva, *Parallel factor analysis of EEM of the fluorescence of carbon dots nanoparticles.* J. Chemometrics 2010. **24**: p. 655–664.

Objectives of this Thesis

The main objectives of this doctoral project with the theme "Nanopartículas para a deteção luminescente em fibra ótica de espécies químicas reativas de oxigénio e azoto", are the development of luminescent optical fiber sensors based on NPs for the detection of the principals ROS/RNS in particular hydrogen peroxide (H_2O_2), superoxide ion ($O_2^{\bullet -}$), nitric oxide (NO) and peroxynitrite ($OONO^-$) in biological systems with prospective for "*in vivo*" determinations. Furthermore the most appropriate sensitivity and selectivity of the developed optical sensors should also be characterized by having a fast, continuous and reversible response. It was also a particular objective of this work the synthesis of these reactive species, the preparation of standard solutions and their standardization. Relatively to the NPs, their will be functionalized with luminescent chemical systems or could be used as donors or acceptors in LRET systems. Preferably will be selected biocompatible chemical systems not previously used in the quantification of these biological species. The possibility of determination of other related chemical species, such as antioxidants or potential interfering could be also evaluated. Could be used experimental techniques of fluorescence sensibility increase, like the optimization techniques and/or multivariate calibration in order to increase the sensibility and selectivity.

In order to achieve the objectives of the PhD project, several phases along the work must be successively reached. In these first steps are included the selection of the most suitable chemical systems for the detection of ROS/RNS (Initially based in fluorophores of pharmaceutical origin namely in Lanthanide complexes); the synthesis and functionalization of fluorescent NPs (QDs and CDs); the optimization of the response of selected chemical systems to ROS/RNS; functionalization of NPs with the optimized chemical systems; immobilization of functionalized NPs on the more appropriated membrane and with the more adequate method; optical fiber adhesion of the functionalized NPs on the membrane; optical fiber detection by functionalized NPs immobilized on the membrane; evaluation of optical fiber detection by functionalized NPs.

Bibliographic Research …….

Chapter 1

Carbon nanomaterials for tumor targeting theranostics

João M. M. Leitão, Eliana F. C. Simões, Joaquim C. G. Esteves da Silva

Book: Nanomaterials for Tumor Targeting Theranostics",
Chapter 8, Mingqian Tan and Aiguo Wu Eds., Higher Education Press Limited Company and World Scientific Publishing Company, Inc (2016) ISBN: 10 9814635413, ISBN 13 978-9814635417, Print ISBN: 978-981-4635-41-7



In this work the bibliographic research of the different carbon nanomaterials (carbon nanotubes, graphene, CDs, fullerenes and diamonds) namely their application on therapy and diagnostic was made. The figures and the writing of the book chapter, was made together with Professor João M.M. Leitão under the supervision of Professor Joaquim C. G. Esteves da Silva.

Chapter 8

Carbon Nanomaterials for Tumor Targeting Theranostics

João M. M. Leitão[1], Eliana F.C. Simões[2] and Joaquim C.G. Esteves da Silva[2,*]

[1] *Centro de Investigação em Química (CIQ-UP), Faculty of Pharmacy, University of Coimbra Polo das Ciências da Saúde, Coimbra 3000-548, Portugal*

[2] *Centro de Investigação em Química (CIQ-UP), Department of Chemistry and Biochemistry, Faculty of Sciences, University of Porto,Rua do Campo Alegre 687, Porto 4169-007, Portugal*

Carbon nanomaterials are the focus of an intense research in several areas of science. Due to their apparent low toxicity, when compared to other nanomaterials, carbon based nanoparticles found particularly important applications in biomedicine. Indeed, carbon shows many nanoallotropic forms like carbon nanotubes, graphene, carbon dots, fullerene and nanodiamonds. Some of them show fluorescence in the visible wavelength range, like graphene and carbon dots, but all have in common being nanosized with the corresponding properties. The main theranostics applications of carbon based nanomaterials (the fluorescent nanoallotropes) are for improving tumor imaging, allowing earlier detection, and specific drug delivery allowing high treatment efficient and reduced side effects. This chapter will describe the carbon nanomaterials mostly used for tumor targeting theranostics, their properties and the engineering strategies used to modify them. Also, the most successful biomedical applications of the carbon nanomaterials will be described.

8.1. Introduction

Theranostic is the term used to refer the combination of therapy and diagnostic of disease. The cancer therapy and diagnostic has been the main field of research of theranostic applications namely the utilization of nanoparticles in theranostic.[1−3] The development of earlier diagnostic methodologies and more efficient and safer therapeutic agents is of crucial importance in cancer therapy. The selective cancer cell targeting is essential in order to avoid any unwanted damage to the normal cells and corresponding secondary health effects. Concurrent *in vivo* bioimaging allows the detection of tumors at a much earlier stage, which may improve the success of treatment, and provide information about its efficacy. The number and type of the applications in theranostics have been multiplied and diversified. Fig. 8-1 illustrates

*Corresponding author E-mail: jcsilva@fc.up.pt

some of theranostic applications in therapy and diagnostic.

In the last few years there was a growing interest in the study of the nanomaterials as both therapeutic and diagnostic options for the cancer treatment and many other diseases due to the advantages associated with the nanomaterials including spatially and temporally controllable drug release, localizing therapy and avoiding invasive treatment.[4−8] The theranostic nanoparticles may include a wide range of materials such as polymeric nanoparticles, emulsions, nanocapsules, nanospheres, micelles, liposomes, dendrimers, quantum dots, carbon nanotubes and fullerenes.[2−3] It is possible to use nanocarriers that are capable of active targeting using cell-specific ligands and transport multiple therapeutic and imaging agents for accurate diagnosis and controlled drug delivery. These materials are being used to encapsulate or solubilize chemotherapeutic agents for improved drug delivery *in vivo* or to provide unique optical, magnetic and electrical properties for imaging.[6]

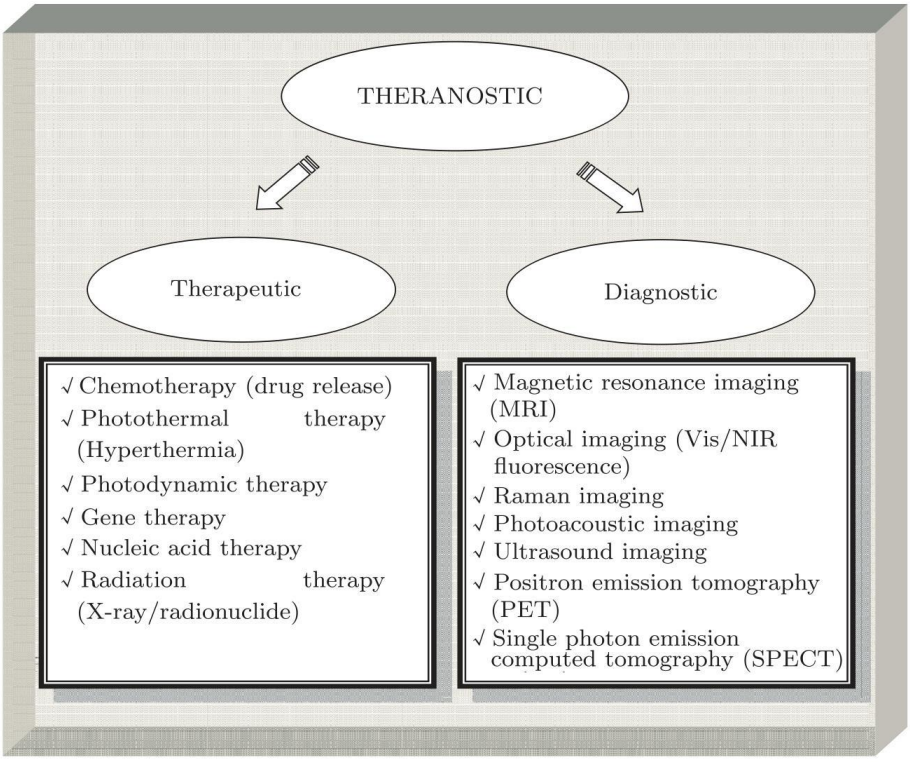


Fig. 8.1. Theranostic applications.

Carbon is capable of forming many allotropes due to its unique valency. Besides the bulk allotropic forms of carbon (diamante, graphite and amorphous carbon), different nanoallotropic forms of carbon as the fullerene forms [fullerene (FL), carbon nanotubes (CNT), graphene (GP)], nanodiamonds (ND) and carbon dots (CD) have also been discovered.[9−10] Having versatile properties, these different nano forms of carbon play important roles in different fields of application. The nano forms of

carbon are gaining relevance in the tumor target theranostics.[10] Most of the tumor theranostics applications found in the literature uses CNT.[3–8] Other applications are also found using graphene, carbon dots, fullerene and nanodiamonds. Fig. 8-2 depicts the variety of carbon nanomaterials used in tumor targeting theranostic.

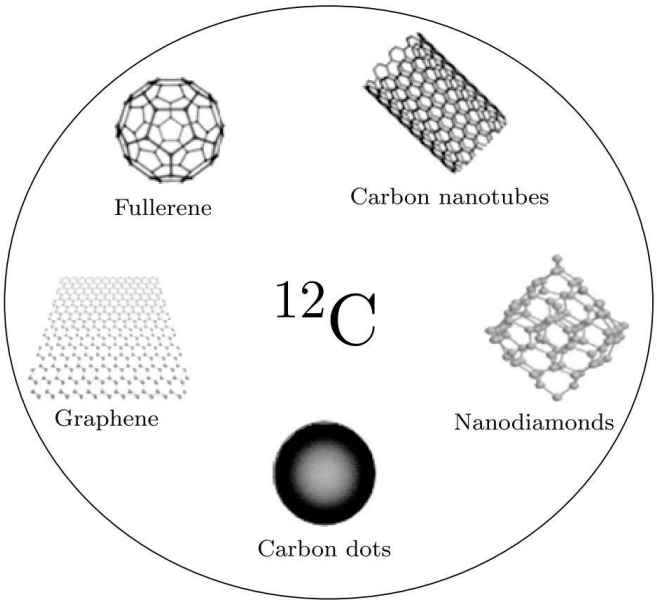


Fig. 8.2. Carbon nanomaterials used in tumor targeting theranostics.

The potential of carbon based nanoparticles in biomedical applications is enormous because the major component, carbon, is a nontoxic element. The carbon based nanomaterials consequently have lower toxicity compared to other nanomaterials. Furthermore, the availability of carbon nanoparticles for conjugation with other materials makes it possible to exploit their attributes in cancer theranostics. The photothermal properties of some carbon nanomaterials, such as the NTC, also allows them to be used in conjunction with near infrared radiation and lasers to thermally ablate cancer cells. This chapter presents mainly the carbon nanomaterials used as theranostic agents and their bioanalytical and biomedical applications.

8.2. Tumor Theranostic Applications of Carbon Nanomaterials

8.2.1. *Tumor Theranostics Applications of Carbon Nanotubes*

CNT are a member of the structural family of fullerenes with a cylindrical nanostructure constituted with carbon atoms arranged in condensed aromatic rings.[11] Raw CNT have highly hydrophobic surfaces and are not soluble in aqueous solutions. Their name is derived from their long, hollow structure with their walls formed by a one-atom-thick concentric graphene sheet. CNT, depending on their formation by one or more graphene sheets, are classified respectively as single-walled

carbon nanotubes (SWCNT), with 0.4-2.0 nm of diameter and a few μm of length, or as multi-walled carbon nanotubes (MWCNT), with diameter up to 100 nm and a length from 1 to several μm. The graphene sheets are rolled at specific and discrete ("chiral") angles, and the combination of the rolling angle and radius decide the properties of CNT. Individual CNT naturally tend to align themselves into "ropes" held together by van der Waals forces, more specifically, pi-stacking.[12−13]

Due to their high length-to-diameter ratio, high mechanical strength, large surface areas, chemical and thermal stability, electronic and optical properties, CNT become valuable for nanotechnology, electronics, optics and other fields of materials science and technology.[11,14] Their unique mechanical strength are due to the strength of the chemical bonds of CNT entirely composed of sp^2 bonds, similar to those of graphite, stronger than the sp^3 bonds found in alkanes and diamond.[14] These cylindrical CNT have been constructed with a length-to-diameter ratio significantly larger than any other material with a very large surface area, which makes CNT amenable for high sensitivity molecular detection and recognition in biological systems. Moreover, SWCNT have very high optical absorbance in the NIR range where the biological systems are transparent.[12] Nevertheless, some CNT toxicity and biodegradable issues are still under discussion.[8,11,15]

The CNT functionalization decreases the citotoxicity, improves the biocompatibility, increases the solubility and gives the opportunity to append drugs molecules, proteins or genes, for the construction of delivery systems. The CNT functionalization can be done using several different processes. Functionalization can be done at the covalent ends or at the defect sites with an initial oxidation procedure. On the other hand, covalent sidewall functionalization can be achieved where reagents with high chemical reactivity are involved, due to carbon bonds with lower reactivity. On the contrary, a noncovalent functionalization through an amphiphilic substance or ionic interaction has the advantage of no destruction of the conjugation in the CNT.[11−13,16] Besides the functionalization with one substance, CNT can also be multifunctionalized allowing the immobilization of different types of bioactive molecules such as peptide, proteins, nucleic acids and small drugs, to make them able to act in different ways simultaneously.[17]

Intense research was performed with CNT in the theranostics field that has been reflected in the high number of reviews featuring this carbon nanomaterial.[2−8,12−13,16−19] In cancer theranostic, CNT have been used in photothermal,[4,6,8,16−17,19] photodynamic,[19] radio frequency ablation and photoacustic therapy;[17] in nucleic acid or gene[2,4,7−8,12−13,19] and drug delivery[2−5,7−8,12−13,16−18] and in diagnosis as imaging agents.[2,4−8,12] Although, most of the theranostics applications with CNT involved drug delivery coupled with different types of imaging techniques, but in some cases other kinds of therapy were performed. Due to their inherent characteristics, the multifuncionalization of CNT has been extensively used to generate complex nanocomposites with different properties. Among the several theranostics applications developed with CNT, the

most representative applications will be discussed in this chapter. Fig. 8-3 presents the main cancer theranostics application with CNT.

Some complex multifunctionalized CNT for tumour theranostics applications have been established.[20−24] While SWCNT were used in four of these multifunctionalized CNT,[20−22,24] MWCNT has also been used in one case.[23] Water soluble pristine SWCNT that were noncovalently functionalized by single-strand DNA (ssDNA) have been modified with silver (Ag) or gold (Au) and then coated with folic acid (FA) conjugated lipoic acid modified polyethylenoglicol (PEG-FA). In the SWCNT-ssDNA-Au-PEG-FA, the over expressed FA cancer cell gives the selectivity and Au provokes the enhancement of Raman signal of SWNTC. Strong surface plasmon resonance absorption allows the use of these nanocomposites in Raman imaging and photothermal ablation of KB and HeLa cancer cells.[20]

Water soluble SWCNT were conjugated with Cy3 labeled with ssDNA and covalently functionalized with a mixture of phospholipids PEG-FA and PEG fluorescein. The multifunctionalized nanocomposites was used to target cancer Hella cells by the FA and for optical bioimaging by the fluorescein probe and NIR photothermal therapy based in the intense SWCNT NIR absorption.[24] Magnetic SWCNT conjugating doxorubicin (DOX) and transferrin (TF) with silica coated CdTe quantum dots (SiO_2-CdTe) linked to SWCNT filled with Fe_3O_4 were synthesized. This SWCNT nanocomposite provides a Fe_3O_4 and TF dual-targeted DOX delivery system to HeLa cancer cells with the possibility of visible fluorescence optical imaging by the SiO_2-CdTe fluorescent probe.[21] Oxidized SWCNT were also functionalized with DOX anticancer drug, 5(6)-carboxyfluorescein fluorescent probe and with a carcinoembryonic antigen (CEA) monoclonal antibody for targeting cancer cells. DOX was noncovalently linked to SWCNT and monoclonal antibody and 5(6)-carboxyfluorescein were covalently linked using bovine serum albumin (BSA) as multifunctional linker. The synthesized nanocomposite was used for DOX delivery and visible optical imaging for human cancer colon cells.[22]

In the theranostics application with multifunctionalized MWCNT Das et al conjugated oxidized MWCNT with the fluorescent label Alexa-fluor (AF), a Technitium radionuclide (^{99m}Tc), tumor targeting molecule (FA) and an anticancer drug methotrexate (MTX). The ^{99m}Tc was coordinated and the other three compounds were covalently functionalized at MWCNT surface. For the MTX functionalization, a glycidylated MWCNT-FA-AF was previously synthesized. The MWCNT-FA-AF-MTX was used for selectively targeting lung (A549) and breast cancer (MCF7) cells *in vitro* and *in vivo* by the FA and for multimodal visible optical and radio imaging by respectively the AF and ^{99m}Tc.[23]

Simpler SWCNT nanocomposites[25] or nonfunctionalized SWCNT[26] were used for theranostics tumor targeting. SWCNT, functionalized only with a mixture of two PEGylated phospholipids 1,2-distearoylphosphatidylethanol-amine-methyl-polyethyleneglycol and poly(maleic anhydride-alt-1-octadecene)-poly(ethylene glycol) methyl ether, were used for in vivo tumor NIR optical imaging and for pho-

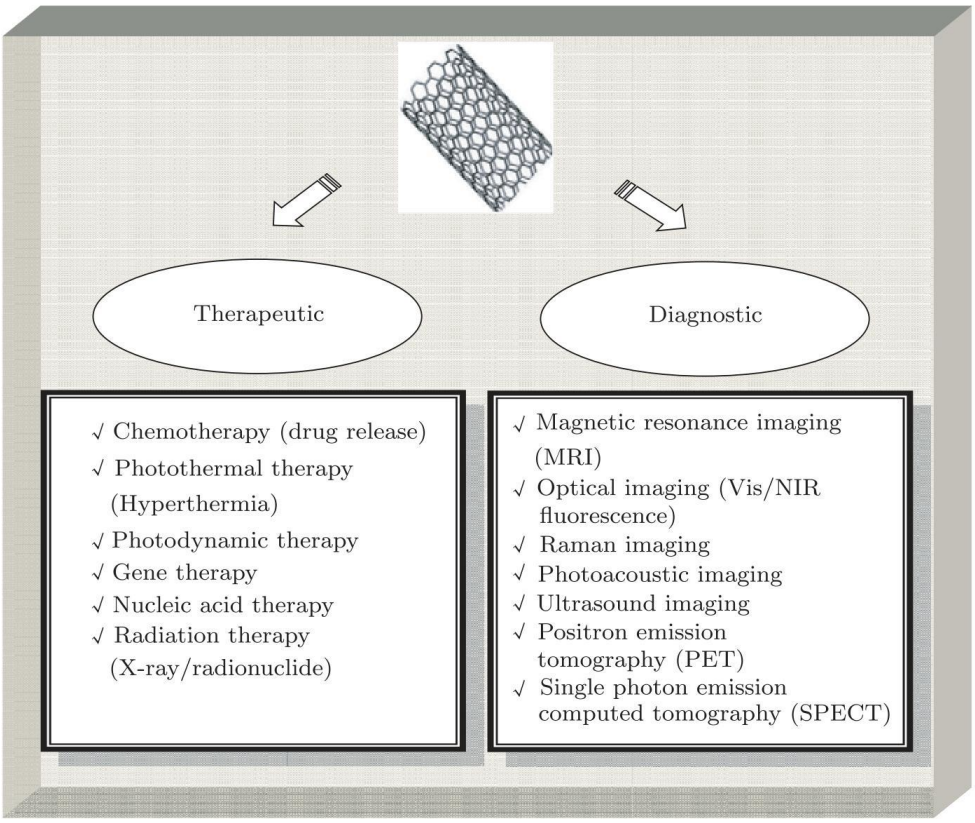


Fig. 8.3. Cancer theranostic applications of carbon nanotubes.

tothermal ablation of tumor with a referred high tumor uptake.[25] Nonfunctionalized SWCNT were used in tissues-mimicking materials and the response to the enhancement of the dielectric and temperature of that materials can be attributed to the utilization of these SWCNT for simultaneous microwave detection and hyperthermic treatment of breast cancer.[26]

Similar CNT nanocomposites were also developed for therapeutic or diagnostic applications with potential for cancer theranostics applications. Several kind of SWCNT or MWCNT nanocomposites of more or less complexity were developed for DOX,[27−28] cyclosporine (CY),[29] etopoxide (ETO)[30] and gemcitabine (GEM)[31] drug delivery; DNA[32−33] and small interfering RNA (siRNA)[34−35] delivery and PET and Raman imaging.[36] Similar CNT nanomaterial, with a different conical shape designed as nanohorns, were used as multifunctionalized nanocomposites for photodynamic and hyperthermic therapy.[37]

8.2.2. *Tumor Theranostics Applications of Graphene*

GP is a two dimensional material, and similar to CNT, is composed of sp^2-bonded carbon atoms arranged in a regular hexagonal pattern. GP has a tunable planar

structure (sheet, ribbon, triangle and hexagon), with a thickness from 0.34 to 100 nm and lateral size from 0.3 to 10 μm and can have a mono or multilayer structure.[38] The main derivatives of GP are the graphene oxide (GO) and reduced graphene oxide (RGO). GO can be considered as consisting of individual sheets of GP decorated with oxygen functional groups on both the basal planes and edges.[39] The physicochemical features of GP and their derivatives are characterized by a low aspect ratio, larger surface area, and overall better dispersibility in most solvents compared to CNT. Colloidal dispersions of individual GP or other derivatives sheets can easily be engineered without metallic impurities, with high stability and less aggregation.[38]

A quite important property of GP nanostructures is that they are not fiber-shaped. Theoretically this characteristic offers significant advantages in terms of toxicity and biocompatibility over inhomogeneous dispersions of fiber-shaped CNT. However, studies that directly compare GP and CNT are uncommon, making comparative considerations of their overall safety and risk assessment challenging.[38] Their unique mechanical, optical and electronic properties, being different from the CNT, allow their application in different areas including quantum physics, nanoelectronic devices and for nanocomposites materials. GO is soluble in water and is been used for the detection of biomolecules.[40–42]

An intense research is being done in the last years with the GP in the theranostics field and some reviews dealing with theranostics applications of GP were published.[6,40–45] In cancer theranostic, GP have been used in photothermic[6,40,42–44] and photodynamic therapy[6,43]; in nucleic acid or gene therapy[43–45]; drug delivery;[40–45] and, in diagnosis as imaging agents.[41–45] Fig.8-4 presents the main cancer theranostics applications of GP.

Most of the GP theranostics applications for cancer involved multifunctionalized single layer GO.[46–50] GO was linked to hyaluronic acid conjugated with chlorin e6 (Ce6) by non-covalent functionalization and it was used for NIR fluorescence and photothermal and photodynamic induced therapy of A549 cancer cells.[46] In other application, aminated PEG, of molecular weight of 6000 g (PEG6000N), and FA as the targeting ligands were initially covalently linked to GO and then the GO-PEG-FA were noncovalently and covalently functionalized, respectively with a gadolinium salt (Gd), as a MRI probe, and DOX, for drug delivery where the GO-PEG6000N-FA-Gd-DOX nanocomposites were tested in HepG2 cancer cells.[47] Moreover, GO was covalently functionalized with branched PEG and with an antibody anti-CD20, for selective targeting, for DOX drug delivery and it was also used for NIR optical imaging of B and T cancer cells.[48]

Multifunctionalized GO for theranostics applications using GO magnetic nanocomposites were also synthesized with iron oxide nanoparticles.[49–50] One of the GO linked to iron oxide was covalently linked with branched PEG and DOX and used for targeted drug delivery and photothermal therapy in $4T_1$ cancer cells and in vivo MRI using the nanocomposites as the T_2 contrast agent.[49] The other GO linked

with iron oxide was noncovalently functionalized with poly (maleic anhydride-alt-1-octadecene) (PMA–PEG) and used for photothermal therapy and MRI, visible optical and photoacoustic imaging.[50]

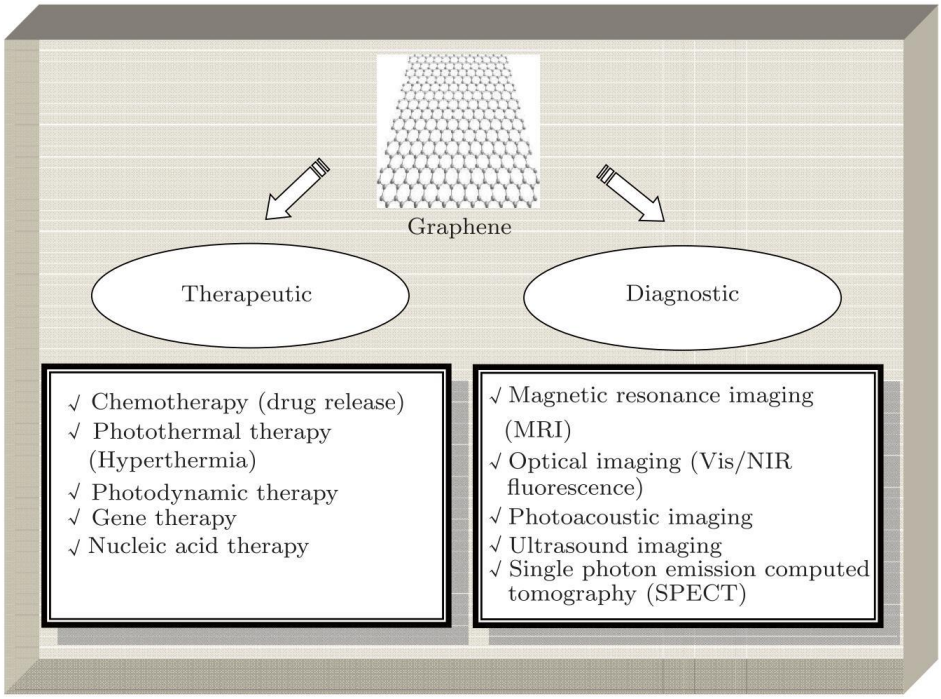


Fig. 8.4. Cancer theranostic applications of graphene.

A different kind of multifunctional GO nanocomposites was synthesized by coating poly(lactic acid) (PAA) microcapsules, containing Au nanoparticles, with GO by an electrostatic layer by layer technique. The Au-PAA-GO nanocomposites were used *in vivo* photothermal therapy, due to the strong NIR absorption of GO, and *in vivo* bimodal ultrasound and computed tomography imaging, due to the enhancement of ultrasound imaging by the PAA microcapsules and the use of Au nanoparticles as contrast agent, respectively. [51]

Simpler nanocomposites were developed for cancer theranostics applications with single layer RGO.[52–53] RGO were only functionalized with bovine serum albumin (BSA) and the synthesized RGO-BSA nanocomposites were used for photothermal therapy of MCF-7 cancer cells and for *in vivo* photoacoustic and ultrasounds imaging.[52] In another application, RGO was linked with CdSe/ZnS QD after surface adsorption of poly(L-lysine) amphiphlic polypeptide. The synthesized RGO-CdSE/ZnS nanocomposites were also used for photothermal therapy of MCF-7 and HeLa cancer cells, and were used for in vivo visible optical imaging. Graphene sheets of different size, linked with FA, were also evaluated for their internalization in the two lines of cancer cells.[53]

Nonetheless, some GO nanocomposites, constituted by single layer GO, were developed only for therapeutic or diagnostic applications with potential for cancer theranostics applications.[54–66] Some of these nanocomposites were developed for DOX,[54–55] adryamicincamptothecin analog[56] and iressa drug delivery[57]. Others were developed for DNA,[58] siRNA[59] and single stranded RNA (ssRNA)[60] delivery. Some nanocomposites were developed for visible[61] and NIR[62] optical imaging. Several applications were developed for photothermal[54,64] and photodynamic[65–66] therapy. With RGO, a photothermal therapeutic[67] and PET imaging diagnostic applications [68] were also developed.

8.2.3. *Tumor Theranostics Applications of Carbon Dots*

Carbon dots (CDs) are small photoluminescent carbon nanoparticles usually of-dimensions less than 10 nm, suspending in water or in other solvents. Their properties are similar to the classical nanocrystalline semiconductors quantum dots (QD) but the CDs had been developed as a biocompatible and nontoxic alternative.

All the theranostics applications involving CDs are of functionalized CDs.[69–71] In one application, CD were passivated with aminated polyethileno glycol of molecular weight 2000 g (PEG2000N) and was linked to the CD-PEG2000N chlorin e6 (Ce6).[69] In another case, CDs of silica nanocomposites (CD-SiO_2) was coated with PEG900N.[70] In a third application, CDs were passivated with branched polyethylenimine (BPEI).[71] For the CD-PEG2000N-Ce6, the possibility of simultaneously enhanced photosensitizer fluorescence detection, by a fluorescence Förster resonance energy transfer (FRET) mechanism between the CDs and Ce6 in MGC803 cancer cells, and of in vivo visible optical imaging and photodynamic therapy of gastric cancer was demonstrated.[69] For the other two CD applications, their diagnostic ability by visible bioimaging and the capability of drug[70] and gene[71] delivery were

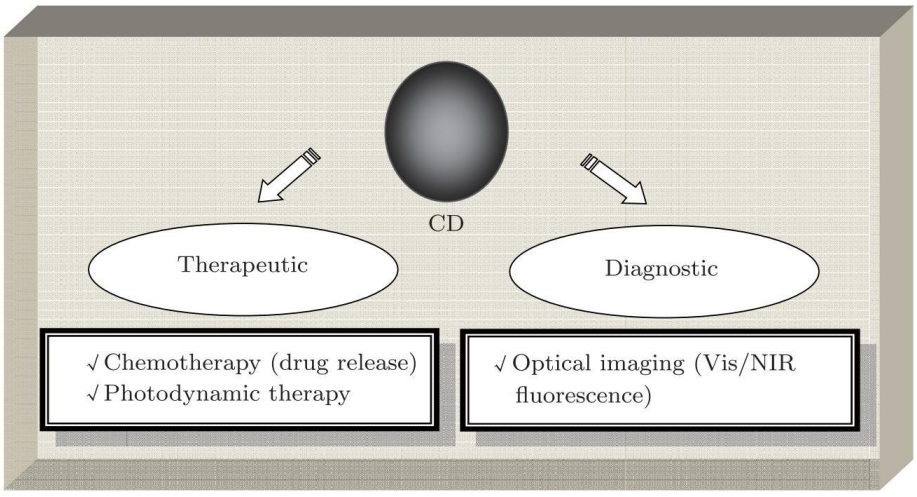


Fig. 8.5. Cancer theranostic applications of Carbon dots.

exhibited after functionalization with the anti-cancer drug DOX in HeLa and vector/pDNA complexes (pDNA) in COS7 and HepG2 cancer cells. The capability of DOX drug release was done by evaluating ratiometric changes of the fluorescence of CDs (blue emission) and DOX (red emission) at the cytoplasm and nucleus, and the capability of gene transfection of the CD-BPEI-pDNA nanocomposites was verified. Fig. 8-5 schematically shows the cancer theranostics applications of CD.

Cell cytotoxicity assays suggested that mesoporous carbon dots (MCD) could be used for drug delivery. The MCNs served as effective carriers for camptothecin which efficiently inhibited the growth of MCF-7 cancer cells after its sustained release therein.[72] Iron based carbon magnetic nanoparticle DOX drug delivery systems were also reported.[73]

8.2.4. *Tumor Theranostics Applications of Fullerene*

Fullerences (FLs) are three dimensional polyhedron forms of carbon with a molecular formula of C_{2n} (n = 30–41) and a diameter around 1 nm. They are composed of carbon in the form of a hollow sphere, ellipsoid or tube. Spherical FLs are called buckyballs. Their structure is similar to graphite, which is composed of stacked graphene sheets of linked hexagonal rings, but they may also contain pentagonal (or sometimes heptagonal) rings.[74] Their poor solubility and the difficulty in purifying and processing have impaired the application of FLs, and functionalization is required in order to modify their physical and chemical properties.[75] Studies on functionalization of FLs for various applications in the field of biomedical sciences have been significantly increased. The ultimate goal towards employing these functionalized fullerenes involves their use in the diagnosis and in the therapy of cancer and others human diseases.[75–77]

The preparation of specific multifunctionalized derivatives, mostly of C_{60}, with organic addends for biomedical applications is currently undergoing in several research groups.[76–77] Two fullerenes derivatives have recently gained [77]relevance in the therapy and diagnostic of cancer, the polyhydroxy fullerenes (fullerenols, PHFL)[78] and the endohedral metallofullerenes (EMFL).[75,79] The water soluble FLOH, with a molecular formula $C_{60}(OH)_n$ (n = 12–26), are considered to be excellent antioxidants due to their free radical scavenging ability and it is expected that they have a large biomedical use.[78] The EMFL, a new class of hybrid molecules, are formed by encapsulation of metallic species inside fullerene cages. They exhibit unique properties that differ from those of empty fullerenes due to the presence of metals and their hybridization effects via electron transfer. The introduction of metallic species inside fullerene cages provides a novel platform for developing future nanomedicines with multiple functions. The most important advantage that these EMF offer is the cage protection from the toxic metal ions inside the large surface area of the fullerene, associated with the possibility of multiple hydrophilic functionalization with the attachment of some tissue-targeting ligands. For example, these EMFL have the possibility to accommodate one or more gadollinium atoms

to obtain gadofullerenes and, due to their own characteristics, these gadofullerenes can be used for MRI.[75–78,79] In cancer therapy and diagnostic the functionalized FL have been used for: drug[76] and DNA[75,76] delivery; in photothermal,[77,78,80] photodynamic,[76] photoacoustic[77,78] and radio therapy;[77,79] in MRI;[75–78,79]and, as chemoterapeutic pharmaceutical.[77,79] The FL usually used is the buckyball C_{60} fullerene. In Fig.8-6, some cancer theranostics applications of FL are presented.

Few theranostic applications have been developed until now with FL or its derivatives.[80,81–82] PHFL $C_{60}(OH)_n$, (n = 18-22) functionalized with chitosan (CS) were used for in vivo photothermal therapy and photoacoustic imaging. Besides these PHFL-CS nanocomposites, some other nanocomposites with fluorescein isotiocianate doped silica nanoparticles were synthesized in different ways.[80] C_{60} FL was functionalized with HA in the presence of lithium hydroxide. The synthesized C_{60}-HA nanocomposites was used for in vivo photothermal therapy, for optical NIR fluorescence imaging and in HCT 116 and KB cancer cells.[81] EMFL with trigadolinium nitride (Gd_3N) inside a C_{80} FL was functionalized with^{177}Lu isotope after previously linked with bifunctional 2-(4-aminobenzyl)-1,4,7,10-tetraazacyclododecane -1,4,7,10-tetraacetic acid (p-NH2-Bn-DOTA, DOTA). The synthesized radiolabeled metallofullerene was used for radiation therapy and for MRI and radioactive labeling in U87MG and GBM_{12} cancer cell lines.[82]

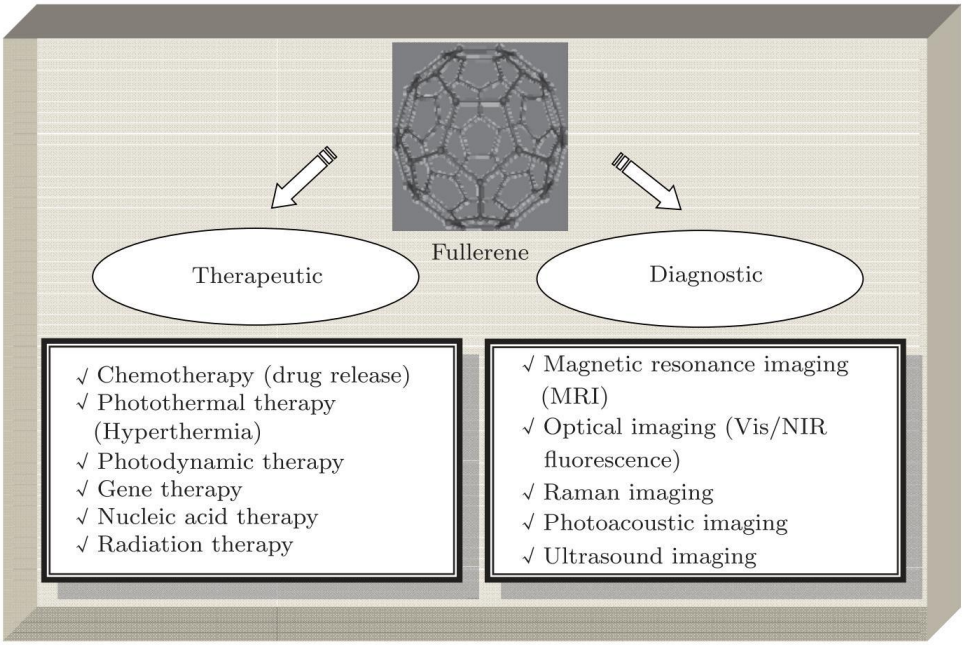


Fig. 8.6. Cancer theranostic applications of fullerene.

Most of the FL, PHFL or EMFL nanocomposites for cancer applications used C_{60} only for therapeutic or diagnostic application with potential for cancer theranostics.[83–87] They were used for DOX,[83,85] paclitaxel (PTX)[87] and

docetaxel[84] drug delivery and photodynamic therapy.[83,85,87] Besides these applications, some FLs and their derivatives with potential in chemotherapy as active chemotherapeutic pharmaceutical drug was also demonstrated.[88–90] The therapeutic activity was demonstrated with C_{60}^{88} and with gadolinium metallofullerenol $[Gd@C_{82}(OH)_{22}]_n^{89-91}$ for *in vivo* and *in vitro* cancer cells. Furthermore, $[Gd@C_{82}(OH)_{22}]_n$ nanoparticles overcome tumor resistance to cisplatin by increasing its intracellular accumulation through the mechanism of restoring defective endocytosis.[92]

8.2.5. *Tumor Theranostics Applications of Nanodiamonds*

Nanodiamonds (NDs) are monodisperse nanometre-sized diamond particles with an irregular tetrahedral structure containing 46 carbon atoms. NDs can be produced by detonation, high-pressure, high temperature, ultrananocrystalline diamonds and single/polycrystalline diamond films. The NDs have a size around 4 to 5 nm and are soluble in water and they are a chemically inert material with low cytotoxicity, good biocompatibility and a large surface area.[93–94]

Based on ND's chemical, biological, and physical (optical, mechanical, electrical, thermal) properties, they can be used in several biomedical applications such as drug delivery, sensing and imaging.[93–98] They can be functionalized with different types of pharmaceutical drugs and can be suspended easily in water, which makes them important drug delivery systems.[99] Nanocrystalline diamond films have also been used in the coating of biomedical implants.[100]

In theranostics applications, NDs nanocomposites act as a chemotherapeutic pharmaceutical drug[101] or as a drug delivery system.[102–105] It was used for the diagnostic application in visible wavelength range. When ND acts as chemotherapeutic pharmaceutical drug, the fluorescent nanomaterial was covalently functionalized with chlorotoxin peptide BmK CT, known as active to glioma cancer cells. The activity of the synthetized ND-BmK CT nanocomposites and the visible optical imaging capability were demonstrated in C6 glioma cancer cells.[101]

For the nanocomposites used for drug delivery, a ND multifunctional PTX drug delivery agent was obtained by covalently linking a fluorescently labeled oligonucleotide PTX-DNA conjugate strands and a monoclonal antibody anti-EGFR (mAbs) as targeting ligand. The synthesized nanocomposites were used in MCF7 and MDA-MB-231 cancer cells.[103] Simpler nanocomposites functionalized with fluorescein and DOX were synthetized for the DOX drug delivery and visible optical imaging and used in human breast adenocarcinoma. It was demonstrated for this nanocomposites that the liberation of PTX drug depends on the pH.[103] For the other ND nanocomposites that act as a drug delivery system, fluorescent ND were functionalized with a porous silica coating using tetraethoxy orthosilicate (TEOS) and posterior coupled with PEG-polyethylenimine (PEI) copolymer. The synthetized nanocomposites were used for visible optical bioimaging of HeLa cancer cells and their potential for drug delivery was investigated after linking a red

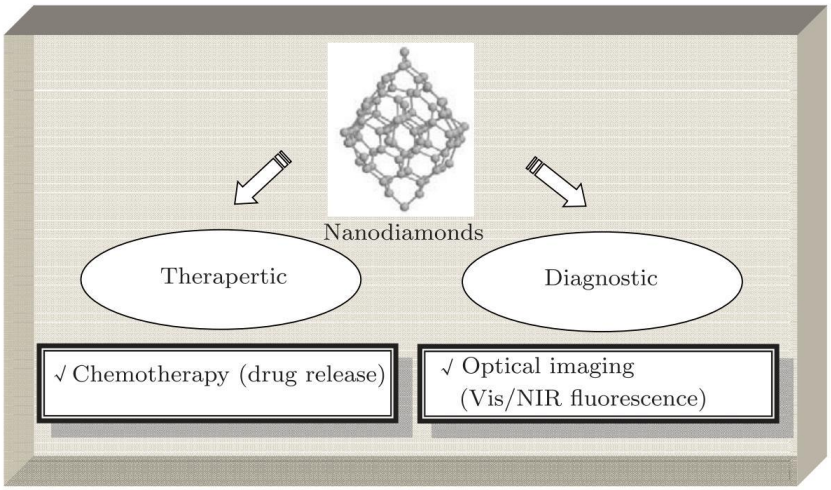


Fig. 8.7. Cancer theranostic applications of nanodiamonds.

fluorescent dye.[105] Fig. 8-7 presents the principal cancer theranostic applications of NDs.

Besides the described applications of NDs, some therapeutic or diagnostic applications with different nanocomposites were also developed with potential use in cancer theranostics applications[106−112] including DOX,[106−107,109] PTX,[110] 10-hydroxycamptothecin (HCPT)[111] drug delivery, radio-frequency hyperthermic[108] therapy and visible optical imaging.[109,112]

8.3. Future Perspectives

Different carbon nanoallotropes forms are being developed for human theranostic applications. The large majority of theranostic applications that have been developed are focused on cancer diseases. Indeed, nanomaterials in general are particularly suited for cancer theranostics because the success of the cancer treatment is highly dependent on the yearly diagnostics and on the selective cytotoxic drug delivery. Carbon nanomaterials have the nanosized properties coupled with a potential low toxicity and biocompatibility and, consequently, are highly promising nanomaterials for cancer theranostics. Nevertheless, some of the carbon nanoallotropes raised some toxicity questions, e.g., CNT, which must be investigated and clarified further.

The intense research observed in the last decade about the use of carbon nanomaterials for *in vitro* cancer theranostics set up the basic strategies. In diagnostics, the development of intrinsically high fluorescent nanomaterials, coupled with the paramagnetic materials and/or specific functionalization, improved earlier tumor detection methodologies. In drug delivery, they have an important role as agents for the selective drug delivery of classic cytotoxic drugs or gene/protein oriented therapies. Indeed, besides the major advances that are occurring in cancer thera-

pies that resulted from of the identification of the oncogenes pathways associated with selected cancers, nanosized carbon materials will have an important role in the development of these new therapies.

Acknowledgments. Financial support from Fundação para a Ciência e Tecnologia (FCT, Lisbon) project PEST and a PhD grant to Eliana Simões SFRH/BD/81074/2011 is acknowledged.

References

1. Kelkar, S. S.; Reineke, T. M., Theranostics: Combining imaging and therapy. *Bioconjug Chem* **2011**, 22 (10), 1879–903.
2. Duncan, R.; Gaspar, R., Nanomedicine(s) under the microscope. *Mol Pharm* **2011**, 8 (6), 2101–41.
3. Svenson, S., Theranostics: Are we there yet? *Mol Pharm* **2013**, 10 (3), 848–56.
4. Choi, K. Y.; Liu, G.; Lee, S.; Chen, X., Theranostic nanoplatforms for simultaneous cancer imaging and therapy: Current approaches and future perspectives. *Nanoscale* **2012**, 4 (2), 330–42.
5. Menon, J. U.; Jadeja, P.; Tambe, P.; Vu, K.; Yuan, B.; Nguyen, K. T., Nanomaterials for photo-based diagnostic and therapeutic applications. *Theranostics* **2013**, 3 (3), 152–66.
6. Shibu, E. S.; Hamada, M.; Murase, N.; Biju, V., Nanomaterials formulations for photothermal and photodynamic therapy of cancer. *J Photoch Photobio C* **2013**, 15, 53–72.
7. Ahmed, N.; Fessi, H.; Elaissari, A., Theranostic applications of nanoparticles in cancer. *Drug Discov Today* **2012**, 17 (17-18), 928–34.
8. Huang, H. C.; Barua, S.; Sharma, G.; Dey, S. K.; Rege, K., Inorganic nanoparticles for cancer imaging and therapy. *J Control Release* **2011**, 155 (3), 344–57.
9. Terrones, M.; Terrones, H., The carbon nanocosmos: Novel materials for the twenty-first century. *Philos Trans A Math Phys Eng Sci* **2003**, 361 (1813), 2789–806.
10. Liu, Z.; Liang, X. J., Nano-carbons as theranostics. *Theranostics* **2012**, 2 (3), 235–7.
11. Moradi, O.; Yari, M.; Zare, K.; Mirza, B.; Najafi, F., Carbon nanotubes: A review of chemistry principles and reactions. *Fuller Nanotub Car N* **2012**, 20 (2), 138–151.
12. Liu, Z.; Tabakman, S.; Welsher, K.; Dai, H. J., Carbon nanotubes in biology and medicine: In vitro and in vivo detection, imaging and drug delivery. *Nano Res* **2009**, 2 (2), 85–120.
13. Zhang, W. X.; Zhang, Z. Z.; Zhang, Y. G., The application of carbon nanotubes in target drug delivery systems for cancer therapies. *Nanoscale Res Lett* **2011**, 6.
14. Yang, W.; Ratinac, K. R.; Ringer, S. P.; Thordarson, P.; Gooding, J. J.; Braet, F., Carbon nanomaterials in biosensors: Should you use nanotubes or graphene? *Angew Chem Int Ed Engl* **2010**, 49 (12), 2114–38.
15. Bianco, A.; Kostarelos, K.; Prato, M., Making carbon nanotubes biocompatible and biodegradable. *Chem Commun (Camb)* **2011**, 47 (37), 10182–8.
16. Zhang, Y.; Bai, Y. H.; Yan, B., Functionalized carbon nanotubes for potential medicinal applications. *Drug Discov Today* **2010**, 15 (11-12), 428–435.
17. Lamanna, G.; Battigelli, A.; M é nard-Moyon, C.; Bianco, A., Multifunctionalized carbon nanotubes as advanced multimodal nanomaterials for biomedical applications. *Nanotechnol Rev* **2012**, 1, 17–29.
18. Boncel, S.; Muller, K. H.; Skepper, J. N.; Walczak, K. Z.; Koziol, K. K., Tunable

chemistry and morphology of multi-wall carbon nanotubes as a route to non-toxic, theranostic systems. *Biomaterials* **2011**, 32 (30), 7677–86.
19. Ji, S. R.; Liu, C.; Zhang, B.; Yang, F.; Xu, J.; Long, J. A.; Jin, C.; Fu, D. L.; Ni, Q. X.; Yu, X. J., Carbon nanotubes in cancer diagnosis and therapy. *Bba-Rev Cancer* **2010**, 1806 (1), 29–35.
20. Wang, X.; Wang, C.; Cheng, L.; Lee, S. T.; Liu, Z., Noble metal coated single-walled carbon nanotubes for applications in surface enhanced raman scattering imaging and photothermal therapy. *J Am Chem Soc* **2012**, 134 (17), 7414–22.
21. Chen, M. L.; He, Y. J.; Chen, X. W.; Wang, J. H., Quantum dots conjugated with fe3o4-filled carbon nanotubes for cancer-targeted imaging and magnetically guided drug delivery. *Langmuir* **2012**, 28 (47), 16469–76.
22. Heister, E.; Neves, V.; Tilmaciu, C.; Lipert, K.; Beltran, V. S.; Coley, H. M.; Silva, S. R. P.; McFadden, J., Triple functionalisation of single-walled carbon nanotubes with doxorubicin, a monoclonal antibody, and a fluorescent marker for targeted cancer therapy. *Carbon* **2009**, 47 (9), 2152–2160.
23. Das, M.; Datir, S. R.; Singh, R. P.; Jain, S., Augmented anticancer activity of a targeted, intracellularly activatable, theranostic nanomedicine based on fluorescent and radiolabeled, methotrexate-folic acid-multiwalled carbon nanotube conjugate. *Mol Pharm* **2013**, 10 (7), 2543–2557.
24. Kam, N. W. S.; O'Connell, M.; Wisdom, J. A.; Dai, H. J., Carbon nanotubes as multifunctional biological transporters and near-infrared agents for selective cancer cell destruction. *Proc Natl Acad Sci USA* **2005**, 102 (33), 11600–11605.
25. Robinson, J. T.; Welsher, K.; Tabakman, S. M.; Sherlock, S. P.; Wang, H.; Luong, R.; Dai, H., High performance in vivo near-ir (>1 mum) imaging and photothermal cancer therapy with carbon nanotubes. *Nano Res* **2010**, 3 (11), 779–793.
26. Mashal, A.; Sitharaman, B.; Li, X.; Avti, P. K.; Sahakian, A. V.; Booske, J. H.; Hagness, S. C., Toward carbon-nanotube-based theranostic agents for microwave detection and treatment of breast cancer: Enhanced dielectric and heating response of tissue-mimicking materials. *IEEE T Bio-Med Eng.* **2010**, 57 (8), 1831–1834.
27. Liu, Z.; Fan, A. C.; Rakhra, K.; Sherlock, S.; Goodwin, A.; Chen, X.; Yang, Q.; Felsher, D. W.; Dai, H., Supramolecular stacking of doxorubicin on carbon nanotubes for in vivo cancer therapy. *Angew Chem Int Ed Engl* **2009**, 48 (41), 7668–72.
28. Ali-Boucetta, H.; Al-Jamal, K. T.; McCarthy, D.; Prato, M.; Bianco, A.; Kostarelos, K., Multiwalled carbon nanotube-doxorubicin supramolecular complexes for cancer therapeutics. *Chem Commun (Camb)* **2008**, (4), 459–61.
29. Hadidi, N.; Kobarfard, F.; Nafissi-Varcheh, N.; Aboofazeli, R., Pegylated single-walled carbon nanotubes as nanocarriers for cyclosporin a delivery. *AAPS PharmSciTech* **2013**, 14 (2), 593–600.
30. Chen, C.; Xie, X. X.; Zhou, Q.; Zhang, F. Y.; Wang, Q. L.; Liu, Y. Q.; Zou, Y.; Tao, Q.; Ji, X. M.; Yu, S. Q., Egf-functionalized single-walled carbon nanotubes for targeting delivery of etoposide. *Nanotechnology* **2012**, 23 (4), 045104.
31. Yang, F.; Jin, C.; Yang, D.; Jiang, Y.; Li, J.; Di, Y.; Hu, J.; Wang, C.; Ni, Q.; Fu, D., Magnetic functionalised carbon nanotubes as drug vehicles for cancer lymph node metastasis treatment. *Eur J Cancer* **2011**, 47 (12), 1873–82.
32. Singh, R.; Pantarotto, D.; McCarthy, D.; Chaloin, O.; Hoebeke, J.; Partidos, C. D.; Briand, J.-P.; Prato, M.; Bianco, A.; Kostarelos, K., Binding and condensation of plasmid DNA onto functionalized carbon nanotubes:? Toward the construction of nanotube-based gene delivery vectors. *J Am Chem Soc* **2005**, 127 (12), 4388–4396.
33. Liu, Y.; Wu, D. C.; Zhang, W. D.; Jiang, X.; He, C. B.; Chung, T. S.; Goh, S. H.; Leong, K. W., Polyethylenimine-grafted multiwalled carbon nanotubes for secure

noncovalent immobilization and efficient delivery of DNA. *Angew Chem Int Ed Engl* **2005**, 44 (30), 4782–5.
34. Bartholomeusz, G.; Cherukuri, P.; Kingston, J.; Cognet, L.; Lemos, R., Jr.; Leeuw, T.; Gumbiner-Russo, L.; Weisman, R. B.; Powis, G., In vivo therapeutic silencing of hypoxia-inducible factor 1 alpha (hif-1α) using single-walled carbon nanotubes noncovalently coated with sirna. *Nano Res* **2009**, 2 (4), 279–291.
35. Podesta, J. E.; Al-Jamal, K. T.; Herrero, M. A.; Tian, B.; Ali-Boucetta, H.; Hegde, V.; Bianco, A.; Prato, M.; Kostarelos, K., Antitumor activity and prolonged survival by carbon-nanotube-mediated therapeutic sirna silencing in a human lung xenograft model. *Small* **2009**, 5 (10), 1176–85.
36. Liu, Z.; Cai, W.; He, L.; Nakayama, N.; Chen, K.; Sun, X.; Chen, X.; Dai, H., In vivo biodistribution and highly efficient tumour targeting of carbon nanotubes in mice. *Nat Nanotechnol* **2007**, 2 (1), 47–52.
37. Zhang, M.; Murakami, T.; Ajima, K.; Tsuchida, K.; Sandanayaka, A. S.; Ito, O.; Iijima, S.; Yudasaka, M., Fabrication of znpc/protein nanohorns for double photodynamic and hyperthermic cancer phototherapy. *Proc Natl Acad Sci USA* **2008**, 105 (39), 14773–8.
38. Bussy, C.; Ali-Boucetta, H.; Kostarelos, K., Safety considerations for graphene: Lessons learnt from carbon nanotubes. *Accounts Chem Res* **2012**, 46 (3), 692–701.
39. Chen, D.; Feng, H.; Li, J., Graphene oxide: Preparation, functionalization, and electrochemical applications. *Chem Rev* **2012**, 112 (11), 6027–53.
40. Bao, H.; Pan, Y.; Li, L., Recent advances in graphene-based nanomaterials for biomedical applications. *Nano Life* **2012**, 02 (01), 1230001–15.
41. Shen, H.; Zhang, L. M.; Liu, M.; Zhang, Z. J., Biomedical applications of graphene. *Theranostics* **2012**, 2 (3), 283–294.
42. Mao, H. Y.; Laurent, S.; Chen, W.; Akhavan, O.; Imani, M.; Ashkarran, A. A.; Mahmoudi, M., Graphene: Promises, facts, opportunities, and challenges in nanomedicine. *Chem Rev* **2013**, 113 (5), 3407–24.
43. Yang, K.; Feng, L. Z.; Shi, X. Z.; Liu, Z., Nano-graphene in biomedicine: Theranostic applications. *Chem Soc Rev* **2013**, 42 (2), 530–547.
44. Feng, L.; Wu, L.; Qu, X., New horizons for diagnostics and therapeutic applications of graphene and graphene oxide. *Adv Mater* **2013**, 25 (2), 168–86.
45. Zhang, Y.; Nayak, T. R.; Hong, H.; Cai, W. B., Graphene: A versatile nanoplatform for biomedical applications. *Nanoscale* **2012**, 4 (13), 3833–3842.
46. Cho, Y.; Kim, H.; Choi, Y., A graphene oxide-photosensitizer complex as an enzyme-activatable theranostic agent. *Chem Commun (Camb)* **2013**, 49 (12), 1202–4.
47. Shen, A. J.; Li, D. L.; Cai, X. J.; Dong, C. Y.; Dong, H. Q.; Wen, H. Y.; Dai, G. H.; Wang, P. J.; Li, Y. Y., Multifunctional nanocomposite based on graphene oxide for in vitro hepatocarcinoma diagnosis and treatment. *J Biomed Mater Res A* **2012**, 100 (9), 2499–506.
48. Sun, X. M.; Liu, Z.; Welsher, K.; Robinson, J. T.; Goodwin, A.; Zaric, S.; Dai, H. J., Nano-graphene oxide for cellular imaging and drug delivery. *Nano Res* **2008**, 1 (3), 203–212.
49. Ma, X. X.; Tao, H. Q.; Yang, K.; Feng, L. Z.; Cheng, L.; Shi, X. Z.; Li, Y. G.; Guo, L.; Liu, Z., A functionalized graphene oxide-iron oxide nanocomposite for magnetically targeted drug delivery, photothermal therapy, and magnetic resonance imaging. *Nano Res* **2012**, 5 (3), 199–212.
50. Yang, K.; Hu, L.; Ma, X.; Ye, S.; Cheng, L.; Shi, X.; Li, C.; Li, Y.; Liu, Z., Multimodal imaging guided photothermal therapy using functionalized graphene nanosheets anchored with magnetic nanoparticles. *Adv Mater* **2012**, 24 (14), 1868–

72.
51. Jin, Y.; Wang, J.; Ke, H.; Wang, S.; Dai, Z., Graphene oxide modified pla microcapsules containing gold nanoparticles for ultrasonic/ct bimodal imaging guided photothermal tumor therapy. *Biomaterials* **2013**, 34 (20), 4794–802.
52. Sheng, Z.; Song, L.; Zheng, J.; Hu, D.; He, M.; Zheng, M.; Gao, G.; Gong, P.; Zhang, P.; Ma, Y.; Cai, L., Protein-assisted fabrication of nano-reduced graphene oxide for combined in vivo photoacoustic imaging and photothermal therapy. *Biomaterials* **2013**, 34 (21), 5236–43.
53. Hu, S. H.; Chen, Y. W.; Hung, W. T.; Chen, I. W.; Chen, S. Y., Quantum-dot-tagged reduced graphene oxide nanocomposites for bright fluorescence bioimaging and photothermal therapy monitored in situ. *Adv Mater* **2012**, 24 (13), 1748–54.
54. Qin, X. C.; Guo, Z. Y.; Liu, Z. M.; Zhang, W.; Wan, M. M.; Yang, B. W., Folic acid-conjugated graphene oxide for cancer targeted chemo-photothermal therapy. *J Photoch Photobio B* **2013**, 120, 156–162.
55. Kurapati, R.; Raichur, A. M., Graphene oxide based multilayer capsules with unique permeability properties: Facile encapsulation of multiple drugs. *Chem Commun (Camb)* **2012**.
56. Wu, J.; Wang, Y. S.; Yang, X. Y.; Liu, Y. Y.; Yang, J. R.; Yang, R.; Zhang, N., Graphene oxide used as a carrier for adriamycin can reverse drug resistance in breast cancer cells. *Nanotechnology* **2012**, 23 (35), 355101.
57. Liu, Z.; Robinson, J. T.; Sun, X. M.; Dai, H. J., Pegylated nanographene oxide for delivery of water-insoluble cancer drugs. *J Am Chem Soc* **2008**, 130 (33), 10876–10877.
58. Feng, L.; Yang, X.; Shi, X.; Tan, X.; Peng, R.; Wang, J.; Liu, Z., Polyethylene glycol and polyethylenimine dual-functionalized nano-graphene oxide for photothermally enhanced gene delivery. *Small* **2013**, 9 (11), 1989–97.
59. Yang, X. Y.; Niu, G. L.; Cao, X. F.; Wen, Y. K.; Xiang, R.; Duan, H. Q.; Chen, Y. S., The preparation of functionalized graphene oxide for targeted intracellular delivery of sirna. *J Mater Chem* **2012**, 22 (14), 6649–6654.
60. Zhang, L. M.; Wang, Z. L.; Lu, Z. X.; Shen, H.; Huang, J.; Zhao, Q. H.; Liu, M.; He, N. Y.; Zhang, Z. J., Pegylated reduced graphene oxide as a superior ssrna delivery system. *J Mater Chem B* **2013**, 1 (6), 749–755.
61. Qian, J.; Wang, D.; Cai, F. H.; Xi, W.; Peng, L.; Zhu, Z. F.; He, H.; Hu, M. L.; He, S., Observation of multiphoton-induced fluorescence from graphene oxide nanoparticles and applications in in vivo functional bioimaging. *Angew Chem Int Ed Engl* **2012**, 51 (42), 10570–5.
62. Yue, Z.; Lv, P.; Yue, H.; Gao, Y.; Ma, D.; Wei, W.; Ma, G., Inducible graphene oxide probe for high-specific tumor diagnosis. *Chem Commun (Camb)* **2013**, 49 (37), 3902–4.
63. Hong, H.; Zhang, Y.; Engle, J. W.; Nayak, T. R.; Theuer, C. P.; Nickles, R. J.; Barnhart, T. E.; Cai, W., In vivo targeting and positron emission tomography imaging of tumor vasculature with (66)ga-labeled nano-graphene. *Biomaterials* **2012**, 33 (16), 4147–56.
64. Yang, K.; Wan, J.; Zhang, S.; Tian, B.; Zhang, Y.; Liu, Z., The influence of surface chemistry and size of nanoscale graphene oxide on photothermal therapy of cancer using ultra-low laser power. *Biomaterials* **2012**, 33 (7), 2206–14.
65. Li, F.; Park, S.; Ling, D.; Park, W.; Han, J. Y.; Na, K.; Char, K., Hyaluronic acid-conjugated graphene oxide/photosensitizer nanohybrids for cancer targeted photodynamic therapy. *J Mater Chem B* **2013**, 1 (12), 1678–1686.
66. Cho, Y.; Choi, Y., Graphene oxide-photosensitizer conjugate as a redox-responsive

theranostic agent. *Chem Commun (Camb)* **2012**, 48 (79), 9912–4.
67. Robinson, J. T.; Tabakman, S. M.; Liang, Y.; Wang, H.; Casalongue, H. S.; Vinh, D.; Dai, H., Ultrasmall reduced graphene oxide with high near-infrared absorbance for photothermal therapy. *J Am Chem Soc* **2011**, 133 (17), 6825–31.
68. Shi, S.; Yang, K.; Hong, H.; Valdovinos, H. F.; Nayak, T. R.; Zhang, Y.; Theuer, C. P.; Barnhart, T. E.; Liu, Z.; Cai, W., Tumor vasculature targeting and imaging in living mice with reduced graphene oxide. *Biomaterials* **2013**, 34 (12), 3002–9.
69. Huang, P.; Lin, J.; Wang, X.; Wang, Z.; Zhang, C.; He, M.; Wang, K.; Chen, F.; Li, Z.; Shen, G.; Cui, D.; Chen, X., Light-triggered theranostics based on photosensitizer-conjugated carbon dots for simultaneous enhanced-fluorescence imaging and photodynamic therapy. *Adv Mater* **2012**, 24 (37), 5104–10.
70. Lai, C. W.; Hsiao, Y. H.; Peng, Y. K.; Chou, P. T., Facile synthesis of highly emissive carbon dots from pyrolysis of glycerol; gram scale production of carbon dots/msio(2) for cell imaging and drug release. *J Mater Chem* **2012**, 22 (29), 14403–14409.
71. Liu, C.; Zhang, P.; Zhai, X.; Tian, F.; Li, W.; Yang, J.; Liu, Y.; Wang, H.; Wang, W.; Liu, W., Nano-carrier for gene delivery and bioimaging based on carbon dots with pei-passivation enhanced fluorescence. *Biomaterials* **2012**, 33 (13), 3604–13.
72. Gu, J.; Su, S.; Li, Y.; He, Q.; Shi, J., Hydrophilic mesoporous carbon nanoparticles as carriers for sustained release of hydrophobic anti-cancer drugs. *Chem Commun (Camb)* **2011**, 47 (7), 2101–3.
73. Ma, Y. H.; Manolache, S.; Denes, F. S.; Thamm, D. H.; Kurzman, I. D.; Vail, D. M., Plasma synthesis of carbon magnetic nanoparticles and immobilization of doxorubicin for targeted drug delivery. *J Biomat Sci-Polym E* **2004**, 15 (8), 1033–1049.
74. Kroto, H. W.; Heath, J. R.; Obrien, S. C.; Curl, R. F.; Smalley, R. E., C-60-buckminsterfullerene. *Nature* **1985**, 318 (6042), 162–163.
75. Nakamura, E.; Isobe, H., Functionalized fullerenes in water. The first 10 years of their chemistry, biology, and nanoscience. *Accounts Chem Res* **2003**, 36 (11), 807–815.
76. Partha, R.; Conyers, J. L., Biomedical applications of functionalized fullerene-based nanomaterials. *Int J Nanomed* **2009**, 4, 261–275.
77. Chen, Z.; Ma, L.; Liu, Y.; Chen, C., Applications of functionalized fullerenes in tumor theranostics. *Theranostics* **2012**, 2 (3), 238–50.
78. Grobmyer, S. R.; Krishna, V., Minimally invasive cancer therapy using polyhydroxy fullerenes. *Eur J Radiol* **2012**, 81 (S1), S51–S53.
79. Lu, X.; Feng, L.; Akasaka, T.; Nagase, S., Current status and future developments of endohedral metallofullerenes. *Chem Soc Rev* **2012**, 41 (23), 7723–7760.
80. Krishna, V.; Singh, A.; Sharma, P.; Iwakuma, N.; Wang, Q.; Zhang, Q.; Knapik, J.; Jiang, H.; Grobmyer, S. R.; Koopman, B.; Moudgil, B., Polyhydroxy fullerenes for non-invasive cancer imaging and therapy. *Small* **2010**, 6 (20), 2236–41.
81. Kwag, D. S.; Park, K.; Oh, K. T.; Lee, E. S., Hyaluronated fullerenes with photoluminescent and antitumoral activity. *Chem Commun (Camb)* **2013**, 49 (3), 282–4.
82. Wilson, J. D.; Broaddus, W. C.; Dorn, H. C.; Fatouros, P. P.; Chalfant, C. E.; Shultz, M. D., Metallofullerene-nanoplatform-delivered interstitial brachytherapy improved survival in a murine model of glioblastoma multiforme. *Bioconjug Chem* **2012**, 23 (9), 1873–1880.
83. Fan, J.; Fang, G.; Zeng, F.; Wang, X.; Wu, S., Water-dispersible fullerene aggregates as a targeted anticancer prodrug with both chemo- and photodynamic therapeutic actions. *Small* **2013**, 9 (4), 613–21.
84. Kotelnikov, A. I.; Rybkin, A. Y.; Khakina, E. A.; Kornev, A. B.; Barinov, A. V.; Goryachev, N. S.; Ivanchikhina, A. V.; Peregudov, A. S.; Martynenko, V. M.; Troshin, P. A., Hybrid photoactive fullerene derivative-ruboxyl nanostructures for

photodynamic therapy. *Org Biomol Chem* **2013**, 11 (26), 4397–404.
85. Lucafo, M.; Pacor, S.; Fabbro, C.; Da Ros, T.; Zorzet, S.; Prato, M.; Sava, G., Study of a potential drug delivery system based on carbon nanoparticles: Effects of fullerene derivatives in mcf7 mammary carcinoma cells. *J Nanopart Res* **2012**, 14 (4).
86. Kwag, D. S.; Oh, N. M.; Oh, Y. T.; Oh, K. T.; Youn, Y. S.; Lee, E. S., Photodynamic therapy using glycol chitosan grafted fullerenes. *Int J Pharm* **2012**, 431 (1-2), 204–9.
87. Zakharian, T. Y.; Seryshev, A.; Sitharaman, B.; Gilbert, B. E.; Knight, V.; Wilson, L. J., A fullerene-paclitaxel chemotherapeutic: Synthesis, characterization, and study of biological activity in tissue culture. *J Am Chem Soc* **2005**, 127 (36), 12508–12509.
88. Didenko, G.; Prylutska, S.; Kichmarenko, Y.; Potebnya, G.; Prylutskyy, Y.; Slobodyanik, N.; Ritter, U.; Scharff, P., Evaluation of the antitumor immune response to c-60 fullerene. *Materialwiss Werkst* **2013**, 44 (2-3), 124–128.
89. Meng, H.; Xing, G.; Blanco, E.; Song, Y.; Zhao, L.; Sun, B.; Li, X.; Wang, P. C.; Korotcov, A.; Li, W.; Liang, X. J.; Chen, C.; Yuan, H.; Zhao, F.; Chen, Z.; Sun, T.; Chai, Z.; Ferrari, M.; Zhao, Y., Gadolinium metallofullerenol nanoparticles inhibit cancer metastasis through matrix metalloproteinase inhibition: Imprisoning instead of poisoning cancer cells. *Nanomedicine* **2012**, 8 (2), 136–46.
90. Chen, C. Y.; Xing, G. M.; Wang, J. X.; Zhao, Y. L.; Li, B.; Tang, J.; Jia, G.; Wang, T. C.; Sun, J.; Xing, L.; Yuan, H.; Gao, Y. X.; Meng, H.; Chen, Z.; Zhao, F.; Chai, Z. F.; Fang, X. H., Multi hydroxylated [gd@c-82(oh)(22)](n) nanoparticles: Antineoplastic activity of high efficiency and low toxicity. *Nano Lett* **2005**, 5 (10), 2050–2057.
91. Meng, H.; Xing, G.; Sun, B.; Zhao, F.; Lei, H.; Li, W.; Song, Y.; Chen, Z.; Yuan, H.; Wang, X.; Long, J.; Chen, C.; Liang, X.; Zhang, N.; Chai, Z.; Zhao, Y., Potent angiogenesis inhibition by the particulate form of fullerene derivatives. *ACS Nano* **2010**, 4 (5), 2773–2783.
92. Xing-Jie Lianga, H. M., Yingze Wanga, Haiyong Hea, Jie Menga, Juan Lua, Paul C. Wangc, Yuliang Zhao, Xueyun Gaob, Baoyun Sunb, Chunying Chena, Genmei Xingb, Dingwu Shend, Michael M. Gottesmand, Yan Wua, Jun-jie Yine, and Lee Jia, Metallofullerene nanoparticles circumvent tumor resistance to cisplatin by reactivating endocytosis. *Proc Natl Acad Sci USA* **2010**, 107, 7449–7454.
93. Schrand, A. M.; Hens, S. A. C.; Shenderova, O. A., Nanodiamond particles: Properties and perspectives for bioapplications. *Crit Rev Solid State* **2009**, 34 (1-2), 18–74.
94. Mochalin, V. N.; Shenderova, O.; Ho, D.; Gogotsi, Y., The properties and applications of nanodiamonds. *Nat Nanotechnol* **2012**, 7 (1), 11–23.
95. Man, H. B.; Ho, D., Diamond as a nanomedical agent for versatile applications in drug delivery, imaging, and sensing. *Phys Status Solidi A* **2012**, 209 (9), 1609–1618.
96. Kaur, R.; Badea, I., Nanodiamonds as novel nanomaterials for biomedical applications: Drug delivery and imaging systems. *Int J Nanomedicine* **2013**, 8, 203–20.
97. Say, J. M.; van Vreden, C.; Reilly, D. J.; Brown, L. J.; Rabeau, J. R.; King, N. J. C., Luminescent nanodiamonds for biomedical applications. *Biophys Rev* **2011**, 3 (4), 171–184.
98. Hui, Y. Y.; Cheng, C. L.; Chang, H. C., Nanodiamonds for optical bioimaging. *J Phys D Appl Phys* **2010**, 43 (37).
99. Zhu, Y.; Li, J.; Li, W.; Zhang, Y.; Yang, X.; Chen, N.; Sun, Y.; Zhao, Y.; Fan, C.; Huang, Q., The biocompatibility of nanodiamonds and their application in drug delivery systems. *Theranostics* **2012**, 2 (3), 302–12.
100. Bajaj, P.; Akin, D.; Gupta, A.; Sherman, D.; Shi, B.; Auciello, O.; Bashir, R., Ultrananocrystalline diamond film as an optimal cell interface for biomedical applications.

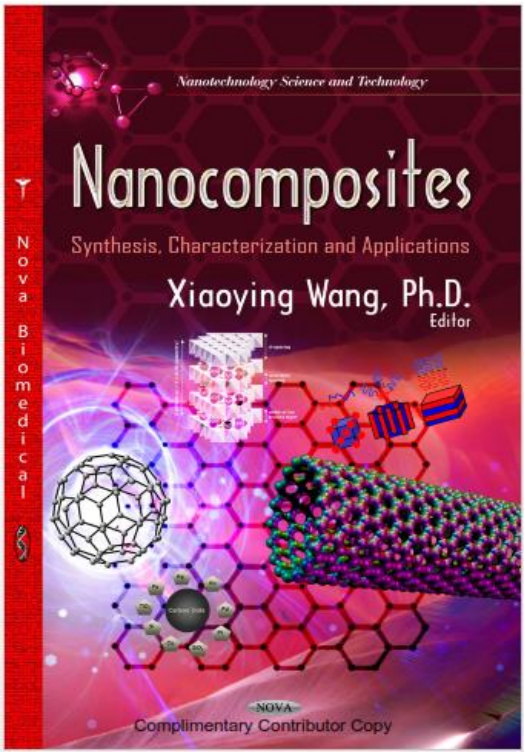
Biomed Microdevices **2007**, 9 (6), 787–94.
101. Fu, Y. J.; An, N.; Zheng, S. H.; Liang, A. H.; Li, Y. Q., Bmk ct-conjugated fluorescence nanodiamond as potential glioma-targeted imaging and drug. *Diam Relat Mater* **2012**, 21, 73–76.
102. Zhang, X. Q.; Lam, R.; Xu, X. Y.; Chow, E. K.; Kim, H. J.; Ho, D., Multimodal nanodiamond drug delivery carriers for selective targeting, imaging, and enhanced chemotherapeutic efficacy. *Adv Mater* **2011**, 23 (41), 4770–+.
103. Yan, J. J.; Guo, Y.; Altawashi, A.; Moosa, B.; Lecommandoux, S.; Khashab, N. M., Experimental and theoretical evaluation of nanodiamonds as ph triggered drug carriers. *New J Chem* **2012**, 36 (7), 1479–1484.
104. von Haartman, E.; Jiang, H.; Khomich, A. A.; Zhang, J. X.; Burikov, S. A.; Dolenko, T. A.; Ruokolainen, J.; Gu, H. C.; Shenderova, O. A.; Vlasov, I. I.; Rosenholm, J. M., Core-shell designs of photoluminescent nanodiamonds with porous silica coatings for bioimaging and drug delivery i: Fabrication. *J Mater Chem B* **2013**, 1 (18), 2358–2366.
105. Prabhakar, N.; Nareoja, T.; von Haartman, E.; Karaman, D. S.; Jiang, H.; Koho, S.; Dolenko, T. A.; Hanninen, P. E.; Vlasov, D. I.; Ralchenko, V. G.; Hosomi, S.; Vlasov, II; Sahlgren, C.; Rosenholm, J. M., Core-shell designs of photoluminescent nanodiamonds with porous silica coatings for bioimaging and drug delivery ii: Application. *Nanoscale* **2013**, 5 (9), 3713–22.
106. Wang, D. X.; Tong, Y. L.; Li, Y. Q.; Tian, Z. M.; Cao, R. X.; Yang, B. S., Pegylated nanodiamond for chemotherapeutic drug delivery. *Diam Relat Mater* **2013**, 36, 26–34.
107. Orel, V. E.; Shevchenko, A. D.; Bogatyreva, G. P.; Leshchenko, O. V.; Romanov, A. V.; Rykhal's'kii, O. Y.; Dzyatkovskaya, I. I.; Nikolov, N. A.; Dzyatkovskaya, N. N.; Shchepotin, I. B., Magnetic characteristics and anticancer activity of a nanocomplex consisting of detonation nanodiamond and doxorubicin. *J Superhard Mater* **2012**, 34 (3), 179–185.
108. Vaijayanthimala, V.; Cheng, P. Y.; Yeh, S. H.; Liu, K. K.; Hsiao, C. H.; Chao, J. I.; Chang, H. C., The long-term stability and biocompatibility of fluorescent nanodiamond as an in vivo contrast agent. *Biomaterials* **2012**, 33 (31), 7794–802.
109. Huang, S. S.; Shao, J. Q.; Gao, L. F.; Qi, Y. Z.; Ye, L., Adsorption of cathepsin b-sensitive peptide conjugated dox on nanodiamonds. *Appl Surf Sci* **2011**, 257 (20), 8617–8622.
110. Liu, K. K.; Zheng, W. W.; Wang, C. C.; Chiu, Y. C.; Cheng, C. L.; Lo, Y. S.; Chen, C.; Chao, J. I., Covalent linkage of nanodiamond-paclitaxel for drug delivery and cancer therapy. *Nanotechnology* **2010**, 21 (31), 315106.
111. Li, J.; Zhu, Y.; Li, W. X.; Zhang, X. Y.; Peng, Y.; Huang, Q., Nanodiamonds as intracellular transporters of chemotherapeutic drug. *Biomaterials* **2010**, 31 (32), 8410–8418.
112. Chang, I. P.; Hwang, K. C.; Chiang, C. S., Preparation of fluorescent magnetic nanodiamonds and cellular imaging. *J Am Chem Soc* **2008**, 130 (46), 15476–15481.

Chapter 2

Synthesis and applications of carbon dots nanocomposites

João M. M. Leitão, Eliana F. C. Simões, Joaquim C. G. Esteves da Silva

Book: Nanocomposites: Synthesis, Characterization and Applications" chapter 6, pp.121-138, Xiaoying Wang Ed., Nova Science Publishers, Inc New York, United States of America (2013) Print ISBN-10: 1629482269, Print ISBN-13:978-1629482262, eBook ISBN: 978-1-62948-227-9



In this work the bibliographic research of the different methods of synthesis of CDs nanocomposites and their main applications was made. The writing of the book chapter and the design of the figures was made together with Professor João M.M. Leitão under the supervision of Professor Joaquim C. G. Esteves da Silva.

Chapter

Synthesis and applications of carbon dots nanocomposites

João M. M. Leitão[1], Eliana F.C. Simões[2], Joaquim C.G. Esteves da Silva[2*]
[1]Centro de Investigação em Química (CIQ), Faculty of Pharmacy, University of Coimbra, Polo das Ciências da Saúde, Coimbra 3000-548, Portugal
[2]Centro de Investigação em Química (CIQ), Department of Chemistry and Biochemistry, Faculty of Sciences, University of Porto, Rua do Campo Alegre 687, Porto 4169-007, Portugal

ABSTRACT

Carbon dots (CD) are a new class of fluorescent carbon nanomaterials with no toxic and biocompatible properties. Because the fluorescence properties of CD can be tuned in the visible wavelength range, they are being design as substitutes of the well known, but potentially toxic, quantum dots for the *in vivo* applications development. Nanocomposites of CD are being developed in order to improve the fluorescence quantum yield, to shift the absorption and emission wavelengths into the red, to acquire a specific reactivity and to make them selective towards a specific target. Nanocomposites of CD result from their coupling with polymers, simple organic substances, biomolecules, inorganic substances, semiconductor quantum dots and organosilanes. This chapter will describe the synthesis of CD nanocomposites and their analytical and bioanalytical chemistry, bioimaging and drug delivery applications.

Keywords: Carbon dots; Nanocomposites; Polymers; Organic substances; Inorganic substances; Quantum dots; Synthesis; Photoluminescence; Bioimaging; Sensing.

INTRODUCTION

Carbon is an element that exist in abundance in the nature. Several forms of carbon that differ in its size and shape are known. Beside the bulk allotropic forms of carbon as the diamante, graphite and amorphous carbon, also different forms in a nano range scale (nanoallotropes) are

* Corresponding Author address: Department of Chemistry and Biochemistry, Faculty of Sciences, University of Porto, Rua do Campo Alegre 687, Porto 4169-007, Portugal
Email:jcsilva@fc.up.pt

being discovered, as the fullerene forms (buckyballs, carbon nanotubes, graphene) nano diamonds, nano fibers and carbon dots (CD). Each of these different forms of carbon have different properties and are now fundamental in different fields of application.

Beside carbon nanotubes and graphene sheets, with several analytical and bioanalytical applications[1, 2], also the recently discovered CD [3-5] are now being extensively used. In these applications the different forms of carbon can be used alone or they are conjugated with other substances resulting in the formation of new composite structures. These new nanocomposites can have the characteristics of their components or can have new characteristics due to the cooperative effects of the different constituents. The possibility of formation of composites structures, and particularly nanocomposites structures, could enlarge the field and improved the quality of the applications of each of these different forms of nanocarbon. The utilization of these nanocomposites structures depends on the possibility of their synthesis and of their surface modification.

CD are small photoluminescent carbon nanoparticles usually with dimensions less than 10 nm suspending in water or in other solvents. Their properties are similar to the classical nanocrystaline semiconductors quantum dots (QD) but the CD had been developed as a biocompatibly and non toxic alternative. A great number of methods for the synthesis of CD have been proposed. They are classified as ''bottow-up'' and ''top-down'' methodologies of synthesis. The main ''bottow-up'' methods are thermal decomposition, microwave or autoclave and acid dehydratation. The main ''top-down'' methods of synthesis are the laser ablation and electrochemical techniques. In the synthesis of the CD nanocomposites, after the synthesis of raw CD, they are coupled to a selected substance or the CD nanocomposites can be obtained in one step synthesis.

In this chapter a revision of the synthesised CD nanocomposites will be done. Also, their methods of synthesis, the substances used and their main applications, with focus on the analytical and bioanalytical, will be described. This chapter is structured taking into consideration the type of substance linked to the CD nanocomposites.

CARBON DOTS/POLYMERS NANOCOMPOSITES

Several CD nanocomposites are composed by attaching polymers to passivate the synthesized raw CD. Fig. 1 presents the principal polymers used for CD passivation. One of the most used polymer for CD passivation is polyethilenoglicol (PEG) [6-41], namely PEG200 [7, 8, 11-16, 20, 31-33] and PEG1500 [6, 10, 17-19, 21-23, 25-27, 29, 30, 34-36, 40]. Several of these nanocomposites are synthesized using amine or diamine PEG200 or PEG1500. Using these polymers an amidation reaction occurs that allows to obtained free amino groups on the CD surface. Synthesized no native fluorescent CD, obtained by laser ablation [6, 11-19, 25-29, 31, 35], or native fluorescent CD, obtained by microwave [20, 24, 32], carbonization of carbon precursors [8-10, 21-23, 30, 33, 34, 40, 41], and ultrasonic [7] methodologies, were passivated with PEG. The passivation by PEG was done in order to obtain photoluminescent CDs [6, 11-16, 24-29, 31, 35] or to obtain an enhancement of their native fluorescence [10, 20, 24, 41]. Beside the effect on the quantum yield, PEG passivation generally improves the stability of CD and increases their bio-compatibility.

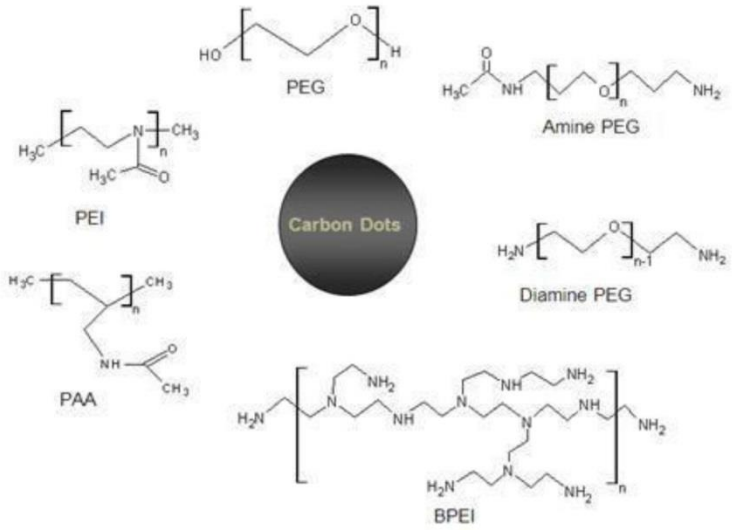


Fig. 1 Polymers used for CDs passivation.

PEG200 passivation of CD obtained by laser ablation synthesis was done in one step [28], or by reflux with PEG200 [11-16], after activation by reflux in nitric acid. Hu *et al* synthesize passivated CD with different precursors, solvents and different molecular weights of PEG [28]. It was observed that the precursor do not affect the photoluminescent characteristics of the CD nanocomposites, the solvent and the molecular weight of PEG affects the maxima of excitation and emissions wavelengths, with a shift of these wavelengths to higher wavelengths with the PEG molecular weight. To the passivated CD-PEG200, obtained by refluxing the synthesized raw CD with PEG200, Esteves da Silva group linked N-acetyl-L-cysteine (NAC) [11-15] or mercaptosuccinic acid (MSA) [16], also by reflux through the reaction of the CD-PEG200 amine groups with the thiol group of these two compounds. The synthesized CD-PEG200-NAC and CD-PEG200-MSA were tested in the sensing of several metallic ions. Good results were found with CD-PEG200-NAC by quenching of the fluorescence with Hg(II) and Cu(II) and with CD-PEG200-MSA by quenching of the fluorescence with iodide. With both nanocomposites a good sensitivity to the pH was also observed [15, 16]. Also an optical fibre sensor for Hg(II) was successfully obtained by immobilization the CD-PEG200-NAC in a sol gel matrix and, in order to increase the sensitivity of Hg(II) quantification, immobilization the CD-PEG200-NAC with a new approach based in a layer by layer deposition method with polyethylenimine (PEI) [11, 14]. The fluorescence excitation-emission matrices of the CD-PEG200-NAC, collected varying the Hg(II) [12, 13] and the pH [13], were analyzed by three-way decompositions methodologies in order to know its inner structure and their performance was assessed in order to their potential use in real samples. The enhancement of the intensities and improved photostabilities of CD-PEG200 in plasmon supporting materials was also observed [31].

When the CD were synthesized by microwave, the PEG200 passivation was done in one step by mixing the glucose, precursor of CD, and PEG200 [20, 24, 32]. With a similar CD-PEG200 microwave synthesizes procedure, Zhu *et al* demonstrate the electroluminescence properties of the synthesized CD-PEG200 [20] and Liu *et al* linked to the CD-PEG200 nanocomposites bovine serum albumin (BSA) through the cross-linking chemistry of 1-ethyl-3-[3-

dimethylaminopropyl]carbodiimide hydrochloride (EDC). The CD-PEG200-BSA was then applied to the Cu(II) quantification by the quenching of fluorescence of CD-PEG200-BSA after lysine fluorescence enhancement[24]. Also the CD-PEG200 synthesis was done by refluxing [8], sonicating [7] PEG200 or heating different carbohydrates as carbon precursors in different solvents [33]. These CD-PEG200 were used for the Hg(II) detection [8] and for bioimaging [7, 33]. In one of this bioimaging applications the synthesized CD-PEG200 were functionalized with folic acid and TAT peptide.[33]

The PEG1500 passivation of CD obtained by laser ablation synthesis [6, 17-19, 25-27, 29, 35] and some obtained by carbonization of carbon precursors [21, 23, 30, 40] was done by heating the nanomaterial with PEG1500, after activation by refluxing in nitric acid. In some of this CD-PEG1500 synthesis a previous thyonyl chloride treatment was done before the PEG1500 passivation in order to subsequent amidation by PEG1500 [6, 18, 26]. Also PEG1500 passivation was done without previous refluxing with nitric acid, for CD synthesized by carbonization of a carbon precursor [10], or heating in a microwave oven [36] simultaneously with PEG1500 in one step synthesis. Also, a similar procedure was used for CD obtained by heating citric acid [34] or refluxing lampblack, for posterior heating of the synthesized CD with PEG1500 [22]. Sun group studied the photoluminescent properties of laser ablation synthesized CD passivated with PEG1500 [17, 27]. They were classified as an electron donor or acceptor [18] and their photoluminescent properties were compared with the photoluminescent properties of CD passivated with polypropionylethyleneimine-*co*-ethyleneimine (PPEI-EI) [17, 25], polyallylamine (PAA) [25] and PEG1500 passivated ZnS doped CD (CD-ZnS-PEG1500) [19]. The CD-PEG1500 were tested in bioimaging [19, 25, 29] with a great focus in the evaluation of toxicity of these CD-PEG1500 nanocomposites [25, 29]. Platinum (Pt) and gold (Au) coated CD-PEG1500 were also used as photocatalysts for the reduction of CO_2 [26] and their quenching of the fluorescence effect was shown [35]. Beside this study, the synthesized CD-PEG1500 were cross-linked with dimethylpimelimidate (DMP) to stabilize the CD and to obtain ultra-bright multi CD fluorescent probes [6]. For the CD-PEG1500 obtained by microwave synthesis their chemiluminescence properties were demonstrated [36].

Several authors synthesized CD-PEG1500 nanocomposites by carbonization of carbon precursors using different substances [21-23, 30, 40], and evaluated them comparatively[21-23, 30, 40] using different solvents[10], different polymers[30] or organic molecules[23] for surface passivation. Different CD-PEG1500 strategies were used in some synthesis. Yang *et al*, previous to the carbonization step of 1,3,5-trimethylbenzene (TMB), diaminebenzene (DAB), pyrene (PY) and phenanthroline (PHA), used the copolymer Pluronic P123 as a soft template and mesoporous silica (OMS) SBA-15 as a hard template to obtain CD by chemically etching of the initially CD-OMS nanocomposites [40]. Li *et al* used resols as carbon precursors and silica colloid spheres functionalized with amphiphilic triblock polymer copolymer as carriers for the CD synthesis [21]. The synthesized CD by these two strategies were acid activated and passivated with PEG1500. Li *et al* also used PEG1500, triblock copolymer (PEI-PEG-PEI) and 4-armed PEG for CD passivation. The synthesized CD-PEG1500, CD-PEI-PEG-PEI and CD-4-armed PEG nanocomposites were then used for target cancer cells *in vitro* [21, 30]. In order to increase the cell recognition, the amine groups of CD were conjugated with transferrin by the cross-linking 1-(3-dimethylaminopropyl)-3-ethylcarbodiimide hydrochloride (EDC) chemistry [30].

Other types of CD-PEG nanocomposites as the CD-PEG600 [39], CD-PEG900 [41] and CD-PEG2000 [9, 37, 38] were also synthesized. The PEG600 graphitized CD were synthesized by hydrothermal carbonization of cetyltrimethylammonium bromide (CTAB). The as obtained CD were then oxidized with nitric acid before the synthesis of CD-PEG600 [39]. CD-PEG900 was obtained from glycerol, as carbon precursor, and it was simultaneous heated with amino PEG900

[41]. The photoluminescence characteristics of the CD-PEG600 and CD-PEG900 were evaluated. With the CD-PEG900 nanocomposite their photoluminescence characteristics were evaluated comparatively with CD silica (SiO_2) and CD-SiO_2-PEG900 nanocomposites synthesized in a similar way [41]. In the two applications with PEG2000 diamine, Daxiang *et al* synthesized CD-PEG2000 from clean soot by refluxing with nitric acid and after passivation with PEG2000 by heating at 120 ºC [37, 38]. The toxicity of the CD-PEG2000 was evaluated [37] and the CD-PEG2000 was linking to the chlorin e6 (Ce6) by EDC and *N*-hydroxysuccinimide (NHS) cross-linking reaction [38]. The CD-PEG2000-Ce6 was then applied for the simultaneous bioimaging and photodynamic therapy by a fluorescence Förster resonance energy transfer (FRET) mechanism. Also, in another application using PEG2000, Goh *et al*, after obtained the CD-PEG2000, link hyaluronic acid (HA) for bioimaging specific targets of HA in cells [9]. The CD-PEG2000-HA synthesized nanocomposites were obtained through the carbonization of the citric acid as carbon precursor simultaneous with PEG2000 and posterior HA conjugation.

The great majority of the other synthesized CD polymers nanocomposites without PEG, use some kind of ethylene polymer as PEI, polypropionylethyleneimine (PPEI), PPEI-EI or branched polyethylenimine (BPEI) [17, 25, 30, 42-49]. For the PEG200 and PEG1500, the ethylene polymers passivation of the CD obtained by laser ablation synthesis [17, 25, 45] and some obtained by carbonization of carbon precursors [30, 42, 44] was done by heating with the ethylene polymer after activation by reflux in nitric acid. The synthesis of these CD polymers nanocomposites was also performed in one-step by refluxing the PEI with acid [42], microwave [43, 46] or pyrolyzing [48, 49] of a carbon precursor with BPEI. These polymers CD nanocomposites were evaluated in bioimaging [17, 25, 43, 45, 47]. Beside this application it was also shown that the CD-PEI is pH sensitive[42], that could be used for Cu(II) detection[46] and for drug [30] or gene [43] delivery. The citotoxicity of these CD ethylene polymers nanocomposites were also evaluated [25, 44, 46, 47]. In one of these studies the CD-PEI was conjugated with the CEA8 antibody and the cell viability in the presence of CD-PEI-CEA8 was compared with the cytotoxicity of the CdTe QD [47]. The CD have a minor effect in the cell viability and have better biocompatibility. Dong *et al* and Liu *et al* use CD-BPEI for Cu(II) detection [48, 49] and for drug delivery[43], respectively.

Beside the CD-PAA, CD-PEG and CD-PEI nanocomposites, other nanomaterials were prepared with CD/polymer with polyallylamine hydrochloride (PAH) [50], polysodium-4-styrensulfonate (PSS) [50] and with an amphilic polymer (AP) constituted by polyethylene glycol hydrophilic units and hydrophobic decyl chains along a common poly(methyl methacrylate) backbone [51]. The CD were first obtained by laser ablation in the CD-PAA and by carbonization of citric acid for the CD-PAH, CD-PSS and CD-AP synthesis. The posterior passivation was done for the CD-PAH and CD-PSS by a layer by layer technique and for the CD-PAA and CD-AP heating the CD with the polymer. In the CD-PAH and CD-PSS the initially CD synthesis was performed using mesoporous silica spheres as nanoreactors and in the CD-PAA the passivation was done after activation by reflux in nitric acid. The toxicity of CD-PAA and CD-AP nanocomposites were evaluated.

CARBON DOTS/SIMPLE ORGANIC SUBSTANCES NANOCOMPOSITES

Most of the organic molecules used for the synthesis of CD nanocomposites had amine groups in their structure that allows the linking to the carboxyl groups of CD through an amidation reaction [23, 52-67]. Fig. 2 presents some of the organic compounds used for CD nanocomposites synthesis. Some of the authors use ethylenediamine (EDA) for CD passivation [52-54, 65, 66]. The CD-EDA nanocomposites were synthesized in one step microwave synthesis [53, 54],

hydrothermal carbonization [65] of citric acid with EDA, a one step microwave synthesis of glycerol with EDA [66] or obtaining initially the CD from benzene in an arc plasma reactor with posterior linking of EDA [52]. Beside EDA, Liu group also used acrylic acid and other amines as diethylamine (DEA), triethylamine (TEA) and 1,4-butanediamine (BDA) for the CD passivation [53, 54]. The different kinds of amine compounds were compared and were used in bioimaging [53]. Acrylic acid was simultaneous used with DEA in a microwave one step synthesis to give CD enriched with amine groups. These CD were functionalized with glycidyl methacrylate (GMA) to produce CD-GMA with epoxy groups at the surface that allows linking N-isopropylacrylamide (NIPAM) and methyl methacrylate (MMA), to obtain CD-GMA-NIPAM and CD-GMA-MMA nanocomposites. Also CD-GMA containing hydrogels with different CD contents were synthesized [54]. The CD nanocomposites were used in bioimaging and the cytotoxicity was evaluated. In one step hydrothermal synthesis, the CD-EDA nanocomposites were functionalized with polyvinyl alcohol (PVA), obtaining nanofibers by electrospinning, and *N,N'*-dimethylacrylamide (DMAA) resulting in poly*N,N'*-dimethylacrylamide (PDMAA) nanocomposites [65]. The CD-EDA nanocomposites were use as printing inks and could be used as a biocompatible Fe(III) sensor. Also, after the preparation of CD-EDA nanocomposites with a great number of amine groups in their surface, they were functionalized with an organic dye (naphthalimide azide derivative) by the EDC-NHS cross-linking reaction and used as a fluorescence resonance energy transfer (FRET) probe for hydrogen sulfide (H_2S) detection in aqueous media and living cells [66].

Other high molecular weigth amines containing sulfur or oxygen atoms, were also used for CD passivation by different authors [23, 55-64, 67]. Two of the most used amines are the *N*-(2-aminoethyl)-*N,N,N'*-tris(pyridin-2-ylmethyl) ethane-1,2-diamine (TEPA) and 4,7,10-trioxa-1,13-tridecanediamine (TTDDA). Tiang and Shi *et al* synthesized CD nanocomposites with TEPA from raw CD obtained electrochemically and after heating by reflux with TEPA [55, 56]. The synthesized CD-TEPA nanocomposites were used for Cu(II) fluorescent cell bioimaging [55] and for electrochemical cerebral Cu(II) monitoring [56]. In the electrochemical Cu(II) monitoring the CD-TEPA nanocomposites were deposited in a glassy carbon electrode by an EDC and NHS cross-linking reaction after the enrichment of the glassy carbon electrode with methoxy functional groups. The TTDDA was used for CD passivation by several authors. The CD passivation with TTDDA was done after the synthesis of CD through the chemical oxidation by nitric acid of activated carbon [23] or the carbonization of carbohydrates in sulfuric acid [57]. Also, one step microwave synthesis was used to obtain the CD-TTDDA nanocomposites [58, 59]. The fluorescent characteristics of the CD-TTDDA were compared with CD-PEG1500 [23] and it was used in bioimaging applications[23, 58] and for distinguish cancer cells after functionalization with folic acid (FA) [59]. In the CD-TTDDA-FA synthesis, the linking with FA was done using NHS chemistry.

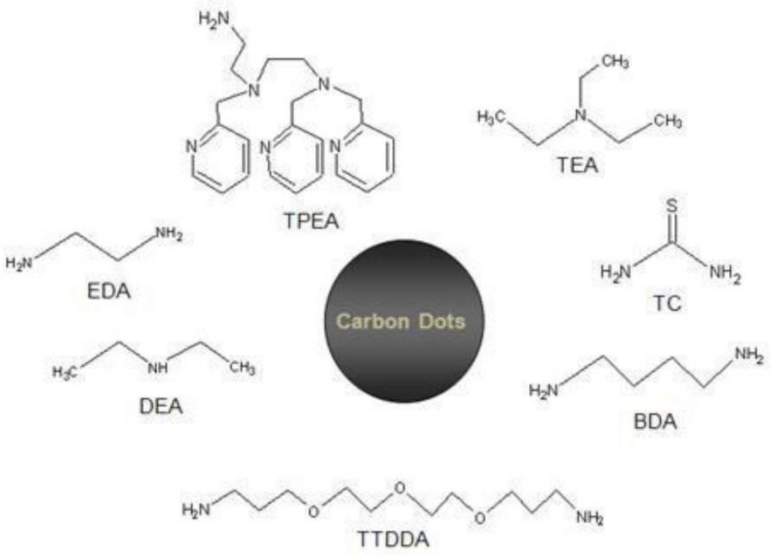


Fig. 2 Organic compounds used for CD nanocomposites synthesis.

The 4′-(Aminomethylphenyl)-2,2′:6′,2″-terpyridine (ATPY) [62], thiocarbamide (TC) [61], 1-hexadecylamine (HDA) [60], 11-aminoundecanoic acid (AUA) [64] and octacedyl ammonium (ODA), 2-(2-aminoethoxy)-ethanol (2AEE) or 4-aminoantipyrine (4AAP) [67] were also used as passivation agents. With these amines different methods of synthesis and different applications were found. The CD-ATPY was obtained by an EDC-NHS cross-linking reaction and used in two photon bioimaging and pH sensing in living cells and tissues [62]. The fluorescence characteristics of CD-TC, synthesized by carbonization of kerosene soot in nitric acid and heating with TC, were established [61].The CD-HAD, obtained in one step synthesis by carbonization of citric acid with HDA in hot octadecene, was used as white light emitting device attending to their electroluminescence properties [60]. The CD-AUA was synthesized by heating simultaneous the citric acid and the AUA, and was used for inorganic phosphate detection in complex matrices [63, 64]. The mechanism for the phosphate quantification is based in the quenching of the CD-AUA fluorescence by the europium ion followed by the recovery of fluorescence by the inorganic phosphate. CD-ODA, CD-2AEE and CD-4AAP were synthesized and the optical properties of the nanocomposites were established. The synthesis of these nanocomposites were performed in a similar one-step thermal carbonization of octadecyl ammonium citrate salt, 2-(2-aminoethoxy)-ethanol salt or 4AAP resulting in organophilic or hydrophilic CD [67].

The only examples of CD nanocomposites of organic molecules without an amine group in their structure are the ibuprofen [68], ionic liquids (IL) [69, 70] and complex nickel(II) dithiolene [71]. The CD-Ibuprofen nanocomposites used for drug delivery was synthesized after the CD production by carbonization of the carbon precursor, polypyrrole (PPy) nanoparticles, and enrichment of the CD surface with amino groups for the condensation reaction with ibuprofen.[68] Two ionic liquids were used for CD functionalization. The 1-butyl-3-methylimidazolium glutamine salt [69] and 1-methyl-3-butyl imidazolium tetrafluoroborate [70]. The nanocomposites synthesis was done by microwave [69] or electrochemically [70] one step synthesis, and the

fluorescence characteristics of the synthesized CD-IL nanocomposites were established. The synthesis of the nickel(II) dithiolene CD nanocomposites was done by an initially wood wool carbonization, after nitric acid activation and, in opposition to the others CD nanocomposites, by doping tris(hydroxymethyl)aminomethane (Tris) and betaine hydrochloridenickel(II) dithiolene complex with the synthesized CD [71].

CARBON DOTS/BIOMOLECULES NANOCOMPOSITES

Few examples were found in the literature of CD nanocomposites with biomolecules or a derivative [72-74]. CD were linked to an aminoacid derivative [74], to a fluorescent labeled single-stranded DNA (ssDNA) [72] and to antibodies GAM immunoglobulins [73]. Fig. 3 presents the biomolecules used for CD nanocomposites synthesis.

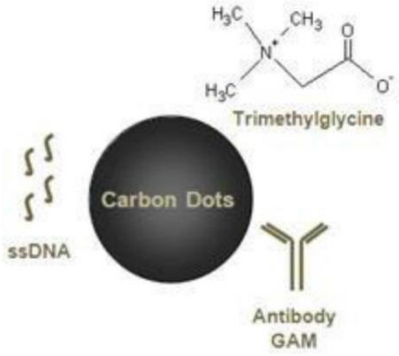


Fig. 3 Biomolecules used for CD nanocomposites synthesis.

The CD-ssDNA nanocomposites were used for the DNA detection [72]. This detection is based in the formation of a double-stranded DNA (dsDNA) and consequent recovery of the fluorescence of the labeled dye. For the CD-ssDNA nanocomposites synthesis the functionalization of the CD with ssDNA was done by physical adsorption after CD synthesis from combustion of candle soot through an oxidative acid treatment. Luminescent CD nanocomposites were obtained with trimethylglycine [74]. For the synthesis of the CD aminoacid derivative nanocomposites the tris(hydroxymethyl)aminomethane (Tris) and betaine hydrochloride were simultaneous heated at 250 ºC. One interesting application is the use of CD in an immunochromatographic assay where the CD where labeled with the antibodies GAM immunoglobulins for the detection and quantification of a synthetic plant regulator forchlorfenuron in food samples [73]. Essentially the CD are linked to GAM immunoglobulins by a sonication procedure, and the CD-GAM immunoglobulins were immobilized in nitrocellulose membranes for detection and quantification of the phytoregulator forchlorfenuron.

CARBON DOTS/INORGANIC SUBSTANCES NANOCOMPOSITES

Some inorganic compounds as iron (Fe), iron oxides, Au, silver (Ag), Pt, palladium (Pd), copper (Cu), silicon (Si), SiO_2 and titanium oxide (TiO_2) were used for CD nanocomposites synthesis [26, 35, 41, 75-84]. Fig.4 presents the inorganic compounds used for CD

nanocomposites synthesis. Nanocomposites with magnetic properties were obtained when Fe or iron oxide were used. As in a previous CD-EDA nanocomposites synthesis [52] a plasma reactor was used for the synthesis of functionalized iron or iron oxide carbon magnetic nanoparticles [75]. The magnetic nanoparticles were first synthesized from an arc sustained between iron electrodes in benzene, leading to the formation of a carbon based structure in which the iron or iron oxides particles are dispersed. These magnetic nanoparticles were then aminated with EDA, activated with glutaric dialdehyde (GD) and covalently functionalized with doxorubicin (DOX) in a plasma reactor. Attending to their *in vitro* antiproliferative activity in cell cytotoxicity assays, it was suggested that this DOX functionalized magnetic CD could be used for drug delivery.

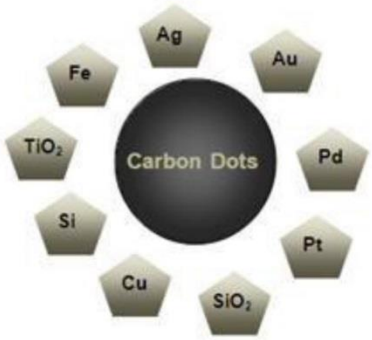


Fig. 4 Inorganic compounds used for CD nanocomposites synthesis.

Most of the CD nanocomposites with metals use gold or silver. In some of these nanocomposites, CD were immobilized in the gold or silver nanoparticles core [76, 77] or the gold or platinum metals coat CD-PEG1500 nanocomposites [26, 35]. In these CD-Au synthetic procedures, CD were linked to Au nanoparticles [76, 77]. Tian *et al* synthesized the CD-Au nanocomposites by heating $HAuCl_4$ with electrochemically synthesized CD. Au nanoparticles are linked to CD in an ultrathin shell of around 2 nm. This CD-Au nanocomposites was then used for surface enhanced Raman scattering [77]. Chandra *et al* synthesized the CD-Au nanocomposites by simply mixing Au nanoparticles and CD. The CD synthesis was done by refluxing thiomalic acid in acid medium. Their fluorescence characteristics were characterized [76].

Two CD-Ag nanocomposites with a SiO_2 interlayer between the Ag nanoparticle and the CD were obtained and their metal-enhanced fluorescence properties were evaluated.[78, 79] For both nanocomposites, layer by layer electrostatic assemblies, each of them with a different procedure, were used to link the CD to the Ag nanoparticles. In both, tetraethylorthosilicate (TEOS) was used as silica source for the SiO_2 interlayer deposition and for the layer by layer assembly, in order to add a positive charge at the surface, positively charged polyelectrolytes [poly allylamine hydrochloride, (PAH)] [78] and 3-aminopropyltrimethoxysilane (APS) [79] were used. The previous CD synthesis was done by a hydrothermal method [79] or using an impregnation method with mesoporous silica spheres as nanoreactors and citric acid as carbon precursor [78]. Using Ag, Pd or Cu salts, different CD-Ag, CD-Pd and CD-Cu nanocomposites were synthesized [80]. Previous to the metal nanostructures deposition on CD, the synthesis of CD was done refluxing combustion soot of natural gas in nitric acid. The fluorescence characteristics of these synthesized nanocomposites was established and their electrochemically behavior was shown. Besides the synthesis of CD-PEG1500-Au or CD-PEG1500-Pt nanocomposites, they were used as

photocatalysts for the reduction of CO_2 [26] and their quenching of fluorescence effect was followed [35].

The previously synthesized CD-SiO_2-Ag nanocomposites [78, 79] were coated with PEG900 [41]. Also, other CD-SiO_2 nanocomposites were synthesized [84] and, in another nanocomposites, CD were trapped in Si microspheres [81]. The synthesis of CD-SiO_2 without coating, by linking the CD to the SiO_2 surface, was done using electrochemically synthesized CD and SiO_2 nanoparticles. The SiO_2 nanoparticles were obtained by a sol-gel methodology using TEOS. The fluorescence and photocatalyst properties of the CD-SiO_2 nanocomposites were established [84]. The CD-SiO_2-PEG900 nanocomposites were functionalized with DOX by simple mixing the CD-SiO_2-PEG900 with DOX. The cytotoxicity of the synthesized CD-SiO_2-PEG900-DOX nanocomposites was evaluated and was used for bioimaging and drug delivery [41]. The CD-Si microspheres nanocomposites synthesis was performed through a solvent evaporation induced aggregating assembly. In this synthesis, an amphiphilic poly(ethylene oxide)-*b*-polystyrene (PEO-*b*-PS) and TEOS were used, respectively, as a carbon precursor and silica source, obtaining mesoporous silica microspheres with sulfonated CD trapped in the silica microspheres.

TiO_2 was used in three nanocomposites synthesis [82-84]. In one of them, the CD previously synthesized were doped with TiO_2 [83]. In another, the CD were linked to the TiO_2 [84] and in the third they were linked into TiO_2 nanostructured fibers [82]. Capping the CD surface with TiO_2 (CD-TiO_2) was done after a previous CD laser ablation synthesis and activation by refluxing in nitric acid. The preparation of CD-TiO_2 was done by a sol-gel process using titanium(IV) ethoxide, followed by sonication and reflux. The synthesized CD-TiO_2 were capped with PEG1500 (CD-TiO_2-PEG1500) and their fluorescent properties were evaluated [83]. In a similar process, CD-SiO_2 was prepared by linking the CD to the SiO_2 surface. Also the synthesis of CD-TiO_2 was done by mixing electrochemically prepared CD to a TiO_2 surface of nanoparticles and posterior drying in a vacuum oven. Also the TiO_2 nanoparticles synthesis was done by a sol-gel methodology but using tetrabutyl titanate. The fluorescence and photocatalytic properties of the CD-TiO_2 were established [84]. Structured fibers of CD-TiO_2 nanocomposites were synthesized combining an electrospinning technique and a reflux method. Initially the TiO_2 nanostructured fibers, obtained by an electrospinning technique, and CD, were synthesized by an impregnation method using mesoporous silica spheres as nanoreactors. After APS addition, to connect the TiO_2 structured fibers and the CD, CD-TiO_2 nanocomposites synthesis was done refluxing the mixture of both the precursors [82].

CARBON DOTS/QUANTUM DOTS NANOCOMPOSITES

CD are being proposed as non-toxic alternatives to crystalline semiconductors nanoparticles commonly known as quantum dots (QD). Nevertheless some nanocomposites were obtained by doping the synthesized CD with QD to improve their fluorescence performance [19, 83, 85-88]. Fig.5 presents the QD used for CD nanocomposites synthesis. Beside the already discussed CD-ZnS-PEG1500 synthesis by Sun group, CD-ZnO-PEG1500 nanocomposites were synthesized in a similar way [83]. After a previous CD laser ablation synthesis and activation in nitric acid, the suspensions were sonicated and zinc acetate was mixed with sodium sulfide or sodium hydroxide to obtained CD-ZnS or CD-ZnO. PEG1500 was after linked to the synthesized CD-ZnS or CD-ZnO [19, 83, 87, 88]. Their fluorescent properties were evaluated by comparison with CD-PEG1500 and CD-TiO_2-PEG1500 and the bioimaging capabilities of the CD-ZnS-PEG1500 were evaluated. Beside Sun group, Yu *et al* also synthesized CD-ZnO nanocomposites. The CD-ZnO nanocomposites synthesis was done using an autoclave hydrothermal method by mixing zinc acetate with an electrochemically synthesized CD solution. The photocatalytic ability for toxic gas

degradation under visible light of the CD-ZnO was demonstrated in comparison with N-TiO_2 and ZnO nanoparticles [86].

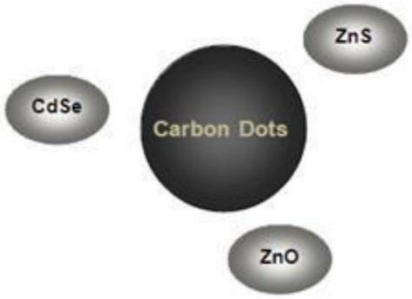


Fig. 5 Crystalline semiconductors nanoparticles used for CD nanocomposites synthesis.

CdSe QD also used for the synthesis of CD nanocomposites. The CD-CdSe nanocomposites were also functionalized with TPEA. The synthesis of CD-CdSe-TPEA were obtained from first CD produced by an electrochemical method and CdSe-SiO_2 particles were obtained through a sol-gel method y mixing the QD with TEOS. The CD-CdSe-TPEA was then obtained after the enrichment of the CdSe-SiO_2 particles surface with amine groups by addition of APS. The final step of the CD-CdSe-TPEA nanocomposites synthesis was the linking of TEPA with CD-CdSe by an EDC-NHS cross-linking reaction. This nanocomposites were used for *in vivo* fluorescence sensing of Cu(II) [85].

CARBON DOTS/ORGANOSILANES NANOCOMPOSITES

Beside TEOS, used as precursor of the SiO_2 in the CD-SiO_2 nanocomposites synthesis, different organosilanes compounds (OS) were also used for CD-OS nanocomposites preparations [89-91]. Fig. 6 presents the principal organosilanes used for CD nanocomposites synthesis. From the different CD-OS synthesized by a simple one-step hydrothermal autoclave method, in which the initially added OS is simultaneous used as carbon precursor and functionalizing agent, it was found that the CD-APS have greater quantum yield and greater solubility. All the synthesized CD-OS are photoluminescent and sensitive to temperature, have a reversible respond and have potential applications in the fabrication of temperature sensitive probes [89].

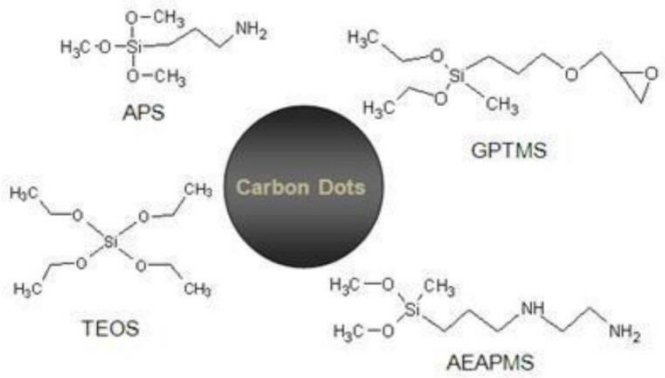


Fig. 6 Organosilanes compounds used for CD nanocomposites synthesis.

Also Wang and Xie *et al* synthesized CD-OS by two similar methodologies [90, 91]. In one the CD-OS nanocomposites synthesis was done by carbonization of citric acid in *N*-(*β*-aminoethyl)- *γ* -aminopropyl methyldimethoxy silane (AEAPMS) [91] after previous heating of the AEAPMS. In the other synthesis, OS is heated up to a desired temperature and an organic polybasic substance was quickly added [90]. CD-SiO_2 nanocomposites were also synthesized by addition of TEOS to the CD-AEAPMS nanocomposites solution [91]. The synthesized CD-OS were used in bioimaging [91] and, due to the methoxy groups of the CD-AEAPMS, they could be used to form films and monoliths [91]. If methyltriethoxysilane, 3-aminopropyl triethoxysilane or 3-glycidoxypropyl methyldiethoxysilane (GPTMS) were used they could form different kind of gels [90].

SUMMARY/PERSPECTIVES

Several methods of CD nanocomposites synthesis are now available. Beside the initially used laser ablation method, microwave and/or hydrothermal methods are being preferred for CD nanocomposites preparation. The majority of the nanocomposites are CD polymers nanocomposites that use polymers for the CD passivation. Beside some examples of nanocomposites with simple aminated organic substances or inorganic substances few examples of CD nanocomposites are found with other kind of substances as biomolecules, organosilanes or even crystalline semiconductors nanoparticles.

The majority of the developed analytical applications were based in the CD fluorescence characteristics. Most of the synthesized CD nanocomposites were used in bioimaging and analytical sensing. The great number of analytical sensing applications developed were done in order to the detection and/or quantification of metallic ions as the Hg(II) or Cu(II). All of these sensing applications are based in the quenching of the CD nanocomposites fluorescence. Only one electrochemical sensing application was found.

New simple methods of synthesis, as the microwave or thermal autoclave synthesis are now emerging as the preferred one for CD raw and nanocomposites synthesis. Attending to their own characteristics the use of biological molecules or even crystalline semiconductors nanoparticles for the CD nanocomposites synthesis is an area that could enlarge the range of analytical and bioanalytical applications. After a great effort development in the methods of synthesis the focus

of the future research could be the functionalization of the CD in order to increase the quantum yield in bioimaging and selectivity in sensing applications.

REFERENCES

1. Scida, K., Stege, P.W., Haby, G., Messina, G.A., and Garcia, C.D. (2011). Recent applications of carbon-based nanomaterials in analytical chemistry: critical review *Anal Chim Acta.* 691, 6-17.
2. Pérez-López, B. and Merkoçi, A. (2012). Carbon nanotubes and graphene in analytical sciences *Microchim. Acta.* 179, 1-16.
3. Luo, P.G., Sahu, S., Yang, S.-T., Sonkar, S.K., Wang, J., Wang, H., et al. (2013). Carbon "quantum" dots for optical bioimaging *J. Mater. Chem. B.* 1, 2116.
4. Li, H., Kang, Z., Liu, Y., and Lee, S.-T. (2012). Carbon nanodots: synthesis, properties and applications *J. Mater. Chem.* 22, 24230.
5. Esteves da Silva, J.C.G. and Gonçalves, H.M.R. (2011). Analytical and bioanalytical applications of carbon dots *TrAC, Trends Anal. Chem.* 30, 1327-1336.
6. Anilkumar, P., Cao, L., Yu, J.J., Tackett, K.N., 2nd, Wang, P., Meziani, M.J., et al. (2013). Crosslinked carbon dots as ultra-bright fluorescence probes *Small.* 9, 545-551.
7. Mitra, S., Chandra, S., Pathan, S.H., Sikdar, N., Pramanik, P., and Goswami, A. (2013). Room temperature and solvothermal green synthesis of self passivated carbon quantum dots *RSC Adv.* 3, 3189-3193.
8. Liu, R., Li, H., Kong, W., Liu, J., Liu, Y., Tong, C., et al. (2013). Ultra-sensitive and selective Hg2+ detection based on fluorescent carbon dots *Mater. Res. Bull.* 48, 2529-2534.
9. Goh, E.J., Kim, K.S., Kim, Y.R., Jung, H.S., Beack, S., Kong, W.H., et al. (2012). Bioimaging of hyaluronic acid derivatives using nanosized carbon dots *Biomacromolecules.* 13, 2554-2561.
10. Wang, F., Pang, S., Wang, L., Li, Q., Kreiter, M., and Liu, C.-y. (2010). One-Step Synthesis of Highly Luminescent Carbon Dots in Noncoordinating Solvents *Chem. Mater.* 22, 4528-4530.
11. Goncalves, H.M., Duarte, A.J., Davis, F., Higson, S.P., and Esteves da Silva, J.C. (2012). Layer-by-layer immobilization of carbon dots fluorescent nanomaterials on single optical fiber *Anal Chim Acta.* 735, 90-95.
12. Leitao, J.M., Tauler, R., and da Silva, J.C. (2011). Chemometric analysis of excitation emission matrices of fluorescent nanocomposites *J Fluoresc.* 21, 1987-1996.
13. Leitão, J.M.M., Gonçalves, H., and da Silva, J.C.G.E. (2010). Parallel factor analysis of EEM of the fluorescence of carbon dots nanoparticles *J. Chemom.* 24, 655-664.
14. Goncalves, H.M., Duarte, A.J., and Esteves da Silva, J.C. (2010). Optical fiber sensor for Hg(II) based on carbon dots *Biosens Bioelectron.* 26, 1302-1306.
15. Gonçalves, H., Jorge, P.A.S., Fernandes, J.R.A., and Esteves da Silva, J.C.G. (2010). Hg(II) sensing based on functionalized carbon dots obtained by direct laser ablation *Sens. Actuators, B.* 145, 702-707.
16. Goncalves, H. and Esteves da Silva, J.C. (2010). Fluorescent carbon dots capped with PEG200 and mercaptosuccinic acid *J Fluoresc.* 20, 1023-1028.
17. Sun, Y.-P., Zhou, B., Lin, Y., Wang, W., Fernando, K.A.S., Pathak, P., et al. (2006). Quantum-Sized Carbon Dots for Bright and Colorful Photoluminescence *J. Am. Chem. Soc.* 128, 7756-7757.
18. Wang, X., Cao, L., Lu, F., Meziani, M.J., Li, H., Qi, G., et al. (2009). Photoinduced electron transfers with carbon dots *Chem. Commun.* 0, 3774-3776.
19. Yang, S.-T., Cao, L., Luo, P.G., Lu, F., Wang, X., Wang, H., et al. (2009). Carbon Dots for Optical Imaging in Vivo *J. Am. Chem. Soc.* 131, 11308-11309.

20. Zhu, H., Wang, X., Li, Y., Wang, Z., Yang, F., and Yang, X. (2009). Microwave synthesis of fluorescent carbon nanoparticles with electrochemiluminescence properties *Chem Commun (Camb)*. 5118-5120.
21. Liu, R., Wu, D., Liu, S., Koynov, K., Knoll, W., and Li, Q. (2009). An aqueous route to multicolor photoluminescent carbon dots using silica spheres as carriers *Angew Chem Int Ed Engl*. 48, 4598-4601.
22. Mao, X.J., Zheng, H.Z., Long, Y.J., Du, J., Hao, J.Y., Wang, L.L., et al. (2010). Study on the fluorescence characteristics of carbon dots *Spectrochim Acta A Mol Biomol Spectrosc*. 75, 553-557.
23. Qiao, Z.A., Wang, Y., Gao, Y., Li, H., Dai, T., Liu, Y., et al. (2010). Commercially activated carbon as the source for producing multicolor photoluminescent carbon dots by chemical oxidation *Chem Commun (Camb)*. 46, 8812-8814.
24. Liu, J.M., Lin, L.P., Wang, X.X., Lin, S.Q., Cai, W.L., Zhang, L.H., et al. (2012). Highly selective and sensitive detection of Cu2+ with lysine enhancing bovine serum albumin modified-carbon dots fluorescent probe *Analyst*. 137, 2637-2642.
25. Wang, Y., Anilkumar, P., Cao, L., Liu, J.H., Luo, P.G., Tackett, K.N., 2nd, et al. (2011). Carbon dots of different composition and surface functionalization: cytotoxicity issues relevant to fluorescence cell imaging *Exp Biol Med (Maywood)*. 236, 1231-1238.
26. Cao, L., Sahu, S., Anilkumar, P., Bunker, C.E., Xu, J., Fernando, K.A., et al. (2011). Carbon nanoparticles as visible-light photocatalysts for efficient CO2 conversion and beyond *J Am Chem Soc*. 133, 4754-4757.
27. Wang, X., Cao, L., Yang, S.T., Lu, F., Meziani, M.J., Tian, L., et al. (2010). Bandgap-like strong fluorescence in functionalized carbon nanoparticles *Angew Chem Int Ed Engl*. 49, 5310-5314.
28. Hu, S.-L., Niu, K.-Y., Sun, J., Yang, J., Zhao, N.-Q., and Du, X.-W. (2009). One-step synthesis of fluorescent carbon nanoparticles by laser irradiation *J. Mater. Chem.* 19, 484-488.
29. Yang, S.-T., Wang, X., Wang, H., Lu, F., Luo, P.G., Cao, L., et al. (2009). Carbon Dots as Nontoxic and High-Performance Fluorescence Imaging Agents *J. Phys. Chem. C*. 113, 18110-18114.
30. Li, Q., Ohulchanskyy, T.Y., Liu, R., Koynov, K., Wu, D., Best, A., et al. (2010). Photoluminescent Carbon Dots as Biocompatible Nanoprobes for Targeting Cancer Cells in Vitro *J. Phys. Chem. C*. 114, 12062-12068.
31. Zhang, Y., Goncalves, H., da Silva, J.C., and Geddes, C.D. (2011). Metal-enhanced photoluminescence from carbon nanodots *Chem Commun (Camb)*. 47, 5313-5315.
32. Lin, L.P., Wang, X.X., Lin, S.Q., Zhang, L.H., Lin, C.Q., Li, Z.M., et al. (2012). Research on the spectral properties of luminescent carbon dots *Spectrochim Acta A Mol Biomol Spectrosc*. 95, 555-561.
33. Bhunia, S.K., Saha, A., Maity, A.R., Ray, S.C., and Jana, N.R. (2013). Carbon nanoparticle-based fluorescent bioimaging probes *Sci Rep*. 3, 1473.
34. Wang, F., Kreiter, M., He, B., Pang, S., and Liu, C.Y. (2010). Synthesis of direct white-light emitting carbogenic quantum dots *Chem Commun (Camb)*. 46, 3309-3311.
35. Xu, J., Sahu, S., Cao, L., Bunker, C.E., Peng, G., Liu, Y., et al. (2012). Efficient fluorescence quenching in carbon dots by surface-doped metals--disruption of excited state redox processes and mechanistic implications *Langmuir*. 28, 16141-16147.
36. Zhao, L., Di, F., Wang, D., Guo, L.-H., Yang, Y., Wan, B., et al. (2013). Chemiluminescence of carbon dots under strong alkaline solutions: a novel insight into carbon dot optical properties *Nanoscale*. 5, 2655-2658.
37. Wang, K., Gao, Z., Gao, G., Wo, Y., Wang, Y., Shen, G., et al. (2013). Systematic safety evaluation on photoluminescent carbon dots *Nanoscale Res. Lett*. 8, 122.
38. Huang, P., Lin, J., Wang, X., Wang, Z., Zhang, C., He, M., et al. (2012). Light-triggered theranostics based on photosensitizer-conjugated carbon dots for simultaneous enhanced-fluorescence imaging and photodynamic therapy *Adv Mater*. 24, 5104-5110.

39. Liu, Y., Liu, C.Y., and Zhang, Z.Y. (2011). Synthesis and surface photochemistry of graphitized carbon quantum dots *J Colloid Interface Sci.* 356, 416-421.
40. Yang, Y., Wu, D., Han, S., Hu, P., and Liu, R. (2013). Bottom-up fabrication of photoluminescent carbon dots with uniform morphology via a soft-hard template approach *Chem Commun (Camb).* 49, 4920-4922.
41. Lai, C.-W., Hsiao, Y.-H., Peng, Y.-K., and Chou, P.-T. (2012). Facile synthesis of highly emissive carbon dots from pyrolysis of glycerol; gram scale production of carbon dots/mSiO2 for cell imaging and drug release *J. Mater. Chem.* 22, 14403.
42. Shen, L., Zhang, L., Chen, M., Chen, X., and Wang, J. (2013). The production of pH-sensitive photoluminescent carbon nanoparticles by the carbonization of polyethylenimine and their use for bioimaging *Carbon.* 55, 343-349.
43. Liu, C., Zhang, P., Zhai, X., Tian, F., Li, W., Yang, J., et al. (2012). Nano-carrier for gene delivery and bioimaging based on carbon dots with PEI-passivation enhanced fluorescence *Biomaterials.* 33, 3604-3613.
44. Liu, J.-H., Anilkumar, P., Cao, L.I., Wang, X.I.N., Yang, S.-T., Luo, P.G., et al. (2010). Cytotoxicity Evaluations of Fluorescent Carbon Nanoparticles *Nano LIFE.* 01, 153-161.
45. Cao, L., Wang, X., Meziani, M.J., Lu, F., Wang, H., Luo, P.G., et al. (2007). Carbon Dots for Multiphoton Bioimaging *J. Am. Chem. Soc.* 129, 11318-11319.
46. Salinas-Castillo, A., Ariza-Avidad, M., Pritz, C., Camprubi-Robles, M., Fernandez, B., Ruedas-Rama, M.J., et al. (2013). Carbon dots for copper detection with down and upconversion fluorescent properties as excitation sources *Chem Commun (Camb).* 49, 1103-1105.
47. Han, B., Wang, W., Wu, H., Fang, F., Wang, N., Zhang, X., et al. (2012). Polyethyleneimine modified fluorescent carbon dots and their application in cell labeling *Colloids Surf B Biointerfaces.* 100, 209-214.
48. Dong, Y., Wang, R., Li, H., Shao, J., Chi, Y., Lin, X., et al. (2012). Polyamine-functionalized carbon quantum dots for chemical sensing *Carbon.* 50, 2810-2815.
49. Dong, Y., Wang, R., Li, G., Chen, C., Chi, Y., and Chen, G. (2012). Polyamine-functionalized carbon quantum dots as fluorescent probes for selective and sensitive detection of copper ions *Anal Chem.* 84, 6220-6224.
50. Yang, X., Peng, L., Zong, J., and Zhu, Y. (2013). Preparation of photoluminescent carbon dots-embedded polyelectrolyte microcapsules *Particuology.* 11, 334-339.
51. Fowley, C., McCaughan, B., Devlin, A., Yildiz, I., Raymo, F.M., and Callan, J.F. (2012). Highly luminescent biocompatible Carbon Quantum Dots by encapsulation with an amphiphilic polymer *Chem Commun (Camb).* 48, 9361-9363.
52. Jiang, H., Chen, F., Lagally, M.G., and Denes, F.S. (2010). New strategy for synthesis and functionalization of carbon nanoparticles *Langmuir.* 26, 1991-1995.
53. Zhai, X., Zhang, P., Liu, C., Bai, T., Li, W., Dai, L., et al. (2012). Highly luminescent carbon nanodots by microwave-assisted pyrolysis *Chem Commun (Camb).* 48, 7955-7957.
54. Zhang, P., Li, W., Zhai, X., Liu, C., Dai, L., and Liu, W. (2012). A facile and versatile approach to biocompatible "fluorescent polymers" from polymerizable carbon nanodots *Chem Commun (Camb).* 48, 10431-10433.
55. Qu, Q., Zhu, A., Shao, X., Shi, G., and Tian, Y. (2012). Development of a carbon quantum dots-based fluorescent Cu2+ probe suitable for living cell imaging *Chem Commun (Camb).* 48, 5473-5475.
56. Shao, X., Gu, H., Wang, Z., Chai, X., Tian, Y., and Shi, G. (2013). Highly Selective Electrochemical Strategy for Monitoring of Cerebral Cu2+ Based on a Carbon Dot-TPEA Hybridized Surface *Anal. Chem.* 85, 418-425.
57. Peng, H. and Travas-Sejdic, J. (2009). Simple Aqueous Solution Route to Luminescent Carbogenic Dots from Carbohydrates *Chem. Mater.* 21, 5563-5565.

58. Liu, C., Zhang, P., Tian, F., Li, W., Li, F., and Liu, W. (2011). One-step synthesis of surface passivated carbon nanodots by microwave assisted pyrolysis for enhanced multicolor photoluminescence and bioimaging *J. Mater. Chem.* 21, 13163.
59. Song, Y., Shi, W., Chen, W., Li, X., and Ma, H. (2012). Fluorescent carbon nanodots conjugated with folic acid for distinguishing folate-receptor-positive cancer cells from normal cells *J. Mater. Chem.* 22, 12568.
60. Wang, F., Chen, Y.H., Liu, C.Y., and Ma, D.G. (2011). White light-emitting devices based on carbon dots' electroluminescence *Chem Commun (Camb).* 47, 3502-3504.
61. Zhang, S., He, Q., Li, R., Wang, Q., Hu, Z., Liu, X., et al. (2011). Study on the fluorescence carbon nanoparticles *Mater. Lett.* 65, 2371-2373.
62. Kong, B., Zhu, A., Ding, C., Zhao, X., Li, B., and Tian, Y. (2012). Carbon dot-based inorganic-organic nanosystem for two-photon imaging and biosensing of pH variation in living cells and tissues *Adv Mater.* 24, 5844-5848.
63. Zhao, H.X., Liu, L.Q., Liu, Z.D., Wang, Y., Zhao, X.J., and Huang, C.Z. (2011). Highly selective detection of phosphate in very complicated matrixes with an off-on fluorescent probe of europium-adjusted carbon dots *Chem Commun (Camb).* 47, 2604-2606.
64. Bourlinos, A.B., Stassinopoulos, A., Anglos, D., Zboril, R., Georgakilas, V., and Giannelis, E.P. (2008). Photoluminescent Carbogenic Dots *Chem. Mater.* 20, 4539-4541.
65. Zhu, S., Meng, Q., Wang, L., Zhang, J., Song, Y., Jin, H., et al. (2013). Highly photoluminescent carbon dots for multicolor patterning, sensors, and bioimaging *Angew Chem Int Ed Engl.* 52, 3953-3957.
66. Yu, C., Li, X., Zeng, F., Zheng, F., and Wu, S. (2013). Carbon-dot-based ratiometric fluorescent sensor for detecting hydrogen sulfide in aqueous media and inside live cells *Chem Commun (Camb).* 49, 403-405.
67. Bourlinos, A.B., Stassinopoulos, A., Anglos, D., Zboril, R., Karakassides, M., and Giannelis, E.P. (2008). Surface functionalized carbogenic quantum dots *Small.* 4, 455-458.
68. Oh, W.K., Yoon, H., and Jang, J. (2010). Size control of magnetic carbon nanoparticles for drug delivery *Biomaterials.* 31, 1342-1348.
69. Wei, Y., Liu, Y., Li, H., He, X., Zhang, Q., Kang, Z., et al. (2011). Carbon nanoparticle ionic liquid hybrids and their photoluminescence properties *J Colloid Interface Sci.* 358, 146-150.
70. Lu, J., Yang, J.-x., Wang, J., Lim, A., Wang, S., and Loh, K.P. (2009). One-Pot Synthesis of Fluorescent Carbon Nanoribbons, Nanoparticles, and Graphene by the Exfoliation of Graphite in Ionic Liquids *ACS Nano.* 3, 2367-2375.
71. Begum, A., Sonkar, S.K., Saxena, M., and Sarkar, S. (2011). Nanocomposites of carbon quantum dots-nickel(ii) dithiolene as nanolights *J. Mater. Chem.* 21, 19210-19213.
72. Li, H., Zhang, Y., Wang, L., Tian, J., and Sun, X. (2011). Nucleic acid detection using carbon nanoparticles as a fluorescent sensing platform *Chem Commun (Camb).* 47, 961-963.
73. Suarez-Pantaleon, C., Wichers, J., Abad-Somovilla, A., van Amerongen, A., and Abad-Fuentes, A. (2013). Development of an immunochromatographic assay based on carbon nanoparticles for the determination of the phytoregulator forchlorfenuron *Biosens Bioelectron.* 42, 170-176.
74. Bourlinos, A.B., Zbořil, R., Petr, J., Bakandritsos, A., Krysmann, M., and Giannelis, E.P. (2012). Luminescent Surface Quaternized Carbon Dots *Chem. Mater.* 24, 6-8.
75. Ma, Y., Manolache, S., Denes, F.S., Thamm, D.H., Kurzman, I.D., and Vail, D.M. (2004). Plasma synthesis of carbon magnetic nanoparticles and immobilization of doxorubicin for targeted drug delivery *Journal of Biomaterials Science, Polymer Edition.* 15, 1033-1049.
76. Chandra, S., Patra, P., Pathan, S.H., Roy, S., Mitra, S., Layek, A., et al. (2013). Luminescent S-doped carbon dots: an emergent architecture for multimodal applications *J. Mater. Chem. B.* 1, 2375.

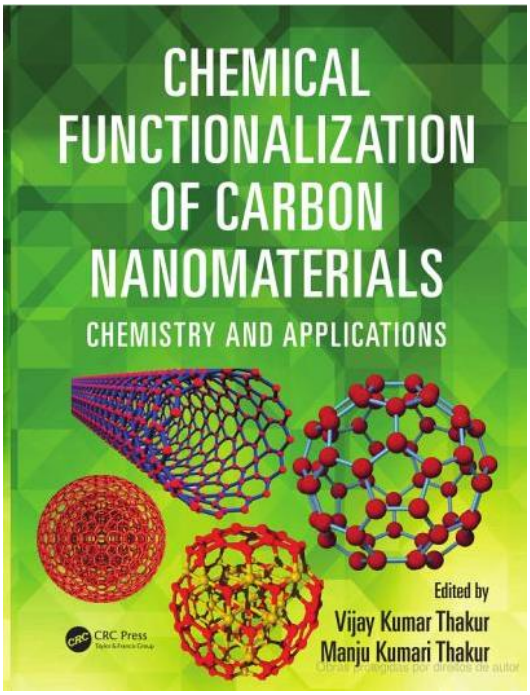
77. Luo, P., Li, C., and Shi, G. (2012). Synthesis of gold@carbon dots composite nanoparticles for surface enhanced Raman scattering *Phys Chem Chem Phys.* 14, 7360-7366.
78. Li, C., Zhu, Y., Zhang, X., Yang, X., and Li, C. (2012). Metal-enhanced fluorescence of carbon dots adsorbed Ag@SiO2 core-shell nanoparticles *RSC Adv.* 2, 1765.
79. Li, J., Zhang, B., Wang, F., and Liu, C.-y. (2011). Silver/carbon-quantum-dot plasmonic luminescent nanoparticles *New J. Chem.* 35, 554.
80. Tian, L., Ghosh, D., Chen, W., Pradhan, S., Chang, X., and Chen, S. (2009). Nanosized Carbon Particles From Natural Gas Soot *Chem. Mater.* 21, 2803-2809.
81. Yue, Q., Wang, M., Wei, J., Deng, Y., Liu, T., Che, R., et al. (2012). A template carbonization strategy to synthesize ordered mesoporous silica microspheres with trapped sulfonated carbon nanoparticles for efficient catalysis *Angew Chem Int Ed Engl.* 51, 10368-10372.
82. Li, H., Zhu, Y., Cao, H., Yang, X., and Li, C. (2013). Preparation and characterization of photocatalytic carbon dots-sensitized electrospun titania nanostructured fibers *Mater. Res. Bull.* 48, 232-237.
83. Anilkumar, P., Wang, X., Cao, L., Sahu, S., Liu, J.H., Wang, P., et al. (2011). Toward quantitatively fluorescent carbon-based "quantum" dots *Nanoscale.* 3, 2023-2027.
84. Li, H., He, X., Kang, Z., Huang, H., Liu, Y., Liu, J., et al. (2010). Water-soluble fluorescent carbon quantum dots and photocatalyst design *Angew Chem Int Ed Engl.* 49, 4430-4434.
85. Zhu, A., Qu, Q., Shao, X., Kong, B., and Tian, Y. (2012). Carbon-dot-based dual-emission nanohybrid produces a ratiometric fluorescent sensor for in vivo imaging of cellular copper ions *Angew Chem Int Ed Engl.* 51, 7185-7189.
86. Yu, H., Zhang, H., Huang, H., Liu, Y., Li, H., Ming, H., et al. (2012). ZnO/carbon quantum dots nanocomposites: one-step fabrication and superior photocatalytic ability for toxic gas degradation under visible light at room temperature *New J. Chem.* 36, 1031.
87. Cao, L., Yang, S.T., Wang, X., Luo, P.G., Liu, J.H., Sahu, S., et al. (2012). Competitive performance of carbon "quantum" dots in optical bioimaging *Theranostics.* 2, 295-301.
88. Sun, Y.-P., Wang, X., Lu, F., Cao, L., Meziani, M.J., Luo, P.G., et al. (2008). Doped Carbon Nanoparticles as a New Platform for Highly Photoluminescent Dots *J. Phys. Chem. C.* 112, 18295-18298.
89. Chen, P.C., Chen, Y.N., Hsu, P.C., Shih, C.C., and Chang, H.T. (2013). Photoluminescent organosilane-functionalized carbon dots as temperature probes *Chem Commun (Camb).* 49, 1639-1641.
90. Xie, Z., Wang, F., and Liu, C.Y. (2012). Organic-inorganic hybrid functional carbon dot gel glasses *Adv Mater.* 24, 1716-1721.
91. Wang, F., Xie, Z., Zhang, H., Liu, C.-y., and Zhang, Y.-g. (2011). Highly Luminescent Organosilane-Functionalized Carbon Dots *Adv. Funct. Mater.* 21, 1027-1031.

Chapter 3

Fluorescence sensing by functionalized carbon dots nanoparticles

João M. M. Leitão, Eliana F. C. Simões, Joaquim C. G. Esteves da Silva

Book: Chemical Functionalization of Carbon Nanomaterials: Chemistry and Applications, Chapter 11, pp. 292-309, Vijay Kumar Thakur and Manju Kumari Thakur Eds., CRC Press Taylor & Francis Group, Boca Raton, United States of America, (2015) Print ISBN: 978-1-4822-5394-, eBook ISBN: 978-1-4822-5396-2, DOI: 10.1201/b187247-13, July 2015



In this work the bibliographic research of the different functionalized CDs and their main applications in fluorescence sensing was made. The writing of the book chapter was made together with Professor João M. M. Leitão under the supervision of Professor Joaquim C. G. Esteves da Silva.

CHAPTER 11

CONTENTS

11.1 Introduction 293

11.2 CDs Fluorescence Mechanism 294

11.3 CDs Fluorescence Sensing 294

References 305

© 2016 by Taylor & Francis Group, LLC

11 Fluorescence Sensing by Functionalized Carbon Dots Nanoparticles

João M.M. Leitão, Eliana F.C. Simões, and Joaquim C.G. Esteves da Silva

Downloaded by [João Leitão] at 08:46 30 August 2015

11.1 INTRODUCTION

Fluorescent carbon dots (CDs) nanoparticles are usually referred as the natural and sustainable alternative to the semiconductor quantum dots (QDs). Indeed, CDs can easily be synthesized from renewable biomass. Compared to QDs, they have a higher solubility in water, have higher resistance to photo degradation, show a nonblinking luminescence, and have lower toxicity and generally good biocompatibility. The color-tuning properties in the visible wavelength range and quantum yields (QYs) of CDs are usually referred as less favorable properties when compared with QDs, but recent research advances are markedly improving these characteristics of CDs (Esteves da Silva 2011, 2012; Zhang et al. 2013).

Since their accidental discovery in 2004 in arc-discharged soot (Xu et al. 2004), other techniques have been used in CDs synthesis, like top-down physical methods and bottom-up chemical methodologies, and their multiple applications in diverse fields of science (Baker and Baker 2010; Esteves da Silva et al. 2011; Li et al. 2012; Ruedas-Rama et al. 2012; Luo et al. 2013). Some of the synthesized CDs are intrinsically fluorescent, but they also can be modified to alter their luminescence properties (Zhang et al. 2013; Ding et al. 2014). The carbon surface of bare CDs can be easily modified by oxidation, passivation, and/or functionalization with different types of compounds that modified the intrinsically fluorescent properties. Indeed, the properties of bare CDs can be changed only by oxidation; passivation of their surface; functionalization, by linking some species to the surface of bare CDs; or yet functionalization of oxidized or passivated CDs. The passivation and/or functionalization of bare CDs is done in order to obtain fluorescence, increasing the QY, to achieve sensitive and/or selective sensing of some compounds, or for the delivery of some therapeutic drug.

The characteristic feature of CDs is the intrinsically fluorescent properties of the synthesized bare or functionalized CDs that confers them a particularly useful role in sensing and/or bioimaging (Esteves da Silva et al. 2011; Li et al. 2012; Ruedas-Rama et al. 2012; Luo et al. 2013; Zhang et al. 2013; Ding et al. 2014). The increasing trend in the relatively high QY and recent advances in the tunable fluorescent properties open new areas for CDs applications that could be yet enlarge as a consequence of their functionalization. In preliminary applications of CDs, the non fluorescent raw CDs, were surface passivated with diamine-terminated poly(ethylene glycol), with an average molecular weight of 1500 (PEG1500N), and poly(propionylethyleneimine-*co*-ethyleneimine), an ethyleneimine copolymer (PPEI-EI), was then used for bioimaging (Sun et al. 2006; Cao et al. 2007). Since these first applications, the CDs have been used for drug delivery, biological labeling, biomedicine, inks, solar cells patterning, and optoelectronic devices in electronic, photonic, energy, catalysis, and medicine fields.

Beside the former top-down methods of synthesis, several bottom-up methods as thermal decomposition, ultrasound, microwave, autoclave, and acid dehydration and similar top-down methods of synthesis were developed for the synthesis of raw CDs and/or posterior passivation and/or

© 2016 by Taylor & Francis Group, LLC

functionalization (Esteves da Silva et al. 2011; Li et al. 2012; Zhang et al. 2013). All the bottom-up chemical methods are based on thermal or acid digestion of some CDs precursor. Several different types of CDs precursors have been used. Based on these methods of synthesis, the functionalized CDs could be obtained in one or more steps of synthesis.

The focus of this chapter is the uorescence sensing by functionalized CDs, including the surface oxidation and passivation. This chapter presents an overview of the main functionalized CDs designed as nanosensors for selected analytical species. The CDs uorescence sensing will be discussed as well as the methods of synthesis of the functionalized CDs, the functionalization labels, and the target species.

11.2 CDs FLUORESCENCE MECHANISM

CDs belong to the family of carbon nanomaterials together with nanodiamonds, graphene, nanotubes, and fullerenes. CDs are mainly composed of graphitic carbon, that is, the predominate carbon atoms have a sp^2 hybridization and show high percentages of oxygen functional groups. These structural characteristics contrast, for example, with nanodiamonds, where carbon has a sp^3 hybridization, but are similar to nanographene (viz., the oxidized form, graphene oxide).

Both CDs and nanographene (particularly graphene oxide) nanoparticles are uorescent nanomaterials that have the characteristic feature of multicolor emission when different excitation wavelengths are used (Liu et al. 2007, 2009; Peng and Travas-Sejdic 2009; Zhu et al. 2009; Li et al. 2010; Mao et al. 2010, 2014; Kozák et al. 2013; Cushing et al. 2014). This property is a major advantage of these uorescent nanomaterials because it allows tuning of the emission spectra simply by changing the excitation wavelength (keeping the size of the nanoparticle). Indeed, inorganic semiconductors like the QDs show the *normal* excitation-independent emission spectra, and, because they have a strong quantum con nement effect, the emission can be tuned by varying the size of the nanoparticle (Esteves da Silva 2011, 2012).

The justi cation for the existence of uorescence in graphite-like nanomaterials is still not clearly understood, but it has long been proposed that it should be due to surface defects, which originates energy levels that justi es the light emission. These levels would allow radiative recombination of excitons (Peng and Travas-Sejdic 2009; Zhu et al. 2009). The existence of surface defect, and the corresponding energy states/bands, was proposed based on the observations that the uorescence appears and/or the QY increased when the nanoparticles are subjected to polymer passivation and nitric acid treatment (Liu et al. 2007, 2009; Peng and Travas-Sejdic 2009; Zhu et al. 2009; Li et al. 2010; Mao et al. 2010).

Recently, the origin of the strong excitation dependence of the emission spectra of graphene oxide has been attributed to *giant red-edge effect* (Cushing et al. 2014). Taking into consideration the structural and chemical similarities of graphene oxide and CDs, the existence of a similar *edge effect* in CDs is expected (the previously discussed surface defects), and the resulting edge states/bands are responsible for the existence of unique uorescence properties.

11.3 CDs FLUORESCENCE SENSING

The uorescence sensing by functionalized CDs nanoparticles is being done in the analysis of different analytical ionic or molecular species using CDs synthesized by different methods of different carbon precursors. In sensor development, the main objective of the functionalization is to increase the sensitivity and selectivity. The main uorescence strategies used and the kind of analytical species evaluated by functionalized CDs are presented in Figure 11.1.

Most of the analytical applications have been done in the quanti cation of ionic species, namely, cations. Also different types of biological molecules, some of them small molecules, were the focus of the uorescence sensing by functionalized CDs. Besides the uorescence sensing based on quenching or uorescence enhancement of the intrinsic CDs uorescence, also, ratiometric analytical, turn off/on, turn on/off, and uorescence resonance energy transfer (FRET) uorescence sensing strategies have been proposed.

Downloaded by [João Leitão] at 08:46 30 August 2015

© 2016 by Taylor & Francis Group, LLC

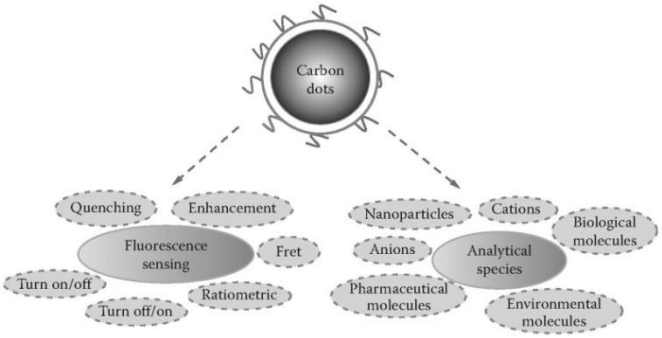


FIGURE 11.1
Fluorescence sensing strategies and analytical species evaluated by functionalized CDs.

11.3.1 Ionic Species

Several types of ionic species have been sensed by functionalized CDs. Tables 11.1 through 11.4 present the cationic species and Table 11.5 the anionic species analyzed using uorescence sensing by functionalized CDs, the functionalization label used, the methods of synthesis of the functionalized CDs, and the observed limit of detection (LOD). Examples of the uorescence sensing strategies for the ionic species evaluation by functionalized CDs are presented in Figure 11.2.

The highest number of analytical applications of functionalized CDs was in the uorescence sensing of cationic species. Fewer applications were observed in the uorescence sensing of anionic species. Different functionalization labels were used for the uorescence sensing by the functionalized CDs of the ionic species. In most of the applications, CDs are functionalized with some amine. Other less speci c functionalization/passivation labels for the ionic sensing of CDs are some types

TABLE 11.1 Cu^{2+} Fluorescence Sensing by Functionalized CDs Nanoparticles

References	Functionalization Label	CDs Synthesis	CDs Functionalization	LOD (μM)
Liu et al. (2014a)	AEAPMS/Si nanoparticles doped with rhodamine B	Thermic	Mixing/two steps	0.0352
Zhu et al. (2014)	HNO_3/AE-TPEA	Electrochemical	1-Ethyl-3-(3-dimethylaminopropyl) carbodiimide hydrochloride (EDC)–NHS/two steps	—
Zhang et al. (2014)	HNO_3	Thermic	Thermic/one step	—
Liu et al. (2014b)	Branched polyethylenimine (BPEI)	Autoclave	Mixing/two steps	0.115
Salinas-Castillo et al. (2013)	PEI	Microwave	Microwave/one step	0.09/0.12
Dong et al. (2012)	BPEI	Thermic	Thermic/one step	0.006
Liu et al. (2012)	PEG200/bovine serum albumin (BSA)/lysine	Microwave	EDC–NHS/mixing/three steps	—
Zhu et al. (2012)	CdSe-ZnS/AE-TPEA	Electrochemical	Mixing/EDC–NHS/three steps	1
Qu et al. (2012)	AE-TPEA	Electrochemical	EDC–NHS/two steps	0.010
Gonçalves et al. (2010)	HNO_3/PEG200N/NAC	Laser ablation	Thermic refluxing/three steps	—

© 2016 by Taylor & Francis Group, LLC

Downloaded by [João Leitão] at 08:46 30 August 2015

TABLE 11.2 Hg^{2+} Fluorescence Sensing by Functionalized CDs Nanoparticles

References	Functionalization Label	CDs Synthesis	CDs Functionalization	LOD (μM)
Yuan et al. (2014)	4,7,10-Trioxa-1,13-tridecanediamine (TTDDA)/bis(dithiocarbamato) copper (II) complex ($CuDTC_2$)	Thermic	Mixing/two steps	0.05
Yan et al. (2014)	1,2-Ethylenediamine (EDA)	Autoclave	Autoclave/one step	0.226
—	AEAPMS	Thermic	Thermic/one step	0.845
Zhang and Chen (2014)	Ethylene glycol (EG)	Autoclave	Autoclave/one step	0.23
Gonçalves et al. (2010a,b, 2012)	HNO_3/PEG200N/NAC	Laser ablation	Thermic refluxing/three steps	0.1/0.1/0.01
Li et al. (2011b)	FAM/ssDNA	Thermic	Adsorption/two steps	0.01

TABLE 11.3 H^+ Fluorescence Sensing by Functionalized CDs Nanoparticles

References	Functionalization Label	CDs Synthesis	CDs Functionalization	LOD (μM)
Du et al. (2013a)	EDA/fluorescein isothiocyanate (FITC)	Microwave	Mixing/two steps	—
Nie et al. (2014)	Diethylamine (DEA)/FITC	Thermic refluxing	Mixing/two steps	—
Kong et al. (2014)	AEAPMS	Thermic	Thermic/one step	—
Qu et al. (2013)	Urea	Microwave	Microwave/one step	—
Shen et al. (2013)	HNO_3/PEI	Thermic refluxing	Thermic refluxing/one step	—
Shi et al. (2012)	TTDDA/FITC/rhodamine B isothiocyanate (RBITC)	Thermic	Mixing/two steps	—
Kong et al. (2012)	4′-(Aminomethylphenyl)-2,2′:6′,2″-terpyridine (AE-TPY)	Electrochemical	EDC–NHS/two steps	—
Gonçalves et al. (2010)	HNO_3/PEG200N/NAC	Laser ablation	Thermic refluxing/three steps	—
Gonçalves and Esteves da Silva (2010)	HNO_3/PEG200N/mercaptosuccinic acid (MSA)	Laser ablation	Thermic refluxing/three steps	—

of poly(ethylene glycol) or oxidation by a strong acid. Most CDs are synthesized by a bottom-up method of synthesis based on a thermal digestion of a carbon precursor. Usually, the CDs functionalization is done in one step by thermal treatment of the carbon precursor and the functionalization label. Another common method of CDs functionalization is the carbodiimide cross-linking chemistry that allows covalent bonding of a carboxyl group in the CDs surface with an amine group of the functionalization label.

The principal cationic species analyzed by uorescence sensing of functionalized CDs were Cu^{2+} (Gonçalves et al. 2010b; Dong et al. 2012; Liu et al. 2012, 2014a,b; Qu et al. 2012; Zhu et al. 2012; Salinas-Castillo et al. 2013; Zhu et al. 2014; Zhang et al. 2014), Hg^{2+} (Gonçalves et al. 2010a,b, 2012; Li et al. 2011b; Yan et al. 2014; Yuan et al. 2014; Zhang and Chen 2014), and pH (Gonçalves and Esteves da Silva 2010; Gonçalves et al. 2010b; Kong et al. 2012; Shi et al. 2012; Du et al. 2013a; Shen et al. 2013; Qu et al. 2013; Kong et al. 2014; Nie et al. 2014). Besides these cations, Fe^{3+}, K^+, Ca^{2+}, Ag^+, and Be^{2+} and the organometallic cation CH_3Hg^+ were also synthesized by functionalized CDs for their uorescence sensing (Sun et al. 2010; Li et al. 2011a; Wei et al. 2012; Krishna et al. 2013; Qu et al. 2013; Zhu et al. 2013; Algarra et al. 2014; Costas-Mora et al. 2014; Li et al. 2014; Song et al. 2014).

Downloaded by [João Leitão] at 08:46 30 August 2015

© 2016 by Taylor & Francis Group, LLC

Downloaded by [João Leitão] at 08:46 30 August 2015

TABLE 11.4 Fluorescence Sensing of Other Cationic Species by Functionalized CDs Nanoparticles

References	Cationic Species	Functionalization Label	CDs Synthesis	CDs Functionalization	LOD (μM)
Song et al. (2014)	Fe^{3+}	EDA	Autoclave	Autoclave/one step	—
Zhu et al. (2013)	—	EDA	Autoclave	Autoclave/one step	17.91
Qu et al. (2013)	—	Urea	Microwave	Microwave/one step	0.04
Sun et al. (2010)	—	2-(2-Aminoethoxy)-ethanol	Autoclave	Autoclave/one step	11.2
Li et al. (2014)	—	Urea/polyvinyl pyrrolidone (PVP), polyacrylamide (PAM), or polyacrylic acid (PAA)	Autoclave	Autoclave/two steps	—
Wei et al. (2012)	K^+	EDA	Thermic refluxing	EDC–NHS/two steps	10
Krishna et al. (2013)	Ca^{2+}	PEG1500N/glutamic acid and hyaluronic acid	Thermic	EDC/two steps	—
Algarra et al. (2014)	Ag^+	H_2SO_4/MSA	Ultrasonic	Mixing/two steps	0.386
Li et al. (2011a)	—	ROX dye labeled ssDNA	Ultrasonic	Mixing/two steps	0.0005
Li et al. (2014)	Be^{2+}	Urea/PVP, PAM, or PAA	Autoclave	Autoclave/two steps	23
Costas-Mora et al. (2014)	CH_3Hg^+	PEG200	Ultrasonic	Ultrasonic/one step	0.0059

TABLE 11.5 Fluorescence Sensing of Anionic Species by Functionalized CDs Nanoparticles

References	Anionic Species	Functionalization Label	CDs Synthesis	CDs Functionalization	LOD (μM)
Liu et al. (2013)	F^-	PEG200/$Zr(H_2O)_2EDTA$	Microwave	Mixing/two steps	0.031
Du et al. (2013b)	I^-	EDA	Microwave	Microwave/one step	0.430
Gonçalves and Esteves da Silva (2010)	—	HNO_3/PEG200N/MSA	Laser ablation	Thermic refluxing/two steps	—
Hou et al. (2013)	S^{2-}	EDA/*N*,*N*′-bis(2-(ethylthio)ethyl) propane-1,3-diamine	Microwave	EDC–NHS/two steps	0.78
Zhang et al. (2014)	$C_2O_4^{2-}$	HNO_3	Thermic	Thermic/one step	1.0
Zhao et al. (2011)	PO_4^{3-}	11-Aminoundecanoic acid	Thermic refluxing	Thermic/one step	0.051

The sensing of these cationic species is quite important in environmental analysis where some of these cationic species are environmental pollutants, like the inorganic mercury ion (Hg^{2+}) and methylmercury (CH_3Hg^+). Heavy metal ions contamination, including Cu^{2+}, is monitored due to their critical role in some physiological and pathological events. Cu^{2+} ion sensing is based on the quenching of the uorescence of CDs at the maximum excitation and emission wavelengths. For the polyethylenimine (PEI)-CDs, due to their upconversion properties, and in order to eliminate the Fe^{3+} interference, the Cu^{2+} uorescence sensing was done at a different wavelength (850 nm) (Salinas-Castillo et al. 2013). Two of the developed CDs sensors are ratiometric and are based on the calculation of a uorescence ratio of the quenching provoked by Cu^{2+} concentration and a constant uorescence reference signal, in order to correct some instrumental variations or sample effects

© 2016 by Taylor & Francis Group, LLC

(Liu et al. 2014a). In one of the sensors, rhodamine B-doped Si nanoparticles were coated with functionalized CDs, and the quenching effect at 467 nm of the functionalized CDs was compared with the uorescence emission of the rhodamine B at 585 nm (Liu et al. 2014a). In the other sensor, a nanocomposite of CDs and CdSe/ZnS QD were functionalized with *N*-(2-aminoethyl)-*N,N,N′*-tris(pyridin-2-ylmethyl)ethane-1,2-diamine (AE-TPEA). The quenching effect of the nanocomposite CdSe/ZnS-C-TPEA at 485 nm was compared with the uorescence emission at 644 nm of CdSe/ZnS embedded in silica shells (Zhu et al. 2012).

Most of the Hg^{2+} uorescence sensing by the functionalized CDs is also based on the uorescence dynamic quenching by the Hg^{2+} (Gonçalves et al. 2010a,b, 2012; Yan et al. 2014; Zhang and Chen 2014). An optical sensor was developed based on the dynamic uorescence extinction of the *N*-acetyl- -cysteine (NAC)–amine poly(ethylene glycol)-200 (PEG200N)–CDs after immobilization of the functionalized CDs sensor in the tip of the optical ber by a sol-gel (Gonçalves et al. 2010a) and by a layer-by-layer deposition technique (Gonçalves et al. 2012). Also, the optical ber detection of Cu^{2+} with a lower sensitivity, considered as interfering on the Hg^{2+} sensing, was evaluated (Gonçalves et al. 2010a, 2012). Based on the enhancement of uorescence, two different turn off/on sensors were developed for the uorescence sensing of Hg^{2+} (Li et al. 2011b; Yuan et al. 2014): the recovery of uorescence by the Hg^{2+} was achieved after the quenching of the CDs induced by the linked $CuDTC_2$ complex (Yuan et al. 2014) and the quenching of the uorescence of linked uorescein amidite (FAM)–ssDNA induced by the CDs (Li et al. 2011b).

An extensive work has been done in order to develop functionalized CDs as uorescence sensor for pH. A tunable uorescent emission functionalized CD was synthesized for the pH uorescence sensing (Nie et al. 2014). The developed sensors are based on the decrease (Shi et al. 2012; Du et al. 2013a; Qu et al. 2013; Kong et al. 2014; Nie et al. 2014) or in the increase (Gonçalves and Esteves da Silva 2010; Gonçalves et al. 2010b; Kong et al. 2012; Shen et al. 2013) of the uorescence intensity of a pH-sensitive label with

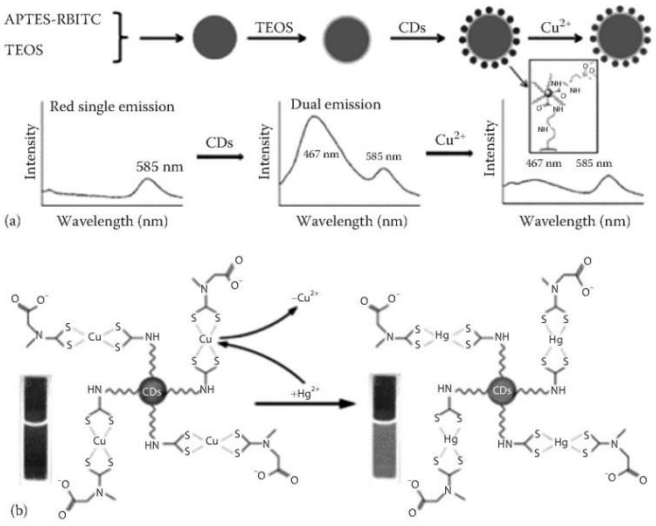


FIGURE 11.2
Examples of fluorescence sensing strategies for the ionic species evaluation by functionalized CDs nanoparticles. (a) Cu^{2+} ratiometric sensor. (Reprinted with permission from Liu, X., Zhang, N., Bing, T., and Shangguan, D., Carbon dots based dual-emission silica nanoparticles as a ratiometric nanosensor for Cu(2+), *Anal. Chem.*, 86(5), 2289. Copyright 2014a American Chemical Society.) (b) Hg^{2+} turn off/on sensor. (Reprinted with permission from Yuan, C., Liu, B., Liu, F., Han, M. Y., and Zhang, Z., Fluorescence "turn on" detection of mercuric ion based on bis(dithiocarbamato) copper(II) complex functionalized carbon nanodots. *Anal. Chem.*, 86(2), 1123. Copyright 2014 American Chemical Society.) (*Continued*)

Downloaded by [João Leitão] at 08:46 30 August 2015

© 2016 by Taylor & Francis Group, LLC

Downloaded by [João Leitão] at 08:46 30 August 2015

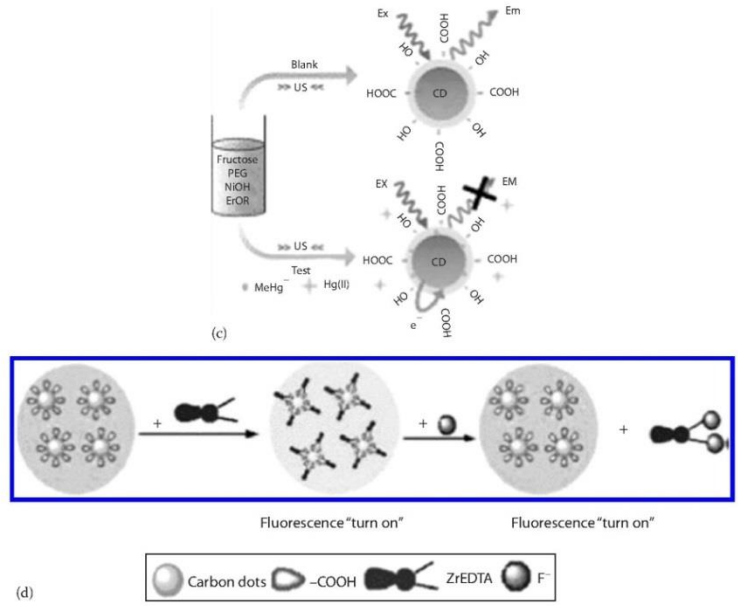


FIGURE 11.2 (*Continued*)
Examples of fluorescence sensing strategies for the ionic species evaluation by functionalized CDs nanoparticles. (c) CH_3Hg^+ in situ fluorescence quenching sensor. (Reprinted with permission from Costas-Mora, I., Romero, V., Lavilla, I., and Bendicho, C., In situ building of a nanoprobe based on fluorescent carbon dots for methylmercury detection, *Anal. Chem.*, 86(9), 4536. Copyright 2014 American Chemical Society.) (d) F^- turn on/off sensor. (Liu, J. M., Lin, L. P., Wang, X. X. et al., Zr(H_2O)2EDTA modulated luminescent carbon dots as fluorescent probes for fluoride detection, *Analyst*, 138(1), 278, 2013. Reproduced by permission of The Royal Society of Chemistry.)

the increase of the H^+ concentration. The FICT is one of the preferentially used pH-sensitive labels. Some of the pH sensors are ratiometric sensors (Shi et al. 2012; Du et al. 2013a; Nie et al. 2014). In all of these ratiometric sensors, the calculated ratio decreases with the proton concentration. In two of these sensors, the ratio of the uorescence intensity of a pH-sensitive label and of the CDs (Du et al. 2013a; Nie et al. 2014) is calculated, and in the other, the ratio of the uorescence intensity of two pH-sensitive labels used for the functionalization (Shi et al. 2012) is used. One of the ratiometric sensors developed is also a FRET-based sensor where the CD also acts as a donor and the FICT, used as pH-sensitive label, also acts as an acceptor of a FRET mechanism (Du et al. 2013a).

Besides these species (Cu^{2+}, Hg^{2+}, and pH), the majority of the uorescence sensing of other cations studied by uorescence functionalized CDs are based on the uorescence quenching induced by them (Sun et al. 2010; Krishna et al. 2013; Qu et al. 2013; Zhu et al. 2013; Algarra et al. 2014; Costas-Mora et al. 2014; Li et al. 2014; Song et al. 2014). Also, based on the uorescence quenching, CDs were in situ synthesized in order to sense CH_3Hg^+ (Costas-Mora et al. 2014), and, based on the uorescence quenching at two wavelengths (455 and 520 nm), a ratiometric sensor was developed for the Fe^{3+} sensing (Qu et al. 2013). Based on the enhancement of uorescence intensity, the sensing of K^+, by a FRET pair of uorescence functionalized CDs and graphene and an ion-selective crown ether (Wei et al. 2012), and the sensing of Ag^+, by a dye-labeled single-stranded DNA (ssDNA) (Li et al. 2011a), were done.

The anionic uorescence sensing by functionalized CDs nanoparticles was done for the F^-, I^-, S^{2-}, $C_2O_4^{2-}$, and PO_4^{3-} anions (Table 11.5). The main strategy used for the uorescence anion sensing is based on a previous uorescence enhancement or quenching followed by a uorescence quenching or enhancement, respectively, by the anion under analysis (Zhao et al. 2011; Du et al.

© 2016 by Taylor & Francis Group, LLC

2013b; Hou et al. 2013; Liu et al. 2013; Zhang et al. 2014). Fluoride sensing was done after a previous enhancement of CDs uorescence by the $Zr(H_2O)_2EDTA$ (Liu et al. 2013). Also, the sensing of S^{2-} and $C_2O_4^{2-}$ was done after the CDs uorescence quenching by the Cu^{2+} (Hou et al. 2013; Zhang et al. 2014), I^-, and PO_4^{3-}, after the CDs uorescence quenching by the Hg^{2+} (Du et al. 2013b) and Eu^{3+} (Zhao et al. 2011) cations.

11.3.2 Molecular Species

Several types of molecular species had been uorescence sensed by functionalized CDs. The biological, pharmaceutical, and the environmental molecular species evaluated by uorescence sensing, the functionalization label used, the methods of synthesis of the functionalized CDs, and the LOD found are presented in Tables 11.6 through 11.8. Examples of the uorescence sensing strategies for the molecular species evaluation by functionalized CDs are presented in Figure 11.3.

The main applications of functionalized CDs were for the uorescence sensing of molecular biological species (Li et al. 2011c; Liu et al. 2011; Mao et al. 2012; Xu et al. 2012; Baruah et al. 2013; Wang et al. 2013; Yeh et al. 2013; Yu et al. 2013a,b; Shan et al. 2014; Shi et al. 2014; Song et al. 2014; Wang et al. 2014; Zhu et al. 2014). Fewer examples were found in the uorescence sensing of molecular pharmaceutical (Sun et al. 2010; Yang et al. 2014) or environmental species (Cayuela et al. 2013; Bu et al. 2014; Huang et al. 2014). A greater number of functionalization labels speci c for a certain molecule were used for the molecular uorescence sensing by functionalized CDs. Except for one top-down electrochemical CDs synthesis, all the CDs are also synthesized by a bottom-up method of synthesis based in a thermal digestion of a carbon precursor. As for the ionic species, the CDs functionalization was also mainly done in one-step thermal treatment of both the carbon precursor and the functionalization label. The CDs functionalization based on the carbodiimide cross-linking chemistry was also frequently used for the CDs functionalization.

Glucose is one of the chemical species most frequently screened in clinical analysis, and it was also the focus of the uorescence sensing by functionalized CDs. Both of the developed sensors

TABLE 11.6 Fluorescence Sensing of Biological Molecules by Functionalized CDs Nanoparticles

References	Molecular Species	Functionalization Label	CDs Synthesis	CDs Functionalization	LOD (μM)
Shan et al. (2014)	Glucose	BBr_3	Autoclave	Autoclave/one step	8
Yeh et al. (2013)	—	RGO	Autoclave	Autoclave/one step	0.140/0.230
Wang et al. (2013)	Acetylcholine	RGO	Autoclave	Autoclave/one step	3×10^{-5}
Mao et al. (2012)	Dopamine	AEAPMS/APTES/TEOS	Thermic	Mixing/two steps	0.017
Song et al. (2014)	Hemin	EDA	Autoclave	Autoclave/one step	—
Baruah et al. (2013)	—	β-cyclodextrin/lactose monohydrate/sucrose	Microwave	Mixing/two steps	—
Liu et al. (2011)	Thrombin	FAM-labeled thrombin aptamer	Thermic	Mixing/two steps	0.020
Xu et al. (2012)	—	Thrombin aptamers (TBA_{15}/TBA_{29})	Microwave	EDC–NHS/two steps	0.001
Wang et al. (2014)	Insulin	HNO_3	Thermic	Thermic/one step	—
Li et al. (2011c)	dsDNA	FAM-labeled ssDNA	Thermic	Mixing/two steps	—
Shi et al. (2014)	GSH	2,20-(Ethylene-dioxy) bis(ethylamine)	Microwave	Microwave/one step	0.050

Downloaded by [João Leitão] at 08:46 30 August 2015

© 2016 by Taylor & Francis Group, LLC

TABLE 11.7 Fluorescence Sensing of Small Biological Molecules by Functionalized CDs Nanoparticles

References	Molecular Species	Functionalization Label	CDs Synthesis	CDs Functionalization	LOD (μM)
Yu et al. (2013b)	NO	EDA/naphthalimide with an *o*-phenylenediamine group	Microwave	EDC–*N*-hydroxy sulfosuccinimide (sulfo-NHS)/two steps	0.003
Shan et al. (2014)	H_2O_2	BBr_3	Autoclave	Autoclave/one step	—
Song et al. (2014)	—	EDA	Autoclave	Autoclave/one step	0.0265
Yeh et al. (2013)	—	RGO	Autoclave	Autoclave/one step	—
Wang et al. (2013)	—	RGO	Autoclave	Autoclave/one step	3×10^{-5}
Zhu et al. (2014)	H_2S	HNO_3/AE-TPEA-Cu^{2+}	Electrochemical	EDC–NHS/two steps	0.7
Yu et al. (2013a)	—	EDA/naphthalimide azide	Microwave	EDC–sulfo-NHS/two steps	0.01

TABLE 11.8 Fluorescence Sensing of Pharmaceutical, Environmental, and Biological Molecules by Functionalized CDs Nanoparticles

References	Molecular Species	Functionalization Label	CDs Synthesis	CDs Functionalization	LOD (μM)
Pharmaceutical					
Sun et al. (2010)	Ferrous succinate	2-(2-Aminoethoxy)-ethanol	Autoclave	Autoclave/one step	11.2
Yang et al. (2014)	Tetracyclines	P_2O_5	Mixing	Mixing/one step	0.042–0.075
Environmental					
Huang et al. (2014)	HClO/ClO^-	H_3PO_4	Microwave	Mixing/two steps	0.015
Bu et al. (2014)	PBB15	PEG-200/antigen PBB15	Microwave	Microwave/one step	0.125
Cayuela et al. (2013)	DNP/DMQ	H_2SO_4/HNO_3/acetone	Thermic refluxing	Thermic/two steps	2.176/5.676

were also H_2O_2 sensors, and the glucose fluorescence sensing was obtained indirectly through sensing of H_2O_2 after the oxidation of glucose by the glucose oxidase in gluconic acid and H_2O_2 (Yeh et al. 2013; Shan et al. 2014). In one of the developed glucose sensors, the H_2O_2 induces a decrease of fluorescence of boron-doped CDs (Shan et al. 2014), and in the other, the H_2O_2 induces an increase of fluorescence of CDs attached to reduced graphene oxide (RGO) by reaction of the H_2O_2 with reactive oxygen species that quenched the fluorescence of the RGO-CDs (Yeh et al. 2013).

Using the same mechanism for glucose sensing (Yeh et al. 2013), the fluorescence sensing of the acetylcholine neurotransmitter by RGO-CDs was successfully achieved using the acetylcholinesterase and the choline oxidase enzymes (Wang et al. 2013). However, in this last work, a different fluorescence sensing strategy is based on the fluorescence quenching by the reactive oxygen species generated by the H_2O_2. Acetylcholinesterase converts the acetylcholine to choline, which is then oxidized by the choline oxidase in betaine and H_2O_2, which generates the reactive oxygen species that induce the fluorescence quenching of the FGO-CDs (Wang et al. 2013). Besides the acetylcholine neurotransmitter, also, the fluorescence sensing of the most important catecholamine neurotransmitter dopamine was done by functionalized CDs. Based on the fluorescence quenching, the dopamine sensing was performed with *N*-(β-aminoethyl)-γ-aminopropyl methyldimethoxysilane

© 2016 by Taylor & Francis Group, LLC

Downloaded by [João Leitão] at 08:46 30 August 2015

(AEAPMS)-CDs encapsulated with a silica imprinted sol-gel lm obtained with tetraethoxysilane (TEOS) and 3-aminopropyltriethoxysilane (APTES) (Mao et al. 2012).

The uorescence quenching of functionalized CDs by the Fe^{3+} ion is the bases of several molecular sensors (Sun et al. 2010; Baruah et al. 2013; Song et al. 2014). The uorescence quenching of Fe^{3+} due to iron-containing porphyrin is the bases of a hemin sensor and, due to its role on the Fenton reaction, of a H_2O_2 sensor (Song et al. 2014). Based on the same principle, another hemin sensor was developed (Baruah et al. 2013). However, the sensitivity of the uorescence quenching of the β-cyclodextrin, lactose, or sucrose-CDs by the hemin is higher than that observed with Fe^{3+} or Fe^{2+}, and the uorescence quenching by amine depends on the number of hydroxyl groups of the functionalization label (Baruah et al. 2013). Also, in other work, the ferrous succinate was indirectly quanti ed after the conversion of Fe^{2+} to Fe^{3+} by the H_2O_2 and consequent uorescence quenching of the uorescence functionalized CDs by the Fe^{3+} (Sun et al. 2010).

Arti cial DNA oligonucleotides known as aptamers were used for the CDs uorescence sensing of thrombin, insulin, and double-stranded DNA (dsDNA) (Li et al. 2011c; Liu et al. 2011; Xu et al. 2012; Wang et al. 2014). Different uorescence strategies were used for the uorescence sensing of

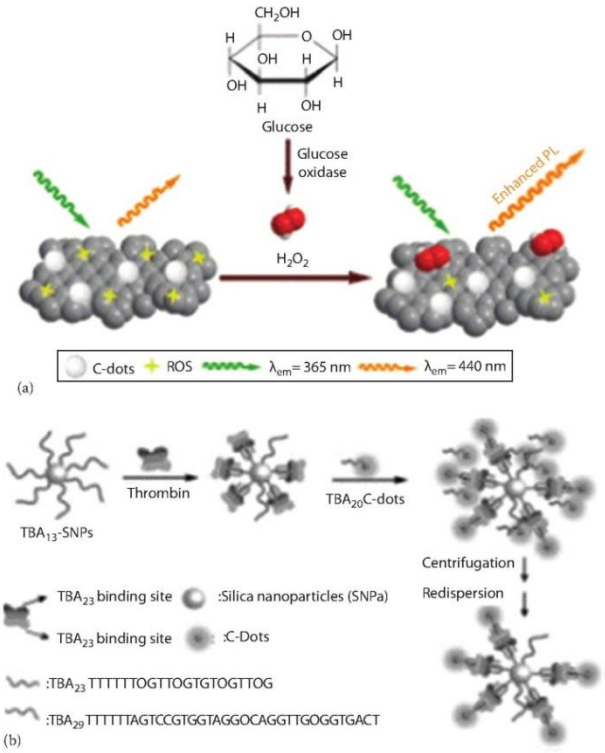


FIGURE 11.3
Examples of fluorescence sensing strategies for the molecular species evaluation by functionalized CDs nanoparticles: (a) Glucose turn off/on sensor. (Reprinted from *Talanta*, 115, Yeh, T., Wang, C., and Chang, H. T., Photoluminescent C-dots@RGO for sensitive detection of hydrogen peroxide and glucose, 718–723, Copyright 2013, with permission from Elsevier.) (b) Thrombin aptamer sandwich sensor. (Xu, B., Zhao, C., Wei, W. et al., Aptamer carbon nanodot sandwich used for fluorescent detection of protein, *Analyst*, 137(23), 5483, 2012. Reproduced by permission of The Royal Society of Chemistry.) (*Continued*)

Downloaded by [João Leitão] at 08:46 30 August 2015

© 2016 by Taylor & Francis Group, LLC

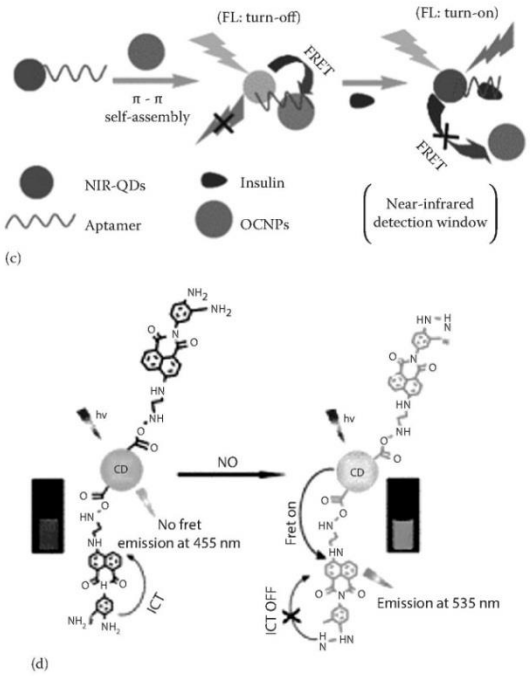


FIGURE 11.3 (*Continued*)
Examples of fluorescence sensing strategies for the molecular species evaluation by functionalized CDs nanoparticles: (c) Insulin turn off/on–based FRET aptamer sensor. (Wang, Y., Gao, D., Zhang P. et al., A near infrared fluorescence resonance energy transfer based aptamer biosensor for insulin detection in human plasma, *Chem. Commun. (Camb.)*, 50(7), 811, 2014. Reproduced by permission of The Royal Society of Chemistry.) (d) NO ratiometric sensor. (Yu, C., Wu, Y., Zeng, F., and Wu, S., A fluorescent ratiometric nanosensor for detecting NO in aqueous media and imaging exogenous and endogenous NO in live cells, *J. Mater. Chem. B*, 1(33), 4152, 2013b. Reproduced by permission of The Royal Society of Chemistry.)

these biological compounds. The sensing of thrombin was performed by linking thrombin aptamers to the CDs (Liu et al. 2011; Xu et al. 2012). In one of the developed sensors, the thrombin uorescence sensing was achieved by the recovery of the uorescence of a FAM-labeled thrombin aptamer after the uorescence quenching of the FAM uorophore by the CDs due to the lowest af nity of the thrombin aptamer complex to the CDs (Liu et al. 2011). In the other, TBA_{15} and TBA_{29} aptamers, which binds at different sites of thrombin, were, respectively, linked to Si nanoparticles and CDs. An enhancement of uorescence was observed with the thrombin due to the successively sandwich structure formed by the thrombin with the TBA_{29}–CDs and TBA_{15}–Si nanoparticles (Xu et al. 2012). The sensing of insulin was done by a FRET mechanism between an insulin aptamer functionalized near infrared (NIR) QDs as a donor and an oxidized CDs as an acceptor was developed for the uorescence sensing of insulin. In this insulin uorescence sensing strategy, the CDs quenched the NIR uorescence that is recovered by higher af nity of the insulin to the aptamer (Wang et al. 2014). As for the thrombin uorescence sensing based on the recovery of the FAM-labeled thrombin aptamer after the uorescence quenching of the FAM uorophore by the CDs, also, the dsDNA uorescence sensing was done by the same principle. In the dsDNA-developed CDs uorescent sensor, the recovery of uorescence was achieved through the hybridization of the ssDNA forming the dsDNA and consequent desorption from the CDs surface (Li et al. 2011c).

© 2016 by Taylor & Francis Group, LLC

Downloaded by [João Leitão] at 08:46 30 August 2015

The sensing of the glutathione (GSH) thiol tripeptide was done by a FRET mechanism between the uorescent functionalized CD as a donor and Au nanoparticle as an acceptor and posterior recover of uorescence by GSH. Besides the GSH sensing by this uorescent turn off/on sensor, also, the spectrophotometric GSH sensing was done using the absorbance ratio at the two maximum wavelengths of Au nanoparticles. Good results were found with this dual nanosensor. The possibility of the GSH sensing in the presence of cysteine and homocysteine-related compounds was also established (Shi et al. 2014).

Besides the previously described hydrogen peroxide sensors, used as sensors of glucose and acetylcholine, some functionalized CDs were also developed for the uorescence sensing of two important small biological molecules such as NO (Yu et al. 2013b) and H_2S (Yu et al. 2013a; Zhu et al. 2014) in different physiological and pathological processes. With the same approach, a ratiometric uorescent sensor based on a FRET mechanism of a naphthalimide-derived functionalized CDs was developed for NO (Yu et al. 2013b) and for H_2S (Yu et al. 2013a) uorescence sensing. These two ratiometric uorescence sensors were used for NO in a naphthalimide with an *o*-phenylenediamine group and for H_2S in a naphthalimide azide functionalized CDs. With both developed sensors, a reaction of NO and H_2S with the naphthalimide-derived CDs allows a FRET mechanism, between the CDs and the product of the reaction of the derived naphthalimide linked to CDs, which induces a uorescence decrease of the naphthalimide-derived functionalized CDs at 455 and 425 nm and an increase at 535 and 526 nm, respectively, for NO and H_2S. Both the calculated ratios increase with NO and H_2S concentrations. Also, for H_2S, a two-photon turn on/off sensor based on a previous Cu^{2+} uorescence quenching of an AE-TPEA functionalized CDs and posterior recovery of uorescence was developed (Zhu et al. 2014).

For the sensing of pharmaceutical molecules, and besides the previously described uorescence sensing of ferrous succinate (Sun et al. 2010), only for the tetracycline was developed a uorescent sensor based on functionalized CDs. The tetracycline uorescent sensing is based in the uorescence quenching of the functionalized CDs by the tetracyclines (Yang et al. 2014).

Environmental molecules subject to uorescence sensing by functionalized CDs were hypochlorous acid (HClO) (Huang et al. 2014), 4,4′-dibrominated biphenyl (PBB15) (Bu et al. 2014), and 2,4-dinitrophenol (DNP) and 2-amino-3,4,8-trimethyl-3*H*-imidazo[4,5-f] quinoxaline (DMQ) (Cayuela et al. 2013). The HClO uorescence sensing was done with tunable uorescent emission CDs by quenching induced by HClO (Huang et al. 2014). The uorescence sensing by functionalized CDs of the three environmental organic pollutants (PBB15, DNP, and DMQ) is done for PBB15 by an immunosensor based in a FRET mechanism (Bu et al. 2014) and for the DNP and DMQ through the uorescence quenching of acetone-passivated CDs (Cayuela et al. 2013). The PBB15 immunosensor is based in the FRET between the antigen PBB15–poly(ethylene glycol)-200 (PEG200)–CDs as a donor and the modi ed anti-PBB15 antibody Au nanoparticles as the acceptor. By reaction of these two modi ed nanoparticles, a decrease of uorescence intensity of the functionalized CDs is observed due to FRET. The recovery of the uorescence of functionalized CDs is obtained due to the competitive immunoreactions with PBB15 (Bu et al. 2014).

11.3.3 Other Species

Besides the uorescence sensing of ionic or molecular species, an application for Au nanoparticles sensing using a CD-based sensor was developed (Cayuela et al. 2014). The developed Au nanoparticle CDs sensor was synthesized in a three-step synthesis by thermal re uxing multiwalled carbon nanotubes (MWCNTs) in an acid medium, passivation with acetone, and posterior functionalization with cysteamine by *N*,*N*′-diisopropylcarbodiimide (DIC)–*N*-hydroxysuccinimide (NHS). The uorescence sensing is based in the static quenching of uorescence of the functionalized cysteamine CDs by the Au nanoparticles. An LOD of 0.0002 M was obtained (Cayuela et al. 2014).

11.3.4 Conclusions/Perspectives

Several uorescence sensing strategies have been exploited for the sensitive and selective detection of different ionic and molecular analytical species by functionalized CDs. A great effort has been

Downloaded by [João Leitão] at 08:46 30 August 2015

© 2016 by Taylor & Francis Group, LLC

done in order to design different methods of synthesis/functionalization of CDs with higher QY to obtain higher sensitivity. The majority of the CD-based analytical methodologies are selective. Even so an intense research in new functionalization labels and functionalization methodologies is still needed in order to achieve the required selectivity and in order to enlarge the application field of the functionalized CDs to new ionic and molecular analytical species.

Some research work was already done in the synthesis of excitation wavelength–dependent tunable emission CDs. Most of the tunable synthesized CDs were applied in bioimaging. A research trend line using CDs excitation wavelength-dependent emission tunability with similar fluorescence intensities could also be explored in order to the sensitivity and selective fluorescence sensing by functionalized CDs.

REFERENCES

Algarra, M., B. B. Campos, K. Radotić et al. 2014. Luminescent carbon nanoparticles: Effects of chemical functionalization, and evaluation of Ag^{+} sensing properties. *Journal of Materials Chemistry A* 2 (22):8342–8351.

Baker, S. N. and G. A. Baker. 2010. Luminescent carbon nanodots: Emergent nanolights. *Angewandte Chemie (International ed. in English)* 49 (38):6726–6744.

Baruah, U., N. Gogoi, G. Majumdar, and D. Chowdhury. 2013. Capped fluorescent carbon dots for detection of Hemin: Role of number of –OH groups of capping agent in fluorescence quenching. *The Scientific World Journal* 2013:1–9.

Bu, D., H. Zhuang, G. Yang, and X. Ping. 2014. An immunosensor designed for polybrominated biphenyl detection based on fluorescence resonance energy transfer (FRET) between carbon dots and gold nanoparticles. *Sensors and Actuators B: Chemical* 195:540–548.

Cao, L., X. Wang, M. J. Meziani et al. 2007. Carbon dots for multiphoton bioimaging. *Journal of American Chemical Society* 129:11318–11319.

Cayuela, A., M. L. Soriano, M. C. Carrion, and M. Valcarcel. 2014. Functionalized carbon dots as sensors for gold nanoparticles in spiked samples: Formation of nanohybrids. *Analytica Chimica Acta* 820:133–138.

Cayuela, A., M. L. Soriano, and M. Valcarcel. 2013. Strong luminescence of carbon dots induced by acetone passivation: Efficient sensor for a rapid analysis of two different pollutants. *Analytica Chimica Acta* 804:246–251.

Costas-Mora, I., V. Romero, I. Lavilla, and C. Bendicho. 2014. In situ building of a nanoprobe based on fluorescent carbon dots for methylmercury detection. *Analytical Chemistry* 86 (9):4536–4543.

Cushing, S. K., M. Li, F. Huang, and N. Wu. 2014. Origin of strong excitation wavelength dependent fluorescence of graphene oxide. *ACS Nano* 8 (1):1002–1013.

Ding, C., A. Zhu, and Y. Tian. 2014. Functional surface engineering of C-dots for fluorescent biosensing and in vivo bioimaging. *Accounts of Chemical Research* 47 (1):20–30.

Dong, Y., R. Wang, G. Li et al. 2012. Polyamine-functionalized carbon quantum dots as fluorescent probes for selective and sensitive detection of copper ions. *Analytical Chemistry* 84 (14):6220–6224.

Du, F., Y. Ming, F. Zeng, C. Yu, and S. Wu. 2013a. A low cytotoxic and ratiometric fluorescent nanosensor based on carbon-dots for intracellular pH sensing and mapping. *Nanotechnology* 24 (36):365101.

Du, F., F. Zeng, Y. Ming, and S. Wu. 2013b. Carbon dots-based fluorescent probes for sensitive and selective detection of iodide. *Microchimica Acta* 180 (5–6):453–460.

Downloaded by [João Leitão] at 08:46 30 August 2015

© 2016 by Taylor & Francis Group, LLC

Esteves da Silva, J. C. G. 2011. Carbon and silicon fluorescent nanomaterials. In *Nanomaterials*, ed. M. M. Rahman. In-Tech, Rijeka, Croatia.

Esteves da Silva, J. C. G. 2012. Localized surface plasmons effect in the fluorescence quantum dots. In *Quantum Dots: Applications, Synthesis an Characterization*, ed. D. O. Ciftja. Nova Publishers, Hauppauge, NY.

Esteves da Silva, J. C. G. and H. M. R. Gonçalves. 2011. Analytical and bioanalytical applications of carbon dots. *TrAC Trends in Analytical Chemistry* 30 (8):1327–1336.

Gonçalves, H. M., A. J. Duarte, F. Davis, S. P. Higson, and J. C. Esteves da Silva. 2012. Layer-by-layer immobilization of carbon dots fluorescent nanomaterials on single optical fiber. *Analytica Chimica Acta* 735:90–95.

Gonçalves, H. M., A. J. Duarte, and J. C. Esteves da Silva. 2010a. Optical fiber sensor for Hg(II) based on carbon dots. *Biosensors and Bioelectronics* 26 (4):1302–1306.

Gonçalves, H. and J. C. Esteves da Silva. 2010. Fluorescent carbon dots capped with PEG200 and mercaptosuccinic acid. *Journal of Fluorescence* 20 (5):1023–1028.

Gonçalves, H., P. A. S. Jorge, J. R. A. Fernandes, and J. C. G. Esteves da Silva. 2010b. Hg(II) sensing based on functionalized carbon dots obtained by direct laser ablation. *Sensors and Actuators B: Chemical* 145 (2):702–707.

Hou, X., F. Zeng, F. Du, and S. Wu. 2013. Carbon-dot-based fluorescent turn-on sensor for selectively detecting sulfide anions in totally aqueous media and imaging inside live cells. *Nanotechnology* 24 (33):335502.

Huang, Z., F. Lin, M. Hu et al. 2014. Carbon dots with tunable emission, controllable size and their application for sensing hypochlorous acid. *Journal of Luminescence* 151:100–105.

Kong, B., A. Zhu, C. Ding et al. 2012. Carbon dot-based inorganic-organic nanosystem for two-photon imaging and biosensing of pH variation in living cells and tissues. *Advanced Materials* 24 (43):5844–5848.

Kong, W., H. Wu, Z. Ye et al. 2014. Optical properties of pH-sensitive carbon-dots with different modifications. *Journal of Luminescence* 148:238–242.

Kozák, O., K. K. R. Datta, M. Greplová et al. 2013. Surfactant-derived amphiphilic carbon dots with tunable photoluminescence. *The Journal of Physical Chemistry C* 117 (47):24991–24996.

Krishna, A. S., C. Radhakumary, and K. Sreenivasan. 2013. In vitro detection of calcium in bone by modified carbon dots. *Analyst* 138 (23):7107–7111.

Li, H., Z. Kang, Y. Liu, and S. Lee. 2012. Carbon nanodots: Synthesis, properties and applications. *Journal of Materials Chemistry* 22 (46):24230–24253.

Li, H., J. Zhai, and X. Sun. 2011a. Sensitive and selective detection of silver(I) ion in aqueous solution using carbon nanoparticles as a cheap, effective fluorescent sensing platform. *Langmuir* 27 (8):4305–4308.

Li, H., J. Zhai, J. Tian, Y. Luo, and X. Sun. 2011b. Carbon nanoparticle for highly sensitive and selective fluorescent detection of mercury(II) ion in aqueous solution. *Biosensors and Bioelectronics* 26 (12):4656–4660.

Li, H., Y. Zhang, L. Wang, J. Tian, and X. Sun. 2011c. Nucleic acid detection using carbon nanoparticles as a fluorescent sensing platform. *Chemical Communications (Cambridge)* 47 (3):961–963.

Li, Q., T. Y. Ohulchanskyy, R. Liu et al. 2010. Photoluminescent carbon dots as biocompatible nanoprobes for targeting cancer cells in vitro. *The Journal of Physical Chemistry C* 114 (28):12062–12068.

Li, X., S. Zhang, S. A. Kulinich, Y. Liu, and H. Zeng. 2014. Engineering surface states of carbon dots to achieve controllable luminescence for solid-luminescent composites and sensitive Be^{2+} detection. *Scientific Reports* 4:4976–4983.

Downloaded by [João Leitão] at 08:46 30 August 2015

© 2016 by Taylor & Francis Group, LLC

Liu, H., T. Ye, and C. Mao. 2007. Fluorescent carbon nanoparticles derived from candle soot. *Angewandte Chemie (International ed. in English)* 46 (34):6473–6475.
Liu, J., J. Li, Y. Jiang et al. 2011. Combination of pi-pi stacking and electrostatic repulsion between carboxylic carbon nanoparticles and fluorescent oligonucleotides for rapid and sensitive detection of thrombin. *Chemical Communications (Cambridge)* 47 (40):11321–11323.
Liu, J. M., L. P. Lin, X. X. Wang et al. 2012. Highly selective and sensitive detection of Cu^{2+} with lysine enhancing bovine serum albumin modified-carbon dots fluorescent probe. *Analyst* 137 (11):2637–2642.
Liu, J. M., L. P. Lin, X. X. Wang et al. 2013. Zr($H_2$0)2EDTA modulated luminescent carbon dots as fluorescent probes for fluoride detection. *Analyst* 138 (1):278–283.
Liu, R., D. Wu, S. Liu et al. 2009. An aqueous route to multicolor photoluminescent carbon dots using silica spheres as carriers. *Angewandte Chemie (International ed. in English)* 48 (25):4598–4601.
Liu, X., N. Zhang, T. Bing, and D. Shangguan. 2014a. Carbon dots based dual-emission silica nanoparticles as a ratiometric nanosensor for Cu(2+). *Analytical Chemistry* 86 (5):2289–2296.
Liu, Y., Y. Zhao, and Y. Zhang. 2014b. One-step green synthesized fluorescent carbon nanodots from bamboo leaves for copper(II) ion detection. *Sensors and Actuators B: Chemical* 196:647–652.
Luo, P. G., S. Sahu, S. Yang et al. 2013. Carbon "quantum" dots for optical bioimaging. *Journal of Materials Chemistry B* 1 (16):2116–2127.
Mao, L., W. Tang, Z. Deng et al. 2014. Facile access to white fluorescent carbon dots toward light-emitting devices. *Industrial and Engineering Chemistry Research* 53 (15):6417–6425.
Mao, X. J., H. Z. Zheng, Y. J. Long et al. 2010. Study on the fluorescence characteristics of carbon dots. *Spectrochimica Acta. Part A, Molecular and Biomolecular Spectroscopy* 75 (2):553–557.
Mao, Y., Y. Bao, D. Han, F. Li, and L. Niu. 2012. Efficient one-pot synthesis of molecularly imprinted silica nanospheres embedded carbon dots for fluorescent dopamine optosensing. *Biosensors and Bioelectronics* 38 (1):55–60.
Nie, H., M. Li, Q. Li et al. 2014. Carbon dots with continuously tunable full-color emission and their application in ratiometric pH sensing. *Chemistry of Materials* 26 (10):3104–3112.
Peng, H. and J. Travas-Sejdic. 2009. Simple aqueous solution route to luminescent carbogenic dots from carbohydrates. *Chemistry of Materials* 21 (23):5563–5565.
Qu, Q., A. Zhu, X. Shao, G. Shi, and Y. Tian. 2012. Development of a carbon quantum dots-based fluorescent Cu^{2+} probe suitable for living cell imaging. *Chemical Communications (Cambridge)* 48 (44):5473–5475.
Qu, S., H. Chen, X. Zheng, J. Cao, and X. Liu. 2013. Ratiometric fluorescent nanosensor based on water soluble carbon nanodots with multiple sensing capacities. *Nanoscale* 5 (12):5514–5518.
Ruedas-Rama, M. J., J. D. Walters, A. Orte, and E. A. Hall. 2012. Fluorescent nanoparticles for intracellular sensing: A review. *Analytica Chimica Acta* 751:1–23.
Salinas-Castillo, A., M. Ariza-Avidad, C. Pritz et al. 2013. Carbon dots for copper detection with down and upconversion fluorescent properties as excitation sources. *Chemical Communications (Cambridge)* 49 (11):1103–1105.
Shan, X., L. Chai, J. Ma et al. 2014. B-doped carbon quantum dots as a sensitive fluorescence probe for hydrogen peroxide and glucose detection. *Analyst* 139 (10):2322–2325.

Downloaded by [João Leitão] at 08:46 30 August 2015

© 2016 by Taylor & Francis Group, LLC

Shen, L., L. Zhang, M. Chen, X. Chen, and J. Wang. 2013. The production of pH-sensitive photoluminescent carbon nanoparticles by the carbonization of polyethylenimine and their use for bioimaging. *Carbon* 55:343–349.

Shi, W., X. Li, and H. Ma. 2012. A tunable ratiometric pH sensor based on carbon nanodots for the quantitative measurement of the intracellular pH of whole cells. *Angewandte Chemie (International ed. in English)* 51 (26):6432–6435.

Shi, Y., Y. Pan, H. Zhang et al. 2014. A dual-mode nanosensor based on carbon quantum dots and gold nanoparticles for discriminative detection of glutathione in human plasma. *Biosensors and Bioelectronics* 56:39–45.

Song, Y., S. Zhu, S. Xiang et al. 2014. Investigation into the fluorescence quenching behaviors and applications of carbon dots. *Nanoscale* 6 (9):4676–4682.

Sun, W., Y. Du, and Y. Wang. 2010. Study on fluorescence properties of carbogenic nanoparticles and their application for the determination of ferrous succinate. *Journal of Luminescence* 130 (8):1463–1469.

Sun, Y., B. Zhou, Y. Lin et al. 2006. Quantum-sized carbon dots for bright and colorful photoluminescence. *Journal of the American Chemical Society* 128 (24):7756–7757.

Wang, C. I., A. P. Periasamy, and H. T. Chang. 2013. Photoluminescent C-dots@RGO probe for sensitive and selective detection of acetylcholine. *Analytical Chemistry* 85 (6):3263–3270.

Wang, Y., D. Gao, P. Zhang et al. 2014. A near infrared fluorescence resonance energy transfer based aptamer biosensor for insulin detection in human plasma. *Chemical Communications (Cambridge)* 50 (7):811–813.

Wei, W., C. Xu, J. Ren, B. Xu, and X. Qu. 2012. Sensing metal ions with ion selectivity of a crown ether and fluorescence resonance energy transfer between carbon dots and graphene. *Chemical Communications (Cambridge)* 48 (9):1284–1286.

Xu, B., C. Zhao, W. Wei et al. 2012. Aptamer carbon nanodot sandwich used for fluorescent detection of protein. *Analyst* 137 (23):5483–5486.

Xu, X., R. Ray, Y. Gu et al. 2004. Electrophoretic analysis and purification of fluorescent single-walled carbon nanotube fragments. *Journal of the American Chemical Society* 126 (40):12736–12737.

Yan, F., Y. Zou, M. Wang et al. 2014. Highly photoluminescent carbon dots-based fluorescent chemosensors for sensitive and selective detection of mercury ions and application of imaging in living cells. *Sensors and Actuators B: Chemical* 192:488–495.

Yang, X., Y. Luo, S. Zhu et al. 2014. One-pot synthesis of high fluorescent carbon nanoparticles and their applications as probes for detection of tetracyclines. *Biosensors and Bioelectronics* 56:6–11.

Yeh, T., C. Wang, and H. T. Chang. 2013. Photoluminescent C-dots@RGO for sensitive detection of hydrogen peroxide and glucose. *Talanta* 115:718–723.

Yu, C., X. Li, F. Zeng, F. Zheng, and S. Wu. 2013a. Carbon-dot-based ratiometric fluorescent sensor for detecting hydrogen sulfide in aqueous media and inside live cells. *Chemical Communications (Cambridge)* 49 (4):403–405.

Yu, C., Y. Wu, F. Zeng, and S. Wu. 2013b. A fluorescent ratiometric nanosensor for detecting NO in aqueous media and imaging exogenous and endogenous NO in live cells. *Journal of Materials Chemistry B* 1 (33):4152–4159.

Yuan, C., B. Liu, F. Liu, M. Y. Han, and Z. Zhang. 2014. Fluorescence "turn on" detection of mercuric ion based on bis(dithiocarbamato)copper(II) complex functionalized carbon nanodots. *Analytical Chemistry* 86 (2):1123–1130.

Zhang, L., H. Wei, F. Gao et al. 2013. Controllable synthesis of fluorescent carbon dots and their detection application as nanoprobes. *Nano-Micro Letters* 5 (4):247–259.

Downloaded by [João Leitão] at 08:46 30 August 2015

© 2016 by Taylor & Francis Group, LLC

Zhang, R. and W. Chen. 2014. Nitrogen-doped carbon quantum dots: Facile synthesis and application as a "turn-off" fluorescent probe for detection of Hg^{2+} ions. *Biosensors and Bioelectronics* 55:83–90.

Zhang, S., Q. Wang, G. Tian, and H. Ge. 2014. A fluorescent turn-off/on method for detection of $Cu^{2+}$and oxalate using carbon dots as fluorescent probes in aqueous solution. *Materials Letters* 115:233–236.

Zhao, H. X., L. Q. Liu, Z. D. Liu et al. 2011. Highly selective detection of phosphate in very complicated matrixes with an off-on fluorescent probe of europium-adjusted carbon dots. *Chemical Communications (Cambridge)* 47 (9):2604–2606.

Zhu, A., Z. Luo, C. Ding et al. 2014. A two-photon "turn-on" fluorescent probe based on carbon nanodots for imaging and selective biosensing of hydrogen sulfide in live cells and tissues. *Analyst* 139 (8):1945–1952.

Zhu, A., Q. Qu, X. Shao, B. Kong, and Y. Tian. 2012. Carbon-dot-based dual-emission nanohybrid produces a ratiometric fluorescent sensor for in vivo imaging of cellular copper ions. *Angewandte Chemie (International ed. in English)* 51 (29):7185–7189.

Zhu, H., X. Wang, Y. Li et al. 2009. Microwave synthesis of fluorescent carbon nanoparticles with electrochemiluminescence properties. *Chemical Communications (Cambridge)* (34):5118–5120.

Zhu, S., Q. Meng, L. Wang et al. 2013. Highly photoluminescent carbon dots for multicolor patterning, sensors, and bioimaging. *Angewandte Chemie (International ed. in English)* 52 (14):3953–3957.

Downloaded by [João Leitão] at 08:46 30 August 2015

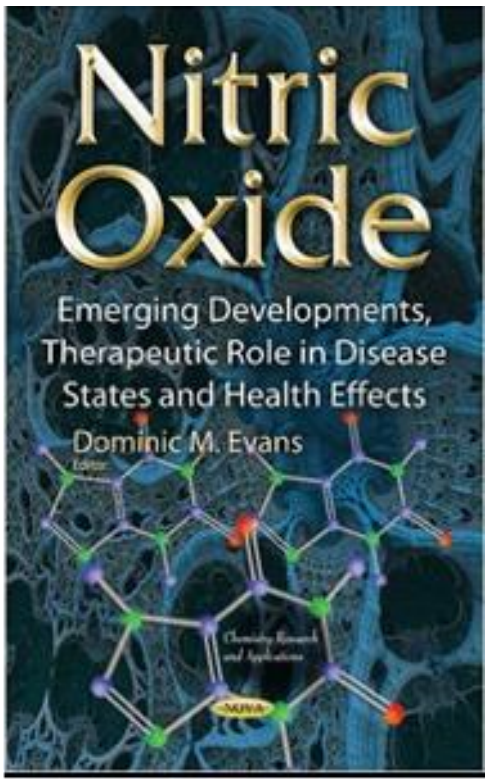
© 2016 by Taylor & Francis Group, LLC

Chapter 4

Nanomaterials for *in vivo* NO sensing

João M. M. Leitão, Eliana F. C. Simões, Joaquim C. G. Esteves da Silva

Book: “Nitric Oxide: Emerging developments, Therapeutic Role in Disease States and Health Effects”, Chapter 4, Dominic M. Evans Ed., Nova science publishers Inc., New York, United States of America (2015) Print ISBN 10 1634829611, ISBN 13 978-1634829618, eBook ISBN: 978-1-63483-016-4, Julho 2015



In this work the bibliographic research of the different nanomaterials applied in the construction of different kinds of electrochemical and optical nanosensors for *in vivo* NO sensing was done. The writing of the book chapter, was made together with Professor João M. M. Leitão under the supervision of Professor Joaquim C. G. Esteves da Silva.

In: Nitric Oxide
Editor: Dominic M. Evans
ISBN: 978-1-63482-961-8
© 2015 Nova Science Publishers, Inc.

Chapter 4

NANOMATERIALS FOR *IN VIVO* NO SENSING

João M. M. Leitão[1], Eliana F. C. Simões[2] and Joaquim C. G. Esteves da Silva[2*]
[1]Centro de Investigação em Química (CIQ), Faculty of Pharmacy, University of Coimbra, Polo das Ciências da Saúde, Coimbra, Portugal
[2]Centro de Investigação em Química (CIQ), Department of Chemistry and Biochemistry, Faculty of Sciences, University of Porto, Porto, Portugal

ABSTRACT

The *in vivo* NO sensing is of outstanding relevance for the comprehension of the diverse physiological and pathological process in which this species is involved. Nevertheless, *in vivo* NO sensing is a complex challenge due to its own physicochemical properties, antioxidant mechanisms and possible interferences. Some electrochemical and optical sensors have already been developed for *in vivo* NO sensing. Most of the electrochemical sensors are amperometric and most of the optical sensors are based on fluorescence. New materials are being developed for new NO electrochemical or optical sensors. Due to their intrinsic properties, the nanomaterials are one of the most promising emergent materials. This

* Corresponding Author address: Department of Chemistry and Biochemistry, Faculty of Sciences, University of Porto, Rua do Campo Alegre 687, Porto 4169-007, Portugal; Email:jcsilva@fc.up.pt.

Complimentary Contributor Copy

chapter review the most promising nanomaterials for the development of electrochemically or optical sensors for *in vivo* NO sensing.

Keywords: NO, *in vivo,* sensing, nanomaterials, optical, electrochemical

1. INTRODUCTION

In vivo sensing [1, 2] and *in vivo* imaging [3, 4] are emerging fields with outstanding relevance that attract the interest of investigators of different scientific fields. Their importance has to do with the *in situ* diagnostic, therapeutic evaluation or study of diverse biological processes in health and disease. An *in vivo* sensor is constituted by a recognition selective phase connected to a transduction element. When the recognition element phase is a biologically component the sensor is designated as a biosensor. Several sensors or biosensors were designed for the *in vitro* sensing. Beside all the characteristics of an *in vitro* sensor, as the sensitivity and selectivity, an *in vivo* sensor must be nontoxic, biocompatible and stable over the time in the biological environment with special and/or temporal resolution. The great progress in the development of *in vivo* sensing is the translation from the *in vitro* to the *in vivo* assays. Indeed some biological processes could not be reproduced or measured *in vitro*.

Nitric oxide (NO) is one of the main reactive oxygen and nitrogen species (ROS/RNS) and one of the more relevant biological molecules in order to understand several physiological or pathological processes. Indeed NO is involved in a variety of physiological and pathological process having a beneficial and injurious role in the human being depending of is concentration level [5, 6]. The *in vivo* sensing of NO allows understanding the physiological or pathological processes in which is involved. Even so the *in vivo* NO sensing is not straightforward due to is short half live, rapid diffusion, usually low concentrations and high reactivity [6-8]. Several analytical methodologies have been developed for their detection and/or quantification. The principal analytical methodologies proposed for their quantification are based on electron paramagnetic resonance (EPR), UV-Visible, electrochemical, quimioluminescence and fluorescence [7, 8]. Most of the developed NO sensors are optical or electrochemical and are essentially based in amperometric or fluorescence analytical techniques, respectively [9, 10].

The definition of nanomaterial focuses mainly on two properties, the size (any material within 1-100 nm) and the size-dependent properties of a given

Complimentary Contributor Copy

material [11, 12]. In the group of nanomaterials are included the different nanoallotropic forms of carbon as the fullerene forms [fullerene (FL), carbon nanotubes (CNT), graphene (GP), nano diamonds (ND) and carbon dots (CD), crystalline semiconductors nanoparticles (quantum dots, QD), metals, dioxide titanium, polymer and silica nanoparticles. Due to their intrinsic properties the nanomaterials are one of the most promising emergent materials for the development of *in vivo* electrochemical or optical sensors [1, 9, 13, 14]. In the development of electrochemical amperometric sensors they can be used as the electrode itself, as the nano matrix of an active recognition compound or they could facilitate the electron transference. In the development of optical fluorescence sensors they could be quite useful due to the high quantum yields, high photo stability, high Stokes shift, excitation and emission wavelengths in the visible range, narrow emission bands and tunable photo luminescent properties.

In this chapter a revision of the main nanomaterials used in the development of NO electrochemical and optical sensors is presented. It will focus on already developed *in vivo* NO sensors. This chapter is structured taking into consideration the class of nanomaterial in the basis of the literature described *in vivo* NO sensors.

2. Carbon Nanotubes

Carbon nanotubes (CNT) is one of the nanoallotropic forms of carbon with a nano cylindrical structure arranged in condensed aromatic rings of graphene that could be found as single wall (SWCNT) or multi wall (MWCNT), if they are formed respectively by one or more than one graphene sheet [15]. Even if the toxicity of CNT could be controversial due to their own physicochemical properties namely, their high length-to-diameter with a high large surface areas, high mechanical strength, chemical and thermal stability and high optical absorbance in the near infrared (NIR), the CNT is one of the most used nanomaterial in the electrochemical *in vivo* sensing but also in the *in vivo* imaging [16]. Based on MWCNT four electrochemical sensors [17-20] and based on SWCNT one optical sensor [21] were developed as *in vivo* NO sensors. In Table 1 are presented the principal analytical performance characteristics of the already developed *in vivo* NO sensors based CNT electrochemical and optical sensors.

Complimentary Contributor Copy

Table 1. Principal analytical performance characteristics of the developed *in vivo* NO electrochemical and optical CNT based sensors*

Ref.	LOD (μM)	LR (μM)	Sensitivity	Selectivity	Stability	Resolution (Spatial / Temporal)
Electrochemical						
[17]	0.025	0.25 - 1	1.72 nA/μM	Ascorbate; NO_2^-; Dopamine; DOPAC; H_2O_2; O_2	Stable	Limited
[18]	0.0076	0.019 - 54	1.73 μA/μM	Glucose; L-arginine; NO_2^-; Dopamine; L-cysteine; Uric acid; Ascorbic acid	Stable	---
[19]	0.0043	1 - 40	1.10 μA/μM	Glucose; L-arginine; Ascorbic acid; H_2O_2; O_2^-	Stable	---
[20]	0.028	0.22 - 120	0.25 μA/μM	L-arginine; NO_2^-; NO_3^-; Ascorbic acid; Dopamine; Several ions	Stable	---
Optical						
[21]	0.070	Exponential decay	---	$ONOO^-$; NO_2^-; NO_3^-; HNO; ClO^-; HO^-; H_2O_2	Stable	Spatial / Temporal

* Ref. – References; LOD – Limit of detection; LR – Linear range; DOPAC – 3,4-dihydroxyphe-nylacetic acid.

In two of the developed *in vivo* NO electrochemical sensors non functionalized MWCNT were immobilized in chitosan (CS) [17, 18]. In the first, hemin and MWCNT were linked to the CS by a cross-linking procedure using N-hidroxysuccinimide (NHS) / 1-[3-(Dimethylamino)propyl]-3-ethyl-carbodiimide methiodide (EDC methiodide). A posterior electrodeposition of the obtained CS film was done on the surface of a carbon fiber microelectrode. Based on the electrocatalytic reduction of NO by the hemin, locally applied exogenous NO was detected by this sensor in a rat brain by squarewave voltammetry (SWV) at a reduction potential of -0.850 V (vs. Ag/AgCl reference electrode) in the presence of oxygen [17]. In the other, MWCNT and Au nanoparticles (AuNPs) were dispersed in CS. The obtained suspension was then deposited on a modified glassy carbon electrode (GCE) and covered with a nafion solution. The NO release in mouse liver, spleen and kidneys was

Complimentary Contributor Copy

evaluated by amperometry at an oxidation potential +0.85 V (vs. saturated calomel reference electrode, SCE) [18].

In the other two electrochemical *in vivo* NO sensors MWCNT were previous functionalized [19, 20]. The first one was functionalized with poly-5,2':5',2''-terthiophene-3'-carboxylic acid (PTTCA) [19] and the other with azocarmine B (ACB) [20]. The functionalized PTTCA-MWCNT were placed in a GCE modified with an AuNPs film. After electrode modification, microperoxidase, catalase and superoxide dismutase enzymes were covalently immobilized in the PTTCA-MWCNT-AuNPs film by a NHS / 1-Ethyl-3-(3-dimethylaminopropyl)carbodiimide (EDC) cross-linking procedure. The microperoxidase enzyme was used as catalyst of the reduction of NO and the catalase and superoxide dismutase enzymes were used in order to eliminate the interferences respectively of the H_2O_2 and $O_2^{\cdot-}$. The released NO was evaluated in rat liver samples, in stomach and intestinal cancer cells by amperometry at a reduction potential of -0.8 V (vs. Ag/AgCl) [19]. The functionalized ACB-MWCNT was deposited in a GCE and the electro-polymerization of ACB was done by cyclic voltametry (CV). The obtained film of polyaxocarmine B-ACB-MWCNT was then covered with nafion. The determination of NO was done in rat liver cells amperometrically at an oxidation potential of + 0.75 V(vs. SCE) [20].

The only developed *in vivo* NO optical sensor based on carbon nanomaterials is a NIR fluorescent sensor able to overcome the auto fluorescence, the possible scattering of living tissues and capable of tissue penetration. The NO evaluation is based in the quenching of fluorescence of the NIR spectra of SWCNT covered with 3,4-diaminophenyl functionalized dextran (DAP-dex) at an excitation wavelength of 785 nm [21]. The NO determination was performed in stimulated macrophage cells and in the abdomen of a mouse after the injection of a NO standard solution. In Figure 1 is presented one example of the *in vivo* NO electrochemical sensing (a) and of the *in vivo* NO optical sensing (b) based in CNT previous described.

Four other NO sensors based in CNT were developed with potential for *in vivo* NO sensing [22-25]. The electrochemical sensors are based on imprinted functional polymer-MWCNT-CS [22], in tetrasulfonated nickel phthalo-cyanine functionalized-SWCNT [23] and the in hematite (α-Fe_2O_3)-CNT-CS [24]. A NIR fluorescence sensor is based in the functionalization of SWCNT with a specific DNA sequence of d(AT)15 oligonucleotides selective to NO [25].

Complimentary Contributor Copy

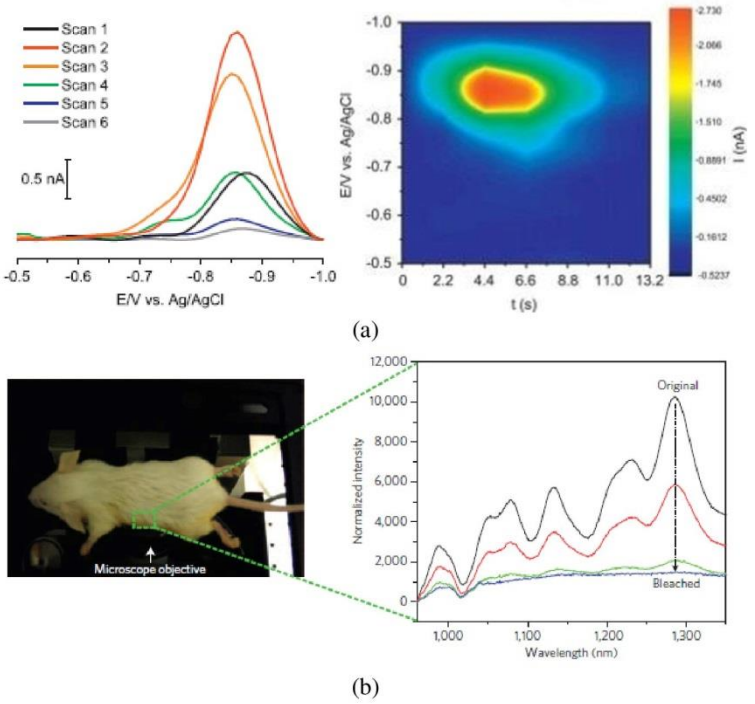


Figure 1. *In vivo* NO electrochemical sensing (a) by MWCNT-Hemin-CS electrodes in a rat brain (reproduced from reference [17] with permission from Elsevier) and *in vivo* NO optical sensing (b) by DAP-Dex-SWCNT in the abdomen of a mouse (reproduced from reference [21] with permission from the Nature Publishing Group).

3. GOLD NANOPARTICLES

The AuNPs, also known as colloidal gold, are generally spherical nanoparticles usually synthesized in solution. Beside the size, the AuNPs also could differ in shape and can be found as nanospheres, nanorods, nanocages, nanocubes, nanopolygons or even nanostars. They have size dependent optical properties, large surface to volume ratio, biocompatibility and low toxicity, which make them useful materials for *in vitro* or *in vivo* sensing and for imaging [26, 27]. Beside the already indicated based CNT sensors, *in vivo* NO detection is based in AuNPs. Also, as for the CNT *in vivo* NO sensors, most of

Complimentary Contributor Copy

the developed AuNPs sensors are electrochemical. Based on AuNPs, and beside the previous indicated electrochemical MWCNT-AuNPs based electrodes [18, 19], four other electrochemical sensors [28-31] and three optical sensors [32-34] were proposed. In Table 2 are presented the principal analytical performance characteristics of the already developed *in vivo* NO based AuNPs electrochemical and optical sensors.

Table 2. Principal analytical performance characteristics of the developed *in vivo* NO electrochemical and optical AuNPs based sensors*

Ref.	LOD (μM)	LR (μM)	Sensitivity	Selectivity	Stability	Resolution (Spatial / Temporal)
Electrochemical						
[28]	0.1	0.4 - 673.9	3.653 mA. cm^{-2}/mM	NO_2^-; Dopamine; Uric acid; Ascorbic acid	---	---
[29]	0.0072	0.036 – 43.2	0.04 μA/μM	Uric acid; several ions	Stable	---
[30]	0.0036	0.0072 - 18	0.56 nA/nM	NO_2^-; Uric acid; Dopamine; Ascorbic acid; Glucose; Cholesterol; L-valine; L-arginine	Stable	---
[31]	0.05	0.1 - 40	---	NO_2^-; NO_3^-; Ascorbic acid; Uric acid; Neurotransmitters	Stable	---
Optical						
[32]	R: 8	R: < 700	R: 0.56 $(\Delta R_0/R)$/ mM	R: NO_2^-; NO_3^-; Cl^-; O_2; H_2O_2; $O_2^{\cdot-}$; $ONOO^-$	R:Stable	R:---
	τ: 30	τ: < 500	τ: 3.9 [Δτ (ns)]/mM	τ: ---	τ:Stable	τ:---
[33]	20	< 1000	0.23 $(\Delta R_0/R)$/ mM	H_2O_2; $O_2^{\cdot-}$; $ONOO^-$	Stable	---
[34]	20	< 1000	0.19 $(\Delta I_0/I)$/ mM	NO_2^-; NO_3^-; O_2; N_2; Ascorbic acid; H_2O_2; $O_2^{\cdot-}$; $ONOO^-$	Stable	---

* Ref. – References; LOD – Limit of detection; LR – Linear range; R – Ratiometric sensor; R_0 – Ratio without NO; R – Ratio at each NO concentration;τ - Lifetime sensor.

Complimentary Contributor Copy

All of the developed *in vivo* NO electrochemical sensors based in AuNPs are amperometric [28-30]. In the first, Au and Pt nanoparticles were placed in a graphene paper electrode. The NO release in living cells were evaluated at an oxidation potential of + 0.75 V(vs. Ag/AgCl) [28]. In another, AuNPs and CS were deposited electrochemically at the surface of a GCE. The release of NO was then evaluated an oxidation potential of +0.85 V (vs. SCE) in rat kidney [29]. AuNPs were deposited in quartz fiber electrode, niacinamide (NA) was electropolymerized above the AuNPs film and posterior coated with nafion. The NO release from a mice liver were done at an oxidation potential of +0.65 V (vs. Ag/AgCl) [30]. In the last electrochemical sensor AuNPs were deposited at a surface of a Pt electrode and then coated with nafion. The NO release from smooth muscle cells was evaluated at an oxidation potential of + 0.74 V (vs. SCE) by differential pulse amperometry [31].

All of the developed *in vivo* NO optical sensors based in AuNPs are based in the fluorescence quenching by NO of a fluorophore previous linked to the heme protein cytochrome c (Cyt-c) highly selective to NO [32-34]. Based in these labeled Cyt-c optical fiber sensors were developed. The AuNPs were used for the attachment of the fluorophore labeled Cyt-c to the optical fibers. By the same authors the fluorophores used were the 4-carboxy-2',7'-difluorofluorescein, succinimidyl ester (Oregon Green 488 carboxylic acid, succinimidyl ester) [32, 33] and 4-carboxy-3,5,6 trifluoro-2',7'-difluorofluorescein, succinimidyl ester (Oregon Green 514 carboxylic acid, succinimidyl ester) [34]. Of the developed optical fiber sensors two are fluorescence ratiometric sensors [32, 33], one is a fluorescence lifetime sensor [32] and, the last one, a single fluorescence intensity determination at maximum fluorescence intensity [34]. For the developed fluorescence ratiometric sensors the detection of NO was done at an excitation wavelength of 488 nm and emission wavelengths of 540 and 545 nm. As fluorescence intensity reference, in the development of these fluorescence ratiometric sensors, it was used a fluorescent carboxylate-modified polystyrene nanospheres with a similar excitation wavelength of the fluorophore used (488 nm) and emission wavelength of 685 nm. For the developed fluorescence lifetime sensor, at an excitation of 488 nm, the lifetime was evaluated at an emission wavelength of 580 nm. The single fluorescence intensity evaluation was done at an emission wavelength of 640 nm and excitation of 530 nm. The NO extracellular release in macrophage cells was performed by the developed single fluorescence intensity and fluorescence ratiometric optical fiber sensors. Also the NO intracellular release in the cytoplasm was done by the developed optical fiber fluorescence lifetime sensor. In Figure 2 is presented one example

Complimentary Contributor Copy

of the *in vivo* NO electrochemical sensing (a) and of the *in vivo* NO optical sensing (b) based in AuNPs previous described.

Some electrochemical amperometric sensors based in AuNPs were also developed for the *in vitro* sensing [35-37]. In the first one, hemoglobin is adsorbed with AuNPs [35], in another AuNPs were assembled with a sol-gel film [36] and, in the last electrochemical sensor, AuNPs were assembled in toluene/water interfaces [37].

4. QUANTUM DOTS

The QD are crystalline semiconductor nanoparticles usually constituted by CdTe, CdSe, CdS, ZnS, CdTe/CdS, CdSe/CdS or CdSe/ZnS. They have a high fluorescence, narrow emission bands, large absorption spectra, large stokes shift, fluorescence tunable size, high surface to volume ratio and they are photostable. Also, varying the QD composition, it is possible to obtain NIR fluorescence emission using for example PbS, PbSe and InAs QD. Because of their composition some toxicity issues were posed. Due to their own optical properties they are essentially used for the optical fluorescence sensing and for imaging [38]. All of the developed NO sensors are based on fluorescence detection [39-50].

Only two of the developed sensors were used for *in vivo* NO sensing [39, 40]. Both sensors are based on a fluorescence quenching mechanism. In the first sensor, CdSe QD were encapsulated in modified hyperbranched polyether (mHP) nanospheres. Also, diazeniumdiolates (NO donors) were linked to the mHP-CdSe QD. The detection of the NO release in mouse fibroblast cells was done by the fluorescence quenching of NO donor-mHP-CdSe QD induced by the NO at an excitation wavelength of 480 nm with a charge coupled device (CCD) detector [39]. In the other sensor, CdTe QD were incorporated in carboxymethyl CS (CMCS). Beside the obtained CMCS-CdTe QDs, diazeniumdiolates (NO fluorescence probes) or O^2-substituted diazenium-diolates (NO donors) were linked to the obtained CMCS-CdTe QD. The detection of the NO release by porcine iliac endothelial cells was performed by the fluorescence quenching of NO donor-CMCS-CdTe QD induced by the NO. A Stern-Volmer fluorescence quenching modelling was done using an excitation wavelength of 400 nm and emission of 560 nm with a linear range below 768 μM [40]. In Figure 3 is presented one example of the *in vivo* NO optical sensing (b) based in QD.

Complimentary Contributor Copy

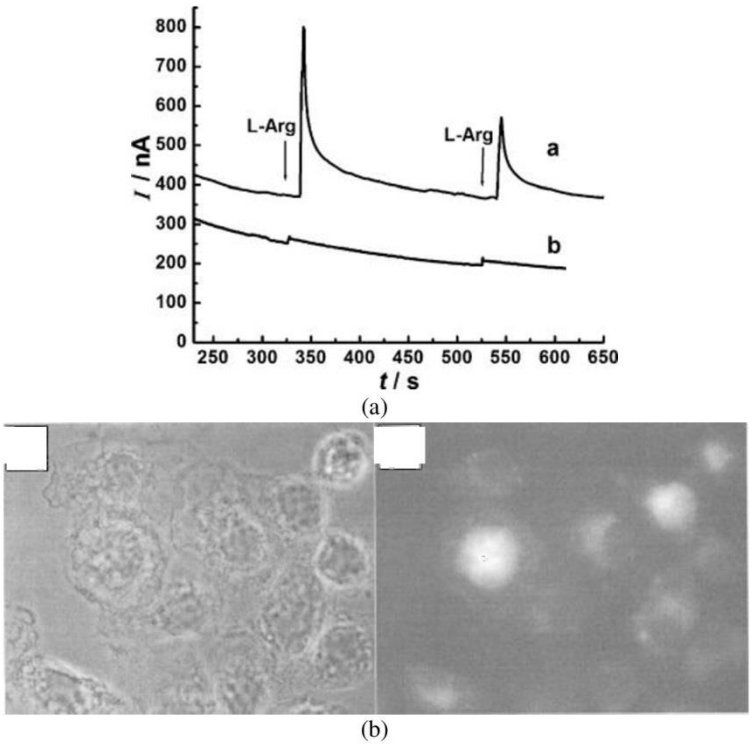


Figure 2. *In vivo* NO electrochemical sensing (a) by AuNPs-NA-Nafion electrode in a mice liver (reproduced from reference [30] with permission from Elsevier) and *in vivo* NO optical sensing (b) in macrophages cells by fluorophore labeled Cyt-c (reproduced from reference [32] with permission from the American Chemical Society).

Most of the developed NO optical sensors have potential to be used for *in vivo* NO sensing [41-50]. These are based in CdTe [44], CdSe [42, 43, 46, 49, 50] or in CdSe/ZnS QD [41, 45, 47, 48]. The response of these sensors is the fluorescence quenching induced by NO [42-47, 49]. Only for the CdSe QD [50] and CdSe/ZnS [41, 48] based sensors, a fluorescence enhancement is observed after quenching by a fluorescence resonance energy transfer (FRET) mechanism.

For the CdTe QD based sensor, the QD were dispersed in a poly(N-isopropylacrylamide) (PNIPAM) hybrid nanogel and diazeniumdiolates (NO donors) were posterior linked to the PNIPAM-CdTe QD [44]. For those

Complimentary Contributor Copy

sensors based on CdSe QD, and in order to stabilize the QD, they were immobilized in CS [42, 46]. In one of them, mercaptosuccinic acid (MSA) was linked to the CS-CdSe QD [42]. The other two were functionalized with triethanolamine (TEA) [49] and trivalent metalloporphyrins [50]. Also, a CdSe QD based optical fiber sensor uses cellulose as sensitive membrane [43]. In two of the developed NO optical sensors based on CdSe/ZnS QD they were dispersed in a polymethacrylate film after stabilization by hexadeylamine [45] and in an organic/inorganic hybrid organogels [47]. In the other two the CdSe/ZnS QD were functionalized with similar ferric dithiocarbamate compounds [41, 48].

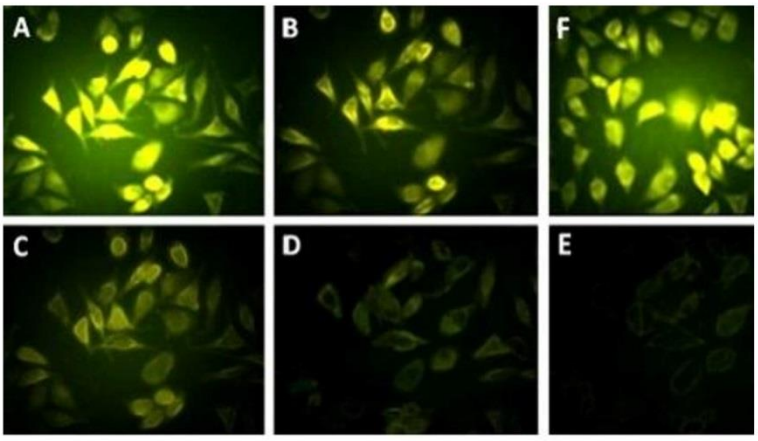


Figure 3. *In vivo* NO optical sensing in culture cells by a NO donor-CMCS-CdTe QD (reproduced from reference [40] with permission from Elsevier).

5. Other Nanomaterials

Beside the already indicated nanomaterials, others were also used for the *in vivo* sensing and/or imaging of NO. The most common nanomaterials families are metal oxides, carbon, silica and polymeric nanoparticles [11, 12]. The nanomaterials already used for the NO sensing are the metal oxide nanoparticles [51-54], silicon [55] and the different nanoallotropic forms of carbon [56, 57]. An *in vivo* NO electrochemical sensor [51] based in Al_2O_3

Complimentary Contributor Copy

nanoparticles (Al_2O_3NPs) and an *in vivo* NO optical sensor [56] based in CD were developed.

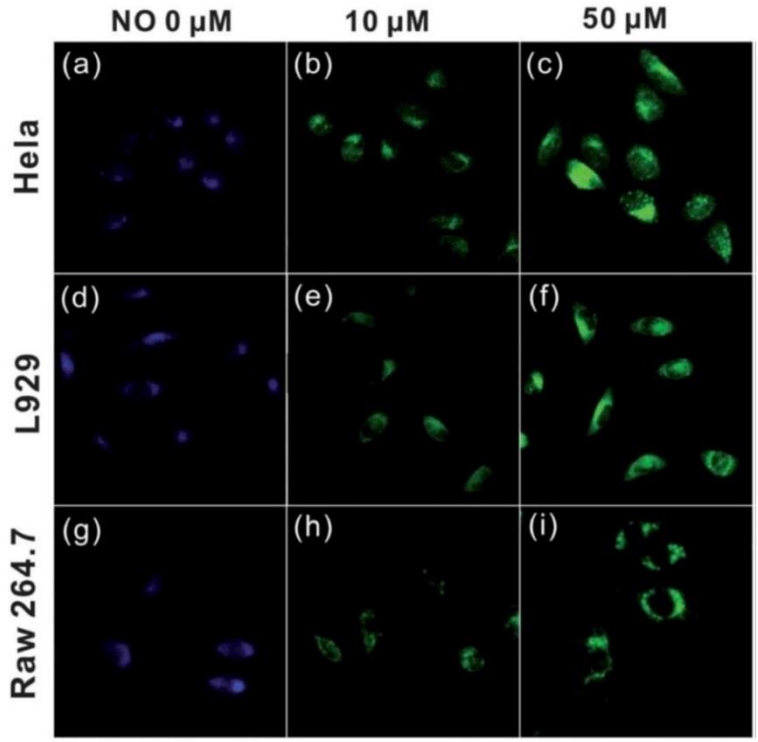


Figure 4. *In vivo* NO optical sensing by NOPD-CD in culture cells (reproduced from reference [56] with permission from the Royal Society of Chemistry).

In the developed *in vivo* NO electrochemical sensor an Al_2O_3NPs film was deposited at the surface of a GCE. With this electrode the detection of NO was achieved with a linear range of 0.04 – 210 μM, sensitivity of 0.037 μA/μM and a LOD of 7.2 nM. The NO detection in rat lung was done at an oxidation potential of + 0.69 V (vs. SCE) by amperometry [51]. In the developed *in vivo* NO optical sensor the CD were functionalized with naphthalimide with an o-phenylenediamine group (NOPD) by N-hydroxysulfosuccinimide sodium salt (Sulfo-NHS) / EDC cross-linking procedure. The fluorescence ratiometric NO

Complimentary Contributor Copy

sensing based in a FRET mechanism was done at an excitation wavelength of 370 nm and emission wavelengths of 455 and 535 nm. In the presence of NO there is a decrease of maximum fluorescence intensity at 455 nm and an increase at 535 nm. The ratio of maximum fluorescence intensity at 535 nm and 455 nm was evaluated in order to NO concentration. A detection limit of 3 nM with selectivity to NO_2^-; NO_3^-; ClO^-; $OH^·$; H_2O_2; $^1O_2$ and ascorbic acid was evaluated. The detection of NO was done at different culture cells [56]. In Figure 4 is presented the *in vivo* NO optical sensing (b) based in CD previous described.

Mostly of the already developed *in vitro* NO sensors with potential for the *in vivo* NO sensing are amperometric electrochemical sensors [24,52-54,57]. Only one of these *in vitro* sensors is a fluorescence optical sensor [55]. The electrochemical sensors were based in Al_2O_3NPs modified with electropolymerized metallo 4′, 4″, 4‴, 4⁗tetra-amine phthalocyanine (poly-MTAPc) covered with nafion [52], in α-Fe_2O_3 nanoparticles (α-Fe_2O_3NPs) alone [53] or with CNT [24] embedded in a CS matrix, in SnO_2 nanoparticles (SnO_2NPs) film in which were immobilized Cyt-c and hemoglobin (Hb) [54] and in a GP nanosheet- hexadecyltrimethylammonium bromide (CTAB) / Hb-CS nanocomposite film [57]. The NO optical sensor was based in the fluorescence enhancement of silicon nanowires (SiNWs) functionalized with reduced fluoresceinamine [55].

CONCLUSION/PERSPECTIVES

The majority of the developed NO sensors based in nanomaterials are for *in vitro* determinations. The *in vivo* nanomaterials based NO sensors uses mainly carbon nanotubes and gold nanoparticles but, also, quantum dots, Al_2O_3 nanoparticles and carbon dots. Almost all the electrochemical sensors are amperometric sensors mainly based in the oxidation of NO. The fluorescent sensors are mainly based in the quenching induced by the NO.

Taking into consideration the characteristics of the nanomaterials under development and the enormous investment in their research, particularly in non toxic/biocompatible nanoparticles and in their functionalization, it is expected that nanomaterials could be increasingly used in the development of *in vivo* NO electrochemical or optical sensors with improved performances.

Complimentary Contributor Copy

ACKNOWLEDGMENTS

Financial support from Fundação para a Ciência e Tecnologia (FCT, Lisbon) project PEST and a PhD grant to Eliana Simões SFRH/BD/ 81074/2011 is acknowledged.

REFERENCES

[1] Eckert, M.A., et al., Novel molecular and nanosensors for in vivo sensing. *Theranostics,* 2013. *3*(8): p. 583-94.
[2] Wilson, G.S. and M.A. Johnson, In-Vivo Electrochemistry: What Can We Learn about Living Systems? C*hemical Reviews,* 2008. *108*(7): p. 2462-2481.
[3] Wessels, J.T., et al., Advances in cellular, subcellular, and nanoscale imaging in vitro and *in vivo. Cytometry* A, 2010. *77*(7): p. 667-76.
[4] Rao, J., A. Dragulescu-Andrasi, and H. Yao, Fluorescence imaging in vivo: recent advances. *Current Opinion in Biotechnology*, 2007. *18*(1): p. 17-25.
[5] Paolo, S., Nitric Oxide in Human Health and Disease. *eLS,* 2013.
[6] Toledo, J.C., Jr. and O. Augusto, Connecting the chemical and biological properties of nitric oxide. *Chem Res Toxicol,* 2012. *25*(5): p. 975-89.
[7] Hetrick, E.M. and M.H. Schoenfisch, Analytical chemistry of nitric oxide. *Annu Rev Anal Chem* (Palo Alto Calif), 2009. *2*: p. 409-33.
[8] Yao, D., A.G. Vlessidis, and N.P. Evmiridis, Determination of Nitric Oxide in Biological Samples. *Microchimica Acta,* 2004. *147*(1-2).
[9] Xu, T., et al., Electrochemical Sensors for Nitric Oxide Detection in Biological Applications. *Electroanalysis,* 2014. *26*(3): p. 449-468.
[10] McQuade, L.E. and S.J. Lippard, Fluorescent probes to investigate nitric oxide and other reactive nitrogen species in biology (truncated form: fluorescent probes of reactive nitrogen species). *Curr Opin Chem Biol,* 2010. *14*(1): p. 43-9.
[11] Zamborini, F.P., L. Bao, and R. Dasari, Nanoparticles in measurement science. *Anal Chem,* 2012. *84*(2): p. 541-76.
[12] Valentini, F. and G. Palleschi, Nanomaterials and Analytical Chemistry. *Analytical Letters,* 2008. *41*(4): p. 479-520.

Complimentary Contributor Copy

[13] Zhu, C., et al., Electrochemical Sensors and Biosensors Based on Nanomaterials and Nanostructures. *Analytical Chemistry,* 2015. *87*(1): p. 230-249.
[14] Ruedas-Rama, M.J., et al., Fluorescent nanoparticles for intracellular sensing: a review. *Anal Chim Acta,* 2012. *751*: p. 1-23.
[15] Moradi, O., et al., Carbon Nanotubes: A Review of Chemistry Principles and Reactions. *Fullerenes, Nanotubes and Carbon Nanostructures,* 2012. *20*(2): p. 138-151.
[16] Liu, Z., et al., Carbon Nanotubes in Biology and Medicine: In vitro and in vivo Detection, Imaging and Drug Delivery. *Nano Res,* 2009. *2*(2): p. 85-120.
[17] Santos, R.M., et al., Biomimetic sensor based on hemin/carbon nanotubes/chitosan modified microelectrode for nitric oxide measurement in the brain. *Biosens Bioelectron,* 2013. *44*: p. 152-9.
[18] Deng, X., F. Wang, and Z. Chen, A novel electrochemical sensor based on nano-structured film electrode for monitoring nitric oxide in living tissues. *Talanta,* 2010. *82*(4): p. 1218-24.
[19] Abdelwahab, A.A., et al., A selective nitric oxide nanocomposite biosensor based on direct electron transfer of microperoxidase: removal of interferences by co-immobilized enzymes. *Biosens Bioelectron,* 2010. *26*(3): p. 1080-6.
[20] Zheng, D., et al., Noncovalently functionalized water-soluble multiwall-nanotubes through azocarmine B and their application in nitric oxide sensor. *Electrochemistry Communications,* 2008. *10*(1): p. 90-94.
[21] Kim, J.-H., et al., The rational design of nitric oxide selectivity in single-walled carbon nanotube near-infrared fluorescence sensors for biological detection. *Nat Chem,* 2009. *1*(6): p. 473-481.
[22] Zhao, L., S. Zhu, and J. Zhou, A novel amperometric nitric oxide sensor based on imprinted microenvironments for controlling metal coordination. *Sensors and Actuators B: Chemical,* 2012. 171-172: p. 563-571.
[23] Porras Gutierrez, A., et al., Hybrid Materials from Carbon Nanotubes, Nickel Tetrasulfonated Phthalocyanine and Thin Polymer Layers for the Selective Electrochemical Activation of Nitric Oxide in Solution. *Electroanalysis,* 2009. *21*(21): p. 2303-2310.
[24] Gong, J., et al., Bifunctional sensor of nitric oxide and oxygen based on hematite nanotubes embedded in chitosan matrix. *Electrochemistry Communications,* 2008. *10*(9): p. 1222-1225.

Complimentary Contributor Copy

[25] Zhang, J., et al., Single Molecule Detection of Nitric Oxide Enabled by d(AT)15 DNA Adsorbed to Near Infrared Fluorescent Single-Walled Carbon Nanotubes. *Journal of the American Chemical Society,* 2011. *133*(3): p. 567-581.

[26] Zhang, X., Gold Nanoparticles: Recent Advances in the Biomedical Applications. Cell Biochem Biophys, 2015.

[27] Yeh, Y.C., B. Creran, and V.M. Rotello, Gold nanoparticles: preparation, properties, and applications in bionanotechnology. *Nanoscale,* 2012. *4*(6): p. 1871-80.

[28] Zan, X., et al., Freestanding graphene paper decorated with 2D-assembly of Au@Pt nanoparticles as flexible biosensors to monitor live cell secretion of nitric oxide. *Biosens Bioelectron,* 2013. *49*: p. 71-8.

[29] Wang, F., et al., Nitric oxide measurement in biological and pharmaceutical samples by an electrochemical sensor. *Journal of Solid State Electrochemistry,* 2011. *15*(4): p. 829-836.

[30] Dang, X., et al., Gold nanoparticle film grown on quartz fiber and its application as a microsensor of nitric oxide. Sensors and Actuators B: Chemical, 2011. *160*(1): p. 260-265.

[31] Zhu, M., et al., Novel nitric oxide microsensor and its application to the study of smooth muscle cells. *Analytica Chimica Acta,* 2002. *455*(2): p. 199-206.

[32] Barker, S.L.R., et al., Ratiometric and Fluorescence-Lifetime-Based Biosensors Incorporating Cytochrome c ' and the Detection of Extra- and Intracellular Macrophage Nitric Oxide. *Analytical Chemistry,* 1999. *71*(9): p. 1767-1772.

[33] Barker, S.L.R. and R. Kopelman, Development and Cellular Applications of Fiber Optic Nitric Oxide Sensors Based on a Gold-Adsorbed Fluorophore. *Analytical Chemistry,* 1998. *70*(23): p. 4902-4906.

[34] Barker, S.L.R., et al., Fiber-Optic Nitric Oxide-Selective Biosensors and Nanosensors. *Analytical Chemistry,* 1998. *70*(5): p. 971-976.

[35] Xu, Y., C. Hu, and S. Hu, A reagentless nitric oxide biosensor based on the direct electrochemistry of hemoglobin adsorbed on the gold colloids modified carbon paste electrode. S*ensors and Actuators B: Chemical,* 2010. *148*(1): p. 253-258.

[36] Kannan, P. and S.A. John, Highly sensitive electrochemical determination of nitric oxide using fused spherical gold nanoparticles modified ITO electrode. *Electrochimica Acta,* 2010. *55*(10): p. 3497-3503.

Complimentary Contributor Copy

[37] Li, Y.-J., et al., Large-scale self-assembly of hydrophilic gold nanoparticles at oil/water interface and their electro-oxidation for nitric oxide in solution. *Journal of Electroanalytical Chemistry,* 2008. *622*(1): p. 103-108.
[38] Kairdolf, B.A., et al., Semiconductor quantum dots for bioimaging and biodiagnostic applications. *Annu Rev Anal Chem (Palo Alto Calif),* 2013. *6*: p. 143-62.
[39] Liu, S., et al., Quantum dots-hyperbranched polyether hybrid nanospheres towards delivery and real-time detection of nitric oxide. *Mater Sci Eng C Mater Biol Appl,* 2014. *45*: p. 37-44.
[40] Tan, L., et al., Novel quantum dots-carboxymethyl chitosan nanocomposite nitric oxide donors capable of detecting release of nitric oxide in situ. *Acta Biomater,* 2012. *8*(10): p. 3744-53.
[41] Sun, J., et al., Fluorescence turn-on detection of gaseous nitric oxide using ferric dithiocarbamate complex functionalized quantum dots. *Anal Chem,* 2014. *86*(12): p. 5628-32.
[42] Simoes, E.F., J.M. Leitao, and J.C. Esteves da Silva, NO Fluorescence Quantification by Chitosan CdSe Quantum Dots Nanocomposites. *J Fluoresc,* 2013.
[43] Ding, L., et al., A sensitive optic fiber sensor based on CdSe QDs fluorophore for nitric oxide detection. *Sensors and Actuators B: Chemical,* 2013. *185*: p. 70-76.
[44] Tan, L., A. Wan, and H. Li, Quantum dots-poly(N-isopropylacrylamide) hybrid nanogel diazeniumdiolates as donors and real-time probes of nitric oxide. *Materials Chemistry and Physics,* 2013. *138*(2-3): p. 956-962.
[45] Fabregat, V., et al., Quantum dot–polymethacrylate composites for the analysis of NOx by fluorescence spectroscopy. *Inorganica Chimica Acta,* 2012. *381*: p. 212-217.
[46] Tan, L., et al., Biocompatible quantum dots–chitosan nanocomposites for fluorescence detection of nitric oxide. *Materials Chemistry and Physics,* 2012. *134*(2–3): p. 562-566.
[47] Wadhavane, P.D., et al., Organogel–quantum dots hybrid materials displaying fluorescence sensitivity and structural stability towards nitric oxide. *Soft Matter,* 2012. *8*(16): p. 4373.
[48] Wang, S., M.-Y. Han, and D. Huang, Nitric Oxide Switches on the Photoluminescence of Molecularly Engineered Quantum Dots. *Journal of the American Chemical Society,* 2009. *131*(33): p. 11692-11694.

Complimentary Contributor Copy

[49] Yan, X.Q., et al., Fluorescence sensing of nitric oxide in aqueous solution by triethanolamine-modified CdSe quantum dots. *Luminescence,* 2009. *24*(4): p. 255-9.

[50] Ivanisevic, A., et al., Photoluminescent Properties of Cadmium Selenide in Contact with Solutions and Films of Metalloporphyrins: Nitric Oxide Sensing and Evidence for the Aversion of an Analyte to a Buried Semiconductor−Film Interface. *Journal of the American Chemical Society,* 2000. *122*(15): p. 3731-3738.

[51] He, Q., D. Zheng, and S. Hu, Development and application of a nano-alumina based nitric oxide sensor. *Microchimica Acta,* 2008. *164*(3-4): p. 459-464.

[52] Yap, C.M., G.Q. Xu, and S.G. Ang, Amperometric nitric oxide sensor based on nanoporous platinum phthalocyanine modified electrodes. *Anal Chem,* 2013. *85*(1): p. 107-13.

[53] Zhang, L., et al., Direct electrocatalytic oxidation of nitric oxide and reduction of hydrogen peroxide based on alpha-Fe2O3 nanoparticles-chitosan composite. *Talanta,* 2010. *82*(1): p. 196-201.

[54] Topoglidis, E., et al., Direct Electrochemistry and Nitric Oxide Interaction of Heme Proteins Adsorbed on Nanocrystalline Tin Oxide Electrodes. *Langmuir,* 2003. *19*(17): p. 6894-6900.

[55] Miao, R., et al., Modified silicon nanowires: a fluorescent nitric oxide biosensor with enhanced selectivity and stability. *Journal of Materials Chemistry,* 2012. *22*(8): p. 3348.

[56] Yu, C., et al., A fluorescent ratiometric nanosensor for detecting NO in aqueous media and imaging exogenous and endogenous NO in live cells. *Journal of Materials Chemistry* B, 2013. *1*(33): p. 4152.

[57] Wen, W., et al., A highly sensitive nitric oxide biosensor based on hemoglobin–chitosan/graphene–hexadecyltrimethylammonium bromide nanomatrix. *Sensors and Actuators B: Chemical,* 2012. *166-167*: p. 444-450.

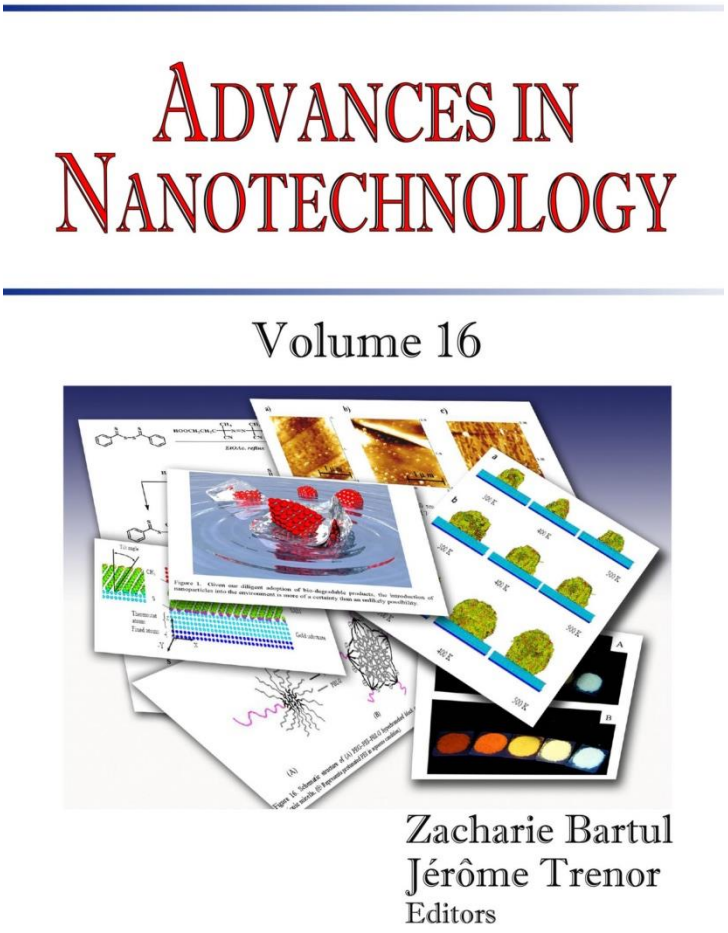
Complimentary Contributor Copy

Chapter 5

Reactive Oxygen/Nitrogen Species Nanoprobes

Eliana F. C. Simões, João M.M. Leitão, Joaquim C.G. Esteves da Silva

Book: Advances in Nanotechnology. Volume 16, Chapter 3, Zacharie Bartul and Jérôme Trenor, Nova Science Publishers Inc., New York. United States of America (2016) ISBN: 978-1-63485-961-5.



In this work the bibliographic research of the different nanomaterials applied in the construction of the main electrochemical and optical nanosensors for ROS/RNS sensing was done. The writing of the book chapter, was made together with Professor João M. M. Leitão under the supervision of Professor Joaquim C. G. Esteves da Silva.

In: Advances in Nanotechnology. Volume 16 ISBN: 978-1-63485-961-5
Editors: Z. Bartul and J. Trenor © 2016 Nova Science Publishers, Inc.

Chapter 3

REACTIVE OXYGEN/NITROGEN SPECIES NANOPROBES

Eliana F. C. Simões[1], João M. M. Leitão[2], and Joaquim C. G. Esteves da Silva[1*]

[1]Centro de Investigação em Química (CIQ), Faculty of Sciences, University of Porto, Porto, Portugal
[2]Centro de Investigação em Química (CIQ), Faculty of Pharmacy, University of Coimbra, Polo das Ciências da Saúde, Coimbra, Portugal

ABSTRACT

Reactive oxygen and nitrogen species (ROS/RNS) are a group of biological substances involved in a variety of physiological and pathological processes. They are easily inter-convert and can easily react with several biological molecules causing changes in the structure and function of cellular components. Even if their determination is of particular interest their detection *in vivo* it's not straightforward and is a continuous challenging due to their short half live, low concentrations, antioxidant mechanisms and interferences. Several analytical methodologies have been proposed for their detection and/or quantification. The majority of these analytical methodologies are electrochemical and optical methodologies.

* Corresponding Author address: Department of Geosciences, Environment and Spatial Planning, Faculty of Sciences, University of Porto, Rua do Campo Alegre 687, Porto 4169-007, Portugal; Email:jcsilva@fc.up.pt.

Complimentary Contributor Copy

Attending to their own specific physical and chemical properties, the nanomaterials becomes to be one of the most promising emerging materials for developing electrochemical or optical sensors or biosensors. Beside their unique own properties, they possess the ability to be "loaded" with a vast variety of molecules, which allows that a significant great number of applications in therapeutic and diagnostic could be developed. Nanomaterials based in carbon as the carbon nanotubes (CNT) or carbon dots (CDs), semiconductor quantum dots (QDs), magnetic, gold (AuNPs) and silver (AgNPs) nanoparticles, and have been extensively investigated for their use as ROS/RNS nanoprobes. This chapter review the most promising nanomaterials for the development of electrochemically or optical sensors for the ROS/RNS electrochemical or optical sensing.

Keywords: reactive oxygen species, reactive nitrogen species, electrochemical sensing, optical sensing, nanoprobes.

1. INTRODUCTION

Reactive oxygen species (ROS) and reactive nitrogen species (RNS) plays a dual role in biological systems. They can be beneficial but can also be injurious in the human being depending of is concentration level [1, 2]. At high concentrations ROS/RNS are directly related with some diseases such as, inflammatory processes, some infections, arteriosclerosis, cancer, age-dependent diseases like neurodegenerative diseases and others. ROS/RNS detection allows to understand several physiological or pathological processes in which they are involved and the possible detection and prevention of diseases [2, 3]. The detection and quantification of these reactive species is not straightforward because they usually are present at low concentrations levels, have high reactivity, short lifetimes, rapid diffusion, possible antioxidants mechanisms and potential interferences in biological media. The main ROS are oxygen (O_2), hydrogen peroxide (H_2O_2), superoxide ion ($O_2^{\bullet-}$), hydroxyl radicals ($^{\bullet}OH$), hypoclorous acid (HClO) and the main RNS are nitric oxide (NO) and peroxynitrite ($ONOO^-$). A variety of analytical methodologies have been developed for their detection and/or quantification. The electrochemical sensors are essentially based in amperometry [4, 5] and the optical sensors and are essentially based in fluorescence analytical techniques [6, 7].

Nanomaterials have become a priority for the scientific research and technological development with particular interest in the areas of health

Complimentary Contributor Copy

sciences as a vehicle for transport of drugs and diagnosis. The definition of nanomaterial focuses mainly on two properties, the size (any material between 1-100 nm in size) and the size-dependent properties of a given material [8, 9]. Due to their own specific physical and chemical properties, the nanomaterials are one of the most promising emergent materials for the development of *in vivo* electrochemical or optical sensors [10-13]. In the group of nanomaterials are included the different nanoallotropic forms of carbon as the fullerene forms, carbon nanotubes (CNT), graphene (GP), nano diamonds (ND) and carbon dots (CDs), gold (AuNPs) and silver nanoparticles (AgNPs), crystalline semiconductors NPs (quantum dots, QDs), metals, dioxide titanium, polymer and silica NPs.

Of the different nanoallotropic forms of carbon the CNT and the CDs are the most used in the development of electrochemical or optical sensors. The CNT are one of the nanoallotropic forms of carbon with a nano cylindrical structure arranged in condensed aromatic rings of GP that could be found as single wall (SWCNT) or multi wall (MWCNT) if they are formed respectively by one or more than one GP sheet [14]. They have physical and chemical properties that allow to predict their behavior, which would ultimately make them more useful for possible nanosensors. Even if the toxicity of CNT could be controversial due to their own physicochemical properties namely their high length-to-diameter with a high large surface areas, high mechanical strength, chemical and thermal stability and high optical absorbance in the near infrared (NIR), the CNT is one of the most used nanomaterial in the electrochemical *in vivo* sensing but also in the *in vivo* imaging [15]. The CDs have been proven to exhibit a lot of advantages, including nontoxicity, biocompatibility, hydrophilicity, and no photobleaching [16]. Due to their high quantum yields, high photostability, high Stokes shift, excitation and emission wavelengths in the visible range, narrow emission bands and tunable photo luminescent properties they could be applied in the development of optical fluorescence sensors [17]. In the development of electrochemical amperometric sensors they can be used as the electrode itself, as the nano matrix of an active recognition compound, or they could facilitate the electron transference.

QDs are crystalline semiconductor NPs with high fluorescence, narrow emission bands, large absorption spectra, large stokes shift, fluorescence tunable size, high surface to volume ratio and are photostable. Most of them are constituted by CdTe, CdSe, CdS, ZnS, CdTe/CdS, CdSe/CdS or CdSe/ZnS. Some problems related with toxicity were detected because of their composition, mainly due to cadmium. Even so the functionalization with other

Complimentary Contributor Copy

compounds allows to increase the QDs biocompatibility. Due to their own optical properties they are essentially used for the optical fluorescence sensing and imaging [18].

Also due to their unique optical and physical properties AuNPs, have been widely used in different fields. AuNPs can diverge in the size and in shape and could be found as nanospheres, nanorods, nanocages, nanocubes, nanopolygons or even nanostars. They have size dependent optical properties, large surface to volume ratio, biocompatibility and low toxicity make them useful materials for the *in vitro* or *in vivo* sensing and imaging [19, 20]. The biocompatibility of AuNPs allows their interaction with some proteins. The functionalization or passivation of AuNPs with a variety of compounds allows their use in therapy and diagnosis [21].

AgNPs presents properties like chemical stability, high electrical and thermal conductivity, surface-enhanced Raman scattering, catalytic activity and nonlinear optical behavior [22]. AgNPs are being used in a diversity of applications in medicine. These NPs reveals antimicrobial protection that allows their use in biomedical sensing applications.

In this chapter a revision of the main nanoprobes used for the ROS/RNS sensing will be done. This chapter is structured taking into consideration the different ROS/RNS and the nanoprobes that have been used to their detection/quantification.

2. Nitric Oxide (NO)

NO is a physiological messenger and effector in mammalian cells and is one of the most studied ROS/RNS. Is a free radical that plays vital roles in vascular and neuronal signal transduction, bioenergetics, immunity and cell death regulation. In high concentrations can be injurious to cells and can be associated with some diseases like hypertension, arthritis, central nervous system diseases and others [1, 23-25]. Some NPs based sensors have been developed for the NO detection.

CNT were used to develop NO sensors with potential for NO sensing. The different kinds of NO sensors based in CNT are presented in Table 1. The majority of the CNT NO sensors are electrochemical sensors.

Complimentary Contributor Copy

Table 1. Main analytical performance of the NO CNT based sensors

CNT nanosensors	Linear range	LOD	References
Electrochemical			
SWCNT/NiTSPc	---	---	[26]
Au/MWCNTs	2.5×10^{-7} - 2.25×10^{-6} M	0.24 nM	[27]
CNT MTAPc	---	---	[28]
SWCNT d(AT)15 oligonucleotides	---	---	[29]
hemin MWCNT CS	0.25 – 1 μM	0.025 μM	[30]
Nafion/MWNTs-CS-AuNPs	0.019 – 54 μM	0.0076 μM	[31]
MP/CAS/SOD - MWCNT-PTTCA	1.0 - 40 μM	4.3 ± 0.2 nM	[32]
MWCNT PACB	2.2×10^{-7}-1.2×10^{-4} M	2.8×10^{-8} M	[33]
Optical			
SWCNT DAP-dex	---	0.070	[34]
SWNT	---	---	[35]

Hybrid materials from SWCNT and tetrasulfonated nickel phthalocyanine (NiTSPc) were electrochemically built to obtain chemically modified electrodes with electrocatalytic activity towards NO [26]. An electrochemical sensor based on a modified glassy carbon electrode (GCE) with MWCNTs decorated with AuNPs showed sensitivity for NO determination (S/N=3) in a range of 2.5×10^{-7} to 2.25×10^{-6} M with limit of detection (LOD) 0.24 nM [27]. An amperometric sensor for NO detection based on nanoporous platinum phthalocyanine modified electrodes was presented. An array of hollow nanotube structures of electropolymerized MTAPc engrained within the nanosized pore channels was constructed and immobilized onto the sputtered Pt at the base. Owing to the nanotube-arrayed morphology and the high electroactive area of the electrocatalytic poly-MTAPc redox mediator, an enhanced sensitivity and a lower LOD was evaluated [28]. The detection of NO supported by specific DNA sequence of d(AT)15 oligonucleotides adsorbed to NIR fluorescent SWCNT was described by Zhang et al. [29]. In other work, a biomimetic microsensor for measuring NO in rat brain *in vivo* the presence of oxygen was developed. The sensor consists of hemin and functionalized MWCNT covalently attached to chitosan (CS) via the carbodiimide crosslinker 1-Ethyl-3-(3-dimethylaminopropyl)-carbodiimide (EDC), followed by CS electrodeposition on the surface of carbon fiber microelectrodes. Based on the electrocatalytic reduction of NO by the hemin locally applied, exogenous NO was sensed by this sensor in a rat brain by

Complimentary Contributor Copy

square wave voltammetry (SWV) at a reduction potential of -0.850 V (vs. Ag/AgCl) in the presence of oxygen [30]. A sensor based on nano-structured film electrode for monitoring NO in living tissues was fabricated by coating Nafion/MWNTs-CS-AuNPs film on GCE. The NO release in mouse liver, spleen and kidneys was evaluated by amperometry at an oxidation potential +0.85 V. The sensor showed a linear variation in the range of 1.90×10^{-8} to 5.40×10^{-5} M and a LOD of 7.60×10^{-9} M (S/N = 3). The monitoring of NO release from living tissues, including mouse kidney, heart, spleen and liver was performed [31]. In other study a selective NO nanocomposite electrochemical biosensor based on three enzymes, including microperoxidase (MP), catalase (CAS), and superoxide dismutase (SOD) immobilized by crosslinking procedure on MWCNT-poly-5,2′:5′,2″-terthiophene-3′-carboxylic acid (PTTCA) nanocomposite layer was constructed. In this sensor the MP was used as a catalyst for the reduction of NO, while CAS and SOD were used to prevent the interferences of H_2O_2 and $O_2^{\cdot-}$. The biosensor showed catalytic response towards the electrochemical reduction of NO in a linear range between 1.0 and 40 μM with a LOD of 4.3 ± 0.2 nM. The NO released was evaluated in rat liver samples and in stomach and intestinal cancer cells by amperometry at a reduction potential of -0.8 V (vs. Ag/AgCl) [32]. Noncovalently functionalized MWCNT through azocarmine B (ACB) was developed as NO sensor. Through a electro-polymerization procedure, a MWNTs and polyazocarmine B (PACB) nanofilm electrode was prepared. The amperometric determination of NO was done in rat liver cells at an oxidation potential of + 0.75 V (vs. SCE). The linear concentration range was of 2.2×10^{-7}–1.2×10^{-4} M with a LOD of 2.8×10^{-8} M [33].

NO optical sensors based in CNT were also developed. In one of them, a NO optical sensor based on SWCNT protected with 3,4-diaminophenylfunctionalized dextran (DAP-dex) with selective fluorescence for NO detection showed capability of real-time and spatially resolved detection of NO produced by stimulating NO synthase in macrophage cells [34]. In another work, the NO detection based on the fluorescence quenching of SWCNT was demonstrated. The NO-detecting SWCNT were administrated in mice by intravenous and subcutaneous routes [35].

The application of CDs as nanoprobe for NO was referenced in two works. In one, the ratiometric sensing of NO based in CDs was made through a fluorescence resonance energy transfer (FRET) process. The CDs serve as both the energy donor and the anchoring site for the NO probe moiety, which turns into the energy acceptor in the presence of NO. This nanosensor, had potential to correlate the fluorescence intensity ratio with the intracellular NO

Complimentary Contributor Copy

level by quantitatively determining the intracellular fluorescence intensities of the donor and the acceptor. A LOD of 3 nM with selectivity to NO_2^-; NO_3^-; ClO^-; OH^-; H_2O_2; $^1O_2$ and ascorbic acid was evaluated. The detection of NO was done in different culture cells [36]. More recently, in other work, a NO sensor based in CDs showed the selective fluorescence sensing of NO and $ONOO^-$ in the presence of the principal ROS/RNS. In this work the CDs were microwave synthesized from citric acid (CA) and ethylenediamine (EDA). The optimum synthesis and sensing conditions for NO were found at pH 4, 2.5 g of CA and 1000 µL of EDA diluted in 15 mL of water exposed for 5 min to a microwave radiation of 700 W. Also, the best conditions for $ONOO^-$ determinations were found, at pH 7, 10, 0.25 g of CA and 500 µL of EDA diluted in 15 mL of water exposed for 5 min to a microwave radiation of 700 W. A greater sensitivity was obtained for the determination of $ONOO^-$ at pH 7 and 10 and a lower sensitivity for the determination of NO at pH 4 [37].

Table 2. Main analytical performance of the NO AuNPs based sensors

AuNPs nanosensors	Linear range	LOD	References
Electrochemical			
AuNPs - Nafion	1.0×10^{-7} - 4.0×10^{-5} M	5.0×10^{-8} M	[39]
AuNP Hb	$1.0\ x10^{-8}$ - $1.0\ x10^{-6}$ M	$5.0x10^{-9}$ M	[40]
Au NPs–3D GH	---	---	[41]
GP paper Au@Pt core-shell	400 nM - 673.9 mM	100 nM	[42]
AuNPs ERGO		133 nM	[43]
AuNPs–CS film	3.6×10^{-8} - 4.3×10^{-5} M	7.2 nM	[44]
AuNPs film nafion polyniacinamide	7.2×10^{-9} - 1.8×10^{-5} M	3.6 nM	[45]
AuNPs-GR-SDS	0.7-7.9 µM	1.2×10^{-8} M	[46]
Optical			
Fluorescein derivative AuNPs	---	---	[47]
Dye-labeled Cyt c' AuNPs.	---	8 µM	[48]

A pyrolytic graphite electrode co-modified with AgNPs and hemoglobin (Hb) was used. NO quantification was done in the linear range of $1.0x10^{-6}$ to $5.0x10^{-5}$ M with a sensitivity of 0.0424 $\mu A \mu M^{-1}$ and LOD of $3.0x10^{-7}$ M [38].

Complimentary Contributor Copy

AuNPs were employed in several methods of NO detection. Most AuNPs sensors are electrochemical sensors. In Table 2 are presented the nanosensors based in AuNPs for the NO detection.

A NO amperometric microsensor modified by AuNPs and nafion was described. The NO detection is based on the AuNPs catalysis of NO oxidation at an anodic potential of +0.74 V (vs. saturated calomel electrode (SCE)) by differential pulse amperometry. The microsensor showed high selectivity and sensitivity for NO determination in a linear range from 1.0×10^{-7} to 4.0×10^{-5} M with a LOD of 5.0×10^{-8} M (S/N = 3) [39]. Another NO cellular biosensor was based on the immobilization of red blood cells (RBCs) containing Hb, on a nanometer-size colloidal gold that is attached to an electrochemically pretreated GCE by linking an EDA monolayer. The immobilized RBCs showed an excellent electrocatalytic response to NO. The electrocatalytic currents are proportional to the NO concentration in the range from $1.0\text{x}10^{-8}$ to $1.0\ \text{x}10^{-6}$ M with LOD of $5.0\text{x}10^{-9}$ M (S/N = 3) [40]. A nanocomposite was also prepared of AuNPs deposited on three-dimensional GP hydrogel (Au NPs–3D GH). This nanocomposite was prepared by a one-step method by in situ reduction of Au^{3+} on 3DGH to build a sensing film in which AuNPs deposited on 3DGH efficiently catalyze the electrochemical oxidation of NO for its sensitive detection [41]. Zan et al. developed an electrochemical biosensor based on GP paper loaded with closely-packed Au@Pt core-shell NPs as a freestanding cell culture substrate for real-time monitoring cell secretion of NO. The electrode demonstrated sensitivity for amperometric detection of NO in a linear range from 400 nM to 673.9 mM and a LOD of 100 nM. The NO release in living cells were evaluated at an oxidation potential of + 0.75 V (vs. Ag/AgCl) [42]. A nanocomposite consisting of AuNPs electrochemically deposited on electrochemically reduced GP oxide (ERGO) was used for NO detection by Ting et al. The synergistic integration of ERGO and AuNPs allows the electrochemical detection of NO with high sensitivity (5.38 μA/μM/cm^2), a LOD of 133 nM (S/N = 5.5) and a fast response time. The use of AuNP-ERGO hybrid electrode to NO detection and its release from live human umbilical vein endothelial cells was demonstrated [43]. Another electrochemical sensor was developed by construction of AuNPs–chitosan nanocomposite sensing film on a GCE surface. The AuNPs–CS film is controllable, stable and exhibits catalytic activity to NO oxidation. The method for NO analysis has a linear range from 3.60×10^{-8} to 4.32×10^{-5} M and a LOD of 7.20 nM. The release of NO was then evaluated an oxidation potential of +0.85 V (vs. SCE) in rat kidney [44]. AuNPs were deposited in a quartz fiber electrode by chemical liquid deposition; niacinamide (NA) was

Complimentary Contributor Copy

electropolymerized above the AuNPs film and posterior coated with nafion. This microsensor displayed high sensitivity based on the catalytic effect of AuNPs and polyniacinamide (PNA) toward the oxidation of NO. The NO detection was made in a range of 7.2×10^{-9} – 1.8×10^{-5} M with a LOD of 3.6 nM (S/N = 3). The NO release from a mice liver was done at an oxidation potential of +0.65 V (vs. Ag/AgCl) [45]. AuNPs-GP composite were used to construct a AuNPs-GR-SDS modified electrode. Hb was successfully immobilized on the surface of a basal plane graphite electrode. The immobilized Hb retained its biological activity for the catalysis toward NO. The biosensor showed sensitivity to NO in a linear range of 0.72–7.92 μM, with a correlation coefficient of 0.9991 and a LOD of 1.2×10^{-8} M (S/N = 3) [46].

Two AuNPs optical sensors to NO detection based on immobilization of AuNPs in a fiber optic were reported [47, 48]. In the first the sensor was composed of a fluorescein derivative dye attached to AuNPs. The fluorophores used were the 4-carboxy-2',7'-difluorofluorescein, succinimidyl ester (Oregon Green 488 carboxylic acid, succinimidyl ester). The fluorescein dye rearranges as NO adsorbs onto the Au, bringing a decrease in the fluorescence intensity of the dye [47]. Ratiometric and fluorescence lifetime-based sensors were considered for detection of extra- and intracellular macrophage NO. These sensors incorporate cytochrome c', a hemoprotein known to bind NO selectively. These sensors are composed of dye-labeled cytochrome c' attached to an optical fiber by AuNPs. In this case it was obtained a LOD of 8 μM [48].

QDs fluorescent sensors have been used for the NO sensing. The NO sensing by QDs is indicated in Table 3. Tan et al. [49] presented biocompatible QDs–CS nanocomposites for the fluorescence detection of NO. These QDs–CS nanocomposites showed sensitivity to NO molecules and can detect NO based on a fluorescence quenching mechanism [49]. The same authors also synthesized CdTe-QD in carboxymethyl chitosan (CMCS) aqueous solutions and incorporated into CMCS. The CdTe QD–CMCS reacted with NO under pressure and subsequently reacted with ethyl bromide to produce CdTe QD–CMCS nanocomposite NO donors. They detect the release of NO by the NO donors in porcine iliac artery endothelial cells based on fluorescence quenching. A Stern-Volmer fluorescence quenching modeling was done using an excitation wavelength of 400 nm and emission of 560 nm with a linear range below 768 μM [50]. A QDs-poly(N-isopropylacrylamide) (PNIPAM) hybrid nanogel diazeniumdiolates (NO donors) system was reported a donor and probes of NO. This system is capable of releasing NO and meanwhile detecting the NO under conditions similar to physiological environment based on the fluorescence quenching by NO [51]. An NO optical

Complimentary Contributor Copy

sensor based on CdSe/ZnS QD was synthetized by adsorption of QDs on polymethacrylate surfaces after stabilization by hexadeylamine ligands. The ability of such materials to sense NO and NOx was tested [52]. The NO quantification, based on fluorescence quenching of a nanocomposite sensor constituted by CdSe QDs stabilized by CS and mercaptosuccinic acid (MSA) was developed by Simoes et al. [53]. The NO quantification with CdSe-MSA-CS was done in linear range from 5 to 200 μM and a LOD of 1.86 μM [53]. A NO optical fiber sensor based on CdSe QD using cellulose as sensitive membrane was developed. In this optical fiber sensor CdSe-QDs were embedded in cellulose acetate via simple hybridized approach. A linear calibration (R^2= 0.9908) was obtained in the concentration range of 1.0×10^{-7} to 1.0×10^{-6} M with a LOD of 1.0×10^{-8} M (S/N = 3) [54]. CdSe functionalized with trivalent porphirin were also used in NO sensing [55].

Table 3. Main analytical performance of the optical NO QDs based sensors

QDs nanosensors	Linear range	LOD	References
CdTe-CS	460-55200 nM	---	[49]
CdTe-CMCS	400-768 μM	---	[50]
TGA-PNIPAM	---	---	[51]
CdSe/ZnS polymethhacrylate	0-33 nM	3 nM	[52]
CdSe-MSA-CS	5-200 μM	1.86 μM	[53]
CdSe cellulose acetate	1.0×10^{-7}-1.0×10^{-6} M	1.0×10^{-8} M	[54]
CdSe trivalent porphirin	---	---	[55]
CdSe-mHP diazeniumdiolates	300-700nM	25 nM	[56]
CdS-PMMA	1.4×10^{-5}- 9.3×10^{-3} M	1.0×10^{-6} M	[57]
CdSe/ZnS QD ferric dithiocarbamate	---	300 nM	[58]
QD ferric dithiocarbamate	---	3.3 μM	[59]
CdSe/ZnS-cyclophane	---	---	[60]
CdSe-TEA	5.9×10^{-7}-1.8×10^{-5} M	3.0×10^{-7} M	[61]
CdSe/ZnSQDs dirhodium complex	---	---	[62]

CdSe QDs-hyperbranched polyether hybrid nanospheres were synthesized for NO donating and real-time detection. The hybrid nanospheres consist of CdSe QDs as NO fluorescent probes, and modified hyperbranched polyether (mHP)-based diazeniumdiolates as NO donors. NO release in mouse fibroblast cells was detected by fluorescence quenching [56]. NO fluorescent probe CdS-polymethyl methacrylate (PMMA) nanocomposites with different molar ratios

Complimentary Contributor Copy

of CdS QDs to PMMA were established via in-situ bulk polymerization method. The detection mechanism was based on the degradation of the PMMA molecule by NO which then influenced the surface properties of the QDs or the formation of ionic complexes between NO and Cd ion on the QDs surface. NO detection was obtained in the range from 1.4×10^{-5} to 9.3×10^{-3} M with a LOD of 1.0×10^{-6} M (S/N = 3) [57]. Two works reported the use of ferric dithiocarbamate compounds in the QDs functionalization. In one of these works CdSe/ZnS QD were functionalized with ferric dithiocarbamate compounds and used for NO detection [58]. In the other one the NO detection was made using QDs ferric functionalized with dithiocarbamate complex with a LOD of 3.3 μM [59]. Organogel–CdSe/ZnS QDs hybrid materials showed fluorescence sensitivity towards NO. The chemical sensing ability of the hybrid organogels towards gaseous NO was investigated by steady-state fluorescence spectroscopy [60]. Triethanolamine (TEA) modified CdSe QDs are significantly quenched in presence of NO. TEA-CdSe-QDs detect NO linear relationship (R^2= 0.9963) was observed over the range 5.92×10^{-7} - 1.85×10^{-5} M with LOD of 3.02×10^{-7} M [61]. A *turn-on* fluorescent probe with sensitivity to NO comprising CdSe/ZnS-QDs coordinated with dirhodium complex was synthesized. Emission from CdSe/ZnS-QDs is quenched when coordinated with the dirhodium complex but can be restored upon the displacement by NO [62].

Nanosensors for NO based in other NPs were used. An *in vivo* NO electrochemical sensor based in Al_2O_3NPs was developed. Al_2O_3NPs film was deposited at the surface of a GCE. The NO detection in rat lung was done at an oxidation potential of + 0.69 V (vs. SCE) by amperometry [63]. Also a NO optical sensor based in the fluorescence enhancement of silicon nanowires (SiNWs) functionalized with reduced fluoresceinamine was presented [64].

3. PEROXYNITRITE ($ONOO^-$)

The formation of $ONOO^-$ *in vivo* is the result of the reaction between NO and superoxide radicals. $ONOO^-$ solutions are prepared by treating acidified H_2O_2 with a solution of sodium nitrite, followed by rapid addition of NaOH. This RNS is a strong oxidant and a powerful nitration agent of biomolecules, is stable in basic media and very unstable in neutral conditions. Due their instability in physiological conditions their detection is very difficult and consequently a small number of sensors based in NPs have been developed

Complimentary Contributor Copy

when compared with other ROS/RNS. $ONOO^-$ sensing based in CDs, AuNPs and QDs was achieved.

Two sensors for $ONOO^-$ detection based in CDs were described. One of them consists in CDs doped with tryptophan (Trp-CD). Trp-CDs were microwave synthesized and used to detect the presence of $ONOO^-$ through quenching of fluorescence probably due to the oxidation of tryptophan added to CDs functionalization. Taking into consideration the nitration and oxidation potential of $ONOO^-$, the aminoacid tryptophan was used to dope the CDs in order to make them reactive toward $ONOO^-$. The evaluated analytical methodology for $ONOO^-$ detection shows a linear response range from 5 to 25 µM with a LOD of 1.5 µM and quantification of 4.9 µM [65]. In the other sensor described also as a NO sensor [37] the $ONOO^-$ determination was made at pH 7, 10, 0.25 g of CA and 500 µL of EDA diluted in 15 mL of water exposed for 5 min to a microwave radiation of 700 W. A greater sensitivity for the determination of $ONOO^-$ at pH 7 and 10 was observed [37].

AuNPs were used in a development of a colorimetric method for detection of ssDNA cleavage induced by $ONOO^-$. The method was based on reducing AuNPs stability by the breakup of adsorbed ssDNA through $ONOO^-$ damage at a pre-selected ionic strength. The $ONOO^-$ concentration was ranged in a linear range from 9.78 mM to 20.77 mM (R=-0.9991). The visual quantitative detection of $ONOO^-$ was obtained [66].

Using QDs as probes for $ONOO^-$, the interaction of cysteine-functionalized CdTe-QDs with $ONOO^-$ was spectroscopically investigated. The photoluminescence of CdTe QDs was quenched to 85% at 86 mM concentration of $ONOO^-$. For CdS QDs, in the same conditions, the loss of PL intensity was only 7% [67]. Another method using QDs for luminescent detection of $ONOO^-$ reports the application of CdTe and CdTe@ZnS QDs capped with 3-mercaptopropionic acid (MPA), thioglycolic acid (TGA), or glutathione (GSH). The strength of the QD–thiolate bond has influence in the sensitivity of the probe. The QD–thiolate bond of CdTe@ZnS is more sensitive to oxidation from $ONOO^-$ than CdTe. QDs capped with MPA showed less selectivity for $ONOO^-$ TGA than GSH. The best LOD of 12.6 nM was obtained for MPA–CdTe@ZnS-QDs [68].

A fluorogenic optical sensor based on oxazine conjugated NPs was applied in the detection *in vivo* of HClO and $ONOO^-$ generation. The sensor consists of along circulating biocompatible NPs that targets phagocytic cells *in vivo* and is coated with oxazine fluorophores that are released by reaction with HOCl or $ONOO^-$ [69].

Complimentary Contributor Copy

4. HYDROGEN PEROXIDE (H_2O_2)

Hydrogen peroxide (H_2O_2) is one of the most important ROS in regards to mitogenic stimulation or cell cycle regulation. Is a powerful oxidant, but it is is unstable that quickly breaks down (through the catalase enzyme present in our body) in water and oxygen. Among all ROS/RNS the mostly studied is H_2O_2.

The main nanoprobes using CNT in the detection of H_2O_2 are described in Table 4.

Table 4. Main analytical performance of the electrochemical H_2O_2 CNT based sensors

CNT nanosensors	Linear range	LOD	References
AgNPs/OxpTTBA/MWCNT	10 - 260 µM	0.24 µM	[70]
MWCNTs/Pt	0.01 - 2 mM	0.3 µM	[71]
CNT-PdNPs	2 µM - 1.3 mM	2 µM	[72]
sensor array SWCNT	---	25 ppm	[73]
Pt/GP–CNT paper	---	10 nM	[74]
RuOHCF/MWCNTs100	0.1 - 10 mM	4.7µM	[75]
RBMWCNT-GCE	0.99 - 28µM 28 - 510µM 0.51 - 1.8µM	0.27µM	[76]
Ag/SnO2 - CNT	0.01 - 35 mM	5.0 µM	[77]
SWNT	---	---	[78]
AgNP–MWNT	6 - 900 µM	4.2 µM	[79]
Ag/MWCNT	2 - 120 µM	0.3 µM	[80]
MWCNTs/Pt NPs-dopamine	0 - 5 mM	0.3441 mM	[81]

An electrochemical sensor to H_2O_2 is proposed using AgNPs modified oxidized poly-2,2':5',2''-terthiophene-3-p-benzoic acid/MWCNT (OxpTTBA/MWCNT). The sensor was built by immobilization of AgNPs on the oxidized pTTA/MWCNT nanocomposite layer. The AgNPs/OxpTTBA/MWCNT nanocomposite showed electrocatalytic activity to H_2O_2. The sensor shows a fast response time less than 5 s, a linear range from 10 to 260 µM and a LOD of 0.24 µM [70]. Miao et al. developed a H_2O_2 biosensor by combining the advantages of CNT and PtNPs, MWCNT/PtNPs nanohybrids. The MWCNTs/Pt-modified electrodes exhibited a favorable catalytic ability in the reduction of H_2O_2. The modified electrodes can be used

Complimentary Contributor Copy

to detect H_2O_2 in the range of 0.01–2 mM with a LOD of 0.3 µM (S/N = 3). The sensitivity to H_2O_2 was 205.80 $\mu AmM^{-1}cm^{-2}$ at working potential of 0 mV [71]. Other electrochemical sensor of H_2O_2 was made with a CNT fiber microelectrode coated with palladium NPs (PdNPs). The microelectrode shows a response time of 2s, a LOD of 2 µM, a sensitivity of 2.75 $Acm^{-2}M^{-1}$, and a linear response range from 2 µM to 1.3 mM (R=0.9994). The sensor is sensitive and selective towards H_2O_2 [72]. The detection of H_2O_2 in the vapor phase was achieved using a nanochemical sensor consisting of SWCNT. A capability of 25 ppm and response and recovery times in the orders of seconds was obtained. The sensor array consisting of 32 sensor elements with variations in sensing materials is capable of discriminating H_2O_2 from water and methanol. Was constructed a sensor array using SWCNT and its variants with functional groups, coatings, and dopings for the trace detection of H_2O_2 in the vapor phase Pristine SWCNT respond well to H_2O_2 but also to water and alcohol, thus making selective discrimination a difficult task. PEI-functionalized SWCNTs, in contrast, provide a strong response only to H_2O_2. A LOD of about 25 ppm was obtained [73]. An electrode based on the sputter deposition of ultrafine PtNPs on freestanding rGO–CNT paper was demonstrated. The nonenzymatic detection of H_2O_2, Pt/GP–CNT paper exhibits high sensitivity, selectivity, stability and reproducibility. The sensitivity obtained was 1.41 $\mu A\ mM^{-1}cm^{-2}$ with a linear range up to 25 µM and a LOD of 10 nM (S/N = 3). The Pt/rGO–CNT electrode demonstrated a improved sensing performance in comparison with Pt/rGO paper and commercial Pt foil electrode toward H_2O_2, and can been used for real-time tracking H_2O_2 secretion by live cells macrophages [74].

An amperometric sensor combining ruthenium oxide hexacyanoferrate RuOHCF films with MWCNT immobilized on a GCE provides a promising platform for H_2O_2 sensing. Experiments indicated that the cathodic reduction of H_2O_2 at the RuOHCF/MWCNTs100/GC modified electrode is facilitated, occurring at 0.0 V vs. Ag/AgCl/KCl. the H_2O_2 determination was made with a LOD (4.7 µM), in a concentration range of (0.1–10 mM) and a sensitivity of 1280 $\mu A\ mmol^{-1}cm^{-2}$ [75]. A H_2O_2 sensor based on a MWCNT-modified GCE and reactive blue 19 (RB) was performed. The RB-MWCNT-GCE shows an increase in the peak current and a decrease in the overvoltage of H_2O_2 electroreduction in comparison with that seen at an RB modified GCE MWCNT modified GCE, and activated GCE. The construction of an RB-MWCNT-GCE and its application in H_2O_2 determination was showed. The

Complimentary Contributor Copy

results showed that RB can be immobilized at the surface of MWCNT-modified GCE. The diffusion coefficient of H_2O_2 was $2.34x10^{-6}$ cm^2/s for experimental conditions using chronoamperometric results. RBMWCNT-GCE exhibits linear ranges of 0.99 -2 8 µM, 28 - 510 µM, and 0.51 - 1.8 µM for H_2O_2 determination by amperometry. The lower LOD is 0.27 µM [76].

Miao et al. obtained electrospun SnO_2 nanotubes by direct sintering of the electrospun poly(vinylpyrrolidone)/SnCl precursor composite fibers. With a fast transport of photogenerated electrons in SnO_2 a synthesis approach of Ag/SnO_2 composite nanotubes is developed by the photocatalytic in situ reduction of Ag^+ using SnO_2 nanotubes as model was developed by nanotubes. The cyclic voltammetry and amperometry results show that the sensor of Ag/SnO_2 composite nanotubes exhibit analytical response to H_2O_2 in a linear detection range from 0.01 to 35 mM with R^2 of 0.998. The LOD estimated to be 5.0 µM (S/N = 3) [77]. In other study an array of fluorescent SWNT that can selectively record, in real time, the quenching that occur as H_2O_2 molecules are emitted from individual human epidermal carcinoma cells stimulated by epidermal growth factor was developed. Such array can distinguish between molecules originating locally on the cell membrane from other contributions. We find that epidermal growth factor induces 2 nmol H_2O_2 locally over a period of 50 min [78].

An amperometric sensor towards H_2O_2 detection is fabricated by immobilization of AgNP–MWCNT on GCE. The sensor responded linearly to H_2O_2 in the concentration of 6 to 900 µM with LOD of 4.2 µM [79]. A H_2O_2 biosensor was fabricated by deposition of AgNPs on the o-MWCNT. The Ag/MWCNT composites were applied to immobilize Mb on the GCE surface. Based on the direct electrochemistry of Mb, a sensitive biosensor for H_2O_2 was obtained. The amperometric determination of H_2O_2 was done with a linear range of 2 to120 µM and a LOD of 0.3 µM [80]. Vitreous carbon electrode modified with MWCNTs and composites of Pt NPs–dopamine were also used as H_2O_2 sensor. This sensor showed a linear response in the 0–5 mM range, with detection and quantification limits of 0.3441 mM and 1.1472 mM, respectively [81].

The application of CDs in the detection of H_2O_2 has markedly increased in the last years. The main methods using CDs in the detection of H_2O_2 are described below (Table 5).

Complimentary Contributor Copy

Table 5. Main analytical performance of the H_2O_2 CDs based sensors

CDs nanosensors	Linear range	LOD	References
Electrochemical			
CDs/Cu_2O	5 µM - 5.3 mM	2.8 µM	[82]
CDs/LDHs	0.1 - 23.1 µM	0.04 µM	[83]
Optical Sensors			
CNDs	1 mM - 100 mM	0.4 mM	[84]
CDs@RGO	---	---	[85]
CDs	10 - 150 µM	3.8 µM	[86]
CDs		5 µM	[87]
CDs	0.025 - 50 µM	---	[88]
SiCDs	---	---	[89]
CD/NP/BE		0.5 mM	[90]
CDs/TPP/PFI	---	0.75 µM	[91]
BCDs	0.1 - 1.0 mM	---	[92]
Hemin/Fe^{3+}/CDs	---	---	[93]

Two electrochemical sensors for H_2O_2 detection based in CDs were described. Li et al. developed a non-enzymatic electrochemical sensor based on CDs/octahedral cuprous oxide (Cu_2O) nanocomposites to detection of glucose and H_2O_2. The CDs/octahedral Cu_2O nanocomposites has good performance to the electrocatalytic reduction of H_2O_2 with a linear response range from 5 µM to 5.3 mM. The amperometric sensor showed a LOD of 2.8 µM (S/N = 3) [82]. Wang et al. developed an electrochemical biosensor for H_2O_2 by immobilization of horseradish peroxidase (HRP) using CDs and CoFe-LDHs composites on the surface of GCE. CDs and CoFe layered double hydroxide composites (CDs/LDHs) were prepared via simply mixing of CoFe-LDHs, CDs and HRP. The nanocomposites were used for the immobilization of HRP on the GCE. The results indicated that HRP immobilized by CDs/LDHs retained the activity of enzyme and displayed quasireversible redox behavior and fast electron transfer. The HRP/CDs/LDHs/GCE displayed good electrocatalytic reduction activity and excellent analytic performance toward H_2O_2. A fast direct electronic transfer behavior and good electrocatalytic reduction toward H_2O_2 due to the synergistic effect between CoFe-LDHs, CDs and HRP was observed. The H_2O_2 biosensor showed a linear range of 0.1–23.1 µM (R^2=0.9942) with a calculated LOD of 0.04 µM (S/N = 3) [83].

Complimentary Contributor Copy

The main nonosensors for the H_2O_2 detection based in CDs are optical. Liu et al. demonstrated a synthesis of photoluminescent carbon nitride dots (CNDs) by microwave heating treatment of organic amines in the presence of acid. These CNDs have intrinsic peroxidase-like activity and have been successfully used as peroxidase mimetics for the colorimetric detection of H_2O_2 and glucose. The linear range to H_2O_2 detection was estimated to be from 1 to100 mM (r = 0.994) and the LOD is estimated to be 0.4 mM [84]. Yeh et al. reported the detection of H_2O_2 and glucose using reduced GP oxide decorated with CDs (CDs@RGO). This method permits the detection of H_2O_2 through a *turn on* process. The sensitivity of H_2O_2 detection was improved in presence of bovine serum albumin (BSA), revealing that this probe has potential to be used for the quantitative detection of H_2O_2 in biological samples [85]. A dielectric barrier discharge (DBD)-assisted one-pot strategy to fabricate CDs using only one reagent N,N-dimethylformamide (DMF) was proposed. The prepared CDs can be used as highly selective and sensitive fluorescence probes for H_2O_2 and glucose. CDs decreases gradually with H_2O_2 concentration. A good linear correlation (R^2=0.9928) can be obtained in the concentration range from 10 to 150 μM with a LOD of 3.8 μM [86]. A synthesis of fluorescent CDs based on application of UV irradiation to carbohydrates was showed. CDs obtained by photochemical treatment from the sucrose/NaOH/poly(ethylene glycol) system showed an increase in the fluorescence (*turn on*) when H_2O_2 is added. Antioxidants such as ascorbic acid and glutathione inhibit the photochemical reaction giving rise to a decrease in fluorescence of the CDs/H_2O_2 system (*turn on–off*). This sensor was applied for the detection of H_2O_2 in contact lens cleaning solutions. The LOD was 5 μM and the repeatability expressed as the relative standard deviation (RSD) was 3.8% (n = 7) [87]. Fluorescent CDs for determination of H_2O_2 in the presence of Fe^{2+} were prepared by a hydrothermal method. These CDs can be directly used for the fluorescence detection of H_2O_2. The production of H_2O_2 from the oxidation of glucose by glucose oxidase results in the fluorescence quenching of CDs in the presence of Fe^{2+}, which can be used to detect glucose. In this work, CDs were used as a fluorescence probe for the *turn-off* detection of H_2O_2 and glucose in the presence of Fe^{2+}. A linear quenching in CDs fluorescence by H_2O_2 was observed in the concentration range between 0.025–50 μM [88]. Specific electron transfer between Si-doped carbon quantum dots (SiCDs) and H_2O_2 allows SiCDs as a sensitive fluorescence sensing platform for H_2O_2 [89]. A CD-based FRET ratiometric nanoprobe (CD-NP-BE) for detecting and imaging H_2O_2 *in vitro* and *in vivo* was performed. This

Complimentary Contributor Copy

nanoprobe showed selectivity and a LOD of 0.5 mM towards H_2O_2. The nanoprobe has been successfully applied in the detection of H_2O_2 in live cells and in zebrafish larvae. In this study, a boronate based H_2O_2 recognition element, 2-(2-aminoethyl)-6-(4,4,5,5tetramethyl-1,3,2 dioxa borolan-2-yl)-1H-benzo[de]isoquinoline 1,3(2H)-dione (NP-BE), was synthesized and covalently linked to CDs. The CDs-based nanoprobe features a small size, high water dispersibility, very low toxicity and fast response toward H_2O_2 [90]. A multifunctional fluorescent CDs-based FRET nanoprobe prepared by covalently linking a mitochondria-targeting ligand (triphenylphosphonium, TPP) and a H_2O_2 recognition element 3-Oxo-3',6'-bis(4,4,5,5-tetramethyl-1,3,2-dioxaborolan-2-yl)-3H-spiro[isobenzofuran-1,9'-xanthene]-6-carboxylic acid (PFl) onto CDs for detecting mitochondrial H_2O_2 was demonstrated. In presence of H_2O_2, the PFl moieties on CDs undergo structural and spectral conversion, affording the nanoplatform a FRET-based ratiometric probe for H_2O_2. This nanoprobe can specifically target and stain the mitochondria; and, it can detect the exogenous H_2O_2 in L929 cells, as well as the endogenously produced mitochondrial H_2O_2 in Raw 264.7 cell upon stimulation by phorbol myristate actate (PMA). For this probe, the CDs serve as the donor of energy transfer and the carrier for the sensing system. The LOD for this nanoprobe was of 0.75 μM [91]. Fluorescent B-doped CDs (BCDs) prepared by a facile one-pot solvothermal route were applied for the of H_2O_2 and glucose detection. The fluorescence intensity decreases with the H_2O_2 concentration increasing. The fluorescence quenching efficiency is linearly correlated with the H_2O_2 concentration from 0.1 to 1.0 mM and remains constant at H_2O_2 concentration values higher than 10.0 mM. Fluorescence quenching of BCDs was observed by increasing the glucose concentration in the presence of GOx [92]. CDs using Fe and hemin were investigated. A hemin sensor based on the Fe^{3+}/CDs system was achieved. A quenching caused by photoluminescent center destruction was caused by hydroxyl radicals (·OH), which were produced by high power UV light and the H_2O_2/Fe^{2+} system; consequently the detection of H_2O_2 by quenching with a low LOD (LOD, 0.9 ppb) using the Fe^{2+} system was realized [93].

AgNPs have catalytic ability for decomposition of H_2O_2, producing silver ions and superoxide. Table 6 shows the main nanoprobes using AgNPs in the detection of H_2O_2. The majority are electrochemical nanoprobes.

Complimentary Contributor Copy

Table 6. Main analytical performance of the H_2O_2 AgNPs based sensors

AgNPs Nanosensors	Linear range	LOD	References
Electrochemical			
AgNPs-carbon nanoflakes	0.02-14 mM	2.2 mM	[94]
AgNPs-PQ11	1×10^{-4} - 0.18 M	3.39×10^{-5} M	[95]
AgNPs/MB	1 µM - 3 mM	0.088 µM	[96]
Ag–DNA hybrid NPs	2.0 µM - 2.5 mM	0.6 µM	[97]
Ag/GC	0.25 - 1.4 µM	1 µM	[98]
AgNPs poly(alizarin yellow R)	1.0 - 450 µM	0.32 µM	[99]
AgNP/DNA/GCE	4-16 µM	1.7 µM	[100]
AgNPsMWNT/GCE.	6 - 900 µM	4.2 µM	[79]
Mb-AgNPs-MWCNT	2 -120 µM	0.3 µM	[80]
AgNPs-GO	10 - 20 mM	0.5 mM	[101]
AgNPs-1-PPy/GCE	0.1 - 5mM 5-120 mM	0.115 µM 0.256 µM	[102]
Hb–Ag film	1×10^{-6} - 2.5×10^{-2} M	1×10^{-7} M	[103]
AgNPs-PDDA-rGO	100 µM - 41 mM	35 µM	[104]
HRP/DNA-Ag/PDDA–Au/DNA-Ag/Au	7.0 µM-7.8 mM	2.0 µM	[105]
Mb- AgNPs -CNTs	2.0×10^{-6}–1.2×10^{-3} M	3.6×10^{-7} M	[106]
AgNGs-PEDOT	---	7 mM	[107]
HRP AgNPs cysteamine-Au	3.3 µM - 9.4 mM	0.78 µM	[108]
AgNPs-3DG	0.03 - 16.21 mM	14.9 µM	[109]
AgNPs-$FeCl_3$-OPD	100 µM - 80 mM	62 µM	[110]
Ag/GN	100 µM - 40 mM	28 µM	[111]
Urchin-like Ag NWs	50 µM - 10.35 mM	10 µM	[112]
Ag coated nanofibrous membrane	10 µM -16.5 mM	4 µM	[113]
Optical			
BSA-Ag NCs	---	60 nM	[114]
PEI-Ag nanoclusters	500 nM - 100 µM	400 nM	[115]
AgNPs-ZnO	2 µM - 5.5 mM	0.42 µM	[116]
H-terminated SiNW arrays AgNPs	---	0.2 µM	[117]
Colorimetric method AgNPs	---	0.6 mg/l	[118]
AgNPs Benincasa hispida fruit extract	---	---	[119]

Complimentary Contributor Copy

Carbon nanoflakes were prepared by hydrothermal treatment using folic acid and ultrafine AgNPs by self-reduction method. The carbon flakes supported AgNPs were used to construct an electrochemical biosensor for the detection of H_2O_2. The sensor had electrocatalytic activity for the detection of H_2O_2 with a wide linear range from 0.02 to 14 mM(R = 0.997) a rapid response time upon the addition of H_2O_2 and a LOD of 2.2 mM [94]. AgNPs from an aqueous solution of $AgNO_3$ and poly[(2-ethyldimethylammonioethyl methacrylate ethyl sulfate)-co-(1vinylpyrrolidone)] (PQ11), were synthetized. Such dispersion can form stable AgNPs films on GCE. The sensor has a fast amperometric response toward H_2O_2 detection of less than 2 s. The linear range estimated is 1×10^{-4} to 0.18 M (r = 0.998) with LOD of 3.39×10^{-5} M (S/N = 3) [95]. Palanisamy et al. used AgNPs and myoglobin (Mb) for the construction of an Ag-NPs/MB biocomposite that was used for H_2O_2 detection. A good direct electron transfer of MB is observed at AgNPs/MB biocomposite electrode rather than direct drop casting of MB onto AgNPs modified electrode. The electron transfer rate constant is 3.02 s^{-1}. The fast amperometric response for H_2O_2 at Ag-NPs/MB biocomposite modified electrode shows a good catalytic activity of the electrode. The H_2O_2 detection is obtained in the linear response range from 1 µM to 3 mM, with the LOD of 0.088 µM. The sensitivity calculated is 0.357 $\mu A \mu M^{-1} cm^{-2}$ [96]. In another work Ag–DNA hybrid NPs were electrodeposited on an electrode surface by the reduction of silver with DNA. The synthetized NPs showed ability to the reduction of H_2O_2 and O_2. The presence of DNA avoided further aggregation of AgNPs and improved the catalytic ability of the NPs. Such silver–DNA hybrid NPs showed a linear response to H_2O_2 concentration ranging from 2.0 µM to 2.5 mM with a LOD of 0.6 µM and a sensitivity of 773 $\mu A m M^{-1} cm^{-2}$ [97]. A green synthesis of a nanosilver modified electrode (Ag/GC) to H_2O_2 was demonstrated by Shukla et al. [98]. The sensor shows good electro-catalytic activity toward the reduction of H_2O_2 at a low potential so the Ag/GC is an attractive amperometric sensor for H_2O_2. The sensor could achieve the maximum steady-state current within 9 s with a LOD of 1 µM (S/N = 3) in a linear range of 0.25 to 1.4 µM [98]. Another amperometric sensor for H_2O_2 was constructed based on a GCE modified with AgNPs on poly(alizarin yellow R). The polymer was electropolymerized onto the surface of the GCE by cyclic voltammetry and the AgNPs were then electrodeposited onto electrode surface. The electrode shows a catalytic activity towards the reduction of H_2O_2, with a linear response range from 1.0 to 450 µM and a LOD of 0.32 µM [99]. AgNPs electrodeposited on three-dimensional DNA

Complimentary Contributor Copy

networks that were directly dropped on the surface of GC electrode as an electrocatalyst to produce a H_2O_2 sensor. Favorable catalytic ability to reduction of H_2O_2 was showed. The good catalytic activity of the sensor was attributed to the DNA networks that facilitated the formation and homogenous distribution of AgNPs. The resulted sensor achieved 95% of the steady-state current within 2 s with a LOD of 1.7 μM [100].

A H_2O_2 sensor was fabricated by immobilization of AgNP–MWCNT on GCE. AgNPs catalyst has been synthesized using gelatin as organic precursor. GCE modified with AgNPs and MWCNT (AgNPs–MWCNT/GCE) was prepared by casting of the AgNPs–MWCNT solution on GCE. The AgNPs–MWCNT enhanced electrocatalytic activity toward H_2O_2 at the AgNPs/MWCNT/GCE by amperometry in linear range between 6 to 900 μM with LOD of 4.2 μM [79]. A H_2O_2 biosensor based Mb immobilized on AgNPs decorated oxidized multi-MWCNT was fabricated. The conductivity of AgNPs could realize fast electron transfer between Mb and the electrode. The amperometric determination of H_2O_2 was found in a linear range of 2 to 120 μM and a LOD of 0.3 μM [80]. In other sensor AgNPs were deposited onto GP Oxide surface by the electroless deposition process. The H_2O_2 detection was made in a range from 10 to 20 mM with a LOD of 0.5 mM [101]. Electrochemically synthesized polypyrrole (PPy) decorated with AgNPs was prepared by electrochemical deposition and used for H_2O_2 detection. In the H_2O_2 determination were found two linear ranges: the first one is 0.1–5 mM with a LOD of 0.115 μM and the second is 120 mM with a correlation factor of 0.256 μM (S/N = 3) [102]. An amperometric H_2O_2 biosensor based on the direct electron transfer of Hb in Hb–Ag sol gel film was developed. Hb was used as a model to construct Hb–Ag sol gel. The Hb–Ag film proved to exhibit a good electrocatalytic activity for the reduction of H_2O_2. This biosensor showed a sensitive response to the reduction of H_2O_2 without any electron mediator in a linear concentration range of 1×10^{-6} to 2.5×10^{-2} M with LOD of 1×10^{-7} M [103]. Poly(diallydimethylammonium chloride) (PDDA) functionalized reduced GP oxide (PDDA-rGO) modified with AgNPs shown electrocatalytic activity for the detection of H_2O_2 in a linear range from 100 μM to 41 mM (r = 0.997) with a LOD of 35 μM [104]. Ma et al. fabricated an amperometric H_2O_2 biosensor based on the immobilization of HRP on DNA–silver nanohybrids (DNA–Ag) and poly(diallyldimethylammonium chloride) (PDDA)-protected gold NPs (PDDA–Au) by combining the self-assembly technique with an *in situ* electrochemical reduction of the DNA–Ag^+ complex. The resulting biosensor (HRP/DNA–Ag/PDDA–Au/DNA–Ag/Au

Complimentary Contributor Copy

electrode) showed a linear response to H_2O_2 in a concentration range from 7.0 μM to 7.8 mM with a LOD of 2.0 μM (S/N = 3) [105]. A H_2O_2 biosensor based on the direct electrochemistry and electrocatalysis of Mb immobilized on AgNPs doped CNT film with hybrid sol–gel techniques was shown. AgNPs have been electrodeposited and modified onto CNTs. The electrocatalysis towards H_2O_2 has been evaluated by cyclic voltammetry and amperometry with a linear range of 2.0×10^{-6}–1.2×10^{-3} M and a LOD of 3.6×10^{-7} M (S/N = 3) [106]. Was reported a electrochemical sensor with silver nanograins (AgNGs) incorporated on a poly[3,4-ethylenedioxythiophene] PEDOT modified electrode by a simple electrochemical method. The AgNGs incorporated PEDOT modified electrode showed good electrocatalytic activity towards the reduction of H_2O_2 was showed a good amperometric response to H_2O_2 with a LOD of 7 mM and a response time of 5 s [107]. HRP was immobilized on AgNPs adsorbed on a cysteamine monolayer-modified gold electrode, and detected its electrocatalytic response to the reduction of H_2O_2 via cyclic voltammetry and amperometry. One AgNP was able of linking HRP molecules. The two dimensional electrode surface was modified to three dimensional. Also more binding sites were provided by the AgNPs for the immobilization of HRP. The linear range of the biosensor was 3.3 μM to 9.4 mM with a LOD of 0.78 μM [108]. AgNPs decorated three-dimensional GP (3DG) were synthetized via a hydrothermal process. The AgNPs-3DG composites are directly fabricated into a free standing sensing electrode for electrochemical detection of H_2O_2. The results shows that AgNPs-3DG based biosensor have fast amperometric sensing, linear responding range between 0.03 and 16.21 mM, LOD of 14.9 μM and selectivity for non-enzyme H_2O_2 detection [109]. The mixture of aqueous $FeCl_3$ and o-phenylenediamine (OPD) solutions at room temperature leads to supramolecular microfibrils of OPD dimers generated by the oxidation of OPD monomers by $FeCl_3$. The treatment of such microfibrils with a $AgNO_3$ aqueous solution transforms them into nanofibers decorated with spherical AgNPs. The AgNPs exhibit good catalytic activity toward the reduction of H_2O_2, leading to an enzymeless sensor with a fast amperometric response time of less than 5 s. The linear detection range is from 100 μM to 80 mM (r = 0.998) with LOD of 62 μM (S/N = 3) [110]. GP nanosheets (GNs) were prepared via chemical reduction of GP oxide (GO) by hydrazine hydrate in the presence of poly[(2-ethyldimethylammonioethyl methacrylate ethyl sulfate)-co-(1-vinylpyrrolidone)] (PQ11), a cationic polyelectrolyte. These Ag/GN nanocomposites exhibit good catalytic activity toward the reduction of H_2O_2 leading to an enzymeless sensor with a fast

Complimentary Contributor Copy

amperometric response time of less than 2 s. The linear range is from 100 μM to 40 mM (r = 0.996), and the LOD is estimated to be 28 μM (S/N = 3) [111]. Urchin-like Ag nanowires were prepared by reacting $AgNO_3$ with Cu metal in the presence of cetyltrimethylammonium chloride and HNO_3 on a screen printed carbon electrode at room temperature. The sensor have a high sensitivity to H_2O_2 of 4705 μA $mM^{-1}mg^{-1}cm^{-2}$ from 50 μM to 10.35 mM and a LOD of 10 μM in amperometric detection [112]. H_2O_2 electrochemical sensor was fabricated by covering a nanofibrous membrane on a GCE. Amperometric measurements indicated that the sensor based on the Ag coated nanofibrous membrane showed a linear response to H_2O_2 concentrations ranging from 10 μM to 16.5 mM with a LOD of 4 μM and a maximum sensitivity of 157 $mAcm^{-2}M^{-1}$ [113].

Based on AgNPs six optical sensors were developed. Fluorescent silver nanoclusters (AgNCs) have been bio-labeled to bovine serum albumin (BSA) protein. BSA-AgNCs display fluorescence quenching with the addition of H_2O_2. A LOD of 60 nM (S/N = 3) was found [114]. Polyethyleneimine-capped silver nanoclusters (PEI-Ag nanoclusters) sensitive to H_2O_2 and glucose were synthetized by Wen et al. The fluorescence intensity quenched linearly for H_2O_2 in the range of 500 nM –100 μM with a LOD of 400 nM [115]. A sensor developed by electrodepositing AgNPs on a modified GCE with a zinc oxide (ZnO) film showed sensibility to H_2O_2. The H_2O_2 sensor exhibits linear behavior in the concentration range 2 μM to 5.5 mM with a LOD of 0.42 μM (S/N = 3) [116]. The ordered H-terminated SiNW arrays via electroless etching method were decorated with AgNPs to fabricate a sensor for the H_2O_2 detection. At an applied potential of −0.45 V at pH 7.5, the sensor can achieve 95% of the maximum steady state current within 4 s and have the LOD of 0.2 μM [117]. A colorimetric probe for H_2O_2 using a flow injection system and AgNPs was developed. H_2O_2 concentration was quantified by monitoring decrease in AgNPs surface plasmon resonance during the decomposition reaction. The LOD for H_2O_2 was 0.6 mg/l [118]. Synthesis of AgNPs from silver nitrate using fruit extract of Benincasa hispida and the study of its ability for H_2O_2 detection by a colorimetric method was made. The AgNPs were found to detect H_2O_2 instantly [119].

The main nanoprobes using AuNPs in the detection of H_2O_2 are described in Table 7.

Complimentary Contributor Copy

Table 7. Main analytical performance of the H_2O_2 AuNPs based sensors

AuNPs nanosensors	Linear range	LOD	References
Electrochemical Sensors			
AuNPs/Thi/MWCNTs-CS	5×10^{-7} -1.5×10^{-3} M	3.75×10^{-8} M	[120]
GNP-TNT/HIL/HRP electrode	15–750 µM	2.2 µM	[121]
AuNPs/CNTs/SPAN hollow spheres	5 µM-0.225 mM 0.225 -8.825 mM	0.4 µM	[122]
HRP-AuNPs-CESM-GCE	10 µM - 2.7 mM	3 µM	[123]
AuNPs - polyvinylpyrrolidone	---	0.7 µM	[124]
AuPs	0.1 - 50 mM	4 µM	[125]
HRP-AuNPs	---	---	[126]
AuNPs	0.1-160 mM	23 µM	[127]
Optical Sensors			
AuNCs	100 nM - 100 µM	30 nM	[128]
HRP-BSA conjugated AuNPs	25 - 400 nM	10 nM	[129]
Au nanoclusters	---	$4.9x10^{-13}$ M	[130]
11-MUA-Au NDs	$0.1\text{-}1x10^{3}$ µM	0.03 µM	[131]
PVPAuNCs/ BSA-AuNCs.	1 - 100 µM	0.8 µM	[132]
Positively-charged AuNPs	$2.0x10^{-6}$ - $2.0x10^{-4}$ M	$5x10^{-7}$ M	[133]

Li et al. developed an amperometric electrochemical biosensor for the detection of H_2O_2, based on AuNPs/thionine (Thi)/AuNPs/MWCNTs–CS composite film. The linear response range of the biosensor to H_2O_2 concentration was from 5×10^{-7} to 1.5×10^{-3} M with a LOD of 3.75×10^{-8} M (S/N = 3) [120]. A composite film, AuNP–dotted TiO (TNTs) and the hydrophobic ionic liquid (HIL), 1-decyl-3-methylimidazolium tetrafluoroborate, as the entrapping agent, was used to facilitate the electron transfer of HRP on a GCE. The GNP–TNT/HIL/HRP electrode was then applied to the detection of H_2O_2. The biosensor exhibited a linear response in the 15–750 µM range, and a LOD of 2.2 µM [121]. An electrochemical non-enzymatic H_2O_2 sensor based on AuNPs/CNT/self-doped polyaniline (AuNPs/CNTs/SPAN) hollow spheres

Complimentary Contributor Copy

modified GCE was developed. The GCE modified with the microspheres showed that the hollow AuNPs/CNTs/SPAN composites improved sensitivity and selectivity to H_2O_2 detection with good stability. Due to the SPAN derivatives composite, the sensor had catalytic effect on the reduction H_2O_2 even under alkaline conditions. Using chronoamperometric method at a constant potential of -0.1 V, the H_2O_2 sensor displays two linear ranges: one from 5 μM to 0.225 mM with a sensitivity of 499.82 $\mu AmM^{-1}cm^{-2}$; another from 0.225 to 8.825 mM with a sensitivity of 152.29 $\mu AmM^{-1}cm^{-2}$. The LOD was estimated as 0.4 μM (S/N = 3) [122]. An amperometric HRP biosensor for H_2O_2 detection was developed by deposition of AuNPs onto a three-dimensional porous carbonized chicken eggshell membrane (CESM). The HRP-AuNPs-CESM-GCE electrode was synthetized by deposition of AuNPs onto a GCE with carbonized eggshell membrane support. The HRP-AuNPs-CESM-GCE electrode, showed good results as H_2O_2 biosensor in range between 10 μM and 2.7 mM, with a LOD of 3 μM and a response time of 3 s [123]. A H_2O_2 biosensor based on AuNPs stabilized in polyvinylpyrrolidone was established. The electrochemical results show electrocatalytic activity of the electrode towards H_2O_2 detection. A large linear range with LOD of 0.7 μM was observed [124]. Ning et al. synthesized Au nanoplates (AuPs) by heating an aqueous solution of $HAuCl_4$ in presence of poly [(2-ethyldimethylammonioethyl methacrylate ethyl sulfate)-co-(1-vinylpyrrolidone)] (PQ11). Direct placing of the dispersion on a GCE surface gives a stable AuPs-containing film with catalytic activity H_2O_2. The sensor shows a fast response time of less than 3 s, a linear range from 0.1 to 50 mM (r = 0.999) and LOD of 4 μM (S/N = 3) [125]. Recently a H_2O_2 biosensor for transports a monolayer of nanocomplex composed of HRP and AuNPs, and responds to H_2O_2 through the highly efficient direct electron transfer at a mild electrode potential without any soluble mediator. The response of electrochemical sensor relatively to H_2O_2 was of +0.15V [126]. AuNPs prepared by reduction of $HAuCl_4$ using CDs as reducing agent showed electrochemical catalytic ability for reduction of H_2O_2, leading to its application of a non-enzymatic H_2O_2 sensor. The H_2O_2 sensor based on AuNPs was performed, with a LOD of 23 μM in a linear range between 0.1–160 mM [127].

Some optical H_2O_2 AuNPs based sensors are described. An enzyme functionalized fluorescent gold nanoclusters AuNCs was fabricated trough a biomineralization process. HRP was used as a model functional template to the direct synthesis of AuNCs to form HRP-AuNCs bioconjugates. The HRP-AuNCs fluorescence is quenched by adding H_2O_2, indicating that HRP

Complimentary Contributor Copy

enzyme remains active and enables catalytic reaction of HRP-AuNCs and H_2O_2. Upon the addition of H_2O_2, the fluorescence intensity quenched linearly over the range of 100 nM to 100 μM with high sensitivity (LOD = 30 nM, S/N = 3) [128]. A sensitive determination of H_2O_2, glucose and uric acid based on FRET using AuNPs as energy acceptors was presented. Based on highly sensitive reaction of tetramethylrhodamine (TMR) labeled tyramide and H_2O_2 catalysed by HRP, and the fluorescence spectrum of TMR partially overlaps with the visible absorption bands of AuNPs. An efficient FRET between tyramide labeled TMR (as energy donors) and HRP (BSA) conjugated AuNPs (as energy acceptors) due to the formation of TMR-labeled HRP–AuNPs or TMR-labeled BSA-AuNPs in the presence of H_2O_2. The analysis results show that the FRET system was applicable for H_2O_2 detection with a low LOD of 10 nM in a linear range from 25 to 400 nM [129]. Colorimetric determination of H_2O_2 using multi-functional Au nanoclusters AuNCs was demonstrated based on the intrinsic peroxidase-like activity of AuNCs stabilized by glutathione (GSH). The color change of 3,3,5,5tetramethylbenzidine (TMB) catalyzed by AuNCs offers an indirect method to glucose determination. The LODs of H_2O_2 and glucose are $4.9x10^{-13}$ M and $1.0x10^{-11}$ M, respectively [130]. More recently a luminescent assay using 11-mercaptoundecanoic acid-bound Au nanodots (11-MUA–Au NDs) for the selective and sensitive detection of H_2O_2 and glucose, based on luminescence quenching was presnted [131]. Also a new IFE based approach using poly(vinylpyrrolidone)-protected AuNPs as an IFE absorber and bovine serum albumin-protected AuNCs (BSA-AuNCs) as an IFE fluorophore for sensing H_2O_2 and cholesterol was developed. The catalytic growth of PVP-AuNCs by H_2O_2 influences the emission of BSA-AuNCs in a delicate yet significant way, which may be due to the overlap between the SPR band of the AuNPs and the excitation band of AuNCs. The quantification results of H_2O_2 and cholesterol was 0.8 and 1.4 μM, respectively in a linear range from 1 to 100 μM [132]. Positively-charged AuNPs possess intrinsic peroxidase like activity and can catalyze oxidation of the peroxidase substrate TMB by H_2O_2 to develop a blue color in aqueous solution providing a method to colorimetric detection of H_2O_2 and glucose. The H_2O_2 determination was made in a linear range between $2.0x10^{-6}$ - $2.0x10^{-4}$ M with a LOD of $5x10^{-7}$M [133].

The H_2O_2 detection methodologies using QDs are described in Table 8.

Complimentary Contributor Copy

Table 8. Main analytical performance of the H_2O_2 QDs based sensors

QDs nanosensors	Linear range	LOD	References
Electrochemical			
ZnSe QDs	2.5×10^{-7} - 6.0×10^{-5} M	1.0×10^{-5} M	[134]
ZnSe QDs	6.10×10^{-7} - 3.10×10^{-4} M	2.00×10^{-7} M	[135]
Optical			
CdTe-MSA-HRP	$1x10^{-6}$ - $1x10^{-3}$ M	$1x10^{-3}$M	[136]
CdTe-GSH-MPA	0.0025% - 0.040%	0.040%	[137]
CdTe/ZnS-MPA-MTAPc	1-16 nM		[138]
QD-HRP-Cy5	10 - 100 nM	10 nM	[139]
GQDs metalloporphyrins	2–300 µM	0.3 µM	[140]
glutathione capped QDs	---	3 µM	[141]

Based on QDs two H_2O_2 electrochemical sensors were developed. The electrogenerated chemiluminescence (ECL) of CdSe nanocrystal thin films was studied by depositing CdSe nanocrystals on a paraffin-impregnated graphite electrode (PIGE). With addition of H_2O_2, an enhancement of the intensity of ECL emission of CdSe nanocrystal thin films was observed. A linear response of ECL relatively to H_2O_2 from $2.5x10^{-7}$ to $6x10^{-5}$ M with a LOD of $1x10^{-5}$ M was observed [134]. The ECL of ZnSe QDs was used to detect H_2O_2. The weak ECL emission of ZnSe QDs was generated when the electrode potential was scanned from 0.0 to −1.4 V (vs Ag/AgCl), and the ECL intensity was greatly enhanced in the presence of H_2O_2. The dynamic range is from 6.10×10^{-7} and 3.10×10^{-4} M the LOD is 2.00×10^{-7} M (S/N = 3) [135].

The majority of the H_2O_2 detection methods based in QDs are optical sensors. Yuan et al. developed a CdTe QDs-enzyme hybrid system combining the properties of QDs and the specificity of enzymatic reactions for both phenolic compounds and H_2O_2 detection. In the presence of H_2O_2 and HRP, phenolic compounds can quench QDs photoluminescence. Using a MSA-capped-QDs-enzyme system, the LODs for H_2O_2 was $1x10^{-7}$ M in a linear range between $1x10^{-6}$ and $1x10^{-3}$ M [136]. In other wok based on reduced glutathione (GSH) induced fluorescent enhancement of mercaptopropionic acid (MPA) capped CdTe-QDs a chemosensor for H_2O_2 determination was developed. H_2O_2 increase the oxidation of glutathione to glutathione disulfide

Complimentary Contributor Copy

and consequently a decrease in SH groups was observed. A linear working calibration curve for H_2O_2 concentrations between 0.0025% and 0.040% (n=6), with a correlation coefficient of 0.9975 and LOD of 0.0012% was obtained [137]. H_2O_2 nanoprobes based on the covalent conjugation of CdTe@ZnS-QDs with three different metals (Al, Ni and Zn) tetraamino-phthalocyanine can be covalently linked to QDs to form a QDs-MTAPc nanoconjugate which can be applied as a luminescence nanosensor for ROS detection. Interaction between the QDs and MTAPc occurred through FRET which in turn *switched off* the fluorescence of the QDs. In the presence of varying concentrations of H_2O_2, the fluorescence of the QDs was *switched on* and the degree of sensitivity/LOD followed the order: QDs-ZnTAPc>QDs-NiTAPc>QDs-AlTAPc [138]. Huang et al. determinate H_2O_2 based on QD-based FRET and tyramide reaction. The principle of FRET is based on sensitive reaction of a carbocyanine dye (Cy5) labeled tyramide and H_2O_2 catalyzed by HRP. Was observed that the fluorescence Cy5 depended linearly on the H_2O_2 concentration in a range from 10 to 100 nM with LOD of 10 nM [139]. Zanhg et al. developed a *turn on* system based on GQDs assembled with metalloporphyrins for H_2O_2 sensing. The *turn on* system for H_2O_2 sensing and can be further extended to the detection of glucose. A linear calibration for H_2O_2 concentration in the range 2–300 µM (R^2 = 0.993), with a LOD of 0.3 µM was obtained [140]. The use of glutathione capped QDs as fluorescence probe for the detection H_2O_2 was validated using a kinetic approach. Was obtained a linear variation (R^2=0.9929) with a slope of 1795 cps µM and LOD of 3 µM [141].

Other families of NPs were also used in H_2O_2 sensing. Bimetallic Platinum (Pt) - ruthenium NPs were prepared and characterized for the H_2O_2 detection [142]. Polypyrrole NPs presented intrinsic peroxidase-like activity and can be employed to monitor H_2O_2 [143]. Hollow graphitic nanocapsules were applied as efficient electrode materials for the H_2O_2 sensing [144]. A H_2O_2 sensor based on Pd NPs and GCE was fabricated by Wang et al. The electrode with an optimized NP coverage of 85 % presented high selectivity to H_2O_2 [145]. A H_2O_2 sensor based on Fe_3O_4 magnetic NPs was fabricated [146]. Polyethyleneimine (PEI)-capped copper nanoclusters were applied as a H_2O_2 fluorescent probe in aqueous solution [147]. An enzyme-free spectrophotometric detection of H_2O_2 was established based on its colorimetric reaction with oxygen deficient cerium oxide NPs immobilized on poly(4-vinylpyridine) self-assembled monolayers [148]. Supramolecular fluorescent NPs self-assembled from fluorescein isothiocyanate modified b-cyclodextrin (FITC-b-CD)/rhodamine B modified ferrocene (Fc-RB)

Complimentary Contributor Copy

amphiphile were prepared through host–guest interaction between FITC-b-CD host and Fc-RB guest for H_2O_2 detection [149]. Mao et al. used poly (thymine)-templated copper NPs as a fluorescent indicator for H_2O_2 [150]. Rhodium NPs-mesoporous silicon nanowire nanohybrids were also used in H_2O_2 detection [151]. The H_2O_2 sensing was made based on Pt-Au bimetallic NPs electrodeposited on reduced graphene sheets [152].

The synthesis of QDs based on graphene (GQDs) with intrinsic peroxidase-like catalytic activity was developed by pyrolysis of the aminoacid, L-glutamic acid. The GQDs showed strong blue, green and red luminescence under the irradiation of ultra-violet, blue and green light, respectively. Moreover, the GQDs emitted near-infrared (NIR) fluorescence. Coupled with 2,2′-azino-bis(3-ethylbenzothiazoline-6-sulphonic acid) (ABTS), the GQDs can be used for the sensitive detection of H_2O_2 with a LOD of 20 μM [153]. A colorimetric procedure based on AgNPs on the surface of GQDs is proposed for H_2O_2 detection. The GQDs/AgNPs hybrid exhibits a absorbance decrease response to the reduction of H_2O_2. In this work a LOD of 33 nM for the detection of H_2O_2 was obtained [154].

5. SUPEROXIDE ($O_2^{\bullet-}$)

The superoxide anion radical ($O_2^{\bullet-}$), briefly called as superoxide, is also one of the more important ROS. Acts as a powerful oxidizing agent and may be produced in living systems. Few nanoprobes were proposed for $O_2^{\bullet-}$ detection.

One method for the detection of $O_2^{\bullet-}$ using CDs was reported. In this analytical methodology the CDs were electrochemically prepared and used as fluorescent biosensor for ratiometric monitoring of $O_2^{\bullet-}$. CDs functionalization was made using the fluorophore hydroethidine (HE), a specific organic molecule toward $O_2^{\bullet-}$. The nonfluorescent HE can react with $O_2^{\bullet-}$ with high selectivity to generate the products which showed an emission peak at 610 nm. The hybrid probe CD-HE only emitted at 525 nm is ascribed to CDs. After reaction with $O_2^{\bullet-}$, a new emission peak attributed to the reaction products of was clearly observed at 610 nm, this peak gradually increases with the concentration of $O_2^{\bullet-}$ while the fluorescence emission at 525 nm ascribed to CDs had no obvious changes, leading to the ratiometric detection $O_2^{\bullet-}$. The sensor shows linearity with the $O_2^{\bullet-}$ concentration from 500 nM to 30 μM with a LOD of 100 nM [155].

Complimentary Contributor Copy

Two analytical methods using AgNPs were reported in $O_2^{\bullet-}$ detection. In the first method a fluorescent nanoprobe DBZTC/Ag@SiO_2 with sensitivity and selectivity for detection and imaging of $O_2^{\bullet-}$ in living cells was synthesized by a simple self-assembly method based on 2-chloro-1,3-dibenzothiazoline-cyclohexene (DBZTC) and Ag@SiO 2 core–shell NPs. The sensitivity and selectivity of the DBZTC/Ag@SiO nanocomposite for detection of $O_2^{\bullet-}$ was showed [156]. In other method colloidal AgNPs were synthetized by reduction of silver nitrate solution using Olax scandens leaf extract were synthetized. A method has been investigated for anti-bacterial and anti-cancer activity of b-AgNPs. The formation of ROS are involved in anticancer activities. Hence, anti-cancer activity of bio-synthesized AgNPs towards A549 and B16 cells may be attributed due to the formation of ROS especially $O_2^{\bullet-}$ and H_2O_2 [157].

The only application of AuNPs in the $O_2^{\bullet-}$ detection was electrochemical. A composite fiberelectrode fabricated by dispersing AuNPs onto poly(methyl methacrylate)(PMMA)–polyaniline (PANI) core–shell electrospun nanofibers was developed. Direct electron transfer is achieved between SOD and the electrode with an electron transfer rate constant of 8.93 s^{-1}. At an applied potential of +300 mV, AuNPs dispersed poly(methylmethacrylate)–polyaniline core–shell nanofibrous membrane (PMMA/PANI–Au_{nano}–ESCFM) shows highly sensitive detection of $O_2^{\bullet-}$ [158]. A different technique based on the layer-by-layer self-assembly of positively charged CTAB wrapped AuNRs and negatively charged SOD from their aqueous solutions on cysteine modified gold electrode, a third generation biosensor ((SOD/AuNRs)/Cys/Au electrode) for $O_2^{\bullet-}$ was developed. The electrochemical biosensor ((SOD/AuNRs)$_2$/Cys/Au) can sense $O_2^{\bullet-}$. The (SOD/AuNRs)/Cys/Au electrode showed good analytical performance in a wider linear range from 200 nM to 0.2 mM with LOD of 100 nm and sensibility of 22.11 $nAcm^{-2}\mu M^{-1}$ [159].

The use of QDs as $O_2^{\bullet-}$ probe was described. The fluorescence intensity of the negatively capped QD-oxidized Cyt c system was enhanced when the $O_2^{\bullet-}$ was generated using pyrogallol assay. The coupling system of negatively capped CdSe/ZnS-QDs with an oxidized Cyt c is capable of the fluorescent imaging of an $O_2^{\bullet-}$ with high sensitivity and specificity in living cells. The oxidized Cyt c provokes fluorescence quenching of the negatively capped QDs, while the reduced form of Cyt c, incubated with negatively capped QDs, leads to the recovery of the fluorescence of the QDs [160]. In other work CdTe@ZnS-QDs and cobalt tetraamino-phthalocyanine were coordinated. The linking of thiol-capped CdTe@ZnS-QDs with cobalt tetraamino-

Complimentary Contributor Copy

phthalocyanine results in the fluorescence quenching of the former. The $O_2^{\bullet-}$ addition results in fluorescence enhancement with LOD of about 2 nM [161].

Some $O_2^{\bullet-}$ sensors based in other kind of nanoparticles are now described. Kim et al. prepared and characterized hydrocyanine-conjugated and CS-functionalized pluronic-based nano-carriers, which can detect ROS including $O_2^{\bullet-}$. The reduction of cyanine to hydrocyanine of the nano-carriers resulted in disappearance of fluorescence emission, and the fluorescence could be recovered by ROS-induced reoxidization [162]. Copper–zinc composite NPs based enzyme-free amperometric sensors were used on a screen-printed electrode for $O_2^{\bullet-}$ sensing [163].

6. HIPOCHLORITE (ClO^-)

Hypochlorous acid (HClO) is a weak acid that dissociates into hypochlorite ion (ClO^-) and hydrogen. Together, HClO and ClO^- are known as free chlorine. The two species are in an equilibrium that is pH dependent. Below a pH of 7.5 hypochlorous acid is the dominant specie and above a pH of 7.5, hypochlorite ion is the dominant specie. HClO oxidize a great number of biological compounds. Myeloperoxidase (MPO) is the neutrophil enzyme recognized to be a source of HClO production [164]. HClO is usually used as antimicrobial agent; is also used in water treatment for natural defense in living organisms. All the ($HClO/ClO^-$) proposed nanoprobes are optical.

Some CDs based sensors were applied in HClO detection. Recently a sensor based on fluorescence quenching mechanism of nitrogen-doped CDs (N-CDs) showed a relatively fast response time and a linear response range for HClO ($R^2 = 0.994$) from 0.03 to 15 μM and a LOD of 1 nM. This method has been successfully applied to the determination of HClO in tap and river water with recoveries in the range of 96.0–104.8% and 95.5–103.6% and presented potential for the detection of HClO in environmental applications [165]. A different sensor for HClO based on the fluorescence of CDs was prepared by one-step microwave-assisted procedure. A decreased of 76 % when the concentration of HClO reached 2.2 μM was observed. There is a good linear relationship (R^2=0.994) in the range from 0.2 to 2.0 μM. The LOD was of 15 nM [166]. Another sensor prepared from sweet pepper based on fluorescence quenching of CDs in the presence of ClO^- in tap water was reported. The HClO detection was made within a wide range of 0.1 to 10 μM to 10 to 300 μM in two consecutive linear ranges with a low LOD of 0.05 and

Complimentary Contributor Copy

0.06 μM using both the down- and up-conversion fluorescence signals (S/N = 3) [167].

CdSe-ZnS-QDs based fluorometric assay for ClO^- quantification, monitoring the HClO generation activity of myeloperoxidase and detecting HClO in the LH60 cell line was demonstrated. The QDs were coated with organic ligands for fluorescence detection of HClO [168]. ClO^- can directly oxidize glucose-derived GP QDs to give increase to chemiluminescence emission, The determination of ClO^- with these method was made in the concentration range from 0.5 μM to 1.0 mM, with a LOD of 0.3 μM [169]. The quantification of endogenous HClO produced by leukocytes *in vitro* and *in vivo* was made with a QD-based sensor. Selectivity assays relatively to other ROS allows to demonstrate high selectivity towards HClO [170]. Another fluorescent assay for simultaneous screening of MPO inhibitors and HClO scavengers was developed using QDs as HClO probe. The fluorescent quenching of QDs.provoked by HClO produced from HL60 cells was showed [171].

Nanoprobes for HClO based in other NPs were reported. A ratiometric sensing system based on core–shell structured silica NPs (SiNPs) was described for the HClO sensing. A phosphorescent ratiometric probe for ClO^- was prepared by incorporation of two iridium (III) complexes into the NPs. This probe was used to detect intracellular exogenous and endogenous ClO^- [172]. Also was reported a fluorogenic optical sensor based on oxazine conjugated NPs for the detection *in vivo* of HClO and $ONOO^-$ generation [69].

7. HYDROXYL RADICAL (•OH)

Hydroxyl radicals (•OH) are an important type of ROS. Is a short-lived radical with high reactivity. Biomolecules such as nucleic acids, proteins, carbo- hydrates, and lipids are susceptible to attack by •OH which leads to many diseases, such as irreparable cellular damage or cell death, embryo teratogenesis, and inflammation [173]. Due to is short lifetime and high instability is detection is very difficult.

Fluorescent CDs, sensible to •OH, were obtained from polyvinylpyrrolidone by a hydrothermal method. The fluorescence intensity of these CDs showed sensibility to •OH based on the fluorescence quenching with great sensitivity. A linear correlation (R^2 = 0.997) is on the basis of the quenching effects on the concentration of l-ascorbate over the range from 50 to 1000 μM. [174]. Other CDs sensor for •OH based on colloidal

Complimentary Contributor Copy

nanocomposites consisting of CDs and dodecylbenzenesulfonate (DBS)-layered double hydroxides (LDHs) was synthetized. The resulting nanocatalyst can function as a heterogeneous Fenton-like catalyst for the decomposition of acidified H_2O_2 to generate •OH associated with an enhancement in the chemiluminescence. The sensor presents a family of Fenton-like nanocatalysts with selectivity for the decomposition of H_2O_2 to •OH. The catalytic performance of this CD-LDH catalyst was used to promote the heterogeneous Fenton-like reaction by evaluating DBS degradation without any external energy input [175].

Two works showed the application of AuNPs in the detection of •OH. In the first, a ratiometric fluorescence biosensor for •OH was developed for bioimaging and biosensing in live cells. In this sensor a gold nanocluster (AuNC) protected by BSA was used as a reference fluorophore and the organic molecule 2-[6-(4'-hydroxy)phenoxy-3H-xanthen-3-on-9-yl]benzoic acid (HPF) acted as both the response signal and specific recognition element for •OH. The sensor showed high selectivity for •OH over other ROS, RNS, metal ions, and other biological species, and sensitivity with low LOD of 0.68 μM in a linear range from 1 to 150 μM [176]. In the second AuNPs based •OH sensor a DNA-based electrochemical sensor has constructed for sensitive detection of •OH based on the silver-enhanced gold NPs label. Thiolated DNA1 was firstly immobilized on the gold electrode through Au-S bonds. The •OH generated from Fenton reaction could induce serious oxidative damage of the DNA1 layer on the electrode surface. Then DNA2-functionalized gold NPs (DNA2-Au NPs) were linked on the electrode through the hybridization between DNA2 and undamaged DNA1. Based on the catalytic reduction of silver ion by Au NPs, a silver layer was formed on the surface of Au NPs. The quantitative assay of •OH was carried out by differential pulse voltammetry (DPV) detection of the deposited silver. Under the optimization conditions, the developed DNA-based biosensor could detect •OH quantitatively with linear range (0.2 - 200 μM) and LOD of 50 nM [177].

A probe based on QDs was developed for determination of •OH by comparative studies between different thiol-capped CdTe and CdTe@ZnS QDs. The results showed that the type of capping agent and QDs influenced the sensitivity and selectivity of the probe with GSH-CdTe@ZnS giving the best sensitivity, and a LOD of 8.5×10^{-8} M [178]. Another work explains the electrochemiluminescence ECL process of the thioglycolic acid-capped CdSe QDs film/peroxide aqueous system CdSe/TGA QDs. The intermediate •OH radical is a key species in the ECL process. Therefore, all •OH radical

Complimentary Contributor Copy

involved reactions will quench the ECL emission, generating a ECL sensor [179].

CONCLUSION/PERSPECTIVES

In this chapter the most promising nanomaterials for the development of electrochemically or optical sensors for the ROS/RNS electrochemical or optical sensing were reviewed. A considerable great number of nanoprobes were already developed for the sensing of the principal ROS/RNS. Is for the H_2O_2 that the major number of nanoprobes were already developed.

The majority of the already developed electrochemical sensors are amperometric sensors based in CNT, AuNPs or AgNPs and the majority of the already developed optical sensors are based in quenching of QDs fluorescence.

Due to their own specifical properties is expected that a greater number of electrochemical and optical nanoprobes will be developed in the near future not only for the NO, $ONOO^-$, H_2O_2. $O_2^{\bullet-}$, ClO^- or $^\bullet OH$ but also for other ROS/RNS. The *in vivo* sensing associated to the diagnostic or even as vehicle of therapeutic drugs is also an objective that could be achieved with the development of nanoprobes.

ACKNOWLEDGMENTS

Financial support from Fundação para a Ciência e Tecnologia (FCT, Lisbon) project PEST and a PhD grant to Eliana Simões SFRH/BD/81074/2011 is acknowledged.

REFERENCES

[1] Bergendi, L., et al., Chemistry, physiology and pathology of free radicals. *Life Sciences,* 1999. 65(18–19): p. 1865-1874.

[2] Valko, M., et al., Free radicals and antioxidants in normal physiological functions and human disease. *Int J Biochem Cell Biol,* 2007. 39(1): p. 44-84.

Complimentary Contributor Copy

[3] Halliwell, B. and M. Whiteman, Measuring reactive species and oxidative damage in vivo and in cell culture: how should you do it and what do the results mean? *Br J Pharmacol*, 2004. 142(2): p. 231-55.
[4] Calas-Blanchard, C., G. Catanante, and T. Noguer, Electrochemical Sensor and Biosensor Strategies for ROS/RNS Detection in Biological Systems. *Electroanalysis,* 2014. 26(6): p. 1277-1286.
[5] Borgmann, S., Electrochemical quantification of reactive oxygen and nitrogen: challenges and opportunities. *Anal Bioanal Chem*, 2009. 394(1): p. 95-105.
[6] McQuade, L.E. and S.J. Lippard, Fluorescent probes to investigate nitric oxide and other reactive nitrogen species in biology (truncated form: fluorescent probes of reactive nitrogen species). *Curr Opin Chem Biol,* 2010. 14(1): p. 43-9.
[7] Chen, X., et al., Fluorescent and luminescent probes for detection of reactive oxygen and nitrogen species. *Chemical Society Reviews*, 2011. 40(9): p. 4783-4804.
[8] Zamborini, F.P., L. Bao, and R. Dasari, Nanoparticles in measurement science. *Anal Chem,* 2012. 84(2): p. 541-76.
[9] Valentini, F. and G. Palleschi, Nanomaterials and Analytical Chemistry. *Analytical Letters*, 2008. 41(4): p. 479-520.
[10] Eckert, M.A., et al., Novel molecular and nanosensors for in vivo sensing. *Theranostics,* 2013. 3(8): p. 583-94.
[11] Xu, T., et al., Electrochemical Sensors for Nitric Oxide Detection in Biological Applications. *Electroanalysis,* 2014. 26(3): p. 449-468.
[12] Zhu, C., et al., Electrochemical Sensors and Biosensors Based on Nanomaterials and Nanostructures. *Analytical Chemistry,* 2015. 87(1): p. 230-249.
[13] Ruedas-Rama, M.J., et al., Fluorescent nanoparticles for intracellular sensing: a review. *Anal Chim Acta,* 2012. 751: p. 1-23.
[14] Moradi, O., et al., Carbon Nanotubes: A Review of Chemistry Principles and Reactions. *Fullerenes, Nanotubes and Carbon Nanostructures*, 2012. 20(2): p. 138-151.
[15] Liu, Z., et al., Carbon Nanotubes in Biology and Medicine: In vitro and in vivo Detection, Imaging and Drug Delivery. *Nano Res,* 2009. 2(2): p. 85-120.
[16] Himaja, A.L., P.S. Karthik, and S.P. Singh, Carbon Dots: The Newest Member of the Carbon Nanomaterials Family. *The Chemical Record,* 2015. 15(3): p. 595-615.

Complimentary Contributor Copy

[17] Zuo, J., et al., Preparation and Application of Fluorescent Carbon Dots. *Journal of Nanomaterials,* 2015. 2015: p. 13.
[18] Kairdolf, B.A., et al., Semiconductor quantum dots for bioimaging and biodiagnostic applications. *Annu Rev Anal Chem* (Palo Alto Calif), 2013. 6: p. 143-62.
[19] Zhang, X., Gold Nanoparticles: Recent Advances in the Biomedical Applications. *Cell Biochem Biophys,* 2015.
[20] Yeh, Y.C., B. Creran, and V.M. Rotello, Gold nanoparticles: preparation, properties, and applications in bionanotechnology. *Nanoscale,* 2012. 4(6): p. 1871-80.
[21] Tiwari, P., et al., Functionalized Gold Nanoparticles and Their Biomedical Applications. *Nanomaterials,* 2011. 1(1): p. 31.
[22] Yu, A.K., et al., Synthesis and properties of silver nanoparticles: advances and prospects. *Russian Chemical Reviews,* 2008. 77(3): p. 233.
[23] Hetrick, E.M. and M.H. Schoenfisch, Analytical chemistry of nitric oxide. *Annu Rev Anal Chem* (Palo Alto Calif), 2009. 2: p. 409-33.
[24] Yao, D., A.G. Vlessidis, and N.P. Evmiridis, Determination of Nitric Oxide in Biological Samples. *Microchimica Acta,* 2004. 147(1-2).
[25] Paolo, S., Nitric Oxide in Human Health and Disease. eLS, 2013.
[26] Porras Gutierrez, A., et al., Hybrid Materials from Carbon Nanotubes, Nickel Tetrasulfonated Phthalocyanine and Thin Polymer Layers for the Selective Electrochemical Activation of Nitric Oxide in Solution. *Electroanalysis*, 2009. 21(21): p. 2303-2310.
[27] Maluta, J.R., T.C. Canevari, and S.A.S. Machado, Sensitive determination of nitric oxide using an electrochemical sensor based on MWCNTs decorated with spherical Au nanoparticles. *Journal of Solid State Electrochemistry,* 2014. 18(9): p. 2497-2504.
[28] Yap, C.M., G.Q. Xu, and S.G. Ang, Amperometric nitric oxide sensor based on nanoporous platinum phthalocyanine modified electrodes. *Anal Chem, 2013.* 85(1): p. 107-13.
[29] Zhang, J., et al., Single Molecule Detection of Nitric Oxide Enabled by d(AT)15 DNA Adsorbed to Near Infrared Fluorescent Single-Walled Carbon Nanotubes. *Journal of the American Chemical Society*, 2011. 133(3): p. 567-581.
[30] Santos, R.M., et al., Biomimetic sensor based on hemin/carbon nanotubes/chitosan modified microelectrode for nitric oxide measurement in the brain. *Biosens Bioelectron,* 2013. 44: p. 152-9.

Complimentary Contributor Copy

[31] Deng, X., F. Wang, and Z. Chen, A novel electrochemical sensor based on nano-structured film electrode for monitoring nitric oxide in living tissues. *Talanta,* 2010. 82(4): p. 1218-24.
[32] Abdelwahab, A.A., et al., A selective nitric oxide nanocomposite biosensor based on direct electron transfer of microperoxidase: removal of interferences by co-immobilized enzymes. *Biosens Bioelectron*, 2010. 26(3): p. 1080-6.
[33] Zheng, D., et al., Noncovalently functionalized water-soluble multiwall-nanotubes through azocarmine B and their application in nitric oxide sensor. *Electrochemistry Communications,* 2008. 10(1): p. 90-94.
[34] Kim, J.-H., et al., The rational design of nitric oxide selectivity in single-walled carbon nanotube near-infrared fluorescence sensors for biological detection. *Nat Chem*, 2009. 1(6): p. 473-481.
[35] Iverson, N.M., M.S. Strano, and G.N. Wogan In Vivo Delivery of Nitric Oxide-Sensing, Single-Walled Carbon Nanotubes. *Current protocols in chemical biology*, 2015. 7, 93-102 DOI: 10.1002/9780470559277.ch140196.
[36] Yu, C., et al., A fluorescent ratiometric nanosensor for detecting NO in aqueous media and imaging exogenous and endogenous NO in live cells. *Journal of Materials Chemistry B,* 2013. 1(33): p. 4152.
[37] Simões, E.F.C., J.C.G. Esteves da Silva, and J.M.M. Leitão, Peroxynitrite and nitric oxide fluorescence sensing by ethylenediamine doped carbon dots. *Sensors and Actuators B: Chemical,* 2015. 220: p. 1043-1049.
[38] Gan, X., et al., An electrochemical biosensor for nitric oxide based on silver nanoparticles and hemoglobin. *Anal Sci*, 2004. 20(9): p. 1271-5.
[39] Zhu, M., et al., Novel nitric oxide microsensor and its application to the study of smooth muscle cells. *Analytica Chimica Acta*, 2002. 455(2): p. 199-206.
[40] Gu, H.Y., et al., A Novel Nitric Oxide Cellular Biosensor Based on Red Blood Cells Immobilized on Gold Nanoparticles. *Analytical Letters,* 2006. 39(15): p. 2849-2859.
[41] Li, J., et al., Au Nanoparticles–3D Graphene Hydrogel Nanocomposite To Boost Synergistically in Situ Detection Sensitivity toward Cell-Released Nitric Oxide. *ACS Applied Materials and Interfaces,* 2015. 7(4): p. 2726-2734.
[42] Zan, X., et al., Freestanding graphene paper decorated with 2D-assembly of Au@Pt nanoparticles as flexible biosensors to monitor live cell secretion of nitric oxide. *Biosens Bioelectron,* 2013. 49: p. 71-8.

Complimentary Contributor Copy

[43] Ting, S.L., et al., Gold nanoparticles decorated reduced graphene oxide for detecting the presence and cellular release of nitric oxide. *Electrochimica Acta,* 2013. 111: p. 441-446.
[44] Wang, F., et al., Nitric oxide measurement in biological and pharmaceutical samples by an electrochemical sensor. *Journal of Solid State Electrochemistry,* 2011. 15(4): p. 829-836.
[45] Dang, X., et al., Gold nanoparticle film grown on quartz fiber and its application as a microsensor of nitric oxide. *Sensors and Actuators B: Chemical,* 2011. 160(1): p. 260-265.
[46] Xu, M.-Q., J.-F. Wu, and G.-C. Zhao, Direct Electrochemistry of Hemoglobin at a Graphene Gold Nanoparticle Composite Film for Nitric Oxide Biosensing. *Sensors,* 2013. 13(6): p. 7492.
[47] Barker, S.L.R. and R. Kopelman, Development and Cellular Applications of Fiber Optic Nitric Oxide Sensors Based on a Gold-Adsorbed Fluorophore. *Analytical Chemistry,* 1998. 70(23): p. 4902-4906.
[48] Barker, S.L.R., et al., Ratiometric and Fluorescence-Lifetime-Based Biosensors Incorporating Cytochrome c ' and the Detection of Extra- and Intracellular Macrophage Nitric Oxide. *Analytical Chemistry*, 1999. 71(9): p. 1767-1772.
[49] Tan, L., et al., Biocompatible quantum dots–chitosan nanocomposites for fluorescence detection of nitric oxide. *Materials Chemistry and Physics,* 2012. 134(2–3): p. 562-566.
[50] Tan, L., et al., Novel quantum dots-carboxymethyl chitosan nanocomposite nitric oxide donors capable of detecting release of nitric oxide in situ. *Acta Biomater,* 2012. 8(10): p. 3744-53.
[51] Tan, L., A. Wan, and H. Li, Quantum dots-poly(N-isopropylacrylamide) hybrid nanogel diazeniumdiolates as donors and real-time probes of nitric oxide. *Materials Chemistry and Physics,* 2013. 138(2-3): p. 956-962.
[52] Fabregat, V., et al., Quantum dot–polymethacrylate composites for the analysis of NOx by fluorescence spectroscopy. *Inorganica Chimica Acta,* 2012. 381: p. 212-217.
[53] Simoes, E.F., J.M. Leitao, and J.C. Esteves da Silva, NO Fluorescence Quantification by Chitosan CdSe Quantum Dots Nanocomposites. *J Fluoresc,* 2013.
[54] Ding, L., et al., A sensitive optic fiber sensor based on CdSe QDs fluorophore for nitric oxide detection. *Sensors and Actuators B: Chemical,* 2013. 185: p. 70-76.

Complimentary Contributor Copy

[55] Ivanisevic, A., et al., Photoluminescent Properties of Cadmium Selenide in Contact with Solutions and Films of Metalloporphyrins: Nitric Oxide Sensing and Evidence for the Aversion of an Analyte to a Buried Semiconductor−Film Interface. *Journal of the American Chemical Society,* 2000. 122(15): p. 3731-3738.

[56] Liu, S., et al., Quantum dots-hyperbranched polyether hybrid nanospheres towards delivery and real-time detection of nitric oxide. *Mater Sci Eng C Mater Biol Appl,* 2014. 45: p. 37-44.

[57] Ding, L., et al., Synthesis and characterization of a novel nitric oxide fluorescent probe CdS-PMMA nanocomposite via in-situ bulk polymerization. *Materials Science and Engineering: C,* 2014. 35: p. 29-35.

[58] Wang, S., M.-Y. Han, and D. Huang, Nitric Oxide Switches on the Photoluminescence of Molecularly Engineered Quantum Dots. *Journal of the American Chemical Society,* 2009. 131(33): p. 11692-11694.

[59] Sun, J., et al., Fluorescence turn-on detection of gaseous nitric oxide using ferric dithiocarbamate complex functionalized quantum dots. *Anal Chem,* 2014. 86(12): p. 5628-32.

[60] Wadhavane, P.D., et al., Organogel–quantum dots hybrid materials displaying fluorescence sensitivity and structural stability towards nitric oxide. *Soft Matter,* 2012. 8(16): p. 4373.

[61] Yan, X.Q., et al., Fluorescence sensing of nitric oxide in aqueous solution by triethanolamine-modified CdSe quantum dots. *Luminescence*, 2009. 24(4): p. 255-9.

[62] Koo, E. and J.-C. Lee, A turn-on fluorescent probe for detecting nitric oxide in aqueous media. *Journal of Nanomaterials,* 2014. 2014: p. 210.

[63] He, Q., D. Zheng, and S. Hu, Development and application of a nano-alumina based nitric oxide sensor. *Microchimica Acta,* 2008. 164(3-4): p. 459-464.

[64] Miao, R., et al., Modified silicon nanowires: a fluorescent nitric oxide biosensor with enhanced selectivity and stability. *Journal of Materials Chemistry,* 2012. 22(8): p. 3348.

[65] Simões, E.F.C., J.C.G.E. da Silva, and J.M.M. Leitão, Carbon dots from tryptophan doped glucose for peroxynitrite sensing. *Analytica Chimica Acta,* 2014. 852: p. 174-180.

[66] Chen, L., et al., Colorimetric detection of peroxynitrite-induced DNA damage using gold nanoparticles, and on the scavenging effects of antioxidants. *Mikrochimica acta,* 2013. 180(7-8): p. 573-580.

Complimentary Contributor Copy

[67] Priyam, A., S.C. Bhattacharya, and A. Saha, Volatile interface of biological oxidant and luminescent CdTe quantum dots: implications in nanodiagnostics. *Phys Chem Chem Phys,* 2009. 11(3): p. 520-7.
[68] Adegoke, O. and T. Nyokong, Probing the sensitive and selective luminescent detection of peroxynitrite using thiol-capped CdTe and CdTe@ZnS quantum dots. *Journal of Luminescence,* 2013. 134: p. 448-455.
[69] Panizzi, P., et al., Oxazine conjugated nanoparticle detects in vivo hypochlorous acid and peroxynitrite generation. *J Am Chem Soc,* 2009. 131(43): p. 15739-44.
[70] Abdelwahab, A.A. and Y.-B. Shim, Nonenzymatic H2O2 sensing based on silver nanoparticles capped polyterthiophene/MWCNT nanocomposite. *Sensors and Actuators B: Chemical,* 2014. 201: p. 51-58.
[71] Miao, Z., D. Zhang, and Q. Chen, Non-enzymatic Hydrogen Peroxide Sensors Based on Multi-wall Carbon Nanotube/Pt Nanoparticle Nanohybrids. *Materials,* 2014. 7(4): p. 2945.
[72] Liu, Y., et al., Highly sensitive detection of hydrogen peroxide at a carbon nanotube fiber microelectrode coated with palladium nanoparticles. *Mikrochimica acta,* 2014. 181(1-2): p. 63-70.
[73] Lu, Y., M. Meyyappan, and J. Li, Trace detection of hydrogen peroxide vapor using a carbon-nanotube-based chemical sensor. *Small,* 2011. 7(12): p. 1714-8.
[74] Sun, Y., et al., Real-time electrochemical detection of hydrogen peroxide secretion in live cells by Pt nanoparticles decorated graphene–carbon nanotube hybrid paper electrode. *Biosensors and Bioelectronics*, 2015. 68: p. 358-364.
[75] Peña, R.C., et al., Hydrogen peroxide monitoring in Fenton reaction by using a ruthenium oxide hexacyanoferrate/multiwalled carbon nanotubes modified electrode. *Journal of Electroanalytical Chemistry,* 2012. 686: p. 1-6.
[76] Nasirizadeh, N., et al., Fabrication of a novel electrochemical sensor for determination of hydrogen peroxide in different fruit juice samples. *Journal of Food and Drug Analysis*, 2016. 24(1): p. 72-82.
[77] Miao, Y.-E., et al., A novel hydrogen peroxide sensor based on Ag/SnO 2 composite nanotubes by electrospinning. *Electrochimica Acta,* 2013. 99: p. 117-123.

Complimentary Contributor Copy

[78] Jin, H., et al., Detection of single-molecule H2O2 signalling from epidermal growth factor receptor using fluorescent single-walled carbon nanotubes. *Nature nanotechnology,* 2010. 5(4): p. 302.
[79] Chekin, F., S. Bagheri, and S.B.A. Hamid, Gel-assisted synthesis of Ag nanoparticles: a novel hydrogen peroxide sensor based on Ag nanoparticles-carbon nanotube composite film. *Russian Journal of Electrochemistry,* 2014. 50(12): p. 1164-1169.
[80] Liu, B. and M. Wang, Hydrogen peroxide biosensor based on myoglobin immobilized on silver nanoparticles decorated oxidized multi-walled carbon nanotubes. *Int. J. Electrochem. Sci,* 2013. 8: p. 9801-9810.
[81] Guzmán, C., et al., Hydrogen peroxide sensor based on modified vitreous carbon with multiwall carbon nanotubes and composites of Pt nanoparticles–dopamine. *Electrochimica Acta,* 2009. 54(6): p. 1728-1732.
[82] Li, Y., et al., Carbon quantum dots/octahedral Cu 2 O nanocomposites for non-enzymatic glucose and hydrogen peroxide amperometric sensor. *Sensors and Actuators B: Chemical*, 2015. 206: p. 735-743.
[83] Wang, Y., et al., Horseradish peroxidase immobilization on carbon nanodots/CoFe layered double hydroxides: Direct electrochemistry and hydrogen peroxide sensing. *Biosensors and Bioelectronics,* 2015. 64: p. 57-62.
[84] Liu, S., et al., A general strategy for the production of photoluminescent carbon nitride dots from organic amines and their application as novel peroxidase-like catalysts for colorimetric detection of H2O2 and glucose. *RSC Advances*, 2012. 2(2): p. 411-413.
[85] Yeh, T.-Y., C.-I. Wang, and H.-T. Chang, Photoluminescent C-dots@RGO for sensitive detection of hydrogen peroxide and glucose. *Talanta*, 2013. 115: p. 718-723.
[86] He, D., et al., Dielectric barrier discharge-assisted one-pot synthesis of carbon quantum dots as fluorescent probes for selective and sensitive detection of hydrogen peroxide and glucose. *Talanta,* 2015. 142: p. 51-56.
[87] Costas-Mora, I., et al., In situ photochemical synthesis of fluorescent carbon dots for optical sensing of hydrogen peroxide and antioxidants. *Talanta,* 2015. 144: p. 1308-1315.
[88] Wei, J., et al., Fluorescence turn-off detection of hydrogen peroxide and glucose directly using carbon nanodots as probes. *Analytical Methods,* 2014. 6(6): p. 1922-1927.

Complimentary Contributor Copy

[89] Qian, Z., et al., Si-doped carbon quantum dots: a facile and general preparation strategy, bioimaging application, and multifunctional sensor. *ACS Appl Mater Interfaces*, 2014. 6(9): p. 6797-805.
[90] Wu, G., et al., A ratiometric fluorescent nanoprobe for H2O2 sensing and in vivo detection of drug-induced oxidative damage to the digestive system. *Journal of Materials Chemistry B,* 2014. 2(48): p. 8528-8537.
[91] Du, F., et al., A targeted and FRET-based ratiometric fluorescent nanoprobe for imaging mitochondrial hydrogen peroxide in living cells. *Small,* 2014. 10(5): p. 964-72.
[92] Shan, X., et al., B-doped carbon quantum dots as a sensitive fluorescence probe for hydrogen peroxide and glucose detection. *Analyst,* 2014. 139(10): p. 2322-2325.
[93] Song, Y., et al., Investigation into the fluorescence quenching behaviors and applications of carbon dots. *Nanoscale*, 2014. 6(9): p. 4676-4682.
[94] Yi-Chen, W. and J. Xiu-E, Hydrogen Peroxide Biosensor Based on Carbon Supported Ultrafine Silver Nanoparticles. *Chinese Journal of Analytical Chemistry,* 2014. 42(5): p. 689-694.
[95] Lu, W., et al., Hydrothermal synthesis of well-stable silver nanoparticles and their application for enzymeless hydrogen peroxide detection. *Electrochimica Acta,* 2011. 56(5): p. 2295-2298.
[96] Palanisamy, S., et al., Direct electrochemistry of myoglobin at silver nanoparticles/myoglobin biocomposite: Application for hydrogen peroxide sensing. *Sensors and Actuators B: Chemical,* 2014. 202: p. 177-184.
[97] Wu, S., et al., Electrodeposition of silver–DNA hybrid nanoparticles for electrochemical sensing of hydrogen peroxide and glucose. *Electrochemistry Communications,* 2006. 8(8): p. 1197-1203.
[98] Shukla, V.K., et al., Green synthesis of nanosilver as a sensor for detection of hydrogen peroxide in water. *Journal of Hazardous Materials,* 2012. 213–214: p. 161-166.
[99] Zhang, K., et al., Amperometric sensing of hydrogen peroxide using a glassy cabon electode modified with silver nanoparticles on poly(alizarin yellow R). *Microchimica Acta,* 2011. 173(1/2): p. 135-141.
[100] Cui, K., et al., A novel hydrogen peroxide sensor based on Ag nanoparticles electrodeposited on DNA-networks modified glassy carbon electrode. *Electrochemistry Communications*, 2008. 10(4): p. 663-667.

Complimentary Contributor Copy

[101] Zhu, J., et al., Electroless Deposition of Silver Nanoparticles on Graphene Oxide Surface and Its Applications for the Detection of Hydrogen Peroxide. *Electroanalysis,* 2014. 26(11): p. 2513-2519.
[102] Nia, P.M., W.P. Meng, and Y. Alias, Hydrogen peroxide sensor: Uniformly decorated silver nanoparticles on polypyrrole for wide detection range. *Applied Surface Science,* 2015. 357, Part B: p. 1565-1572.
[103] Xu, Y., C. Hu, and S. Hu, A hydrogen peroxide biosensor based on direct electrochemistry of hemoglobin in Hb–Ag sol films. *Sensors and Actuators B: Chemical,* 2008. 130(2): p. 816-822.
[104] Liu, X., et al., Synthesis of graphene nanosheets with incorporated silver nanoparticles for enzymeless hydrogen peroxide detection. *Analytical Methods,* 2013. 5(9): p. 2298-2304.
[105] Ma, L., et al., Amperometric hydrogen peroxide biosensor based on the immobilization of HRP on DNA–silver nanohybrids and PDDA-protected gold nanoparticles. *Journal of Molecular Catalysis B: Enzymatic*, 2009. 56(4): p. 215-220.
[106] Liu, C.-Y. and J.-M. Hu, Hydrogen peroxide biosensor based on the direct electrochemistry of myoglobin immobilized on silver nanoparticles doped carbon nanotubes film. *Biosensors and Bioelectronics,* 2009. 24(7): p. 2149-2154.
[107] Balamurugan, A. and S.-M. Chen, Silver Nanograins Incorporated PEDOT Modified Electrode for Electrocatalytic Sensing of Hydrogen Peroxide. *Electroanalysis,* 2009. 21(12): p. 1419-1423.
[108] Ren, C., et al., Hydrogen peroxide sensor based on horseradish peroxidase immobilized on a silver nanoparticles/cysteamine/gold electrode. *Anal Bioanal Chem,* 2005. 381(6): p. 1179-85.
[109] Zhan, B., et al., A hydrogen peroxide electrochemical sensor based on silver nanoparticles decorated three-dimensional graphene. *Applied Physics Letters,* 2014. 104(24): p. 243704.
[110] Tian, J., S. Liu, and X. Sun, Supramolecular Microfibrils of o-Phenylenediamine Dimers: Oxidation-Induced Morphology Change and the Spontaneous Formation of Ag Nanoparticle Decorated Nanofibers. *Langmuir,* 2010. 26(19): p. 15112-15116.
[111] Liu, S., et al., Stable Aqueous Dispersion of Graphene Nanosheets: Noncovalent Functionalization by a Polymeric Reducing Agent and Their Subsequent Decoration with Ag Nanoparticles for Enzymeless Hydrogen Peroxide Detection. *Macromolecules*, 2010. 43(23): p. 10078-10083.

Complimentary Contributor Copy

[112] Hsiao, W.-H., et al., Urchin-like Ag Nanowires as Non-enzymatic Hydrogen Peroxide Sensor. *Journal of the Chinese Chemical Society*, 2012. 59(4): p. 500-506.
[113] Li, D., et al., Amperometric detection of hydrogen peroxide using a nanofibrous membrane sputtered with silver. *RSC Advances,* 2014. 4(8): p. 3857-3863.
[114] Patel, A.S. and T. Mohanty, Silver nanoclusters in BSA template: a selective sensor for hydrogen peroxide. *Journal of Materials Science,* 2014. 49(5): p. 2136-2143.
[115] Wen, T., et al., Polyethyleneimine-capped silver nanoclusters as a fluorescence probe for sensitive detection of hydrogen peroxide and glucose. *Analytica Chimica Acta,* 2012. 749: p. 56-62.
[116] Wang, Q. and J. Zheng, Electrodeposition of silver nanoparticles on a zinc oxide film: improvement of amperometric sensing sensitivity and stability for hydrogen peroxide determination. *Microchimica Acta,* 2010. 169.
[117] Yin, J., et al., A hydrogen peroxide electrochemical sensor based on silver nanoparticles decorated silicon nanowire arrays. *Electrochimica Acta*, 2011. 56(11): p. 3884-3889.
[118] Teerasong, S., et al., Colorimetric Sensor Using Silver Nanoparticles for Determination of Hydrogen Peroxide Based on a Flow Injection System. *Journal of Nanoelectronics and Optoelectronics,* 2013. 8(5): p. 446-449.
[119] Roy, K., K. Sarkar Chandan, and K. Ghosh Chandan, Fast colourimetric detection of H2O2 by biogenic silver nanoparticles synthesised using Benincasa hispida fruit extract, in *Nanotechnology Reviews,* 2016.
[120] Li, S., et al., Hydrogen peroxide biosensor based on gold nanoparticles/thionine/gold nanoparticles/multi-walled carbon nanotubes–chitosans composite film-modified electrode. *Applied Surface Science,* 2012. 258(7): p. 2802-2807.
[121] Liu, X., et al., Hydrogen peroxide detection at a horseradish peroxidase biosensor with a Au nanoparticle-dotted titanate nanotube|hydrophobic ionic liquid scaffold. *Biosens Bioelectron*, 2012. 32(1): p. 188-94.
[122] Chen, X., et al., A Non-Enzymatic Hydrogen Peroxide Sensor Based on Gold Nanoparticles/Carbon Nanotube/Self-Doped Polyaniline Hollow Spheres. *Electroanalysis,* 2014. 26(7): p. 1513-1521.
[123] Zhang, D., et al. A Highly Sensitive and Selective Hydrogen Peroxide Biosensor Based on Gold Nanoparticles and Three-Dimensional Porous Carbonized Chicken Eggshell Membrane. *PloS one,* 2015. 10, e0130156 DOI: 10.1371/journal.pone.0130156.

Complimentary Contributor Copy

[124] Sophia, J. and G. Muralidharan, Gold nanoparticles for sensitive detection of hydrogen peroxide: a simple non-enzymatic approach. *Journal of Applied Electrochemistry*, 2015. 9(45): p. 963-971.
[125] Ning, R., et al., A novel strategy to synthesize Au nanoplates and their application for enzymeless H2O2 detection. *Electrochimica Acta,* 2012. 60: p. 13-16.
[126] Okawa, Y., et al., Direct electron transfer biosensor for hydrogen peroxide carrying nanocomplex composed of horseradish peroxidase and Au-nanoparticle – Characterization and application to bienzyme systems. *Analytical Chemistry Research*, 2015. 5: p. 1-8.
[127] Wang, W., et al., Green preparation of Au nanoparticles for electrochemical detection of H 2 O 2. *Journal of Semiconductors,* 2016. 37(1): p. 013003.
[128] Wen, F., et al., Horseradish Peroxidase Functionalized Fluorescent Gold Nanoclusters for Hydrogen Peroxide Sensing. *Analytical Chemistry,* 2011. 83(4): p. 1193-1196.
[129] Huang, X., et al., Gold nanoparticle-enzyme conjugates based FRET for highly sensitive determination of hydrogen peroxide, glucose and uric acid using tyramide reaction. *Analyst,* 2012. 137(16): p. 3659-66.
[130] Zhao, Q., et al., Colorimetric and ultra-sensitive fluorescence resonance energy transfer determination of H2O2 and glucose by multi-functional Au nanoclusters. *Analyst,* 2014. 139(6): p. 1498-503.
[131] Shiang, Y.-C., C.-C. Huang, and H.-T. Chang, Gold nanodot-based luminescent sensor for the detection of hydrogen peroxide and glucose. *Chemical Communications,* 2009(23): p. 3437-3439.
[132] Chang, H.C. and J.A. Ho, Gold Nanocluster-Assisted Fluorescent Detection for Hydrogen Peroxide and Cholesterol Based on the Inner Filter Effect of Gold Nanoparticles. *Anal Chem,* 2015. 87(20): p. 10362-7.
[133] Jv, Y., B. Li, and R. Cao, Positively-charged gold nanoparticles as peroxidiase mimic and their application in hydrogen peroxide and glucose detection. *Chemical Communications,* 2010. 46(42): p. 8017-8019.
[134] Zou, G. and H. Ju, Electrogenerated Chemiluminescence from a CdSe Nanocrystal Film and Its Sensing Application in Aqueous Solution. *Analytical Chemistry*, 2004. 76(23): p. 6871-6876.
[135] Hu, X., et al., Electrogenerated chemiluminescence of blue emitting ZnSe quantum dots and its biosensing for hydrogen peroxide. *Biosens Bioelectron*, 2010. 25(7): p. 1843-6.

Complimentary Contributor Copy

[136] Yuan, J., W. Guo, and E. Wang, Utilizing a CdTe Quantum Dots−Enzyme Hybrid System for the Determination of Both Phenolic Compounds and Hydrogen Peroxide. *Analytical Chemistry,* 2008. 80(4): p. 1141-1145.
[137] Rodrigues, S.S.M., et al., Fluorescence enhancement of CdTe MPA-capped quantum dots by glutathione for hydrogen peroxide determination. *Talanta,* 2014. 122: p. 157-165.
[138] Adegoke, O., S. Khene, and T. Nyokong, Fluorescence "Switch on" of Conjugates of CdTe@ZnS Quantum Dots with Al, Ni and Zn Tetraamino-Phthalocyanines by Hydrogen Peroxide: Characterization and Applications as Luminescent Nanosensors. *Journal of Fluorescence,* 2013. 23(5): p. 963-974.
[139] Huang, X., et al., Quantum dot-based FRET for sensitive determination of hydrogen peroxide and glucose using tyramide reaction. *Talanta,* 2013. 106: p. 79-84.
[140] Zhang, L., et al., Graphene Quantum Dots Assembled with Metalloporphyrins for "Turn on" Sensing of Hydrogen Peroxide and Glucose. *Chemistry,* 2015. 21(26): p. 9343-8.
[141] Ahmad, I., H. Zhang, and K. Lau, The Reaction Kinetics of Glutathione Capped Quantum Dots for the Detection of Hydrogen Peroxide. *Austin J Biosens and Bioelectron*, 2015. 1(2): p. 1010.
[142] Janyasupab, M., et al., Bimetallic Pt-Ru Nanoparticle Catalyst for Hydrogen Peroxide Detection. *Journal of Nanotechnology,* 2011. 2011: p. 6.
[143] Tao, Y., et al., Polypyrrole nanoparticles as promising enzyme mimics for sensitive hydrogen peroxide detection. *Chemical Communications,* 2014. 50(23): p. 3030-3032.
[144] Liu, W.N., et al., Hollow graphitic nanocapsules as efficient electrode materials for sensitive hydrogen peroxide detection. *Biosens Bioelectron,* 2014. 52: p. 438-44.
[145] Wang, J., et al., Pd nanoparticle-modified electrodes for nonenzymatic hydrogen peroxide detection. *Nanoscale Research Letters,* 2015. 10(1): p. 1-6.
[146] Qu, J., et al., Determination of Hydrogen Peroxide Using a Novel Sensor Based on Fe3O4 Magnetic Nanoparticles. *Analytical Letters,* 2014. 47(11): p. 1797-1807.
[147] Ling, Y., et al., Fluorescent detection of hydrogen peroxide and glucose with polyethyleneimine-templated Cu nanoclusters. *Spectrochimica Acta*

Complimentary Contributor Copy

Part A: Molecular and Biomolecular Spectroscopy, 2014. 118: p. 315-320.

[148] Gaynor, J.D., et al., Enzyme-free detection of hydrogen peroxide from cerium oxide nanoparticles immobilized on poly(4-vinylpyridine) self-assembled monolayers. *Journal of Materials Chemistry B,* 2013. 1(28): p. 3443-3450.

[149] Wei, X., et al., Supramolecular Fluorescent Nanoparticles Constructed via Multiple Non-Covalent Interactions for the Detection of Hydrogen Peroxide in Cancer Cells. *Chemistry,* 2015. 21(32): p. 11427-34.

[150] Mao, Z., et al., Poly(thymine)-Templated Copper Nanoparticles as a Fluorescent Indicator for Hydrogen Peroxide and Oxidase-Based Biosensing. *Analytical Chemistry,* 2015. 87(14): p. 7454-7460.

[151] Song, Z., et al., Rhodium Nanoparticle-mesoporous Silicon Nanowire Nanohybrids for Hydrogen Peroxide Detection with High Selectivity. *Scientific Reports,* 2015. 5: p. 7792.

[152] Yu, G., et al., High sensitive and selective sensing of hydrogen peroxide released from pheochromocytoma cells based on Pt-Au bimetallic nanoparticles electrodeposited on reduced graphene sheets. *Sensors* (Basel), 2015. 15(2): p. 2709-22.

[153] Wu, X., et al., Fabrication of highly fluorescent graphene quantum dots using L-glutamic acid for in vitro/in vivo imaging and sensing. Journal of materials chemistry. *C, Materials for optical and electronic devices,* 2013. 1(31): p. 4676-4684.

[154] Chen, S., et al., In Situ Growth of Silver Nanoparticles on Graphene Quantum Dots for Ultrasensitive Colorimetric Detection of H2O2 and Glucose. *Analytical Chemistry*, 2014. 86(13): p. 6689-6694.

[155] Gao, X., et al., Carbon-Dot-Based Ratiometric Fluorescent Probe for Imaging and Biosensing of Superoxide Anion in Live Cells. *Analytical Chemistry,* 2014. 86(14): p. 7071-7078.

[156] Li, N., et al., A highly selective and sensitive nanoprobe for detection and imaging of the superoxide anion radical in living cells. *Chemical Communications,* 2012. 48(19): p. 2507-2509.

[157] Mukherjee, S., et al., Potential theranostics application of bio-synthesized silver nanoparticles (4-in-1 system). *Theranostics*, 2014. 4(3): p. 316-35.

[158] Santhosh, P., et al., Sensitive electrochemical detection of superoxide anion using gold nanoparticles distributed poly(methyl methacrylate)-polyaniline core-shell electrospun composite electrode. *Analyst,* 2011. 136(8): p. 1557-61.

Complimentary Contributor Copy

[159] WANG MengDong, H.Y., LIU XingXing, NIE Zhou, DENG ChunYan, GUO ManLi, YAO ShouZhuo, Assembly of layer-by-layer films of superoxide dismutase and gold nanorods: A third generation biosensor for superoxide anion. *SCIENCE CHINA Chemistry,* 2011. 54(8): p. 1284-1291.

[160] Li, D.-W., et al., CdSe/ZnS quantum dot–Cytochrome c bioconjugates for selective intracellular O $2^{\cdot-}$ sensing. *Chemical Communications,* 2011. 47(30): p. 8539-8541.

[161] Adegoke, O., E. Antunes, and T. Nyokong, Nanoconjugates of CdTe@ZnS quantum dots with cobalt tetraamino-phthalocyanine: Characterization and implications for the fluorescence recognition of superoxide anion. *Journal of Photochemistry and Photobiology A: Chemistry,* 2013. 257: p. 11-19.

[162] Kim, J.Y., et al., Highly selective in-vivo imaging of tumor as an inflammation site by ROS detection using hydrocyanine-conjugated, functional nano-carriers. *J Control Release,* 2011. 156(3): p. 398-405.

[163] Derkus, B., E. Emregul, and K.C. Emregul, Copper-zinc alloy nanoparticle based enzyme-free superoxide radical sensing on a screen-printed electrode. *Talanta,* 2015. 134: p. 206-14.

[164] Davies, M.J., et al., Mammalian heme peroxidases: from molecular mechanisms to health implications. *Antioxid Redox Signal*, 2008. 10(7): p. 1199-234.

[165] Wang, D., et al., N-doped carbon dots with high sensitivity and selectivity for hypochlorous acid detection and its application in water. *Analytical Methods*, 2015. 7(12): p. 5311-5317.

[166] Huang, Z., et al., Carbon dots with tunable emission, controllable size and their application for sensing hypochlorous acid. *Journal of Luminescence*, 2014. 151: p. 100-105.

[167] Yin, B., et al., Green synthesis of carbon dots with down- and up-conversion fluorescent properties for sensitive detection of hypochlorite with a dual-readout assay. *Analyst*, 2013. 138(21): p. 6551-6557.

[168] Yan, Y., et al., CdSe-ZnS Quantum Dots for Selective and Sensitive Detection and Quantification of Hypochlorite. *Analytical Chemistry,* 2010. 82(23): p. 9775-9781.

[169] Hallaj, T., et al., Chemiluminescence reaction of glucose-derived graphene quantum dots with hypochlorite, and its application to the determination of free chlorine. *Microchimica Acta,* 2014. 182(3): p. 789-796.

Complimentary Contributor Copy

[170] Yang, Y.-C., et al., Selective and Absolute Quantification of Endogenous Hypochlorous Acid with Quantum-Dot Conjugated Microbeads. *Analytical Chemistry,* 2011. 83(21): p. 8267-8272.
[171] Liu, Z., et al., Assaying myeloperoxidase inhibitors and hypochlorous acid scavengers in HL60 cell line using quantum dots. *Am. J. Biomed. Sci,* 2013. 2: p. 140-153.
[172] Zhang, K.Y., et al., Core–shell structured phosphorescent nanoparticles for detection of exogenous and endogenous hypochlorite in live cells via ratiometric imaging and photoluminescence lifetime imaging microscopy. *Chemical Science,* 2015. 6(1): p. 301-307.
[173] Ho, E., et al., Biological markers of oxidative stress: Applications to cardiovascular research and practice. *Redox Biology*, 2013. 1(1): p. 483-491.
[174] Ren, X., et al., Synthesis of Ultra-Stable Fluorescent Carbon Dots from Polyvinylpyrrolidone and Their Application in the Detection of Hydroxyl Radicals. *Chemistry – An Asian Journal,* 2014. 9(4): p. 1054-1059.
[175] Zhang, M., et al., Layered Double Hydroxide-Supported Carbon Dots as an Efficient Heterogeneous Fenton-Like Catalyst for Generation of Hydroxyl Radicals. *The Journal of Physical Chemistry C,* 2014. 118(19): p. 10441-10447.
[176] Zhuang, M., et al., Ratiometric Fluorescence Probe for Monitoring Hydroxyl Radical in Live Cells Based on Gold Nanoclusters. *Analytical Chemistry,* 2014. 86(3): p. 1829-1836.
[177] YANG Yan, Y.P., ZHANG Xiao-hua*, CHEN Jin-hua*, Sensitive Detection of Hydroxyl Radical based on Silver-Enhanced Gold Nanoparticle Label. *Journal of Electrochemistry,* 2015. 21(1): p. 22-28.
[178] Adegoke, O. and T. Nyokong, A comparative study on the sensitive detection of hydroxyl radical using thiol-capped CdTe and CdTe/ZnS quantum dots. *J Fluoresc,* 2012. 22(6): p. 1513-9.
[179] Jiang, H. and H. Ju, Electrochemiluminescence Sensors for Scavengers of Hydroxyl Radical Based on Its Annihilation in CdSe Quantum Dots Film/Peroxide System. *Analytical Chemistry*, 2007. 79(17): p. 6690-6696.

Complimentary Contributor Copy

Experimental Research…….

Chapter 6

Nitric Oxide Fluorescence Sensing by Europium Tetracyclines Complexes in the Presence of Hydrogen Peroxide

Eliana F. C. Simões, João M.M. Leitão, Joaquim C.G. Esteves da Silva
J Fluoresc (2013) 23:681–688
DOI 10.1007/s10895-013-1207-9

The experimental research was begun with the selection of luminescent chemical systems with potential for detection of ROS/RNS. In this phase the optimization of the luminescent systems selected in solution for the individual and/or simultaneous determination of ROS/RNS was done. The response of chemical systems in presence of ROS/RNS namely the enhancement or the quenching of the fluorescence intensity as well the changes in the response of the sensor relatively to the wavelength of the luminescent radiation was evaluated. In the optimization procedures were used multivariate optimization techniques based on the evaluation of response surfaces. The knowledge of the chemical behavior of each ROS/RNS as well as the interfering and antioxidants potentially present in and the biological environment under study is essential for the correct assessment of these species.

One of the first chemical systems evaluated carried out inside the doctoral program was the assessment of a fluorescent chemical system, based in fluorophores of pharmaceutical origin namely Lanthanide complexes of antibiotics of the tetracycline group with lanthanide (III) as europium (III). Studies were carried out with europium: tetracycline complexes (Eu:Tc), europium: oxytetracycline (Eu: OxyTc) and europium: chlortetracycline (Eu: ClTc) at different pH values. The aim of the work was to evaluate the behavior of Eu-Tc complexes with the ROS/RNS (H_2O_2, NO, $OONO^-$, O_2^-). Tests in solutions were carried out, using a light source, two optical fibers to guide the light and a radiation detector. Experimental design methodologies were performed and used in order to evaluate the different variables that affect the reaction of complexation and the

influence of each one of the ROS/RNS in this reaction. The study of detection of the main ROS/RNS was made in three concentration levels (25, 50 and 100 μM), which were evaluated with the [Eu] 130 μM and [tetracyclines] 60 μM (ratio of 2:1, at a constant temperature of 30° C) and at pH 6.00, 7.00 and 8.00.

A fluorescence increase when the complexes Eu: Tc, Eu: OxyTc and Eu: ClTc react with $ONOO^-$, H_2O_2 and $O_2^{\bullet-}$ was observed being the largest increase observed for H_2O_2. Contrary, a fluorescence quenching was observed with NO addition. This behavior was used to develop an analytical methodology for NO detection based on the fluorescence quenching of Eu:Tc complexes in the presence of relatively large amounts of H_2O_2 that resulted in increased sensitivity and elimination of interference (the same approach can be used for $ONOO^-$ or $O_2^{\bullet-}$).

NO detection by the different Eu: Tc complexes, was made at 30° C, pH 7.00 in the presence of H_2O_2 200 μM. The best conditions for the detection were obtained with the complexes Eu 240 μM: Tc 80 μM (3:1), Eu: OxyTc 60 μM 240 μM (4:1) and Eu 560 μM: ClTc 80 μM (7:1). The results of this study were presented, as an article in the scientific journal: Journal of Fluorescence, presented below.

My personal contribution to this work includes the establishment of an initial objective and the bibliographic research of the state of the art related with the determination of ROS/RNS with lanthanide complexes, the protocols set up, the experimental execution and posterior data treatment. The experimental studies beginning on the preparation of the solutions (buffer solutions, Europium and Tetracycline solutions and ROS/RNS solutions) and the characterization of the spectral characteristics of the complexes as the experiments to evaluate the behavior of the complexes in presence of the ROS/RNS were of my personal responsibility. The writing of the paper was performed together with Professor João M. M. Leitão under the supervision of Professor Joaquim C. G. Esteves da Silva.

J Fluoresc (2013) 23:681–688
DOI 10.1007/s10895-013-1207-9

ORIGINAL PAPER

NO Fluorescence Sensing by Europium Tetracyclines Complexes in the Presence of H_2O_2

Eliana F. C. Simões · João M. M. Leitão · Joaquim C. G. Esteves da Silva

Received: 25 January 2013 / Accepted: 24 February 2013 / Published online: 8 March 2013
© Springer Science+Business Media New York 2013

Abstract The effect on the fluorescence of the europium: tetracycline (Eu:Tc), europium:oxytetracycline (Eu:OxyTc) and europium:chlortetracycline (Eu:ClTc) complexes in approximately 2:1 ratio of nitric oxide (NO), peroxynitrite ($ONOO^-$), hydrogen peroxide (H_2O_2) and superoxide ($O_2^{\cdot-}$) was assessed at three ROS/RNS concentrations levels, 30 °C and pH 6.00, 7.00 and 8.00. Except for the NO, an enhancement of fluorescence intensity was observed at pH 7.00 for all the europium tetracyclines complexes—the high enhancement was observed for H_2O_2. The quenching of the fluorescence of the Tc complexes, without and with the presence of other ROS/RNS species, provoked by NO constituted the bases for an analytical strategy for NO detection. The quantification capability was evaluated in a NO donor and in a standard solution. Good quantification results were obtained with the Eu:Tc (3:1) and Eu:OxyTc (4:1) complexes in the presence of H_2O_2 200 μM with a detection limit of about 3 μM (Eu:OxyTc).

Keywords Europium:tetracyclines complexes · Nitric oxide quantification · Fluorescence · Hydrogen peroxide · Peroxynitrite · Superoxide

E. F. C. Simões · J. M. M. Leitão · J. C. G. Esteves da Silva
Centro de Investigação em Química da Universidade do Porto (CIQ-UP), Porto, Portugal

E. F. C. Simões · J. M. M. Leitão
Faculdade de Farmácia da Universidade de Coimbra, 3000-548 Coimbra, Portugal

E. F. C. Simões · J. C. G. Esteves da Silva (✉)
Departamento de Química e Bioquímica, Faculdade de Ciências da Universidade do Porto, R. Campo Alegre 687, 4169-007 Porto, Portugal
e-mail: jcsilva@fc.up.pt

Introduction

Fluorescence sensing uses synthetic organic fluorophores, fluorophores of biological origin, metal-ligand complexes, lanthanide complexes and more recently fluorescent nanoparticles [1]. The demand for alternatives of organic fluorophores with better characteristics is a continuous challenge. Some of the already existing alternatives, as the lantanide complexes, presents specific characteristics that make them more considered in fluorescence sensing [2–6]. The lanthanide complexes presents some interesting luminescence characteristics, as higher emission wavelength, narrow fluorescence emission band, large Stokes shift, long fluorescence lifetime and an intense fluorescence emission in the presence of some compounds that make them especially adequate for their use as fluorescence sensors [7–13]. The europium tetracyclines complexes have been widely used for the detection and quantification of several biochemical species namely hydrogen peroxide (H_2O_2) [14–19], urea hydrogen peroxide [20], low density lipoproteins [21–23], cholesterol [24], bilirubin [25, 26], bile acid [27], lysozyme [28], nucleoside phosphates [29, 30], NADP [31], coenzyme a [32], superoxide dismutase [33], DNA [34], heparin [35], lecithin [36], catalase [37] and glucose [38]. Most of these analytical methodologies are based on the enhancement of the fluorescence intensity by these species [14–24, 28, 31–38]. Only with bilirubin, bile acid and nucleoside phosphates the sensing is based on the fluorescence quenching [25–27, 29, 30]. Catalase and glucose determination was done indirectly thought hydrogen peroxide detection [37, 38].

Reactive oxygen (ROS) and nitrogen (RNS) species, object of this study, are usually involved in several physiological and pathological processes acting as signalling molecules and induce cell damage [39]. The detection and/or quantification of these species in biological samples is not straightforward

due to their high reactivity, short half-life, lower concentrations, rapid diffusion, possible antioxidant mechanisms and potential interferences. The main ROS/RNS are nitric oxide (NO), peroxynitrite ($ONOO^-$), superoxide ($O_2^{\cdot-}$) and hydrogen peroxide (H_2O_2). Their detection is essentially done by electron spin resonance (ESR), fluorescence, chemiluminescence, colorimetric and electrochemical analytical techniques [40–42]. Some applications of lanthanide complexes in ROS/RNS sensing involved the determination of hydroxyl radical [43, 44], singlet oxygen [45, 46] and NO [47].

In this work, the detection of the main ROS/RNS and its mixtures, by the europium:tetracycline (Eu:Tc), europium: oxytetracycline (Eu:OxyTc) and europium:chlortetracycline (Eu:ClTc) complexes was studied at different pH values. At pH 7 the sensing of NO by the europium tetracyclines complexes was optimized and the detection and/or quantification capability was evaluated. The more adequate europium tetracyclines ratio for NO fluorescence sensing in the presence of H_2O_2 was obtained. In the optimized conditions, the NO detection capability was checked varying the NO concentration and the quantification capability was evaluated by the generation of NO with a rapid donor DiEthylAmine NOnoate (DEA/NO) and in standard solutions.

Experimental

Reagents

Europium, tetracycline, oxytetracycline, chlortetracycline, 3-(N-morpholino) propanesulfonic acid (MOPs), potassium superoxide, sodium nitrite, hydrogen peroxide and DiEthylAmine NOnoate diethylammonium salt (DEA/NO) were obtained from Sigma-Aldrich Química S.A. (Spain). Sodium hydroxide and hydrochloric acid were purchased from Merck, Darmstadt (Germany). Mili-Q water with resistivity of 18.2 MΩ.cm at 25 °C was used in all the experiments.

Solutions

All the solutions prepared from a solid powder were done by rigorous weighting to the required final concentration and were prepared daily. Buffer solutions of pH 6.00, 7.00 and 8.00 were obtained by adding, to the MOPs buffer solution previous prepared (pH 10.1), HCl 0.1 M in order to obtain the desired pH. The initially europium and tetracyclines solutions of the desired concentrations were prepared in MOPs buffer of pH 6.00, 7.00 and 8.00. The required europium tetracyclines complexes were then obtained mixing equal volumes of these europium and tetracyclines solutions previously prepared.

The $ONOO^-$ solutions were prepared in a refrigerated beaker under constant stirring by mixing 100 mL of $NaNO_2$ 600 mM, 100 mL of H_2O_2 600 mM in HCl 0.6 M and 100 mL of NaOH 3.6 M. The solution will turn yellow indicating the formation of peroxynitrite. The agitation is maintained until no O_2 is formed. Diluted solutions were done in NaOH 0.1 M to the desired concentrations. The saturated NO solutions (1.9 mM) were prepared from bubbling NO in deoxygenated water (bubbling argon during 15 min). Lower concentrations standard solutions were prepared with deoxygenated water by rigorous dilution. Also H_2O_2 and $O_2^{\cdot-}$ solutions were prepared in water.

The DEA/NO stock solution was prepared in NaOH 10 mM and kept at −20 °C before use. The liberation of NO was done in deoxygenated MOPs pH 7.00.

Instrumentation

The absorbance and the fluorescence emission spectra were collected in a standard 1 cm fluorescence quartz cell respectively in a Jasco V-530 UV-Visible spectrophotometer and in a Jasco FP-6200 spectrofluorimeter. The absorption spectra were obtained in a wavelength range from 220 to 450 nm with a 2 nm interval, slit with 2 nm and wavelength scan rate medium; the Fluorescence emission spectra were obtained in a wavelength range from 420 to 650 nm with a 1 nm interval, slit with 10 nm, sensitivity response medium, response time fast and wavelength scan rate 1,000 nm/min.

All the determinations in the optimization and quantification stages were made at 30 °C using a standard 1 cm fluorescence quartz cell. The control of temperature was done by circulation of water at 30 °C by an external thermostat bath. Also a 395 nm LED, a sampling compartment (CUV-ALL-UV 4-way) and two 1.0 mm core diameter fiber optics (P1000-2-UV–VIS) from Ocean Optics were used. Of the two optical fibers, one guides the light from the source to the sampling compartment and the other guides the emitted light to the detector. The detection was done by a QE65000 charge-coupled device also from Ocean Optics. The reaction time profiles were obtained collecting the signal during 950 s at a wavelength of 616 nm, every 10 s with an integration time of 300 ms. For each reaction time profile the fluorescence intensity before the ROS/RNS addition (I_0) and after 900 s (I) was evaluated and a fluorescence intensity variation ($\Delta I = I - I_0$) was calculated.

Results and Discussion

Figure 1 presents the absorption and emission spectra of the europium, tetracyclines and europium tetracyclines complexes at the ratio and concentrations indicated (initially prepared solutions before the formation of the complexes). These concentrations and their complexes ratio were chosen attending to preliminary evaluations based in previous published results of the Eu:Tc complex with H_2O_2 [19].

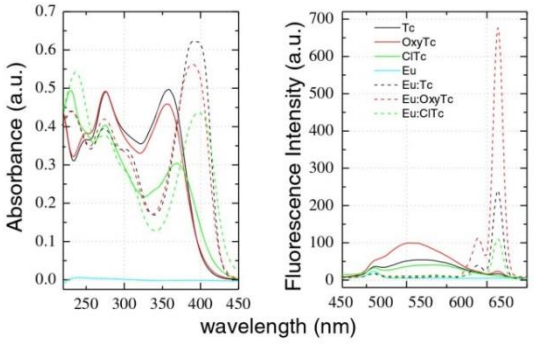


Fig. 1 UV-visible absorption and fluorescence emission spectra at excitation wavelength of 395 nm of Eu 65 μM; Tc, OxyTc and ClTc 30 μM; Eu:Tc, Eu:OxyTc and Eu:ClTc 130 μM:60 μM complexes

The tetracyclines and the corresponding europium tetracyclines complexes have similar absorption and emission spectral shapes with the exception of the absorption spectra of the ClTc and Eu:ClTc complex. The absorption spectra are characterized by two bands at about 276 and 360 nm for the three tetracyclines and at 274 and 390 nm for the related europium tetracyclines complexes. For the emission spectra the wavelength of the main bands are located at about 520 and 614 nm, respectively, for the tetracyclines and europium tetracyclines complexes. For the absorption and emission spectra the highest intensity was observed for the Tc and OxyTc and corresponding complexes.

ROS/RNS Analysis

The detection of the main ROS/RNS (NO, $ONOO^-$, H_2O_2, $O_2^{\cdot-}$), at three concentration levels of 25, 50 and 100 μM were assessed with Eu 130 μM and tetracyclines 60 μM (2:1 ratio, at a constant temperature of 30 °C) and at pH 6.00, 7.00 and 8.00—due to the basicity of the standard $ONOO^-$ solution the final pH of the higher concentration solutions were higher (pH 7.00, 8.00 and 12 with $ONOO^-$ 50 μM; and, of pH 7.60, 11.19 and greater than 12 with $ONOO^-$ 100 μM). The results are presented in Fig. 2.

The analysis of Fig. 2 shows that the presence of the ROS/RNS species affects differently the fluorescence of the Tc complexes and that this effect is dependent of the pH. At pH 7, the presence of the ROS species H_2O_2 and $O_2^{\cdot-}$ provoke an increase of the fluorescence intensity of the three Tc complexes and $ONOO^-$ has a similar behaviour for the Tc and ClTc complexes. The fluorescent enhancement observed at pH 7 with the H_2O_2 from 25 to 100 μM is for Eu:Tc about 115 times, Eu:OxyTc about 150 times and Eu:ClTc about 18 times. Depending of the europium tetracycline complex, these fluorescence enhancement is about 2 and

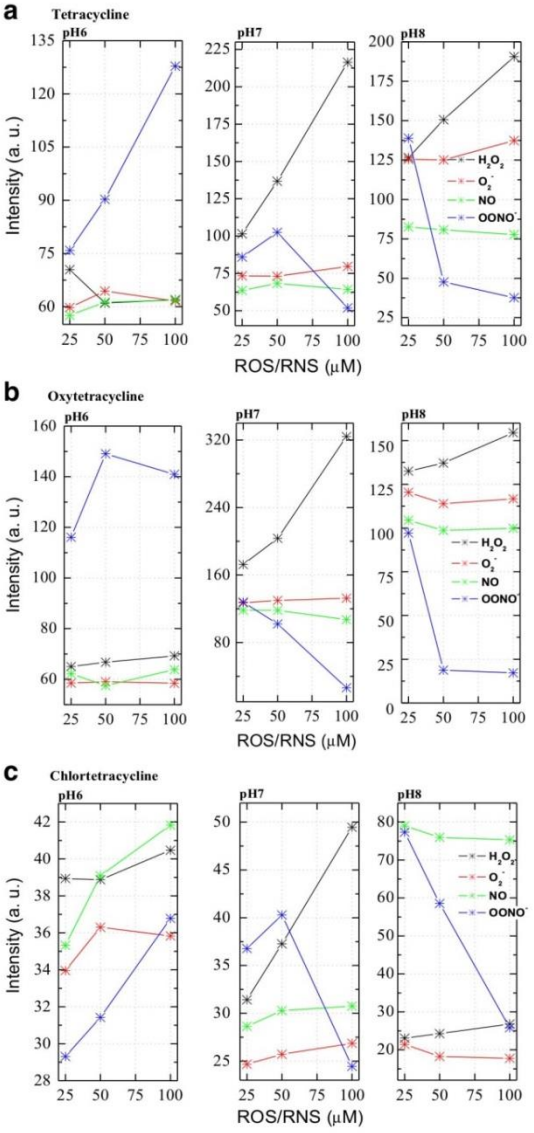


Fig. 2 ROS/RNS 25, 50 and 100 μM detection by Eu:Tc, Eu:OxyTc and ClTc complexes 130 μM:60 μM at a temperature of 30 °C and pH of 6.00, 7.00 and 8.00

19 times greater than the enhancement observed respectively with the $ONOO^-$ (pH 6) and $O_2^{\cdot-}$ (pH 7).

At pH 7.00, NO provokes quenching of the fluorescence intensity of the Eu:Tc and Eu:OxyTc complexes and has no significant effect on the fluorescence intensity of the Eu:ClTc complex. At pH 7.00 this quenching effect is more evident for the Eu:OxyTc complex. A small increase of the fluorescence intensity was also observed with the Eu:Tc

complex at pH 7.00 from 25 to 50 μM and with the Eu:ClTc complex at pH 6.00 and 7.00 from 25 to 100 μM.

NO Sensing Optimization

Due to the different NO effect on the fluorescence of the europium tetracyclines complexes the sensing of NO at pH 7.00 was studied in detail. As shown in the ROS/RNS analysis the quenching effect of NO in the presence of the europium tetracyclines complexes suffers from a lack of sensitivity. To increase the sensitivity, the strategy followed was the NO sensing in the presence of H_2O_2—which would increase the background fluorescent signal. Moreover, the presence of a relatively high concentration of H_2O_2 would allow the detection of NO in systems where H_2O_2 is present. In order to achieve this objective the optimization of the europium tetracyclines complexes in the presence of H_2O_2 was performed and the NO detection in the presence of different levels of H_2O_2 analysed.

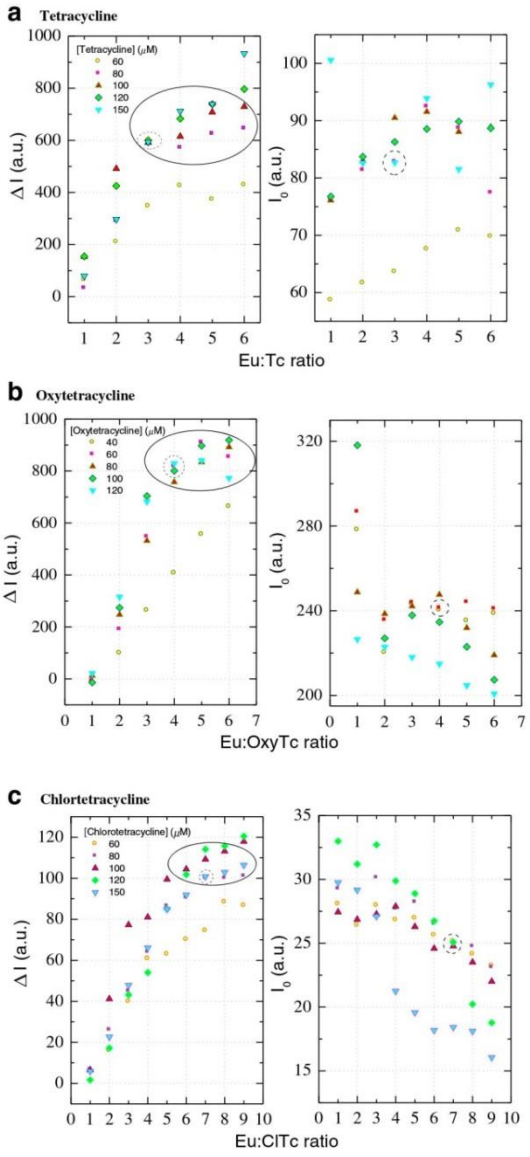


Fig. 3 Fluorescence intensity variation by addition of H_2O_2 100 μM at different Europium:tetracyclines ratios

Europium:Tetracyclines Ratio

The first optimization step was to search for the concentrations of europium and tetracyclines and the ratio of these concentrations that in the presence of H_2O_2 results in a high fluorescence signal. The enhancement of the fluorescence upon addition of H_2O_2 100 μM to europium tetracyclines complexes with ratios for the Eu:Tc and Eu:OxyTc from 1 to 6 and for the Eu:ClTc from 1 to 10 was measured. Figure 3 shows the results obtained in this assessment.

The analysis of Fig. 3 shows that the ΔI increases and stabilises for a higher Eu:Tc ratio for the three Tc and that the intensity shows different trends for the three Tc—Eu:Tc 3:1 (Eu 80 μM:Tc 240 μM); Eu:OxyTc 4:1 (Eu 60 μM:Tc 240 μM); Eu:ClTc 6:1 (Eu 80 μM:Tc 560 μM). A lower I_0 is also found with all the europium tetracyclines complexes at these complex ratios and concentrations.

After this initial study, the response of the europium tetracyclines complexes in the presence of H_2O_2 was evaluated in the complexes ratio and concentrations previous found by variation of the H_2O_2 concentration. Figure 4 shows the typical time profiles and Table 1 the linear regression parameters obtained by addition of H_2O_2 of concentrations from 0.5 to 200 μM. The greatest ΔI variation upon addition of H_2O_2

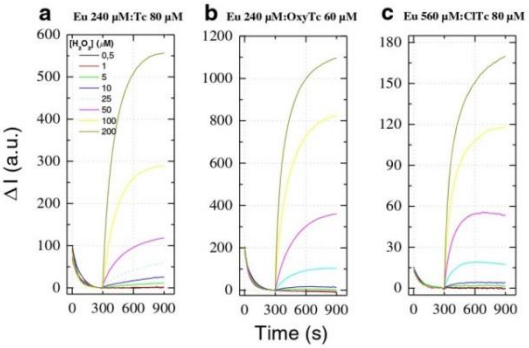


Fig. 4 Typical time profiles of the fluorescence intensity variation by addition of different H_2O_2 concentrations of the **a** Eu:Tc, **b** Eu:OxyTc and **c** Eu:ClTc complexes at the more adequate europium:tetracyclines ratio and concentrations

Table 1 Linear regression of the fluorescence intensity variation of the europium:tetracyclines complexes and the H_2O_2 concentration from 0.5 to 200 μM at the optimized ratio

$y = bx + a[\Delta I = f(C_{H2O2})]$	Eu 240 μM:Tc 80 μM (3:1)	Eu 240 μM:OxyTc 60 μM (4:1)	Eu 560 μM:ClTc 80 μM (7:1)
Lin. range	0.5–200 μM	5–100 μM	5–100 μM
m	8	5	5
a (s_a)	−4.94 (4.15)	−77.76 (22.05)	−8.71 (2.72)
b (s_b)	2.81 (0.05)	8.91 (0.43)	1.25 (0.05)
$s_{y/x}$	9.40	33.26	4.11
R	0.9990	0.9966	0.9973
p ANOVA	<0.0001	0.0002	0.0002

ΔI fluorescence intensity variation; *Lin. range* linear range; *m* number of calibration points; *a* intercept; s_a intercept standard deviation; *b* slope; s_b slope standard deviation; $s_{y/x}$ standard deviation of residuals; *R* linear correlation coefficient; *p ANOVA* ANOVA probability value (p) for a 5 % significance level of the linear regression

was obtained with Eu:OxyTc and the lowest with Eu:ClTc (Fig. 4). Table 1 shows that better linear fit results were obtained with Eu:Tc and generally worse results with the Eu:ClTc complex. Also, a greater sensitivity was found with Eu:OxyTc by variation of the H_2O_2 concentration. Attending to these results we expect identical quantification potential with a similar sensitivity for NO sensing by the Eu:Tc and Eu:OxyTc complexes in the presence of H_2O_2.

H_2O_2 Concentration

The quantification of NO in the presence of a concentration of H_2O_2 from 50 to 400 μM was studied. Table 2 presents the results obtained using the previously optimized europium tetracyclines complexes ratio and concentrations—linear regression of the variation of fluorescence intensity with the NO concentrations in the presence of H_2O_2. Good linear regression

Table 2 Linear regression of the fluorescence intensity variation of the europium:tetracyclines complexes and the NO concentrations from 1 to 200 μM at the optimized ratio in the presence of H_2O_2 from 50 to 400 μM

$[H_2O_2]$ (μM)	$y = bx + a[\Delta I = f(C_{NO})]$									
	a	s_a	b	s_b	$s_{y/x}$	R	m	Lin. range	ΔI_{Lowest}	$\Delta I_{Greatest}$
a) Eu 240 μM:Tc 80 μM (3:1)										
50	n.p.	n.p.	n.p.	n.p.	n.p.	n.p.	n.p.	n.p.	−1.10	−31.57
100	−97.59	4.52	−1.46	0.10	8.15	−0.9914	6	1–100 μM	−88.74	−240.16
200	−163.22	11.43	−1.69	0.11	17.28	−0.9936	5	5–200 μM	−169.57	−491.59
300	−130.32	5.35	−1.15	0.05	6.22	−0.9984	4	25–200 μM	−154.03	−359.73
400	n.p.	n.p.	n.p.	n.p.	n.p.	n.p.	n.p.	n.p.	−859.33	−717.30
b) Eu 240 μM:OxyTc 60 μM (4:1)										
50	−47.37	0.83	−0.32	0.01	1.25	−0.9991	5	5–200 μM	−47.43	−110.77
100	−167.04	6.89	−1.07	0.07	12.22	−0.9908	6	5–200 μM	−169.27	−374.60
200	−142.07	4.72	−1.49	0.05	7.02	−0.9986	5	10–200 μM	−152.27	−436.04
300	−122.10	18.10	−2.23	0.16	22.43	−0.9950	4	10–200 μM	−130.77	−555.52
400	−945.70	7.08	−0.45	0.07	10.53	−0.9671	5	10–200 μM	−943.07	−1031.55
c) Eu 560 μM:ClTc 80 μM (7:1)										
50	n.p.	n.p.	n.p.	n.p.	n.p.	n.p.	n.p.	n.p.	−11.37	−11.49
100	−16.18	1.23	−0.24	0.02	1.53	−0.9923	4	5–100 μM	−17.32	−39.88
200	−15.17	0.32	−0.13	0.003	0.48	−0.9991	5	10–200 μM	−16.56	−40.33
300	−13.23	0.39	−0.14	0.004	0.60	−0.9989	5	5–200 μM	−13.59	−41.12
400	−5.76	0.79	−0.16	0.02	1.22	−0.9864	5	1–100 μM	−4.87	−20.85

n.p. not possible to fit; *a* intercept; s_a intercept standard deviation; *b* slope; s_b slope standard deviation; $s_{y/x}$ standard deviation of residuals; *R* linear correlation coefficient; *m* number of calibration points; *Lin. range* linear range; ΔI_{Lowest} difference of fluorescence intensity at the lowest NO concentration; $\Delta I_{Greatest}$ difference of fluorescence intensity at the greatest NO concentration

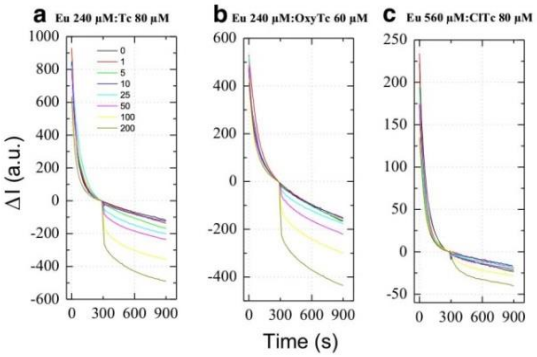


Fig. 5 Typical time profiles of the fluorescence intensity variation by addition of different NO concentrations of the **a** Eu:Tc, **b** Eu:OxyTc and **c** Eu:ClTc complexes in the presence of H_2O_2 200 μM at the more adequate Europium:tetracyclines ratio and concentrations

results were obtained with a H_2O_2 concentration from 100 to 300 μM for the three europium tetracycline complexes and the H_2O_2 concentration of 200 μM was chosen as optimum because it resulted in the highest correlation coefficient and to an adequate linear range. Figure 5 shows typical time profiles of the fluorescence intensity variation by addition of different NO concentrations to the three europium tetracycline complexes in the presence of H2O2 200 μM.

The previous analysis show that the more adequate analytical conditions for the NO sensing at pH 7 are: H_2O_2 200 μM; and one of the following Tc complexes—Eu:Tc 3:1 (Eu 80 μM:Tc 240 μM); Eu:OxyTc 4:1 (Eu 60 μM:Tc 240 μM); or, Eu:ClTc 6:1 (Eu 80 μM:Tc 560 μM).

NO Quantification

Using the previous optimal conditions DEA/NO 25 μM and a NO 50 μM standard solutions were analysed. The results found are presented in Table 3. Similar results for the quantification of NO were obtained with the Eu:Tc and EuOxyTc complexes and worse results with the Eu:ClTc complex. With the DEA/NO solution the liberation of 1.5 mol of NO per mole of DEA/NO (≈37.5 μM) with a half-life at room temperature (≈10′) similar to the expected and with the standard solution an adequate recovery (97 and 102 %) and an acceptable precision (4 and 1 %) were achieved with the two complexes in the NO quantification assessment. The lowest detection limit, evaluated by the intercept standard deviation ($3.s_a/b$), was found for the Eu:OxyTc complex.

Table 3 NO quantification results in a DE/ANO a) and in a standard solution b) obtained by the europium:tetracyclines complexes in the presence of H_2O_2 200 μM

Eu 240 μM:Tc 80 μM (3:1)		Eu 240 μM:OxyTc 60 μM (4:1)		Eu 560 μM:ClTc 80 μM (7:1)	
a) DEA/NO (25 μM)					
Time (min)	C_{NO} ± 4.12 (μM)	Time (min)	C_{NO} ± 6.22 (μM)	Time (min)	C_{NO} ± 6.22 (μM)
20	34.26	20	34.83	20	98.44
40	20.80	40	41.03	40	109.52
60	23.58	60	31.23	60	96.98
Recovery	92.88 %	Recovery	91.36 %	Recovery	262.50 %
$y = bx + a[\Delta I = f(C_{NO})]$					
a=−82.03; s_a=2.79		a=−47.36; s_a=5.60		a=−4.27; s_a=0.49	
b=−1.18; s_b=0.03		b=−1.76; s_b=0.06		b=−0.12; s_b=0.005	
$s_{y/x}$=4.39; R=-0.9992		$s_{y/x}$=10.13; R=-0.9977		$s_{y/x}$=0.73; R=−0.9978	
m=5; 5–200 μM		m=6; Lin. range—1–200 μM		m=5; Lin. range—10–200 μM	
b) Standard (50 μM)					
C_{NO} (μM)	48.41	C_{NO} (μM)	51.06	C_{NO} (μM)	44.09
Recovery	96.82 %	Recovery	102.12 %	Recovery	88.2 %
n	3	n	3	n	2
s	1.87	s	0.35	s	4.39
RSD (%)	3.86	RSD (%)	0.69	RSD (%)	9.96
$DL_{intercept}$	10.81	$DL_{intercept}$	3.11	$DL_{intercept}$	7.74
$y = bx + a[\Delta I = f(C_{NO})]$					
a=−50.67; s_a=3.71		a=3.06; s_a=1.12		a=4.29; s_a=0.49	
b=−1.03; s_b=0.04		b=−1.08; s_b=0.01		b=−0.19; s_b=0.02	
$s_{y/x}$=6.64; R=−0.9971		$s_{y/x}$=2.01; R=−0.9998		$s_{y/x}$=0.76; R=−0.9805	
m=6; Lin. range—1–200 μM		m=6; Lin. range 1–200 μM		m=5; Lin. range 1–50 μM	

The C_{NO} error present is the interpolated standard deviation

ΔI fluorescence intensity variation; a intercept; s_a intercept standard deviation; b slope; s_b slope standard deviation; $s_{y/x}$ standard deviation of residuals; R linear correlation coefficient; m number of calibration points; *Lin. range* linear range; n number of determinations; s mean standard deviation: *RSD* relative standard deviation; $DL_{intercept}$ detection limit estimated by the standard deviation of the intercept

Conclusions

It was observed an enhancement of fluorescence trend when the complexes Eu:Tc, Eu:OxyTc and Eu:ClTc are mixed with $ONOO^-$, H_2O_2 and $O_2^{\cdot-}$ —the highest enhancement was observed for H_2O_2. On the contrary, a quenching trend was observed for NO. This behaviour was used to develop an analytical strategy for NO sensing based on the quenching of fluorescence of the Tc complexes in the presence of relatively high quantities of H_2O_2 which resulted in an increase of sensitivity and interference elimination (although the same approach can be used for $ONOO^-$ or $O_2^{\cdot-}$).

The NO sensing by the different europium tetracyclines complexes was achieved at 30 °C, pH 7.00 in the presence of H_2O_2 200 μM. The better analytical conditions for the NO sensing—Eu 240 μM:Tc 80 μM (3:1), Eu 240 μM: OxyTc 60 μM (4:1) and Eu 560 μM:Tc 80 μM (7:1) complexes. Good quantification results were possible with the Eu:Tc and with the Eu:OxyTc complexes.

Acknowledgments Financial support from Fundação para a Ciência e a Tecnologia (FCT, Lisbon), Programa Operacional Temático Fatores de Competitividade (COMPETE) and comparticipated by Fundo Comunitário Europeu (FEDER) Project PTDC/QUI/71001/2006 is acknowledged. A PhD grant to Eliana Simões SFRH/BD/81074/2011 is acknowledged from FCT, Lisbon. Also the NO gas for the experiences is acknowledged to Rui Barbosa.

References

1. Das S, Powe AM, Baker GA, Valle B, El-Zahab B, Sintim HO, Lowry M, Fakayode SO, McCarroll ME, Patonay G, Li M, Strongin RM, Geng ML, Warner IM (2012) Molecular fluorescence, phosphorescence, and chemiluminescence spectrometry. Anal Chem 84:597–625
2. Gómez-Hens A, Aguilar-Caballos MP (2004) Long-wavelength fluorophores: new trends in their analytical use. Trends Anal Chem 23:127–136
3. Shaner NC, Steinbach PA, Tsien RY (2005) A guide to choosing fluorescent proteins. Nat Methods 2:905–909
4. Piszczek G (2006) Luminescent metal-ligand complexes as probes of macromolecular interactions and biopolymer dynamics. Arch Biochem Biophys 453:54–62
5. Resch-Genger U, Grabolle M, Cavaliere-Jaricot S, Nitschke R, Nann T (2008) Quantum dots versus organic dyes as fluorescent labels. Nat Methods 5:763–775
6. Esteves da Silva JCG, Gonçalves HMR (2011) Analytical and bioanalytical applications of carbon dots. Trends Anal Chem 30:1327–1336
7. Medina AR, Martínez EJL, Barrales PO, Córdova MLF (2011) Lanthanide-sensitized luminescence as a promising tool in clinical analysis. Appl Spectrosc Rev 46:561–580
8. Hagan AK, Zuchner T (2011) Lanthanide-based time-resolved luminescence immunoassays. Anal Bioanal Chem 400:2847–2864
9. Ma Y, Wang Y (2010) Recent advances in the sensitized luminescence of organic europium complexes. Coord Chem Rev 254:972–990
10. Thibon A, Pierre VC (2009) Principles of responsive lanthanide-based luminescent probes for cellular imaging. Anal Bioanal Chem 394:107–120
11. Laurent S, Elst LV, Muller RN (2009) Lanthanide complexes for magnetic resonance and optical molecular imaging. Q J Nucl Med Mol Imaging 53:586–603
12. Grasso AN, Teixeira LS, Vieira ND Jr, Courrol LC (2009) Optical properties of metacycline, oxytetracycline and chlortetracycline europium complexes in the presence of hydrogen peroxide. J Fluoresc 19:715–721
13. Courrola LC, Samad RE (2008) Applications of europium tetracycline complex: a review. Curr Pharm Anal 4:238–248
14. Morandi S, Focardi C, Nocentini M, Puggelli M, Caminati G (2009) Development and validation of europium-sensitized luminescence (ESL) method for the determination of tetracycline residues in milk. Food Anal Methods 2:271–281
15. Chen G, Liu G, Qin F (2011) Use of a portable time-resolved fluorometer to determine oxytetracycline residue in four fruit crops. Food Chem 127:264–269
16. Chen C, Guo C, Wang L, Jiang W (2009) Rapid determination of minocycline in pharmaceutical formulations and human urine/serum samples based on the minocycline-europium-sodium dodecylbenzene sulfonate luminescence system. Anal Lett 42:228–242
17. Mahedero MC, Bohoyo D, Salinas F, Ardila T, Airado D, Roldán B (2005) Improvements in europium sensitized fluorimetric determination of demeclocycline and methacycline. J Pharm Biomed Anal 37:1101–1104
18. Bel'tyukova SV, Vityukova EO, Egorova AV (2007) Spectral luminescence properties of eu (iii) complexes with tetracycline antibiotics and hydrogen peroxide. J Appl Spectrosc 74:344–349
19. Dürkop A, Wolfbeis OS (2005) Nonenzymatic direct assay of hydrogen peroxide at neutral pH using the Eu_3Tc fluorescent probe. J Fluoresc 5:755–761
20. Courrol LC, Bellini MH, Tarelho LVG, Silva FRO, Mansano RD, Gomes L, Vieira ND Jr, Shor N (2006) Urea hydrogen peroxide determination in whole blood using europium tetracycline probe. Anal Biochem 355:140–144
21. Teixeira LS, Grasso AN, Monteiro AM, Neto AMF, Vieira ND Jr, Gidlund M, Steffens J, Courrol LC (2011) Investigation of the europium emission spectra of the europium–oxytetracycline complex in the presence of human low-density lipoproteins. J Fluoresc 21:887–892
22. Teixeira LS, Grasso AN, Monteiro AM, Neto AMF, Vieira ND Jr, Gidlund M, Courrol LC (2010) Enhancement on the europium emission band of europium chlortetracycline complex in the presence of LDL. Anal Biochem 400:19–24
23. Silva FRO, Monteiro AM, Neto AMF, Gidlund M, Vieira ND Jr, Courrol LC (2009) Analytical quantification of low-density lipoprotein using europium tetracycline indicator. J Biolumin Chemilumin 24:189–193
24. Silva FRO, Samad RE, Gomes L, Courrol LC (2008) Enhancement of europium emission band of europium tetracycline complex in the presence of cholesterol. J Fluoresc 18:169–174
25. Bian W, Zhang N, Wang L (2010) Spectrofluorometric determination of total bilirubin in human serum samples using tetracycline-Eu^{3+}. Anal Sci 26:785–789
26. Bian W, Zhang N, Jiang C (2011) Spectrofluorimetric determination of bilirubin in serum samples. J Biolumin Chemilumin 26:54–58
27. Wang T, Wang X, Jiang C (2007) Spectrofluorimetric determination of bile acid using a europium-doxycycline probe. J Clin Lab Anal 21:207–212
28. Chongqiu J, Li L (2004) Lysozyme enhanced europium–metacycline complex fluorescence: a new spectrofluorimetric method for the determination of lysozyme. Anal Chim Acta 511:11–16
29. Schäferling M, Wolfbeis OS (2007) Europium tetracycline as a luminescent probe for nucleoside phosphates and its application to the determination of kinase activity. Chem Eur J 13:4342–4349

30. Hou F, Wang X, Jiang C (2005) Determination of ATP as a fluorescent probe with europium (III)-doxycycline. Anal Sci 21:231–234
31. Peng Q, Hou F, Jiang C (2006) Highly sensitive spectrofluorimetric determination of trace amounts NADP using Europium ion–doxycycline complex probe. Spectrochim Acta A 65:62–66
32. Peng Q, Ge X, Jiang C (2007) A new spectrofluorometric probe for the determination of trace amounts of CoA in injection, human serum and pig livers. Anal Sci 23:557–561
33. Wei W, Wang H, Jiang C (2008) Spectrofluorimetric determination of superoxide dismutase using a Europium-tetracycline probe. Spectrochim Acta A 70:389–393
34. Liu R, Yang J, Wu X (2002) Study of the interaction between nucleic acid and oxytetracycline–Eu^{3+} and its analytical application. J Lumin 96:201–209
35. Zhu X, Wang X, Jiang C (2005) Spectrofluorimetric determination of heparin using a tetracycline–europium probe. Anal Biochem 341:299–307
36. Wang T, Jiang C (2006) Spectrofluorimetric determination of lecithin using a tetracycline–europium probe. Anal Chim Acta 561:204–209
37. Wu M, Lin Z, Wolfbeis O (2003) Determination of the activity of catalase using a europium(III)–tetracycline-derived fluorescent substrate. Anal Biochem 320:129–135
38. Wu M, Lin Z, Wolfbeis O (2004) Time-resolved enzymatic determination of glucose using a fluorescent europium probe for hydrogen peroxide. Anal Bioanal Chem 380:619–626
39. Valko M, Leibfritz D, Moncola J, Cronin MTD, Mazura M, Telser J (2007) Free radicals and antioxidants in normal physiological functions and human disease. Int J Biochem Cell Biol 39:44–84
40. Halliwell B, Whiteman M (2004) Measuring reactive species and oxidative damage in vivo and in cell culture: how should you do it and what do the results mean? Br J Pharmacol 142:231–255
41. Borgmann S (2009) Electrochemical quantification of reactive oxygen and nitrogen: challenges and opportunities. Anal Bioanal Chem 394:95–105
42. Chen X, Tian X, Shin I, Yoon J (2011) Fluorescent and luminescent probes for detection of reactive oxygen and nitrogen species. Chem Soc Rev 40:4783–4804
43. Cui G, Ye Z, Chen J, Wang G, Yuan J (2011) Development of a novel terbium (III) chelate-based luminescent probe for highly sensitive time-resolved luminescence detection of hydroxyl radical. Talanta 84:971–976
44. Page SE, Wilke KT, Pierre VC (2010) Sensitive and selective time-gated luminescence detection of hydroxyl radical in water. Chem Commun 46:2423–2425
45. Song B, Wang G, Tan M, Yuan J (2006) A europium(III) complex as an efficient singlet oxygen luminescence probe. J Am Chem Soc 128:13442–13450
46. Tan M, Song B, Wang G, Yuan J (2006) A new terbium(III) chelate as an efficient singlet oxygen fluorescence probe. Free Radic Biol Med 40:1644–1653
47. Chen Y, Guo W, Ye Z, Wang G, Yuan J (2011) A europium(III) chelate as an efficient time-gated luminescent probe for nitric oxide. Chem Commun 47:6266–6268

Chapter 7

Nitric Oxide Fluorescence Quantification by Chitosan CdSe Quantum Dots Nanocomposites

Eliana F. C. Simões, João M.M. Leitão, Joaquim C.G. Esteves da Silva
J Fluoresc (2014) 24:639–648
DOI 10.1007/s10895-013-1337-0

Due to their properties, crystalline semiconductor NPs based sensors (QDs) are now proposed for detection of NO. In this work the NO detection through the fluorescence quenching of QDs cadmium selenium with chitosan (CS) nanocomposites with mercaptosuccinic acid (QDCdSe-CS-MSA) was made. NO fluorescence quantification by these synthetized QDs was evaluated. Experimental design methodologies were used to make the initial evaluation of the NO response. The response to other ROS/RNS and interference analysis was performed. The NO quantification was obtained on standards and in a donor NO solution in a linear range between 5 and 200 μM, and a detection limit of 1.86 μM. The particle size was evaluated by dynamic light scattering (DLS) and transmission electron microscopy (TEM) techniques. Due to its capacity for the detection and good biocompatibility, QDCdSe-CS-MSA can be used in bioanalitical and biomedical applications. The results of this study, presented below, have been presented as panel communication in XXIII Encontro Nacional da Sociedade Portuguesa de Química and published in an article in Journal of Fluorescence.

My personal contribution to this work includes the establishment of an initial objective and the bibliographic research of the state of the art related with the determination ROS/RNS applying these kinds of NPs and the different methods of NPs synthesis, the protocols set up, the experimental execution and posterior data treatment. After made the bibliographic research the procedures for the characterization of the NPs were done entirely with my contribution. The best experimental conditions were achieved applying experimental design methodologies using the program Unscrambler. The study of the behavior of the NPs with the addition

of the ROS/RNS was after made. Protocols in order to increase the fluorescence intensity signal and enhance the sensibility of the NPs toward ROS/RNS were performed. Then, it was made the characterization of the NPs: that include spectral characterization and size characterizations. The experiments were repeated several times in order to establish if the results were reproducible.

After the experimental part concluded the writing of the paper was made together with Professor João M. M. Leitão under the supervision of Professor Joaquim C. G. Esteves da Silva.

J Fluoresc (2014) 24:639–648
DOI 10.1007/s10895-013-1337-0

ORIGINAL PAPER

NO Fluorescence Quantification by Chitosan CdSe Quantum Dots Nanocomposites

Eliana F. C. Simões · João M. M. Leitão · Joaquim C. G. Esteves da Silva

Received: 14 October 2013 / Accepted: 20 November 2013 / Published online: 11 December 2013
© Springer Science+Business Media New York 2013

Abstract The quantification of nitric oxide (NO) based on the quenching of the fluorescence of a nanocomposites sensor constituted by cadmium/selenium quantum dots (CdSe) stabilized by chitosan (CS) and mercaptosuccinic acid (MSA) is assessed. The optimization of the response of the CS-CdSe-MSA nanocomposites to NO was done by multivariate response surface experimental design methodologies. The highest fluorescence quenching was obtained at pH 5.5 and at room temperature. The NO quantification capability of CS-CdSe-MSA was evaluated using standard solutions and a NO donor reagent. A large linear working range from 5 to 200 μM and a limit of detection of 1.86 μM were obtained. Better quantification results were obtained using the NO donor reagent. Besides NO, the response of the fluorescence of CS-CdSe-MSA to the main reactive oxygen and nitrogen species and similar NO compounds was also assessed.

Keywords Nitric oxide · Chitosan · Quantum dots · Nanocomposites · Fluorescence · Quenching

Introduction

Reactive oxygen species (ROS), as superoxide ($O_2^{\cdot-}$) and hydrogen peroxide (H_2O_2), and reactive nitrogen species (RNS), as nitric oxide (NO) and peroxynitrite ($ONOO^-$), are usually involved in several physiological and pathological processes acting as a signalling molecule. However at higher concentrations these reactive species induce cell damage. Their determination is a matter of great importance in the study of various physiological and pathological processes [1]. Due to their high reactivity, short half-life, lower concentrations, rapid diffusion, possible antioxidant mechanisms and potential interferences, their quantification and/or detection is a continuous challenge. Also the chemistry of these species, namely the preparation and manipulation of standard and sample solutions, is not straightforward due to their reactivity and trace amounts in biological fluids [2,3].

Nitric oxide (NO) and other ROS/RNS regulate many biological processes, such as cardiovascular relaxation, nervous transmission and immunological responses. Disturbs in the NO pathway can provoke disorders such as central nervous system disorders, diabetes mellitus, stroke, hypertension, cardiac failures and others. Due to this regulator role, NO is one of the most studied ROS/RNS and is object of an intense research in order to adequately detect and/or quantify NO by different analytical techniques. The main analytical techniques used are electron spin resonance, chemiluminescence, fluorimetric, colorimetric and electrochemical [2–5]. The fluorescence detection and/or quantification of NO have been done essentially by several classes of organic fluorophores as diaminofluoresceins, diaminorhodamines, dihydrorhodamines, diaminonaphthalene and diaminoanthraquinones [2–7].

Some sensors based in nanocrystalline semiconductors quantum dots (QDs) have been developed as fluorescent probes for NO [8–14]. Most of these sensors are based in CdSe [8–13] and one is based in the CdTe [14] QDs. Also most of the CdSe sensors are based in the quenching of fluorescence [8–12] and only one is based in the enhancement of fluorescence [13]. Sensors based in CdSe fluorescence quenching for NO detection were coupled to fiber optics using cellulose acetate sensitive membranes [8]; biocompatible

E. F. C. Simões · J. M. M. Leitão
Faculdade de Farmácia da Universidade de Coimbra, Pólo das Ciências da Saúde, Centro de Investigação em Química da Universidade do Porto (CIQ-UP), 3000-548, Coimbra, Portugal

J. C. G. Esteves da Silva (✉)
Departamento de Química, Faculdade de Ciências da Universidade do Porto, Centro de Investigação em Química da Universidade do Porto (CIQ-UP), R. Campo Alegre 687, 4169-007 Porto, Portugal
e-mail: jcsilva@fc.up.pt

CdSe QDs chitosan (CS) nanocomposites [9]; CdSe/ZnS QDs in polymethacrylate films [10]; CdSe QDs prepared by changing the oleic acid with tiethanolamine [11]; CdSe QDs coating with metalloporfirins films [12]. Sensor based in the fluorescence enhancement are based in CdSe/ZnS QDs functionalized with tris(dithiocarbamato)iron(III) [13]. A sensor based in CdTe QDs was developed by linked to carboxymethyl chitosan (CMCS) [14]. For the two NO sensors based in CS nanocomposites a linear working range from 5 to 55 μM for CS-CdSe [9] and from 4.6 to 55.2 μM for CMCS-CdTe [14] were obtained.

Nanocomposites resulting of the combination of inorganic molecules with organic molecules (biopolymers as CS) have been used in diagnosis and in cell targeted drug delivery. Indeed chitosan is a biocompatible and biodegradable biopolymer with reduced cytotoxicity and low immunogenicity with a great potential to be used in biomedical applications [15,16]. The combination of QDs and CS allows increasing their biocompatibility and consequently their use in bioapplications. Other nanocomposites composed by QDs and CS, or its derivatives, have been reported [16–18].

In this work, a new CS-CdSe-MSA nanocomposites was synthesized and the potential as NO quantitative sensor was optimized and evaluated. Optimization using response surface experimental design methodologies were used in order to establish the more adequate conditions to the NO quantification by CS-CdSe-MSA. The more adequate pH and temperature conditions for the NO fluorescence sensing with the CS-CdSe-MSA were obtained. In the optimized conditions, the NO detection capability was checked varying the NO concentration and the quantification capability was evaluated in standard solutions and by the generation of NO with a rapid donor diethylamine NONOate (DEA/NO).

Experimental

Reagents

Analytical grade reagents were used: mercaptossucinic acid (MSA), acetic acid, sodium hydroxide (NaOH), sodium borohydride ($NaBH_4$), sodium nitrite, hydrogen peroxide (H_2O_2), hydrogen chloride (HCl), potassium superoxide (KO_2), diethylamine/nitric oxide complex sodium (DEA/NO), sodium nitrate ($NaNO_3$) and sodium nitrite ($NaNO_2$). A low-molecular weight chitosan (CS) sample with a degree of deacetylation greater or equal to 75 % was used (Sigma-Aldrich). Mili-Q water with a resistivity 18 MΩ.cm at 25 °C was used.

Solutions

A CS solution working solution was obtained by filtration of an aqueous solution resulting from the dissolution of 5 g of CS in 500 mL of 0.1 M acetic acid. A hydrogen selenide solution was prepared by mixing 58 mg of Se and 73 mg of $NaBH_4$ with 3 mL of deoxygenated water and kept under nitrogen.

CdSe QDs capped with MSA were prepared by the following procedure: 171 mg of MSA was dissolved in H_2O (50 mL) and the pH was adjusted to 7.0 using a NaOH aqueous solution; next, 28 mg of $CdCl_2$ was added and the pH was again adjusted to 7.0; finally, 200 μL of a hydrogen selenide solution was added to this solution, with continuously stirring yielding an yellow-orange solution.

CS-CdSe-MSA nanocomposites were obtained by the following procedure: 684 mg of MSA was dissolved in H_2O (200 mL) and the pH was adjusted to 7.0 using a NaOH aqueous solution; 112 mg of $CdCl_2$ was added to the previously MSA solution and the pH was again adjusted to 7.0; next, 200 mL of the CS solution was added to the previous solution and well mixed; finally, 1 mL of a hydrogen selenide solution was added to that mixture under a strong continuously stirring, yielding an yellow solution. This mixture was kept under strong stirring for 24 h and it was dialysed for several days against deionised water using a cellulose membrane dialysis tubing (reference D9652 from Sigma). The purified nanocomposites solution is the sensor solution and was stable at room temperature.

Saturated NO solutions (1.9 mM) were prepared by bubbling NO in deoxygenated water, after bubbling argon for 15 min. Standard solutions were prepared in deoxygenated water by rigorous dilution. The DEA/NO stock solution was prepared in NaOH 10 mM and kept at 20 °C before use.

The solutions of H_2O_2, KO_2, $NaNO_3$, $NaNO_2$ were prepared in water. Deoxygenated water was used for the preparation of H_2O_2 and KO_2 solutions. Also solutions of HCl and NaOH 0.1 M were prepared in order to evaluate the influence of pH in the response of the nanocomposites to NO.

Instrumentation

Evaluations were made using a QE65000 charge-coupled detector, a 380 nm light emitting diode (LED), a sampling compartment (CUV-ALL-UV 4-way) and two 1.0 mm core diameter fiber optics (P1000-2-UV–VIS) from Ocean Optics. One of the fibers guides the light from the source to the sampling compartment and the other guide the emitted light to the detector. The reaction time profiles were obtained collecting the signal at the maximum emission wavelength, every 10 s with an integration time of 300 ms. A difference between the initial and the final fluorescence intensity measured after 10 min the addition of NO (intensity variation) were used in all the work.

The absorbance and fluorescence spectra were obtained in a standard 1 cm fluorescence quartz cell and collected respectively in a Jasco V-530 UV-Visible spectrophotometer and in a Jasco FP-6200 spectrofluorimeter. The absorption spectra

were obtained in a wavelength range from 250 to 650 nm with a 2 nm interval, slit widths 2 nm and wavelength scan rate medium; the Fluorescence spectra were obtained in a wavelength range from 300 to 700 nm with a 1 nm interval, slit widths 5 nm, sensitivity response medium, response time fast and wavelength scan rate 1000 nm/min.

The particle size of QDs and nanocomposites and their distribution was obtained by DLS in a Nano Delsa C, Beckman Coulter and by transmission electronic microscopy (TEM) in a FEI Company Tecnai G2 20 S-Twin electronic microscopic. The shape of the particles was also determined by TEM analysis.

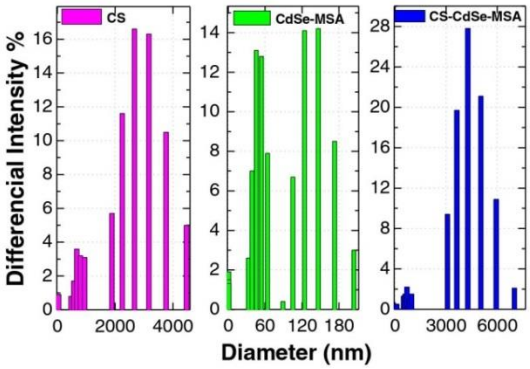


Fig. 2 Particle size distribution of CS, CdSe-MSA and CS-CdSe-MSA obtained by DLS

Data Analysis

The quantum yield (Φ) of the CdSe-MSA QDs and CS-CdSe-MSA nanocomposites were calculated comparing the integrated photoluminescence intensities and the absorbance values of the nanocomposites with the ones of the quinine sulfate [21].

$$\Phi = \Phi_R \times \frac{Grad}{Grad_R} \times \frac{\eta^2}{\eta_R^2}$$

In the equation Φ is the fluorescence quantum yield, Grad is the gradient from the plot of integrated fluorescence intensity *vs*. absorbance and η is the refractive index. The subscripts R refer to reference fluorophore, quinine sulfate of known quantum yield. The Φ of the quinine sulfate is Φ= 0.54. The η of the quinine sulfate in 0.1 M H_2SO_4 and of nanocomposites water solutions used were η=1.33.

A central composite experimental design (CCD) was used for the response surface optimization. This experimental design allows the identification of the optimum response. It also allows the assessment of the significance of the effects of design variables and interactions without confusing their effects. In order to obtain an estimate of errors, a center experiment is included in the experimental design in which the average value

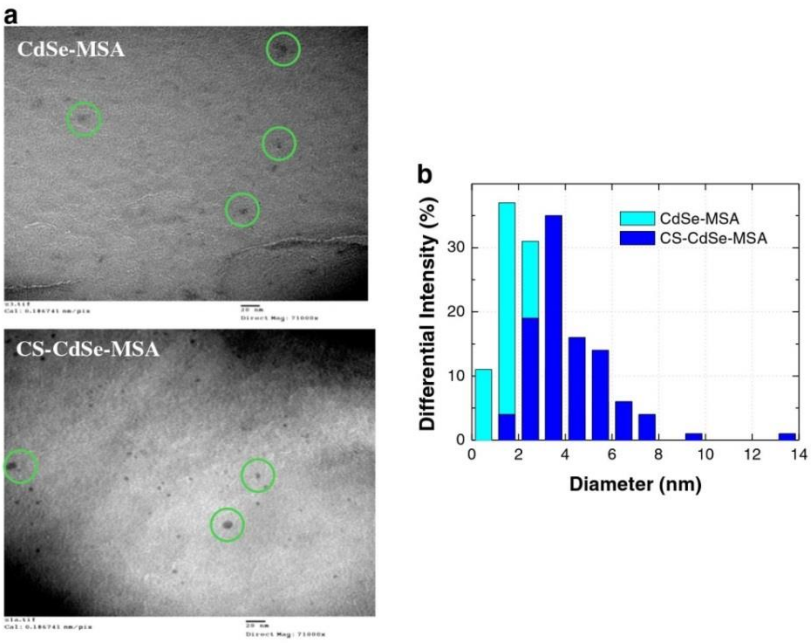


Fig. 1 TEM images (**a**) and particle size distribution plots (**b**) of CdSe-MSA and CS-CdSe-MSA nanocomposites

Table 1 Frequency table of particle size distribution of CS, CdSe-MSA and CS-CdSe-MSA obtained by DLS

Particle size			
	D 10 %	D 50 %	D 90 %
CS	707	2686	44792
CdSe-MSA	35	92	167
CS-CdSe-MSA	2658	3890	5275

of all variables is used. The assessment of the significance of the effects of the design variables and interactions, global linear model, global model quadratic effects and response surfaces was made by analysis of variance (ANOVA) through F-ratio and respective p value. The value of multiple linear regression coefficients of design variables and interactions were also evaluated [19,20]. The CCD was implemented with the Unscrambler® software version 7.51, Camo ASA, Norway.

Results

Characterisation

The size distribution of the nanocomposites was characterized by TEM and DLS and, for comparison purposed, its two main constituents, CS and QDs, were also analyzed.

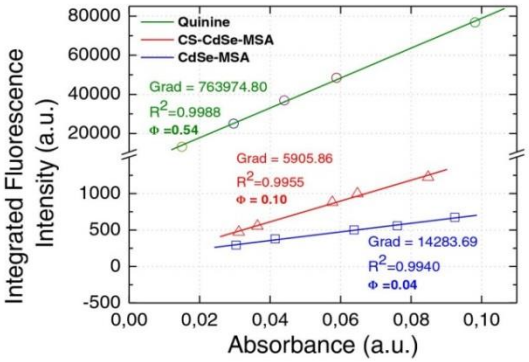


Fig. 4 Quantum yields determinations of CS-CdSe-MSA and CdSe-MSA

TEM

Figure 1 presents the micrographs and the particle core size distribution obtained by TEM analysis. An average particle core size of 2.24 nm (standard deviation - 1.20 nm) for the CdSe-MSA and of 4.19 nm (standard deviation - 1.83 nm) for the CS-CdSe-MSA was observed. This analysis shows that the core of the nanoparticles increases about two times when CS is present.

DLS

Figure 2 and Table 1 present the results, i.e. the size of particles considering the outer salvation sphere, obtained by

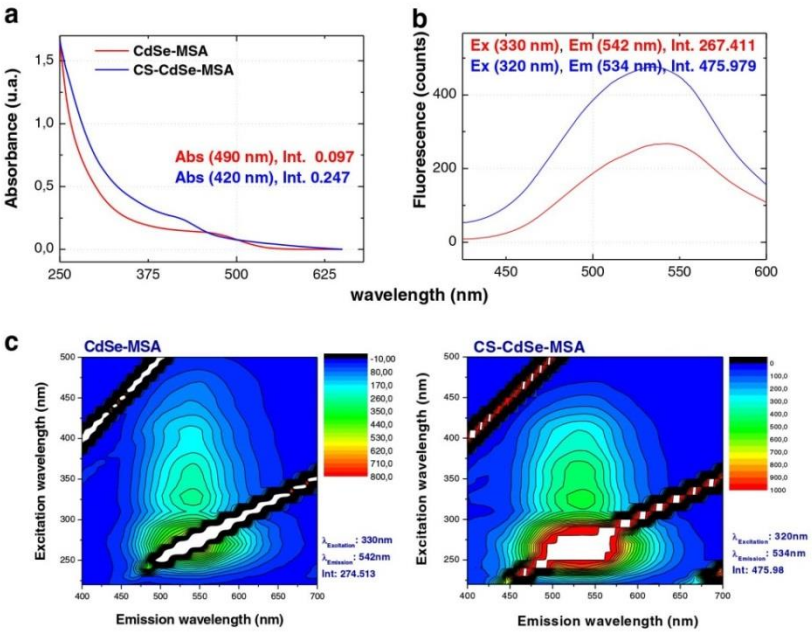


Fig. 3 Absorption (**a**), emission spectra (**b**) and EEM (**c**) of CdSe-MSA and CS-CdSe-MSA

Table 2 Levels of central composite experimental designs

Design variables	Cube levels		Central level
	Low	High	
Central composite design (pH 4-8)			
pH	5	8	6.500
Star levels – Low – 4.385; High –8.615			
Temperature (°C)	25	50	37.500
Star levels – Low – 19.875; High – 55.125			
Central composite design (pH 4-7)			
pH	4.5	6.5	5.500
Star levels – Low – 4.090; High – 6.910			
Temperature (°C)	25	50	37.500
Star levels – Low – 19.875; High – 55.125			

DLS for CS, CdSe-MSA and CS-CdSe-MSA nanoparticles. Taking into consideration the information provided by DLS, and that CS in water is extensively solvated, relatively high dimension particles are expected to be detected.

The analysis of size distribution of the hydrated nanoparticles presented in Fig. 2 shows that the raw QDs (CdSe-MSA) are characterized by nanosized hydrated particles, while when CS is presented (raw CS and the CS nanocomposites), the outer salvation spheres of the particles increase towards the micro-sized dimensions. These results confirm that CS in water is extensively hydrated (it is a gel) as well as the nanocomposites where it is presented.

UVand Fluorescence

Figure 3 shows the absorption and emission spectra and excitation emission matrices (EEM) of CdSe-MSA QDs and CS-CdSe-MSA nanocomposites. The analysis of the EEM shows that the presence of CS on the QDs surface has no significantly effect on photoluminescent properties of the QDs. Indeed, similar fluorescence excitation and emission wavelengths at maximum fluorescence intensity are observed for the QDs ($\lambda_{ExCitation}$ 320 nm, $\lambda_{Emission}$ 542 nm) and nanocomposites QDs (CdSe-MSA - $\lambda_{Excitation}$ 320 nm, $\lambda_{Emission}$ 542 nm; CS-CdSe-MSA - $\lambda_{Excitation}$ 320 nm, $\lambda_{Emission}$ 534 nm). Only a slightly UV-shift of the excitation wavelength and an increase of the fluorescence intensity with the incorporation of CS is observed. This is confirmed by the analysis of the absorption spectra of the two nanocomposites, where a hypsochromic shift, from 490 nm to 420 nm, and a more than two times increase of the absorbance is observed in the CS-CdSe-MSA nanocomposite.

Table 3 ANOVA results for the Δ fluorescent intensity response variable using a central composite optimization experimental design (pH 4 - 8)

ANOVA ($R_{Multiple}$=0.941)						
Effect	SS	d.f.	MS	F-ratio (p-value)	B	$(S.D.)_b$
Model	9.241×10^4	5	1.848×10^4	7.760 (0.021)		
Error	1.191×10^4	5	2.382×10^3			
Adjusted total	1.043×10^5	10	1.043×10^4			
Factor						
Intercept	5.120×10^4	1	5.120×10^4	21.497 (0.006)	-130.640	28.177
pH	6.505×10^4	1	6.505×10^4	27.312 (0.003)	60.206	11.520
Temperature	2.569×10^3	1	2.569×10^3	1.079 (0.347)	1.436	1.382
pH × Temp	789.889	1	789.889	0.332 (0.590)	11.209	19.463
pH × pH	2.400×10^4	1	2.400×10^4	10.076 (0.025)	52.208	16.447
Temp. × Temp.	1.900×10^3	1	1.900×10^3	0.789 (0.413)	14.688	16.447
Model check						
Main	6.762×10^4	2	3.381×10^4			
Int.	789.887	1	789.887	0.332 (0.590)		
Int. + Squ.	2.400×10^4	2	1.200×10^4	5.039 (0.063)		
Squ	2.400×10^4	2	1.200×10^4	5.039 (0.063)		
Error	1.191×10^4	5	2.382×10^3			
Lack of fit						
Lack of fit	1.009×10^4	3	3.362×10^3	3.688 (0.221)		
Pure error	1.823×10^3	2	911.692			
Total error	1.191×10^4	5	2.382×10^3			

RMultiple multiple correlation, *SS* sum of squares; *d.f.* degrees of freedom; *MS* mean squares; *F-ratio* Fisher ratio; *b* beta-regression coefficient; $(S.D.)_b$ standard deviation of b; *Main* main effects; *Int.* interactions effects; *Squ.* squares effects; *p-value* probability value (p) for a 5 % significance level

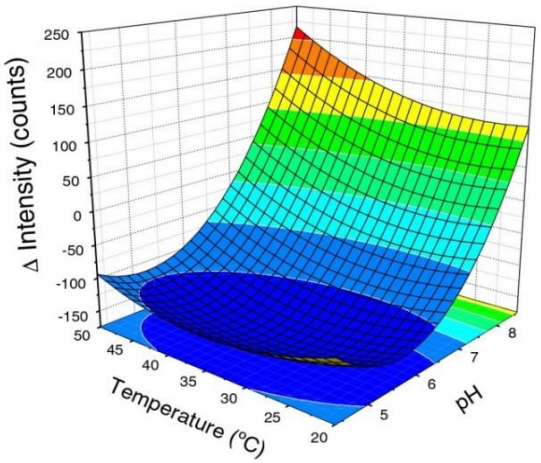


Fig. 5 Response surface fluorescence intensity obtained with the central composite experimental design for pH values between 4 and 8

Figure 4 shows the determination of the quantum yield of the nanoparticles. A relatively lower quantum yield was found for the two nanocomposites. Nevertheless the introduction of CS resulted in a more than two times increase of the Φ found for the CS-CdSe-MSA (Φ = 0.10) relatively of the Φ found for the CdSe-MSA (Φ = 0.04).

Optimization

The optimization of the response of CS-CdSe-MSA to NO was done by response surface methodology using central composite experimental designs (CCD). The evaluated experimental variables were the pH and temperature and the response variable was the difference between the initial and the final fluorescence intensity collected 10 s after the NO addition (Δ Intensity). Two CCD were done with a different pH range and similar temperature range (Table 2).

Table 3 shows the results obtained for the ANOVA of the fluorescence intensity variation as response variable and varying the pH from 4 to 8. Of the global analysis of the model it is possible to conclude that the model adequately fit the data. A statistically significant model (p =0.021), a non-statistically significant lack of fit (p =0.221) with a high $R_{Multiple}$=0.941 it's obtained. By analysis of this table the more relevant is the effect of the pH in the response variable. Indeed, the pH causes a statistically significant increase (p =0.003) of the fluorescence intensity variation and, due to the statistically significant pH square effect (p =0.025), a curvature of the response surface will be expected. Due to the precipitation of CS (pKa=6.5), and possible consequent destruction of the CS-CdSe-MSA structure at a pH higher than 7, a different response to NO with an increase of fluorescence is observed.

Table 4 ANOVA results for the Δ fluorescent intensity response variable using a central composite optimization experimental design (pH 4 - 7)

ANOVA ($R_{Multiple}$=0.978)						
Effect	SS	d.f.	MS	F-ratio (p-value)	B	$(S.D.)_b$
Model	1.094×10^3	5	218.725	21.993 (0.002)		
Error	49.726	5	9.945			
Ajusted total	1.143×10^3	10	114.335			
Factor						
Intercept	702.902	1	702.902	70.677 (0.0004)	-15.307	1.821
pH	635.214	1	635.214	63.871 (0.001)	8.924	1.117
Temperature	275.491	1	275.491	27.701 (0.003)	0.470	8.933×10^{-2}
pH × Temp	157.126	1	157.126	15.799 (0.011)	4.999	1.258
pH × pH	23.46	1	23.46	2.359 (0.185)	-1.632	1.063
Temp × Temp	8.256	1	8.256	0.830 (0.404)	-0.968	1.063
Model check						
Main	910.705	2	455.352			
Int.	157.126	1	157.126	15.799 (0.011)		
Int. + Squ.	25.796	2	12.898	1.297 (0.352)		
Squ	25.796	2	12.898	1.297 (0.352)		
Error	49.726	5	9.945			
Lack of fit						
Lack of fit	11.609	3	3.870	0.203 (0.887)		
Pure error	38.117	2	19.058			
Total error	49.726	5	9.945			

RMultiple multiple correlation, *SS* sum of squares; *d.f.* degrees of freedom; *MS* mean squares; *F-ratio* Fisher ratio; *b* beta-regression coefficient; $(S.D.)_b$ standard deviation of b; *Main* main effects; *Int.* interactions effects; *Squ.* squares effects; *p-value* probability value (p) for a 5 % significance level

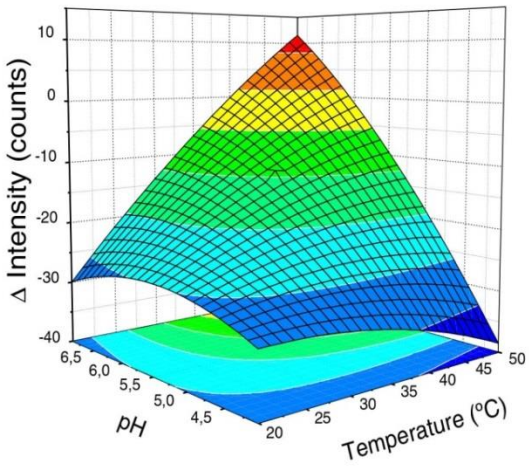


Fig. 6 Response surface fluorescence intensity obtained with the central composite experimental design for pH values between 4 and 7

Figure 5 shows the response surface obtained for the fluorescence intensity variation with the central composite design varying the pH from 4 to 8. The analysis of Fig. 5 confirms that the variable pH affects most significantly the response variable and that the temperature shows a lowest variability in the response variable in the studied range. This figure shows a region where the response variable presents minimum values corresponding to a maximum of fluorescence quenching. This minimum region is observed at a pH from 4.40 to 6.85 at all temperature range. A minimum value of the response variable intensity variation equal to -162.8 was predicted at pH 5.5 and temperature 34.6 °C.

Attending to these results a new central composite design was yet performed now in a pH range from 4 to 7 in the same range of temperatures (Table 2). Table 4 shows the results obtained for the ANOVA for the fluorescence intensity variation as response variable and varying the pH from 4 to 7. Of the global analysis of the model it is possible to conclude that the model adequately fit the data. A statistically significant model ($p=0.002$), a non-statistically significant lack of fit ($p=0.887$) with a high $R_{Multiple}=0.978$ is obtained. By the analysis of this table it is possible to evaluate the statistically significant effects of the pH ($p=0.001$) and of temperature ($p=0.003$) in the response variable. Also the interaction between the two variables is statistically significant ($p=0.011$). Both experimental variables and the interaction induce an increase of the fluorescence intensity variation.

The Fig. 6 shows the response surface obtained for the variable Δ fluorescence intensity with the central composite design restricting the range of the variable pH between 4 and 7. By the analysis of Fig. 6 it is possible to see that there isn't a clearly region of a maximum or minimum of the response variable and even a predicted saddle point was evaluated. Nevertheless, it is possible to define a region of minimum avalues at a pH below 5 at all the temperature range and a region of maximum values at pH above 6.5 at temparature higher than 55 °C of the response variable.

Taking into consideration the relatively small interaction among the two variables a univariate optimization of the pH and temperature was done with a [NO]=50 μM in order to obtain more information about the optimal working regions. The pH was evaluated in a range from 5.5 to 8.5 at temperature 25 °C (Fig. 7) and the temperature was evaluated in a range from 20 to 50 °C at pH 5.5 (Fig. 8).

In Fig. 7, and as previous evaluated, an increase of Δ fluorescence intensity is observed at a basic pH. At pH 7.5 the fluorescence intensity remains almost constant, at pH 7 a lower variation it's observed and only at a pH below 6.5 it's observed the maximum fluorescence quenching. These results show that a stable region of maximum fluorescence quenching is situated at pH values between 5.5 and 6.5.

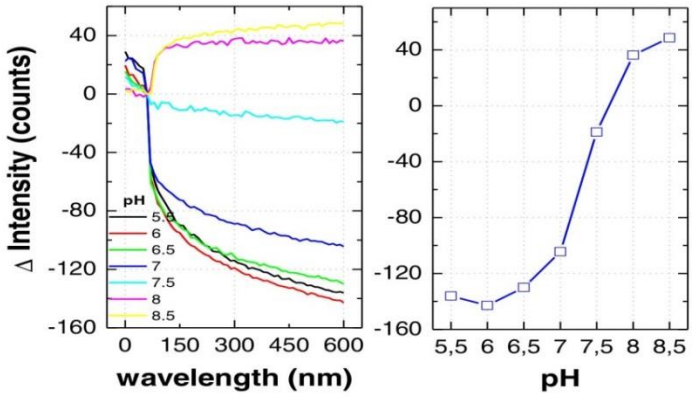


Fig. 7 Fluorescence intensity variation for pH variation at temperature 25 °C and [NO]=50 μM

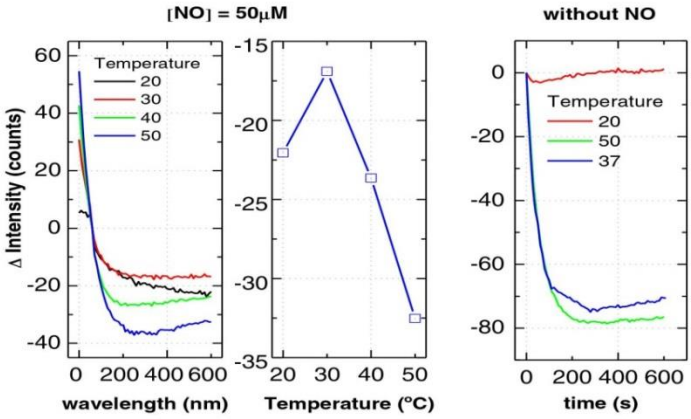


Fig. 8 Fluorescence intensity variation of CS-CdSe-MSA nanocomposite at different temperatures at pH 4.5 by addition of [NO]=50 μM and without NO

In Fig. 8 a small effect on the fluorescence intensity variation is observed in the temperature range evaluated. Nevertheless, the fluorescence intensity becomes somewhat smaller even without NO addition, which provoke a marked effect in the stability of the initial fluorescence intensity of the CS-CdSe-MSA nanocomposite. Consequently, a lower temperature is the more adequate for the NO fluorescence quenching. pH 5.5 and room temperature is the best reaction conditions in order to the NO quantification by the CS-CdSe-MSA.

Quantification of NO

Figure 9 shows typical reaction time profiles of fluorescence intensity variations of the CS-CdSe-MSA nanocomposite with addition of different NO concentrations under the optimized conditions (pH 5.5 and room temperature). From the analysis of Fig. 9 it is possible to observe a marked fluorescence quenching with the addition of NO. A very small variation of the fluorescence intensity of the CdSe-MSA QDs is observed with the addition of NO (data don't shown).

A linear decrease in the fluorescence intensity is observed in the presence of NO concentration from 1.00 to 200 μM. At a reaction time higher than 500 s a fluorescence intensity stabilization is observed. As shown in Table 5, a linear work range from 1 to 200 μM [y=-0.951x+3.856 (m=6); R= 0.99415] with a detection limit of 1.86 μM were obtained. Good quantification results were observed with the solutions under investigation. For the standard solutions and for the DEA/NO solution a recovery around 85 % and for DEA/NO solution of 92 % were found.

The comparison of the response of some ROS/RNS and other NO similar compounds were done in order to evaluate

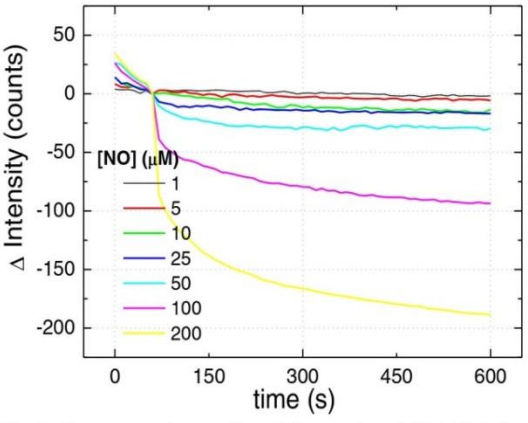


Fig. 9 Fluorescence time profiles of the reaction of CS-CdSe-MSA nanocomposite with NO at different concentrations

Table 5 NO quantification results in a NO donor solution and in standard solutions found by CS-CdSe-MSA in the optimized reaction conditions

NO quantification			
y=- 0.93x - 4.60; m=6; R^2=0.9961; s_a=2.75; s_b=0.03; $s_{y/x}$=4.87; [NO]=5 - 200 μM			
s_{blank}=2.05; LD_{sblank}=1.86 μM; LQ=6.00 μM			
	[NO]=25 μM	[NO]=50 μM	[DEA/NO]=25 μM
[NO] (μM)	20.30±16.10	42.21±15.80	34.45±15.90
Recovery (%)	83.99	84.42	91.88

Calibration equation in form of y = bx + a; m Number of calibration points; R^2 Coefficient of determination, s_a Intercept standard deviation; s_b Slope standard deviation; $s_{y/x}$ Residuals standard deviation; LD_{sblank} Limit of detection calculated by the standard deviation of five determinations of a blank; For the NO estimated concentrations the error is the 95 % confidence interval calculated by the interpolated standard deviation; LQ Limit of quantification

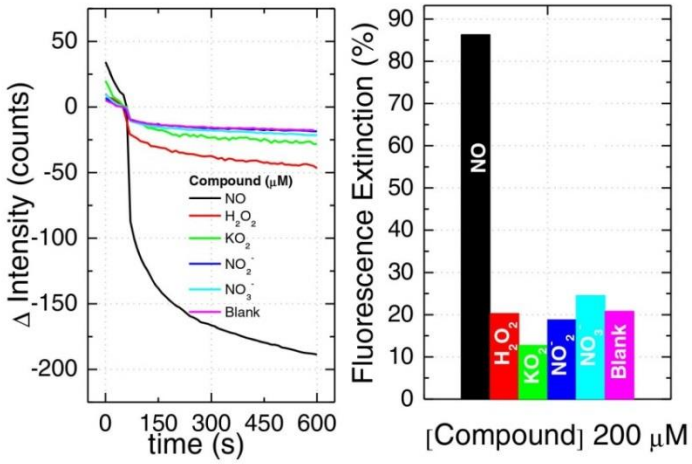


Fig. 10 Comparison of NO fluorescence time profile (**a**) and fluorescence extinction (**b**) with the principal ROS/RNS and NO similar compounds at concentration 200 μM

the selectivity of the CS-CdSe-MSA nanocomposite - 200 μM of each of the compounds were added. In Fig. 10 it is presented the reaction time profile and the percentage of fluorescence extinction for the assessed substances.

From the analysis of Fig. 10 it is possible to observe that only for NO a marked quenching effect on the fluorescence intensity of CS-CdSe-MSA is observed. The decrease of fluorescence intensity with the other evaluated compounds is in the same order to that found with the blank. The fluorescence decrease of the blank and mostly of the fluorescence decrease of the other compounds is probably due to the dilution effect by the increase of the volume added.

Conclusions

New CS-CdSe-MSA nanocomposites were synthesized and were evaluated for the NO detection and/or quantification. Synthetized CS-CdSe-MSA nanocomposite with a regular spherical shape and a size 4.19 nm were obtained. The detection of NO trough the quenching CS-CdSe-MSA fluorescence nanocomposite was verified. A wide linear concentration range 5 – 200 μM, good linear fit (R=0.997) and a lower limit of detection (1.86 μM) were found.

The CS-CdSe-MSA sensor adequately quantifies the NO in a DEA/NO solution. Slightly lowers recoveries were found with the NO standard solutions. Comparing the response of NO with the principal ROS/RNS and NO similar compounds no marked interferences are observed. Due to the proved NO detection and quantification capabilities and potentially good biocompatibility it is expected that the CS-CdSe-MSA nanocomposites could have biological applications.

Acknowledgments Financial support from Fundação para a Ciência e Tecnologia (FCT, Lisbon) project PEST and a PhD grant to Eliana Simões SFRH/BD/81074/2011 is acknowledged. The TEM analyses are also acknowledged to Jorge Nunes and group of de Nanomateriais e Microfabricação of CEMUC.

References

1. Valko M, Leibfritz D, Moncol J, Cronin MT, Mazur M, Telser J (2007) Free radicals and antioxidants in normal physiological functions and human disease. Int J Biochem Cell Biol 39: 44–84
2. Schoenfisch EM, Ha MH (2009) Analytical Chemistry of Nitric Oxide. Annu Rev Anal Chem (Palo Alto Calif) 2:409–433
3. Tarpey MM, Wink DA, Grisham MB (2004) Methods for detection of reactive metabolites of oxygen and nitrogen: in vitro and in vivo considerations. Am J Physiol Regul Integr Comp Physiol 286:R431–R444
4. Tarpey MM, Fridovich I (2001) Methods of detection of vascular reactive species: nitric oxide, superoxide, hydrogen peroxide, and peroxynitrite. Circ Res 89:224–236
5. Taha Z (2003) Nitric oxide measurements in biological samples. Talanta 61:3–10
6. Simões EFC, Leitão JMM, Barbosa RM, Esteves da Silva JCG (2012) Flow injection analysis for nitric oxide quantification based on reduced fluoresceinamine. Anal Methods 4:1089
7. Duarte AJ, Esteves da Silva JCG (2010) Reduced fluoresceinamine as a fluorescent sensor for nitric oxide. Sensors (Basel) 10:1661–1669
8. Ding L, Fan C, Zhong Y, Li T, Huang J (2013) A sensitive optic fiber sensor based on CdSe QDs fluorophore for nitric oxide detection. Sensors Actuators B Chem 185:70–76
9. Tan L, Wan A, Li H, Zhang H, Lu Q (2012) Biocompatible quantum dots–chitosan nanocomposites for fluorescence detection of nitric oxide. Mater Chem Phys 134:562–566
10. Fabregat V, Izquierdo MA, Burguete MI, Galindo F, Luis SV (2012) Quantum dot–polymethacrylate composites for the analysis of NOx by fluorescence spectroscopy. Inorg Chim Acta 381: 212–217

11. Yan XQ, Shang ZB, Zhang Z, Wang Y, Wei JJ (2009) Fluorescence sensing of nitric oxide in aqueous solution by triethanolamine-modified CdSe quantum dots. Luminescence 24:255–259
12. Ivanisevic A, Reynolds MF, Burstyn JN, Ellis AB (2000) Photoluminescent properties of cadmium selenide in contact with solutions and films of metalloporphyrins: Nitric oxide sensing and evidence for the aversion of an analyte to a buried semiconductor-film interface. J Am Chem Soc 122:3731–3738
13. Wang S, Han M-Y, Huang D (2009) Nitric oxide switches on the photoluminescence of molecularly engineered quantum dots. J Am Chem Soc 131:11692–11694
14. Tan L, Wan A, Li H, Lu Q (2012) Novel quantum dots-carboxymethyl chitosan nanocomposite nitric oxide donors capable of detecting release of nitric oxide in situ. Acta Biomater 8:3744–3753
15. Macquarrie DJ, Hardy JJE (2005) Applications of functionalized chitosan in catalysis. Ind Eng Chem Res 44:8499–8520
16. Mansur HS, Mansur AAP, Curti E, De Almeida MV (2013) Functionalized-chitosan/quantum dot nano-hybrids for nanomedicine applications: towards biolabeling and biosorbing phosphate metabolites. J Mater Chem B 1:1696–1711
17. Jiang R, Zhu H, Yao J, Fu Y, Guan Y (2012) Chitosan hydrogel films as a template for mild biosynthesis of CdS quantum dots with highly efficient photocatalytic activity. Appl Surf Sci 258:3513–3518
18. Zhan Li YD, Zhang Z, Pang D (2003) Preparation and characterization of CdS quantum dots chitosan biocomposite. React Funct Polym 55:35–43
19. Bezerra MA, Santelli RE, Oliveira EP, Villar LS, Escaleira LA (2008) Response surface methodology (RSM) as a tool for optimization in analytical chemistry. Talanta 76:965–977
20. Leitao JM, Esteves da Silva JC (2008) Factorial analysis optimization of a Diltiazem kinetic spectrophotometric quantification method. Anal Chim Acta 609:1–12
21. Lakowicz JR (2006) Principles of fluorescence spectroscopy. Springer, New York, pp 54–55

Chapter 8

Carbon Dots from Tryptophan Doped Glucose for Peroxynitrite Sensing

Eliana F. C. Simões, João M.M. Leitão, Joaquim C.G. Esteves da Silva
Analytica Chimica Acta 852 (2014) 174–180
doi.org/10.1016/j.aca.2014.08.050

In this work, and considering that the microwave synthesis of CDs is a rapid, facile and low-cost synthesis method, the CDS were initially synthetized having as precursor only a carbohydrate (glucose (Glc) that are called Bare-CDs. Then, aiming to functionalize these Bare-CDs synthesized by microwave-assisted digestion of Glc, making them by functionalization sensitive to ROS/RNS were added to the microwave synthesis other compounds, such as amino acids and amines.

Considering the ability of nitration and oxidation of $ONOO^-$ and their reactions with some amino acids it was decided add amino acids to the CDs synthesis to make them reactive the $OONO^-$. Firstly was added to the microwave synthesis, some amino acids like tyrosine (Tyr), tryptophan (Trp), phenylalanine (Phe) and cysteine (Cys). This was followed by the characterization of the obtained NPs and verification of sensitivity to ROS/RNS changing conditions of the medium as the temperature and pH. The QY obtained for the synthesized CDs by different forms was of 0.021% for CDs with Tyr, 1.87% for the CDs with Trp, 0.49% for CDs with Phe and 1.41% for CDs with Cys. It was found that the QY of CDs with addition of Trp to the synthesis is higher compared to CDs prepared with addition of other amino acids. Regarding the response to ROS/RNS, it was verified that the CDs with Trp were the only ones with sensitivity for detection and quantification of $OONO^-$.

Then the study of the influence of the masses of Trp and Glc used in the synthesis of these CDs was made in order to establish the ideal conditions for their synthesis. Observing the results of the Bare-CDs microwave synthesis from Glc, the Glc mass of 5 g was fixed and was added growing masses of Trp to the synthesis (100,

200 and 300 mg of Trp) and follow calculated the respective QY. For the CDs synthesized with 5 g of Glc and 100 mg of Trp the QY was 2.02%, to the CDs with 200 mg of Trp was 2.51% and for CDs with 300 mg of Trp was 3.34%. After that optimization experimental design methodologies were using to verify the best masses of Glc and Trp which would synthesize CDs with higher QY. The best conditions for these CDs synthesis called Trp-CDs were for 9 minutes microwave pyrolysis using 2.5 g of Glc and 300 mg of Trp. The Trp-CDs showed an increase in the QY (QY = 9.98%) compared to Bare-CDs (QY = 0.03%) prepared only from Glc and also showed sensitivity and selectivity to the presence of $ONOO^-$ probably due to oxidation of the Trp added these functionalized CDs synthesis. The Trp-CDs synthesized had an average size of 20.3 nm with spherical shape. The $ONOO^-$ causes a decrease in fluorescence intensity of the Trp-CDs ("quenching") probably due to oxidation of Trp residues on the surface of CDs. The $ONOO^-$ detection was performed in a linear scale from 2.5 to 25 µM with a detection limit of 1.49 µM. The quantification of $ONOO^-$ was evaluated in standard solutions and in fortified serum samples. The Trp-CDs have been extensively characterized in contrast with the Bare-CDs by studies of pH, temperature and stability.

The results found from this study were presented, as an article in the scientific journal Analytica Chimica Acta.

My personal contribution to this work includes the establishment of an initial objective and the bibliographic research of the state of the art related with the determination ROS/RNS applying these kinds of CDs, the protocols set up, the experimental execution and posterior data treatment. The study of the main methods for CDs synthesis was made and the microwave pyrolysis method was chosen due to be a facile, rapid and low-cost CDs synthesis method. Protocols in order to produce CDs with increased fluorescence intensity signals and lower sizes were also done with my contribution applying experimental design methodologies. The study of the behavior of the synthetized CDs in the optimized conditions was after made with the addition of the ROS/RNS. The experiments were repeated several times in order to establish if the results were reproducible.

After the experimental part concluded the writing of the paper were made together with Professor João M. M. Leitão under the supervision of Professor Joaquim C. G. Esteves da Silva.

Analytica Chimica Acta 852 (2014) 174–180

Contents lists available at ScienceDirect

Analytica Chimica Acta

journal homepage: www.elsevier.com/locate/aca

Carbon dots from tryptophan doped glucose for peroxynitrite sensing

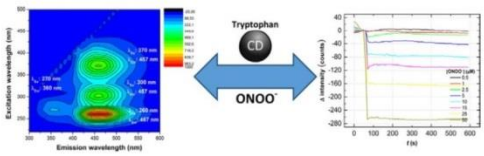
Eliana F.C. Simões [a,b], Joaquim C.G. Esteves da Silva [b], João M.M. Leitão [a,*]

[a] CIQ-UP, Grupo de Ciências Biológicas e Bioanalíticas, Faculdade de Farmácia da Universidade de Coimbra, Pólo das Ciências da Saúde, 3000-548 Coimbra, Portugal
[b] CIQ-UP, Departamento de Química, Faculdade de Ciências da Universidade do Porto, R. Campo Alegre 687, 4169-007 Porto, Portugal

HIGHLIGHTS

- Synthesis of tryptophan doped carbon dots.
- Experimental design optimization of the tryptophan doped carbon dots synthesis.
- Fluorescence sensing of peroxynitrite by tryptophan doped carbon dots.
- Peroxynitrite quantification in serum samples by tryptophan doped carbon dots.

GRAPHICAL ABSTRACT



ARTICLE INFO

Article history:
Received 16 May 2014
Received in revised form 28 July 2014
Accepted 25 August 2014
Available online 2 September 2014

Keywords:
Carbon dots
Tryptophan
Peroxynitrite
Sensing
Fluorescence quenching

ABSTRACT

Tryptophan doped carbon dots (Trp-CD) were microwave synthesized. The optimum conditions of synthesizing of the Trp-CD were established by response surface multivariate optimization methodologies and were the following: 2.5 g of glucose and 300 mg of tryptophan diluted in 15 mL of water exposed for 5 min to a microwave radiation of 700 W. Trp-CD have an average size of 20 nm, were fluorescent with a quantum yield of 12.4% and the presence of peroxynitrite anion ($ONOO^-$) provokes quenching of the fluorescence. The evaluated analytical methodology for $ONOO^-$ detection shows a linear response range from 5 to 25 μM with a limit of detection of 1.5 μM and quantification of 4.9 μM. The capability of the $ONOO^-$ quantification was evaluated in standard solutions and in fortified serum samples.

© 2014 Elsevier B.V. All rights reserved.

1. Introduction

Peroxynitrite anion ($ONOO^-$), one of the main reactive oxygen and nitrogen species (ROS/RNS), is implicated in several physiological or pathological processes. The formation of $ONOO^-$ in vivo is the result of the fast reaction between nitric oxide (NO) and superoxide ($O_2^{\bullet}-$) radicals. The $ONOO^-$ is unstable in acid medium but relatively stable in basic solution. At pH lower than 7.4 $ONOO^-$ is protonated, forming the peroxynitrous acid (ONOOH, $pK_a = 6.8$), followed by decomposition to nitrate [1–3].

The $ONOO^-$ is a strong oxidant and a powerful nitration agent of biomolecules, including proteins, resulting in the modification of their structures and functions. Some of the reactions of $ONOO^-$ with proteins occur through a direct reaction with the cysteine, methionine and tryptophan amino acids residues. Beside this reaction pathway, also the reaction of $ONOO^-$ with proteins could occur through the direct reaction with transition metal centers and selenium-containing amino acids or indirectly by the reaction of secondary $ONOO^-$ derived radicals (hydroxyl, nitrogen dioxide and carbonate radical) with protein residues [3].

Due to the biological role of $ONOO^-$, analytical methodologies for its detection or quantification are of outstanding relevance. However, its reactivity, short half-life, rapid diffusion, low

* Corresponding author. Tel.: +351 239 488 465.
E-mail address: jleitao@ff.uc.pt (J.M.M. Leitão).

http://dx.doi.org/10.1016/j.aca.2014.08.050
0003-2670/© 2014 Elsevier B.V. All rights reserved.

concentration, antioxidant mechanisms, participation in several oxidation and nitration reactions and the presence of possible interferences, makes the detection of $ONOO^-$ challenging [1,2,4–6]. Most of the analytical methodologies for $ONOO^-$ are based in its reactivity. Based on its nitrating ability, the detection of $ONOO^-$ was done through the detection of the product of the tyrosine nitration (3-nitrotyrosine) by immunochemical or chromatographic techniques [4,7–9] and of tryptophan nitration (5- and 6-nitrotryptophan) by liquid-chromatography–mass spectrometry (LC–MS) [10]. The fluorescence and chemiluminescence detection of $ONOO^-$ is based on its oxidation capability. A great number of organic fluorophores probes as the fluorescein [5,8,11–18] and rhodamine [12,19] derivatives were oxidized by the $ONOO^-$ and the related fluorescent oxidation product was evaluated. Fluorescence quenching methods based in the oxidation by the $ONOO^-$ of folic acid [20] or L-tyrosine [21] and chemiluminescence methods based in the quantitative oxidation of the chemiluminescence probes luminol and coelenterazine [5] were developed.

Carbon dots (CD) are fluorescent nanoparticles with attractive analytical properties such water solubility, high quantum yield fluorescence, high biocompatibility and good photostability [22,23]. They can be synthesized by several methods using different carbon precursors [24]. Microwave assisted CD synthesis is a straightforward methodology and several precursors can be used, for example: carbohydrates [25,26], PEG [27], citric acid [28] and dopamine [29]. Due to their fluorescence characteristics, the CD have been proposed for the fluorescence sensing of different analytes [22,24]. For the direct detection of $ONOO^-$ by nanoparticles a quenching fluorescent method based in thiol-capped CdTe or CdTe/ZnS quantum dots (QD) [30] and a colorimetric methodology based on Au nanoparticles have now been proposed [31]. For the fluorescence thiol-capped QD methodology a limit of detection (LOD) of 0.01, 0.02 and 0.07 μM at a pH 9.4 and for the colorimetric Au nanoparticles a linear range from 9.78 to 20.77 mM were calculated.

In this paper we describe the design and synthesis of CD for $ONOO^-$ detection and quantification. Taking into consideration the nitration and oxidation potential of $ONOO^-$, the amino acid tryptophan was used to dope a carbohydrate (glucose) precursor, in order to make them reactive toward peroxynitrite anion. In this study, glucose (Bare-CD) and tryptophan doped glucose (Trp-CD) were used as CD precursors using a microwave pyrolysis methodology. The synthesis process of these two CD samples, Bare-CD and Trp-CD, were optimized using multivariate experimental design methodology. The potential of the CD nanoparticles as $ONOO^-$ sensor was evaluated. Trp-CD synthesized in the presence of glucose and tryptophan has showed an improvement in the quantum yield (Φ) comparatively to Bare-CD prepared only from glucose and showed a greater sensibility to the $ONOO^-$ presence probably due to the oxidation of tryptophan added to CD functionalization.

2. Experimental

2.1. Reagents

Tryptophan, hydrogen peroxide (H_2O_2), sodium hydroxide (NaOH), hydrogen chloride (HCl), sodium phosphate dibasic, monosodium phosphate, potassium superoxide (KO_2), potassium iodide (KI) and sodium nitrite ($NaNO_2$) analytical grade reagents were purchased from Merck, Darmstadt (Germany). Glucose was purchased from Sigma–Aldrich Quimica S.A. (Spain). Mili-Q water with resistivity of 18.2 MΩ cm at 25 °C was used in all experiments.

2.2. Solutions

The $ONOO^-$ and NO standard solutions were prepared as in [13]. The $O_2^{\bullet}-$ and H_2O_2 standard solutions were prepared by rigorous weighing of KO_2 and by rigorous measurement of the required volume of H_2O_2 in deoxygenated water. Diluted standard solutions of the ROS/RNS were prepared by rigorous dilution of the initial standard solutions for $ONOO^-$ in NaOH 0.1 M and for NO, $O_2^{\bullet}-$ and H_2O_2 in deoxygenated water.

The $ONOO^-$ quantification evaluations were performed controlling the pH at 7.4 (neutral physiological pH). Phosphate buffer pH 7.4 was prepared through rigorous weighting of sodium phosphate dibasic and monosodium phosphate for the required volume of solution and posterior addition of NaOH or HCl 0.1 Min order to adjust the pH. In the evaluation of the pH effect in the fluorescence intensity of the synthesized Bare-CD and Trp-CD also the pH was adjusted with NaOH or HCl 0.1 M.

2.3. CD synthesis

Attending to the experimental designs performed in order to establish the optimum conditions of synthesis different masses of glucose and tryptophan were initially solubilized in water and posterior heated in a domestic microwave at the maximum power of 700 W at different heating times. Subsequently the solutions were leaving to cool and were dissolved in water. The obtained solutions were then centrifuged at 9000 rpm for 10 min in order to remove the suspended impurities and a volume of 30 mL were set with water.

2.3.1. Experimental design optimization

Optimization using response surface experimental design methodologies were used in order to establish the more adequate conditions to the Trp-CD synthesis [32–34]. An evaluation of the optimum conditions to the Bare-CD synthesis was previously done. Initial screening fractional or full factorial and posterior optimization central composite experimental designs were implemented with the Unscrambler® software version 7.51, Camo ASA, Norway.

The evaluation of the results found by the experimental design optimization of the Bare and Trp-CD synthesis was performed as previously described [13]. Only for the screening fractional factorial experimental design the initially evaluation of the main effects and variable interactions was done by a comparison with a scale-independent distribution (COSCIND) instead by a higher orders interactions effects (HOIE).

2.4. Instrumentation

2.4.1. Spectrophotometric measurements

The absorbance and the fluorescence spectra were collected, respectively, in a Jasco V-530 UV–vis spectrophotometer and FP-6200 spectrofluorimeter in the required conditions. The reaction time profiles were obtained at the maximum emission wavelength of 496 nm for Bare-CD and of 470 nm for Trp-CD by an optical fiber spectrophotometer using a QE65000 charge-coupled detector and a 380 nm light emitting diode from Ocean Optics.

The fluorescence quantum yield of the CD was evaluated comparing the integrated photoluminescence intensities and the absorbance values of the CD with the ones of the quinine sulphate reference.

$$\Phi = \Phi_R \times \frac{\mathrm{Grad}}{\mathrm{Grad}_R} \times \frac{\eta^2}{\eta_R^2}$$

In the equation Φ is the fluorescence quantum yield, Grad is the gradient from the plot of integrated fluorescence intensity vs. absorbance and η is the refractive index. The subscript R refers to

reference fluorophore quinine sulphate of known Φ. The literature Φ of the quinine sulphate is $\Phi = 0.54$ [30]. The η of the quinine sulphate in 0.1 M H_2SO_4 and of CD aqueous solutions used were $\eta = 1.33$.

The fluorescence lifetimes were calculated using a Horiba Jovin Yvon Fluoromax 4 TCSPC spectrophotometer and the corresponding software (Decay Analysis Software v. 6.4.1, Horiba Jovin Yvon). Fluorescence decays were interpreted in terms of a multi-exponential function: $I(t) = A + \sum B_i \exp - t/\tau_i$, where A and B_i are the pre-exponential factors and τ_i the decay times.

The Fourier transform infrared (FTIR) spectra were obtained by a PerkinElmer FTIR Spectrum 400 spectrophotometer in solid state with an attenuated total reflectance (ATR) accessory in a range of 4000–650 cm^{-1} with 16 accumulation and resolution of 2 cm^{-1}.

The X-ray photoelectron spectroscopy (XPS) analysis was performed using a Kratos AXIS Ultra HSA, with VISION software for data acquisition and CASAXPS software for data analysis. The analysis was carried out with a monochromatic Al Kα X-ray source (1486.7 eV), operating at 15 kV (90 W), in FAT mode (Fixed Analyzer Transmission), with a pass energy of 40 eV for regions ROI and 80 eV for survey. Data acquisition was performed with a pressure lower than 1×10^{-6} Pa, and it was used as a charge neutralization system. The effect of the electric charge was corrected by the reference of the carbon peak (285 eV). The deconvolution of spectra was carried out using CasaXPS programs, in which a peak fitting is performed using Gaussian–Lorentzian peak shape and Shirley type background subtraction.

2.4.2. Particle size measurements

For the evaluation by experimental design synthesis optimization the particle size of CD and their frequency size distribution was obtained by dynamic light scattering (DLS) in a Nano Delsa C, Beckman Coulter. The size and shape of the synthesized CD in the optimum synthesis conditions were also posteriors evaluated by transmission electronic microscopy (TEM) analysis in a Fei Company Tecnai G2 20 S-Twin electronic microscopic.

3. Results and discussion

3.1. CD synthesis

An optimization of CD synthesis was done by experimental designs methodologies in order to define the best conditions for the Bare-CD and Trp-CD synthesis (Supplementary information).

Bare-CD were synthesized from microwave treatment of aqueous solutions of glucose. The objective is to obtain CD with the highest quantum yield and smaller size the possible under this bottom up procedure. In order to optimize these CD features an experimental design of the factors microwave time, mass of glucose and volume of water was done. Bare-CD with the highest fluorescence intensity and smaller size were obtained from 15 mL of water, 5 g of glucose and 9 min of microwave time.

The optimization of the synthesis of the CD from glucose doped with tryptophan (Trp-CD) followed a similar strategy to that of Bare-CD but one more factor was under analysis, the mass of tryptophan. Trp-CD with the highest fluorescence intensity and smaller size were obtained from 15 mL of water, 2.5 g of glucose, 300 mg of tryptophan and 5 min of microwave time.

3.2. CD characterization

The excitation-emission matrices (EEM) of Bare-CD and Trp-CD are shown in Fig. 1. The analysis of these EEM shows that they are quite different and that corresponding of Trp-CD are characterized

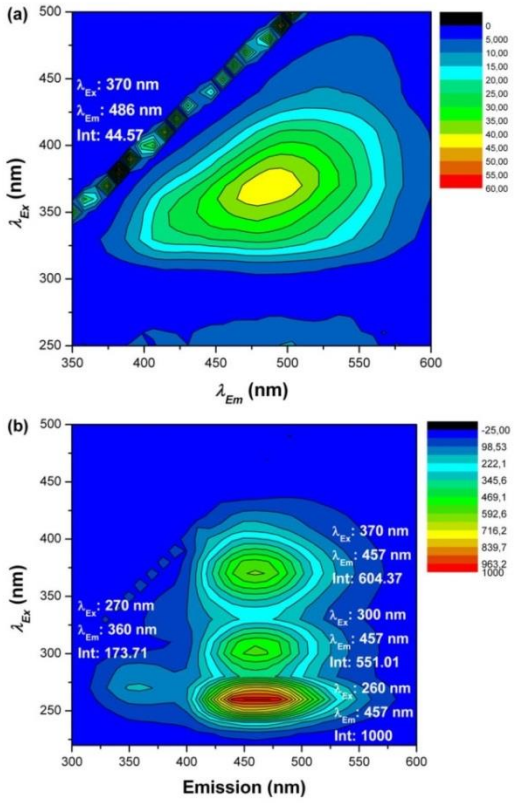


Fig. 1. EEM of Bare (a) and Trp-CD (b) at the optimum synthesis conditions.

by several bands in contrast with Bare-CD that shows only one fluorescence band. A detailed analysis of the EEM of Trp-CD shows:

(i) A band at the same excitation wavelength (370 nm) of the found with the Bare-CD with a slightly different emission wavelength (Bare-CD – 486 nm; Trp-CD – 457 nm) but with a marked difference of the fluorescence intensity (Bare-CD – 44.6; Trp-CD – 604.4).

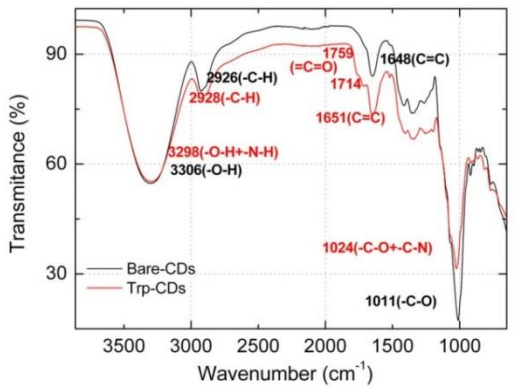


Fig. 2. FTIR spectra of Bare and Trp-CD.

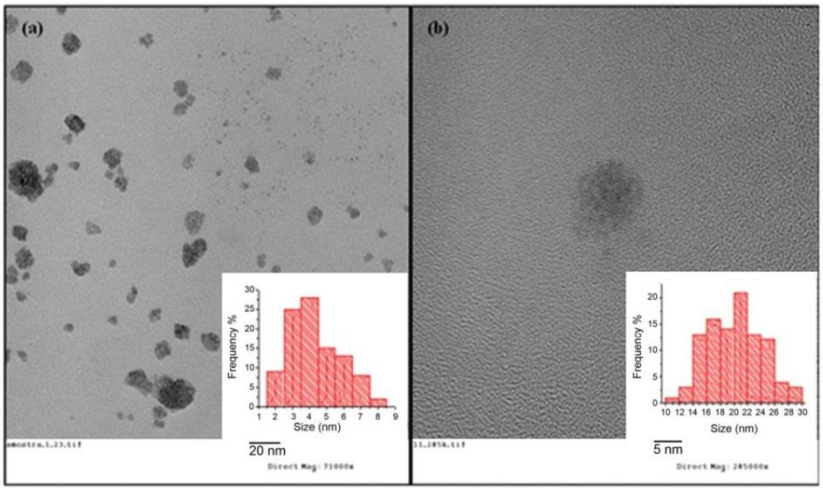


Fig. 3. Images obtained by TEM analysis of the Bare (a) and Trp-CD (b).

(ii) One band at excitation wavelength 270 nm and emission wavelength at 360 nm that could be assigned to the tryptophan residue; and, two other bands at excitation wavelengths (260 and 300 nm) with the same emission wavelength of 457 nm.

The analysis of the Φ of Trp-CD shows a marked increase of 34 times (Φ = 12.4) when compared to that obtained for the Bare-CD (Φ = 0.36). The lifetime decay curves of the fluorescence emission of both CD samples are quite different, and its comparison shows that Trp-CD have components with longer lifetime than Bare-CD. Multicomponent decay models adequately fit the data: Bare-CD – three component decay time model ($\chi^2 = 1.58$) with lifetimes $\tau_1 = 2.77$ ns, $\tau_2 = 0.53$ ns and $\tau_3 = 6.80$; Trp-CD – five component decay time model ($\chi^2 = 1.36$) with lifetimes $\tau_1 = 0.94$ ns, $\tau_2 = 0.89$ ns, $\tau_3 = 0.03$ ns, $\tau_4 = 21.54$ ns and $\tau_5 = 5.67$ ns (Supplementary information). This analysis confirms that the fluorescence lifetime of Trp-CD is longer and is a mixture of fluorophores more complex than that observed for Bare-CD, and shows that tryptophan doping of glucose increases the lifetime as well as the quantum yield. These results confirms that the tryptophan doping have a strong effect on the luminescence properties of the CD.

The mechanism that could explain the fluorescence properties of CD is related to the existence of surface defects and presence of oxygen functional groups [22]. In order to assess if the fluorophores present in Trp-CD are located in the surface of the nanoparticles, iodide anion was added and the dynamic quenching of the fluorescence was measured. The linearization of the quenching profiles observed at the maximum of the four emission bands of Trp-CD with a modified Stern–Volmer equation shows that all the fluorophores are localized at the surface of the nanoparticle but the fluorophores responsible for the band with excitation 270 nm and emission 360 nm. Indeed, only 73% of this class of fluorophores is localized at the surface of the nanoparticles at accessible positions to iodide (Supplementary information). This characteristic is justified because these fluorophores correspond to tryptophan residues and are distributed all over the nanomaterial.

The effect of the pH, temperature and ionic strength in the maximum fluorescence intensity of the bands of Bare-CD and Trp-CD was studied (Supplementary information). The pH has a marked effect in the fluorescence intensity of both samples and is characterized by a general decreasing trend as the pH is raised. Increasing the temperature also provokes a decreasing trend in the fluorescence but the magnitude of the effect is smaller than that observed for the pH. The ionic strength has a relatively small effect on the fluorescence intensity of both CD with no clear trend. The stability of the fluorescence intensity of both samples of CD upon excitation was checked and, besides an initially slight decrease, the fluorescence intensity remains almost constant.

Fig. 2 shows the FTIR spectra of both CD samples. The main common bands observed in both CD samples are: strong band at 3300 cm^{-1} (—OH), strong band at 1020 cm^{-1} (—CO), and two weak bands at 2926 cm^{-1} (—CH) and 1650 cm^{-1}(C=C). Some clear differences are detected in the spectra of the two CD that are due to the —NH and —CN groups presented in Trp-CD. The band assigned to —OH in both samples are markedly sifted (Bare-CD 3306 cm^{-1}; Trp-CD 3298 cm^{-1}), as well as the band assigned to —CO (Bare-CD 1011 cm^{-1}; Trp-CD 1024 cm^{-1}). Also two bands at 1714 cm^{-1} and 1751 cm^{-1} related to =C=O are now clearly evident in the Trp-CD spectrum.

The XPS survey spectrum of the Bare and Trp-CD and the C1s, N1s and O1s core level spectrum are presented in Supplementary information. The XPS survey spectrum of the Bare and Trp-CD shows the presence of carbon (63.8% and 61.8% atomic concentration, respectively) and oxygen (34.5% and 38.2% atomic concentration, respectively) in both samples and a smaller amount of nitrogen in the Trp-CD (1.7% atomic concentration) – a residual band, probably due to nitrogen, is hardly observed in the Bare-CD survey spectrum (<0.05%). The C1s core level spectrum of Trp-CD can be decomposed into four bands at 285.0 eV (26.7%), 286.5 eV (59.1%), 288.0 eV (12.3%) and 289.4 eV (1.9%). The main contribution at low binding energy (285.0 eV) is assigned to the presence of surface methylene group, graphitic and adventitious carbon. The band at 286.5 eV has the highest relative intensity and it may be assigned to C—OH groups. The two low intensity bands can be assigned to C=O, —COO— and C—N moieties. The C1s core level spectrum of Bare-CD has a similar shape to that of Trp-CD but with slightly different proportions: 285.0 eV (14.6%), 286.6 eV (66.1%), 287.9 eV (17.3%) and 289.3 eV (2.0%). The N1s core level spectrum of Trp-CD can be decomposed into two contributions at 400.2 eV (78.6%) and 402.1 eV (21.4%). The

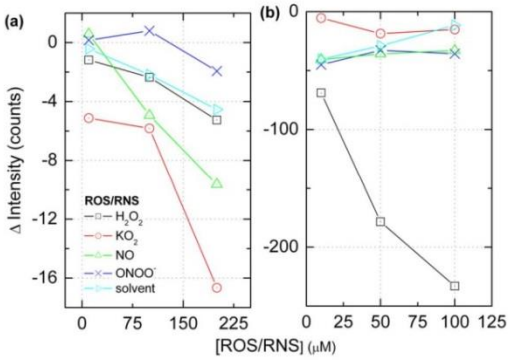


Fig. 4. Effect of $ONOO^-$ on the other ROS/RNS in Bare (a) and Trp-CD (b).

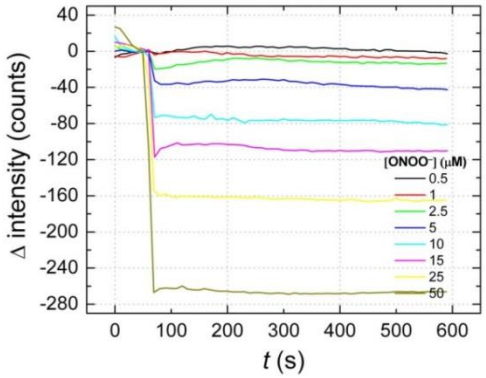


Fig. 5. Typical fluorescence time profiles of the Trp-CD by $ONOO^-$ addition.

main band is due to N—C structures while the minor band is due to N═C and N—O structures. A detailed examination of the N1s core level spectrum region of Bare-CD confirms that the possible band is almost confused with the noise level. The O1s core level spectrum of Trp-CD can be decomposed into three contributions at 531.3 eV (3.7%), 532.9 eV (89.9%) and 534.1 eV (6.5%). The main contribution to the O1s core level spectrum is attributed to oxygen from alcoholic and carbonyl groups. The other minor contributions may be due to CO and/or NO surface structures. The O1 s core level spectrum of Bare-CD has a similar shape to that of Trp-CD but with slightly different proportions: 531.1 eV (1.0%), 532.9 eV (92.2%) and 534.0 eV (6.8%). These results show that the surface of both CD are oxidized with a high degree of oxygen functional structures and the Trp-CD samples also show at the surface some traces of nitrogen containing structures.

The size and shape of both CD samples were determined by TEM analysis (Fig. 3). For the Bare-CD a size of 2 and up to 8 nm is observed with an elliptic or irregular shape. For Trp-CD, nanoparticles with a higher size than Bare-CD of 12 up to 29 nm,with a spherical or irregular shape are observed. A statistical evaluation of the size distribution considering a sample of 100 nanoparticles shows: Bare-CD:$\bar{x} = 4$ nm ($\sigma = 1$); Trp-CD:$\bar{x} = 20$ nm ($\sigma = 4$).

The size distribution of both CD samples in solution was determined by DLS (Supplementary information). These results confirm that Bare-CD ($D_{50\%} = 8$ nm) have a smaller particle size distribution than Trp-CD ($D_{50\%} = 153$ nm). Also, these results show an agglomeration tendency for both samples in solution which is particularly evident for Trp-CD, probably because this sample has a higher density of functional groups due to the tryptophan doping. The low evaluated potential zeta for both kinds of CD (Bare-CD, −6 mV; Trp-CD, +10 mV) confirms the agglomeration tendency of both CD. Even so, evaluations of fluorescence intensity and the quantum yield with the time shows that the fluorescence properties of both CD are not affected by this agglomeration tendency.

3.3. Trp-CD $ONOO^-$ sensing

Fig. 4 presents the plots of the Bare and Trp-CD fluorescence intensity as function of the concentration of the main ROS/RNS, H_2O_2, O_2^-, NO and $ONOO^-$. The analysis of these plots shows that, although a decrease of the fluorescence of the Bare-CD is observed when increasing the ROS/RNS species concentrations, it is not analytically significant (a few fluorescence units) when compared with the quenching of fluorescence provoked by $ONOO^-$ on the fluorescence intensity of Trp-CD (more than one hundred fluorescence units).

Fig. 5 shows typical reaction time profiles of Trp-CD with $ONOO^-$. In the range 0.5–25 μM a linear fit $y = -6.76x - 3.39$ ($m = 7$), $R = -0.9937$, $s_{blank} = 3.35$, LOD = 1.5 μM, LOQ = 5.0 μM are obtained. A worse linear fit is found with a concentration range of $ONOO^-$ up to 50 μM (Supplementary information). The deviation of linearity that is observed for higher $ONOO^-$ concentrations is due to the pH variations induced by the $ONOO^-$ alkaline standard concentrated solution. Comparing to the previous obtained by the already developed nanosensors [30,31], and attending to the lowest $ONOO^-$ concentration evaluated, an intermediary $ONOO^-$ quantification capability by the developed nanosensor was obtained.

The quenching of the fluorescence of Trp-CD by $ONOO^-$ was studied by Stern–Volmer plots and at two temperatures (Fig. 6). The analysis of these plots shows their linear trend with Stern–Volmer constants (K_{SV}) of 9900 ± 800 (20 °C) and 4460 ± 190 (37 °C) M^{-1}. Taking into consideration the magnitude of these constants and its temperature dependence a static quenching is observed probably due to a chemical reaction between $ONOO^-$ and the tryptophan residues in the CD (nitration or oxidation reaction).

In order to assess the Trp-CD based methodology, the analysis of $ONOO^-$ was done in standard solutions and fortified serum samples. Table 1 presents the results found in this analysis which shows that good quantification results were observed with the solutions under investigation.

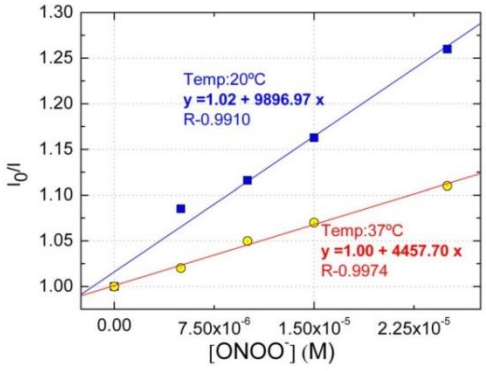


Fig. 6. Stern–Volmer plots at two different temperatures.

Table 1
$ONOO^-$ quantification results in standard solutions and in fortified serum samples.

Trp-CD (m_{Glc} – 2.5 g; m_{Trp} – 300 mg; t_{mic} – 5 min)				
[$ONOO^-$] (μM)	Standard solutions			Fortified serum (10×)
Expected	5	10	15	15
Estimated	5.13	8.78	17.98	15.82
	$s_{xi} = -1.04$	$s_{xi} = -0.97$	$s_{xi} = -0.96$	$s_{xi} = -2.16$
	$IC_{95\%} = \pm 4.48$	$IC_{95\%} = \pm 4.15$	$IC_{95\%} = \pm 4.11$	$IC_{95\%} = \pm 9.29$
Recovery (%)	102.65	87.85	119.89	105.43
$y = bx + a$ [$\Delta I = f([ONOO^-])$]				
$a = -7.09$; $s_a = 2.83$				
$b = -3.25$; $s_b = 0.18$				
$s_{y/x} = 2.86$; $R = 0.9969$				
$m = 4$; 5–25 μM				

s_{xi} – interpolated standard deviation; $IC_{95\%}$ – interpolated 95% confidence interval; a – intercept; s_a – intercept standard deviation; b – slope; s_b – slope standard deviation; $s_{y/x}$ – standard deviation of residuals; R – linear correlation coefficient; m – number of calibration points.

4. Conclusions

Relatively high quantum yield carbon nanoparticles (carbon dots-CD) were successively prepared from glucose doped tryptophan (Trp-CD) by a bottom up one step microwave synthesis. Doping with tryptophan resulted in CD with increased sensitivity and selectivity toward peroxynitrite anion. The synthesis of Trp-CD was optimized with experimental design methodologies. The synthesized carbon nanoparticles had an average size of 20.3 nm with an irregular spherical shape. The $ONOO^-$ anion provokes quenching of the fluorescence intensity of the Trp-CD probably due to the oxidation of tryptophan residues in the surface of the CD. The $ONOO^-$ detection shows a linear range from 2.5 to 25 μM with a limit of detection of 1.5 μM. The $ONOO^-$ quantification capability of the Trp-CD evaluated in standard solutions and in serum fortified samples shows adequate recoveries.

Acknowledgments

A Ph.D. grant SFRH/BD/81074/2011 to Eliana Simões from Fundação para a Ciência e Tecnologia (FCT, Lisbon) is acknowledged. The TEM analyses from Nanomaterials and Micromanufacturing group of Centre for Mechanical Engineering of the University of Coimbra (CEMUC), the XPS analysis from the Materials Centre of the University of Porto (CEMUP) and the FTIR use from UCQ Farma, Pharmacy Faculty of the University of Coimbra are acknowledged.

Appendix A. Supplementary data

Supplementary data associated with this article can be found, in the online version, at http://dx.doi.org/10.1016/j.aca.2014.08.050.

References

[1] M. Valko, D. Leibfritz, J. Moncol, M.T. Cronin, M. Mazur, J. Telser, Free radicals and antioxidants in normal physiological functions and human disease, Int. J. Biochem. Cell Biol. 39 (2007) 44–84.
[2] S.F. Peteu, R. Boukherroub, S. Szunerits, Nitro-oxidative species in vivo biosensing: challenges and advances with focus on peroxynitrite quantification, Biosens. Bioelectron. 58 (2014) 359–373.
[3] B. Alvarez, R. Radi, Peroxynitrite reactivity with amino acids and proteins, Amino Acids 25 (2003) 295–311.
[4] C. Ducrocq, B. Blanchard, B. Pignatelli, H. Ohshima, Peroxynitrite: an endogenous oxidizing and nitrating agent, Cell. Mol. Life Sci. 55 (1999) 1068–1077.
[5] G. Ferrer-Sueta, R. Radi, Chemical biology of peroxynitrite: kinetics, diffusion, and radicals, ACS Chem. Biol. 4 (2009) 161–177.
[6] R. Radi, G. Peluffo, M.N. Alvarez, M. Naviliat, A. Cayota, Unraveling peroxynitrite formation in biological systems, Free Radic. Biol. Med. 30 (2001) 463–488.
[7] M.M. Tarpey, D.A. Wink, M.B. Grisham, Methods for detection of reactive metabolites of oxygen and nitrogen: in vitro and in vivo considerations, Am. J. Physiol. Regul. Integr. Comp. Physiol. 286 (2004) R431–R444.
[8] M.M. Tarpey, I. Fridovich, Methods of detection of vascular reactive species: nitric oxide, superoxide, hydrogen peroxide, and peroxynitrite, Circ. Res. 89 (2001) 224–236.
[9] M.R. Radabaugh, O.V. Nemirovskiy, T.P. Misko, P. Aggarwal, W.R. Mathews, Immunoaffinity liquid chromatography–tandem mass spectrometry detection of nitrotyrosine in biological fluids: development of a clinically translatable biomarker, Anal. Biochem. 380 (2008) 68–76.
[10] B. Alvarez, H. Rubbo, M. Kirk, S. Barnes, B.A. Freeman, R. Radi, Peroxynitrite-dependent tryptophan nitration, Chem. Res. Toxicol. 9 (1996) 390–396.
[11] A. Gomes, E. Fernandes, J.F.C. Lima, Use of fluorescence probes for detection of reactive nitrogen species: a review, J. Fluoresc. 16 (2006) 119–139.
[12] J.P. Crow, Dichlorodihydrofluorescein and dihydrorhodamine 123 are sensitive indicators of peroxynitrite in vitro: implications for intracellular measurement of reactive nitrogen and oxygen species, Nitric Oxide 1 (1997) 145.
[13] E.C. Simões, J.M. Leitão, J.G.E. da Silva, Reduced fluoresceinamine for peroxynitrite quantification in the presence of nitric oxide, J. Fluoresc. 22 (2012) 1127–1140.
[14] A. Keller, A. Mohamed, S. Dröse, U. Brandt, I. Fleming, R.P. Brandes, Analysis of dichlorodihydrofluorescein and dihydrocalcein as probes for the detection of intracellular reactive oxygen species, Free Radic. Res. 38 (2004) 1257–1267.
[15] R. Nakahara, T. Fujimoto, M. Doi, K. Morita, T. Yamaguchi, Y. Fujita, Fluorophotometric determination of hydrogen peroxide and other reactive oxygen species with fluorescein hydrazide (FH) and its crystal structure, Chem. Pharm. Bull. 56 (2008) 977–981.
[16] K. Setsukinai, Y. Urano, K. Kakinuma, H.J. Majima, T. Nagano, Development of novel fluorescence probes that can reliably detect reactive oxygen species and distinguish specific species, J. Biol. Chem. 278 (2003) 3170–3175.
[17] S.L. Hempel, Y.Q. O'Malley, D.A. Wessels, D.M. Flaherty, Dihydrofluorescein diacetate is superior for detecting intracellular oxidants: comparison with 2′,7′-dichlorodihydrofluorescein diacetate, 5(and 6)-carboxy-2′,7′-dichlorodihydrofluorescein diacetate, and dihydrorhodamine 123, Free Radic. Biol. Med. 27 (1999) 146–159.
[18] D. Yang, H.L. Wang, Z.N. Sun, N.W. Chung, J.G. Shen, A highly selective fluorescent probe for the detection and imaging of peroxynitrite in living cells, J. Am. Chem. Soc. 128 (2006) 6004–6005.
[19] X.F. Yang, X.Q. Guo, Y.B. Zhao, Development of a novel rhodamine-type fluorescent probe to determine peroxynitrite, Talanta 57 (2002) 883–890.
[20] J.C. Huang, D.J. Li, J.C. Diao, J. Hou, J.L. Yuan, G.L. Zou, A novel fluorescent method for determination of peroxynitrite using folic acid as a probe, Talanta 72 (2007) 1283–1287.
[21] J. Liang, Z.H. Liu, R.X. Cai, A novel method for determination of peroxynitrite based on hemoglobin catalyzed reaction, Anal. Chim. Acta 530 (2005) 317–324.
[22] J.C.G.E. da Silva, H.M.R. Gonçalves, Analytical and bioanalytical applications of carbon dots, Trends Anal. Chem. 30 (2011) 1327–1336.
[23] Y. Zhang, H. Goncalves, J.C.G.E. da Silva, C.D. Geddes, Metal-enhanced photoluminescence from carbon nanodots, Chem. Commun. 47 (2011) 5313–5315.
[24] E.F. Simoes, J.M. Leitao, J.C.G.E. da Silva, Reduced fluoresceinamine for peroxynitrite quantification in the presence of nitric oxide, J. Fluoresc. 22 (2012) 1127–1140.
[25] X. He, H. Li, Y. Liu, H. Huang, Z. Kang, S.T. Lee, Water soluble carbon nanoparticles: hydrothermal synthesis and excellent photoluminescence properties, Colloids Surf. B Biointerfaces 87 (2011) 326–332.
[26] H. Yan, M. Tan, D. Zhang, F. Cheng, H. Wu, M. Fan, X. Ma, J. Wang, Development of multicolor carbon nanoparticles for cell imaging, Talanta 108 (2013) 59–65.
[27] H. Zhu, X. Wang, Y. Li, Z. Wang, F. Yang, X. Yang, Microwave synthesis of fluorescent carbon nanoparticles with electrochemiluminescence properties, Chem. Commun. 34 (2009) 5118–5120.
[28] S. Zhu, Q. Meng, L. Wang, J. Zhang, Y. Song, H. Jin, K. Zhang, H. Sun, H. Wang, B. Yang, Highly Photoluminescent carbon dots for multicolor patterning, sensors, and bioimaging, Angew. Chem. Int. Ed. 52 (2013) 3953–3957.

[29] K. Qu, J. Wang, J. Ren, X. Qu, Carbon dots prepared by hydrothermal treatment of dopamine as an effective fluorescent sensing platform for the label-free detection of iron(III) ions and dopamine, Chemistry 19 (2013) 7243–7249.
[30] O. Adegoke, T. Nyokong, Probing the sensitive and selective luminescent detection of peroxynitrite using thiol-capped CdTe and CdTe@ZnS quantum dots, J. Lumin. 134 (2013) 448–455.
[31] L. Chen, N. Wu, B. Sun, H. Su, S. Ai, Colorimetric detection of peroxynitrite-induced DNA damage using gold nanoparticles, and on the scavenging effects of antioxidants, Microchim. Acta 180 (2013) 573–580.
[32] M.A. Bezerra, R.E. Santelli, E.P. Oliveira, L.S. Villar, L.A. Escaleira, Response surface methodology (RSM) as a tool for optimization in analytical chemistry, Talanta 76 (2008) 965–977.
[33] T. Lundstedt, E. Seifert, L. Abramo, B. Thelin, Å. Nyström, J. Pettersen, R. Bergman, Experimental design and optimization, Chemometr. Intell. Lab. Syst. 42 (1998) 3–40.
[34] J.M. Leitao, J.C.E. da Silva, Factorial analysis optimization of a Diltiazem kinetic spectrophotometric quantification method, Anal. Chim. Acta 609 (2008) 1–12.

Carbon dots from tryptophan doped glucose for peroxynitrite sensing

Eliana F. C. Simões[a], Joaquim C.G. Esteves da Silva[b] and João M.M. Leitão[a,*]
[a] CIQ-UP, Grupo de Ciências Biológicas e Bioanalíticas, Faculdade de Farmácia da Universidade de Coimbra, Pólo das Ciências da Saúde, 3000-548 Coimbra, Portugal
[b] CIQ-UP, Departamento de Química, Faculdade de Ciências da Universidade do Porto, R. Campo Alegre 687, 4169-007 Porto, Portugal

Supplementary information

1. CD synthesis

1.1. Bare-CD synthesis

In Table S1 are presented the design variables and the levels evaluated for the Bare-CD synthesis optimization.

Table S1 – Levels of design variables under investigation in the experimental designs used for the optimization of the Bare-CD synthesis conditions.

Design variables	Abbreviation	Cube Levels		Central level
		low	high	
Screening fractional factorial experimental design				
Microwave time (min)	t_{mic}	3	15	9
Mass of glucose (g)	m_{Glc}	1	5	3
Volume of water (mL)	V_{water}	5	23	14
Optimization central composite experimental design				
Microwave time (min)	t_{mic}	5	13	9
Star levels – Low – 3.36; **High** – 14.64				
Mass of glucose (g)	m_{Glc}	4	8	6
Star levels – Low – 3.18; **High** – 8.82				

For the screening fractional factorial experimental design three continuous experimental design variables, each one with two levels, without repetitions, three center samples and two response variables were evaluated. A total of seven experiences were done. At the level of resolution of the screening experimental design performed (2^{3-1}) the main effects are confounded with the two interaction effects; For the optimization central composite experimental design two continuous experimental

design variables, each one with two cube levels, two star levels, without repetitions, three center samples and two response variables were evaluated. The optimization experimental design was done with eleven experiments. The responses variables evaluated for both experimental designs are the fluorescence intensity (I_{Flu}) and the frequency size distribution at 50 % (*D50%*).

1.1.1. Screening experimental design

In Table S2 are presented the results found by the COSCIND and Center tests. With the COSCIND test a statistically non-significant and with the Center test a statistically significant curvature checking for the main and two interactions effects were found with the two response variables. Although the main effects are not clearly distinguished the interactions of variables the more relevant from this evaluation is that the t_{mic} and m_{Glc} design variables seems to have an opposite effect in the two response variables to the found with the V_{water}. For the I_{Flu} the t_{mic} and m_{Glc} causes an increase with a positive curvature and the V_{water} causes a decrease with a negative curvature; For the *D50%* the t_{mic} and m_{Glc} causes a decrease with a negative curvature and the V_{water} causes an increase with a positive curvature.

Table S2 – Results obtained with the screening fractional factorial experimental design for the fluorescent intensity (I_{Flu}) for the Bare-CD synthesis.*

	COSCIND		Center	
Variable	**Effect**	**Psi-value (p)**	**Effect**	**F-value (p)**
$t_{mic} = m_{Glc} \times V_{water}$	1.535×10^{6}	---	$1.535\text{x}10^{6}$	18.715 (0.049)
$m_{Glc} = t_{mic} \times V_{water}$	-2.218×10^{6}	1.445 (0.771)	$5.245\text{x}10^{6}$	218.388 (0.004)
$V_{water} = t_{mic} \times m_{Glc}$	5.245×10^{6}	2.750 (0.338)	$-2.218\text{x}10^{6}$	39.055 (0.025)

* Psi-value – Psi value estimated by the Psi statistics; --- – Smallest effect removed.

In Tables S3 and S4 are presented the ANOVA results found. The estimated linear models for the I_{Flu} and *D50%* are respectively globally statistically significant and non-significant with highs $R_{Multiple}$ and with a significant lack of fit. These results could indicated that the models adequately fit the data but also could indicated that a quadratic model, instead a linear model, could better fit the data obtained and confirmed the previous results found by the Center test for the two response variables. Also the *b* coefficients found by ANOVA for the main and interactions effects confirm the previous tendency found with the two response variables for the experimental design

variables by the COSCIND test. The most relevant found by ANOVA is the statically significant increase of I_{Flu} (p = 0.014, b = 1.311×10^{6}) most probably by the increase m_{Glc}.

Table S3 – ANOVA of the fluorescent intensity (I_{Flu}) obtained by the fractional factorial experimental design for the Bare-CD synthesis.*

ANOVA ($R_{Multiple}$ = 0.958)						
Effect	**SS**	**d.f.**	**MS**	**F-ratio (p-value)**	**b**	**$(S.E.)_b$**
Model	3.478×10^{13}	3	1.159×10^{13}	11.093 (0.039)		
Error	3.136×10^{12}	3	1.045×10^{12}			
Adjusted total	3.792×10^{13}	6	6.320×10^{12}			
Factor						
Intercept	1.808×10^{14}	1	1.808×10^{14}	172.964(0.001)	5.082×10^{6}	3.864×10^{5}
$t_{mic} = m_{Glc} \times V_{water}$	2.357×10^{12}	1	2.357×10^{12}	2.255 (0.230)	1.279×10^{5}	8.520×10^{4}
$m_{Glc} = t_{mic} \times V_{water}$	2.751×10^{13}	1	2.751×10^{13}	26.316 (0.014)	1.311×10^{6}	2.556×10^{5}
$V_{water} = t_{mic} \times m_{Glc}$	4.919×10^{12}	1	4.919×10^{12}	4.706 (0.119)	-1.232×10^{5}	5.680×10^{4}
Lack of fit						
Lack of fit	2.884×10^{12}	1	2.884×10^{12}	22.896 (0.041)		
Pure error	2.519×10^{11}	2	1.260×10^{11}			
Total error	3.136×10^{12}	3	1.045×10^{12}			

* $R_{Multiple}$ – Multiple correlation, SS – sum of squares; d.f. – degrees of freedom; MS – mean squares; F-ratio – Fisher ratio; b – beta-regression coefficient; $(S.D.)_b$ – standard deviation of b; Main – main effects; Int. – interactions effects; Squ. – square effects; p-value - probability value (p) for a 5 % significance level.

Table S4 – ANOVA of the frequency particle size distribution at 50 % (*D50%*) obtained by the fractional factorial experimental design for the Bare-CD synthesis.*

ANOVA ($R_{Multiple}$ = 0.935)						
Effect	**SS**	**d.f.**	**MS**	**F-ratio (p-value)**	**b**	**$(S.E.)_b$**
Model	2.259×10^{9}	3	7.530×10^{8}	6.986 (0.072)		
Error	3.234×10^{8}	3	1.078×10^{8}			
Adjusted total	2.582×10^{9}	6	4.304×10^{8}			
Factor						
Intercept	4.324×10^{8}	1	4.324×10^{8}	4.012 (0.139)	7.860×10^{3}	3.924×10^{3}
$t_{mic} = m_{Glc} \times V_{water}$	7.520×10^{8}	1	7.520×10^{8}	6.977 (0.078)	-2.285×10^{3}	865.179
$m_{Glc} = t_{mic} \times V_{water}$	7.522×10^{8}	1	7.522×10^{8}	6.978 (0.078)	-6.856×10^{3}	2.596×10^{3}
$V_{water} = t_{mic} \times m_{Glc}$	7.549×10^{8}	1	7.549×10^{8}	7.003 (0.077)	1.526×10^{3}	576.786
Lack of fit						
Lack of fit	3.234×10^{8}	1	3.234×10^{8}	1.152×10^{7} (0.000)		
Pure error	56.134	2	28.067			
Total error	3.234×10^{8}	3	1.078×10^{8}			

* See footnote of Table S3.

1.1.2. Optimization experimental design

Attending to the found in the screening experimental design, and in order to obtain the higher fluorescence intensity with the smaller size of the Bare-CD, the V_{water} was fixed at 15 mL, the high level of the m_{Glc} was increased and the t_{mic} was evaluated in the same range of variation in the optimization central composite experimental design for the Bare-CD synthesis.

In Tables S5 and S6 are presented the ANOVA results found. Similar results were obtained for the two variables of response in the global evaluation of the quadratic model estimated by ANOVA. In the levels of the experimental design variables evaluated a global statistically non-significant model, a lower $R_{Multiple}$ and a statistically non-significant lack of fit were found with the two quadratic models. These results are according to the fact that the main effects, the variable interactions and the quadratic effects are statistically non-significant and that a non-significant variation it is found with the fit model even if the quadratic model adequately fit the data.

From the analysis of the *b* coefficients is possible to see that the two design variables have opposite effects in the two response variables. The m_{Glc} provokes a

decrease of the I_{Flu} and an increase of *D50%* and the t_{mic} causes an increase of the I_{Flu} and a decrease of the *D50%*. The more relevant found by ANOVA is a maximum for the response variable I_{Flu} predicted at m_{Glc} = 1.50 g and t_{mic} = 8.83 *min*. Also if we considered the average of the frequency size distribution as response variable instead the *D50%* (data don't shown) a minimum it's found at m_{Glc} = 5.23 g and t_{mic} = 7.88 min.

Table S5 – ANOVA of the I_{Flu} obtained by the optimization central composite experimental design for the Bare-CD synthesis.*

ANOVA ($R_{Múltiplo}$ = 0.646)						
Effect	**SS**	**d.f.**	**MS**	**F-ratio (p-value)**	**b**	**$(S.E.)_b$**
Model	2.353×10^{13}	5	4.705×10^{12}	0.715 (0.639)		
Error	3.290×10^{13}	5	6.580×10^{12}			
Adjusted total	5.643×10^{13}	10	5.643×10^{12}			
Factor						
Intercept	7.752×10^{13}	1	7.752×10^{13}	11.780 (0.019)	5.083×10^{6}	1.481×10^{6}
m_{Glc}	1.371×10^{13}	1	1.371×10^{13}	2.084 (0.553)	-6.556×10^{5}	4.541×10^{5}
t_{mic}	7.957×10^{12}	1	7.957×10^{12}	1.209 (0.322)	2.497×10^{5}	4.541×10^{5}
$t_{mic}\times m_{Glc}$	8.476×10^{11}	1	8.476×10^{11}	0.129 (0.734)	3.672×10^{5}	8.645×10^{5}
$t_{mic}\times t_{mic}$	4.944×10^{11}	1	4.944×10^{11}	7.513×10^{-2} (0.795)	-2.370×10^{5}	4.541×10^{5}
$m_{Glc}\times m_{Glc}$	7.930×10^{11}	1	7.930×10^{11}	0.121 (0.743)	-3.001×10^{5}	1.522×10^{5}
Model check						
main	2.167×10^{13}	2	1.084×10^{13}			
Int.	8.476×10^{11}	1	8.476×10^{11}	0.129 (0.734)		
Int. + Squ.	1.008×10^{12}	2	5.041×10^{11}	7.660×10^{-2} (0.927)		
Squ.	1.008×10^{12}	2	5.041×10^{11}	7.660×10^{-2} (0.927)		
Error	3.290×10^{13}	5	6.580×10^{12}			
Lack of fit						
Lack of fit	2.811×10^{13}	3	9.370×10^{12}	3.911 (0.210)		
Pure error	4.791×10^{12}	2	2.396×10^{12}			
Total error	3.290×10^{13}	5	6.580×10^{12}			

* See footnote of Table S3.

Table S6 – ANOVA of the D50% obtained by the optimization central composite experimental design for the Bare-CD synthesis.*

ANOVA ($R_{Multiplo}$ = 0.451)						
Effect	**SS**	**d.f.**	**MS**	**F-ratio (p-value)**	**b**	**(S.E.)$_b$**
Model	8.339×10^3	5	1.668×10^3	0.255 (0.920)		
Error	3.271×10^4	5	6.542×10^3			
Adjusted total	4.105×10^4	10	4.105×10^3			
Factor						
Intercept	1.017×10^4	1	1.017×10^4	1.554 (0.268)	58.218	46.698
m_{Glc}	4.754×10^3	1	4.754×10^3	0.727 (0.433)	12.207	14.320
t_{mic}	1.604×10^3	1	1.604×10^3	0.245 (0.641)	-3.546	7.160
$t_{mic}\times m_{Glc}$	43.340	1	43.340	6.625×10^{-3} (0.938)	2.626	32.258
$m_{Glc}\times m_{Glc}$	34.420	1	34.420	5.261×10^{-3} (0.945)	1.977	27.258
$t_{mic}\times t_{mic}$	1.887×10^3	1	1.887×10^3	0.288 (0.614)	14.638	27.258
Model check						
main	6.359×10^3	2	3.179×10^3			
Int.	43.336	1	43.336	6.624×10^{-3} (0.938)		
Int. + Squ.	1.937×10^3	2	968.559	0.148 (0.866)		
Squ.	1.937×10^3	2	968.559	0.148 (0.866)		
Error	3.271×10^4	5	6.542×10^3			
Lack of fit						
Lack of fit	2.795×10^4	3	9.315×10^3	3.909 (0.210)		
Pure error	4.766×10^3	2	2.383×10^3			
Total error	3.271×10^4	5	6.542×10^3			

* See footnote of Table S3.

Fig. S1 (a) and (b) respectively shows the response surface obtained for the response variables I_{Flu} and *D50%* with the optimization central composite experimental design in the Bare-CD synthesis optimization. It is possible to see that a region of maximum for the I_{Flu} and a region of minimum for the *D50%* are clearly defined. For the I_{Flu} a large region of great stability at maximum I_{Flu} it is found from 3.18 to 6.94 g of m_{Glc} in the entire range of t_{mic} at the lowest mass of glucose and for the *D50%* a region of minimum from 3.18 to 4.80 g of m_{Glc} and in a t_{mic} from 5.5 to 14 min.

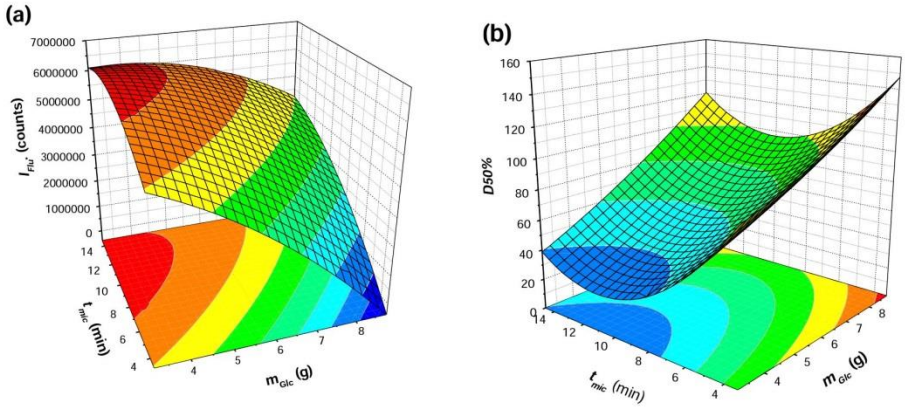


Fig. S1 - Response surface of I_{Flu} (a) and of *D50%* (b) obtained with the optimization central composite experimental design for Bare-CD synthesis.

Attending to the found a compromise must be made between the obtained through the evaluation of the main effects by ANOVA and the obtained by surface response analysis. So a m_{Glc} of 5 g and a t_{mic} of 9 min. allows to obtain Bare-CD nanoparticles with a high fluorescence intensity and small sizes.

1.2. Trp-CD synthesis

The design variables and the levels evaluated for the Trp-CD synthesis optimization are presented in Table S7. Considering the obtained in the Bare-CD synthesis optimization the V_{water} was fixed at 15 mL and a maximum of m_{Glc} of 5 g and a central value of t_{mic} of 9 min. were initially considered. The range of m_{Trp} was defined from a minimum value of 100 mg to a limit of 300 mg taking in consideration the evaluated limit of solubility of 300 mg in the fixed V_{water} of 15 mL.

Table S7 – Levels of design variables under investigation in the experimental designs used for the optimization of the Trp-CD synthesis conditions.

Design variables	Abbreviation	Cube Levels		Central level
		low	high	
Screening full factorial experimental design				
Microwave time (min)	t_{mic}	5	13	9
Mass of glucose (g)	m_{Glc}	1	5	3
Mass of tryptophan (mg)	m_{Trp}	100	300	200
Optimization central composite experimental design				
Microwave time (min)	t_{mic}	5	13	9
Star levels – Low – 3.36; **High** – 14.64				
Mass of glucose (g)	m_{Glc}	2	8	5
Star levels – Low – 0.77; **High** – 9.23				

For the screening full factorial experimental design three continuous experimental design variables, each one with two levels, without repetitions, three center samples and the response variable I_{Flu} were evaluated. A total of thirteen experiences were done; For the optimization central composite experimental design two continuous experimental design variables, each one with two cube levels, two star levels, without repetitions, three center samples and the I_{Flu} and *D50%* response variables were evaluated. The optimization experimental design was done with eleven experiments.

1.2.1. Screening experimental design

In Table S8 are presented the results found by the HOIE and Center tests. A statistically non-significant main and two interactions effects by the HOIE and a statistically non-significant curvature checking for the main and two interactions effects by the Center test were found with all the experimental design variables in the levels of the experimental designs evaluated. Even so it is possible to verify that an increase of the I_{Flu} is favoured by a decrease of m_{Glc} and t_{mic} and an increase of m_{Trp} and that a possible minimum for m_{Glc} and t_{mic} and a possible maximum for m_{Trp} could be found attending respectively to the negative and positive curvature checked by the Center test.

Table S8 – Results obtained with the screening full factorial experimental design for the I_{Flu} for the Trp-CD synthesis.

	HOIE		Center	
Variable	**Effect**	**F-value(p)**	**Effect**	**F-value(p)**
m_{Glc}	-42.497	0.272 (0.629)	-42.497	0.487 (0.524)
m_{Trp}	101.112	1.541 (0.282)	101.112	2.758 (0.172)
t_{mic}	-55.569	0.465 (0.533)	-55.569	0.833 (0.413)

In Table S9 are presented the results obtained by ANOVA.

Table S9 – ANOVA of the I_{Flu} obtained by the full factorial experimental design for the Trp-CD synthesis from glucose and tryptophan.*

ANOVA ($R_{Multiple}$ = 0.809)						
Effect	**SS**	**d.f.**	**MS**	**F-ratio (p-value)**	**b**	**(S.E.)$_b$**
Model	7.526×10^4	6	1.254×10^4	1.888 (0.229)		
Error	3.985×10^4	6	6.542×10^3			
Adjusted total	1.151×10^5	12	9.593×10^3			
Factor						
Intercept	3.382×10^5	1	3.382×10^5	50.920 (0.0004)	161.300	22.604
m_{Glc}	3.612×10^3	1	3.612×10^3	0.544 (0.489)	-10.624	14.407
m_{Trp}	2.045×10^4	1	2.045×10^4	3.078 (0.130)	0.506	0.288
t_{mic}	6.176×10^3	1	6.176×10^3	0.930 (0.372)	-6.946	7.204
$m_{Glc}\times m_{Trp}$	13.023	1	13.023	1.961×10^{-3} (0.966)	0.851	19.210
$m_{Glc}\times t_{mic}$	2.186×10^4	1	2.186×10^4	3.291 (0.120)	-34.848	19.210
$m_{Trp}\times t_{mic}$	2.315×10^4	1	2.315×10^4	3.485 (0.111)	-35.863	19.210
Model check						
Main	3.023×10^4	3	1.008×10^4			
Int.	4.502×10^4	3	1.501×10^4	2.259 (0.182)		
Int. + Squ.	0.000	0	0.000	0.000 (0.000)		
Squ.	0.000	0	0.000	0.000 (0.000)		
Error	3.985×10^4	6	6.642×10^3			
Lack of fit						
Lack of fit	1.020×10^4	2	5.099×10^3	0.688 (0.554)		
Pure error	2.966×10^4	4	7.414×10^3			
Total error	3.985×10^4	6	6.642×10^3			

* See footnote of Table S3.

The ANOVA estimated quadratic model for the I_{Flu} it's globally statistically significant with a high $R_{Multiple}$ and with a statistically non-significant lack of fit which indicated that the model adequately fit the data. The evaluated main effects b coefficients found by ANOVA confirm the previous tendency found by the HOIE test. From the analysis of the response surfaces (data don't shown) it is possible to see that the maximum of I_{Flu} is always found at m_{Trp} from 250 to 300 mg, m_{Glc} from 1 to 5 g and t_{mic} from and 5 to 9 min. or even until 13 min. at a lowest m_{Glc}.

1.2.2. Optimization experimental design

Attending to the found with the full factorial experimental design, and in order to obtain a higher fluorescence intensity with the smaller Trp-CD, the m_{Trp} was fixed at 300 mg, the m_{Glc} was evaluated in a largest range and the t_{mic} was evaluated in the same range of variation.

In Tables S10 and S11 are presented the obtained ANOVA results. Slightly different results were obtained for the two variables of response in the global evaluation of the quadratic model estimated by ANOVA. For I_{Flu} and *D50%* were respectively found a global statistically significant and non-significant model, a high and a lowest $R_{Multiple}$ and a statistically non-significant and significant lack of fit. The statistically non-significant main effects, interactions and quadratic effects for *D50%* and the statistically significant of the two main effects for I_{Flu} explain the results found in the global evaluation of the estimated models.

By ANOVA it´s possible to see that an increase of the experimental design variables provokes a decrease in both response variables. For the I_{Flu} a statistically significant decrease for both experimental design variables (t_{mic}, p = 0.0005; m_{Glc}, p = 0.008) confirm the previous tendency found by the screening full factorial experimental design. Attending to the increase of the high level of m_{Glc} and slightly higher value of the star level of t these results clearly shows that a lowest m_{Glc} and t_{mic} are more favourable in order to a higher I_{Flu}. For the *D50%* both experimental design variables induces a statistically non-significant decrease. All the interactions effects for both response variables are statistically non-significant.

Table S10 – ANOVA of the I_{Flu} obtained by the central composite experimental design for the Trp-CD synthesis from glucose and tryptophan.*

ANOVA ($R_{Multiple}$ = 0.973)						
Effect	**SS**	**d.f.**	**MS**	***F*-ratio (*p*-value)**	**b**	**(S.E.)$_b$**
Model	7.266×10^4	5	1.453×10^4	17.481 (0.003)		
Error	4.157×10^3	5	831.353			
Adjusted total	7.682×10^4	10	7.682×10^3			
Factor						
Intercept	8.537×10^4	1	8.537×10^4	102.694 (0.0002)	168.694	16.647
m_{Glc}	1.486×10^4	1	1.486×10^4	17.874 (0.008)	-14.387	3.403
t_{mic}	5.386×10^4	1	5.386×10^4	64.785 (0.0005)	-20.543	2.552
$m_{Glc}\times t_{mic}$	1.233	1	1.233	1.484×10^{-3} (0.971)	0.443	9.717
$m_{Glc}\times m_{Glc}$	1.671×10^3	1	1.671×10^3	2.010 (0.215)	-13.774	9.717
$t_{mic}\times t_{mic}$	1.137×10^3	1	1.137×10^3	1.367 (0.295)	11.362	19.210
Model check						
Main	6.872×10^4	2	3.436×10^4			
Int.	1.234	1	1.234	1.484×10^{-3} (0.971)		
Int. + Squ.	3.945×10^3	2	1.973×10^3	2.373 (0.189)		
Squ.	3.945×10^3	2	1.973×10^3	2.373 (0.189)		
Error	4.157×10^3	5	831.353			
Lack of fit						
Lack of fit	2.792×10^3	3	930.797	1.364 (0.449)		
Pure error	1.364×10^3	2	682.186			
Total error	4.157×10^3	5	831.353			

* See footnote of Table S3.

Table S11 – ANOVA of the D50% obtained by the optimization central composite experimental design for the Trp-CD synthesis from glucose and tryptophan.*

ANOVA ($R_{Multiple}$ = 0.766)						
Effect	**SS**	**d.f.**	**MS**	**F-ratio (p-value)**	**b**	**$(S.E.)_b$**
Model	1.681×10^{9}	5	3.363×10^{8}	1.421 (0.355)		
Error	1.183×10^{9}	5	2.366×10^{8}			
Adjusted total	2.865×10^{9}	10	2.865×10^{8}			
Factor						
Intercept	2.060×10^{5}	1	2.060×10^{5}	8.704×10^{-4} (0.978)	262.024	16.647
m_{Glc}	7.866×10^{8}	1	7.866×10^{8}	3.324 (0.128)	-3.310×10^{3}	3.403
t_{mic}	1.898×10^{4}	1	1.898×10^{4}	8.021×10^{-5} (0.993)	-12.196	2.552
$m_{Glc}\times t_{mic}$	1.609×10^{3}	1	1.609×10^{3}	6.799×10^{6} (0.998)	15.997	9.717
$m_{Glc}\times m_{Glc}$	6.238×10^{8}	1	6.238×10^{8}	2.636 (0.165)	-8.417×10^{3}	9.717
$t_{mic}\times t_{mic}$	7.179×10^{7}	1	7.179×10^{7}	0.303 (0.605)	-2.855×10^{3}	19.210
Model check						
Main	7.866×10^{8}	2	3.933×10^{8}			
Int.	1.920×10^{3}	1	1.920×10^{3}	8.113×10^{-6} (0.998)		
Int. + Squ.	8.948×10^{8}	2	4.474×10^{8}	1.891 (0.245)		
Squ.	8.948×10^{8}	2	4.474×10^{8}	1.891 (0.245		
Error	1.183×10^{9}	5	2.366×10^{8}			
Lack of fit						
Lack of fit	1.183×10^{9}	3	3.944×10^{8}	1.119×10^{6} (0.000)		
Pure error	705.104	2	352.552			
Total error	1.183×10^{9}	5	2.366×10^{8}			

* See footnote of Table S3.

Fig. S2 (a) and (b) respectively shows the response surface obtained for the response variable I_{Flu} and *D50%* with the optimization central composite experimental design in the Trp-CD synthesis optimization.

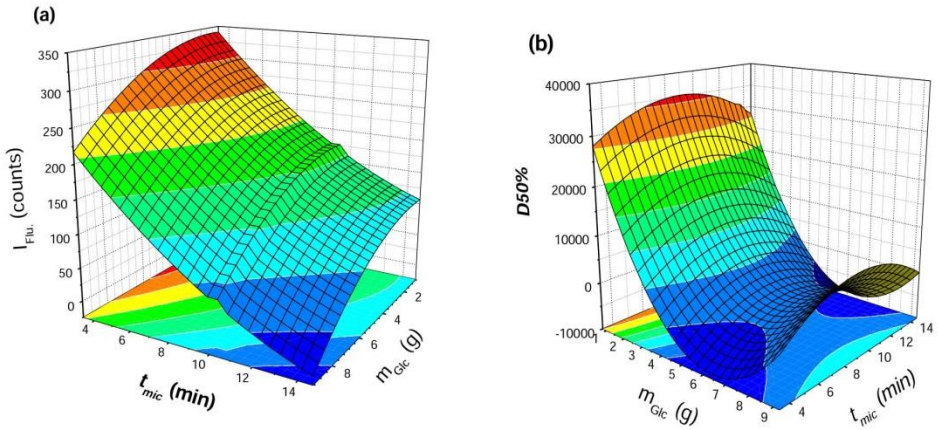


Fig. S2 - Response surface of I_{Flu} (a) and of *D50%* (b) obtained with the optimization central composite experimental design for Trp-CD synthesis.

It´s possible to define for I_{Flu} a region of maximum at lowest t_{mic} and m_{Glc}, at a t_{mic} up to 6 or 8 min and lower m_{Glc} up to 6 g or even for a t_{mic} = 5 min in almost all the range of m_{Glc}; For *D50%* a region of minimum with a saddle shape defined at a m_{Glc} from 4 to 9 g in all the t_{mic}. For m_{Glc} the results by surface response analysis are apparently contradictory in what respect an higher I_{Flu} and lower *D50%* between them and with the found by ANOVA main effect analysis for *D50%*. Even so it's important to stress that even for the *D50%* a lower m_{Glc} of 3 g is a small value of this response variable. A compromise must also be made in order to obtain a higher fluorescent intensity with a smaller size.

1.2.3. Univariate optimization

Considering the principal objective of the Trp-CD synthesis optimization, the possibility of the $ONOO^-$ sensing with a greater sensitivity, a last univariate optimization was done evaluating the quantum yield (Φ) and the *D50%* in conditions that allows a greater I_{Flu}. So the m_{Glc} was changed from 1 to 3 g and were fixed the m_{Trp} at 300 mg and the t_{mic} at 5 min.. In Table S12 and Fig. S3 are presented the results found by this univariate optimization. The synthetized Trp-CD from a m_{Glc} of 2.5g showed an already high Φ with a small particle size. A similar evaluation done with Trp-CD synthetized with a m_{Glc} of glucose 2.5g and t_{mic} 9 min that shows a Φ of 10.0 % and a *D50%* of 311 %.

Table S12 - Evaluated Φ and *D50%* obtained by Trp-CD synthesis varying the m_{Glc}.

Synthesis conditions (m_{Trp} - 300 mg/ t_{mic} - 5 min)		**Φ (%)**	***D50%***
m_{Glc} (g)	1	12.5	47721
	1.5	12.6	35018
	2	10.8	146
	2.5	12.4	153
	3	9.1	171

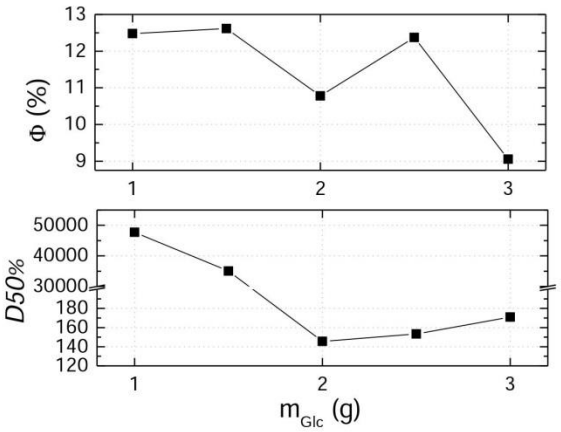


Fig. S3 – Variation of the evaluated Φ and *D50%* obtained by Trp-CD synthesis from different m_{Glc}.

From the overall analysis of the results obtained it is possible to conclude that the optimum conditions of Trp-CD synthesis are: m_{Glc} - 2,5g, m_{Trp} – 300 mg; V_{water} – 15 mL and t_{mic} – 5 min. with a microwave irradiation at maximum power (700 W).

2. Trp-CD characterization

2.1 Fluorescence

In Fig. S4 are presented the excitation-emission matrices (EEM) of tryptophan and of the Bare-CD obtained after simple tryptophan addition. It is possible to observe that only by addition of tryptophan, and beside the band of the tryptophan, no alteration was found relatively to the found EEM obtained with the Bare-CD [Fig. 1 (a)].

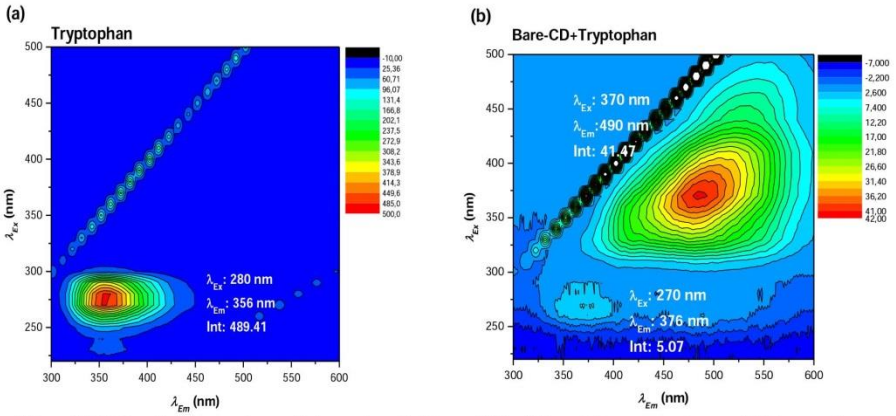


Fig. S4 - EEM of tryptophan (a) and of Bare-CD (b) with posterior addition of tryptophan.

In Fig. S5 are presented the absorption, excitation and emission spectra of the Bare and Trp-CD. A similar absorbance and emission spectra and a different excitation spectrum were found for the Trp-CD.

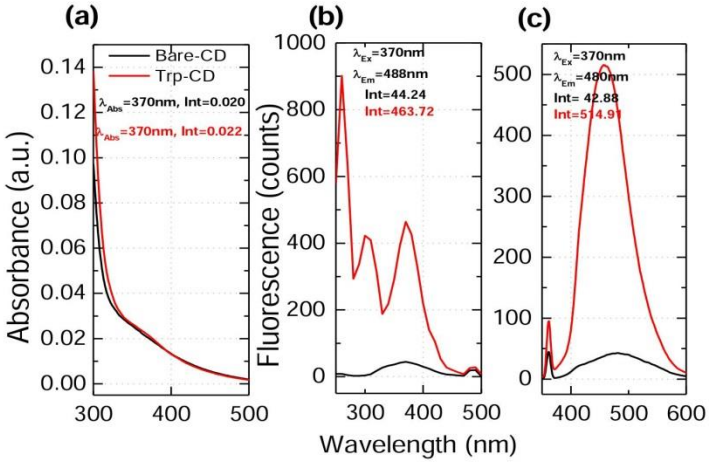


Fig. S5 –Absorbance (a) excitation (b) and emission (c) spectra of Bare and Trp-CD.

In Fig. S6 are presented the emission spectra and the variation of the Φ obtained for Trp-CD and Bare-CD by variation of the m_{Glc} and remaining constants the other synthesis conditions. The Trp-CD synthesis was done in the same optimized conditions of the Bare-CD synthesis (m_{Glc} - 5 g, t_{mic} - 9 min.) with 100, 200 and 300 mg of tryptophan. The Φ of the synthetized CD with m_{Trp} of 300 mg shows a 10 × and a 2 × increase compared to the found respectively by the Bare-CD and Trp-CD with m_{Trp} of 100 mg.

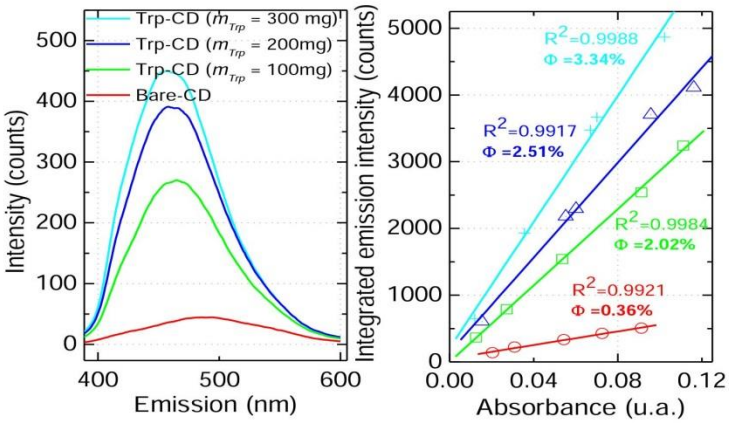


Fig. S6 - Spectra emission and Φ of Bare-Cd and of Trp-CD synthetized from different m_{Trp}, with 5 g of m_{Glc} and t_{mic} of 9 min..

In Table S14 is showed a three component for Bare-CD and a five component decay time model for Trp-CD. In Fig. S12 are also presented typical lifetime decay profiles found for Bare and Trp-CD.

Table S13 - Lifetime intensity decays of Bare-CD and Trp-CD.

CD	N	τ_i (ns)	s	B_i	χ^2
Bare-CD	1	2.77	8.18×10^{-11}	2.46×10^{-2}	1.58
	2	0.53	1.28×10^{-11}	7.63×10^{-2}	
	3	6.80	2.14×10^{-10}	4.16×10^{-2}	
Trp-CD	1	0.94	9.39×10^{-10}	12.55	1.36
	2	0.89	3.01×10^{-11}	-13.38	
	3	0.03	8.96×10^{-8}	4.61×10^{-3}	
	4	21.54	9.37×10^{-11}	0.48	
	5	5.67	1.04×10^{-11}	0.28	

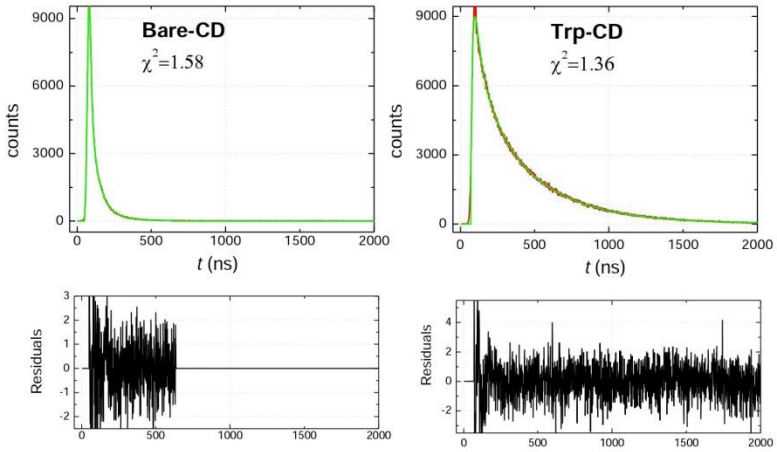


Fig. S7 – Lifetime decay profiles of Bare-CD (a) and Trp-CD (b).

2.2 Effect of pH, temperature and ionic strength

In Fig. S8, S9 and S10 are presented respectively the influence of pH, temperature and ionic strength variables in the fluorescence intensity of the Bare and Trp-CD at excitation and emission wavelengths of maximum fluorescence intensity in the optimized synthesis conditions.

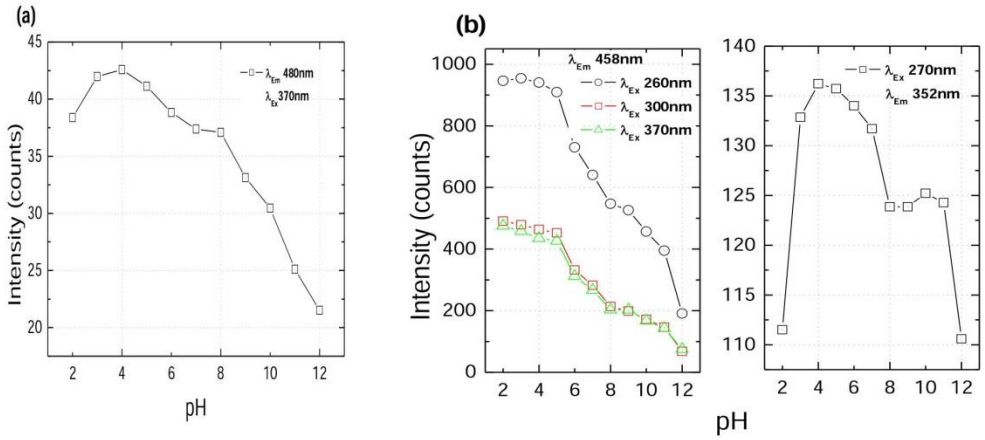


Fig. S8 – Influence of the pH on the maximum fluorescence intensity of Bare (a) and Trp-CDs (b).

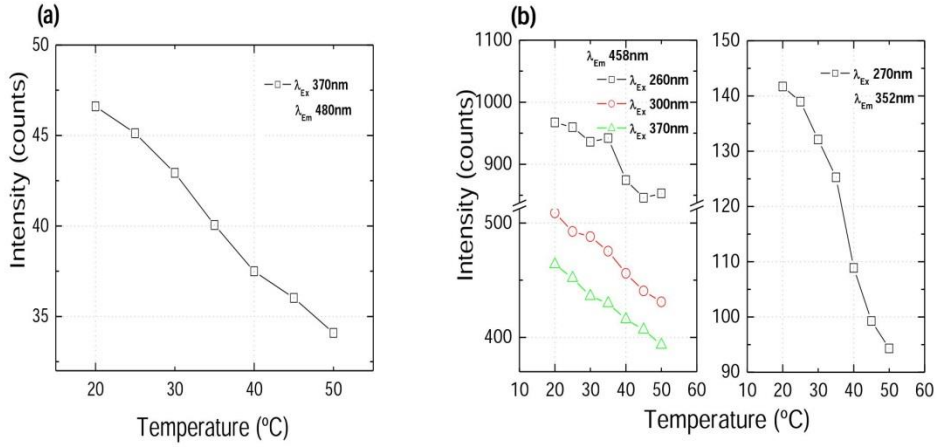


Fig. S9 - Effect of temperature on the maximum fluorescence intensity of Bare (a) and Trp-CD (b).

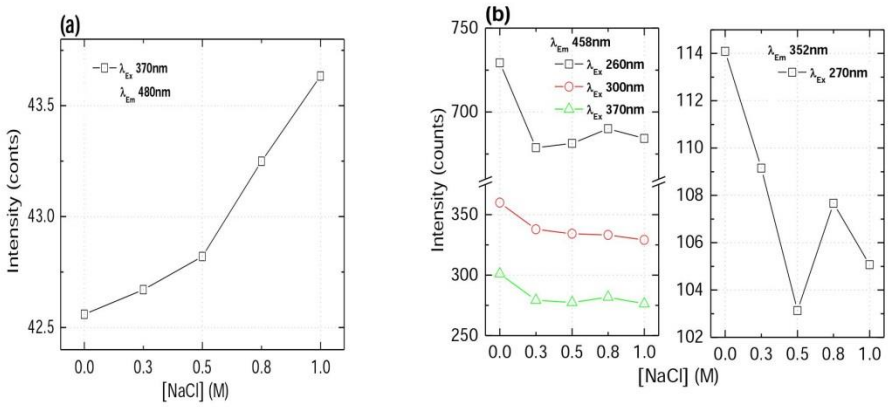


Fig. S10 - Effect of ion strength on the maximum fluorescence intensity of Bare (a) and Trp-CD (b) by addition of NaCl at concentrations from 0.3 to 1 M.

2.3 Photostability

In Fig. S11 is presented the evaluation done for Bare and Trp-CD in the optimized synthesis conditions at excitation wavelength of 370 nm and emission wavelengths of maximum fluorescence intensity respectively for Bare-CD of 486 nm and for Trp-CD of 457 nm. The photostability was evaluated during 1 hour and continuous monitoring the fluorescence intensity. With both CD a non significant decrease in the fluorescence intensity of both CD it's observed.

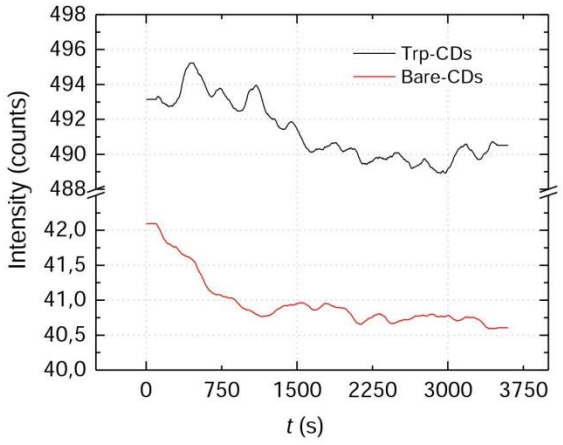


Fig. S11 – Photostability of Bare and Trp-CD with time at a wavelength of 370 nm.

2.4 Surface XPS analysis

In Fig. S12 the XPS the survey spectra and in Fig. S13, S14 and S15 respectively the C1s, N1s and O1s core level spectra of Bare (a) and Trp-CD (b) are presented.

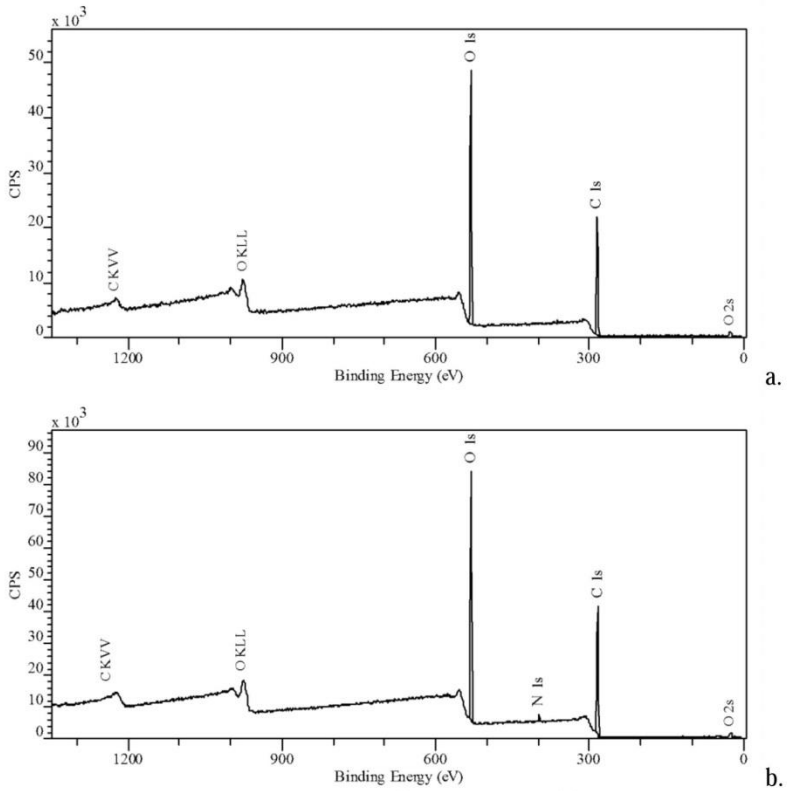


Fig. S12 – XPS survey spectra of Bare (a) and Trp-CD (b).

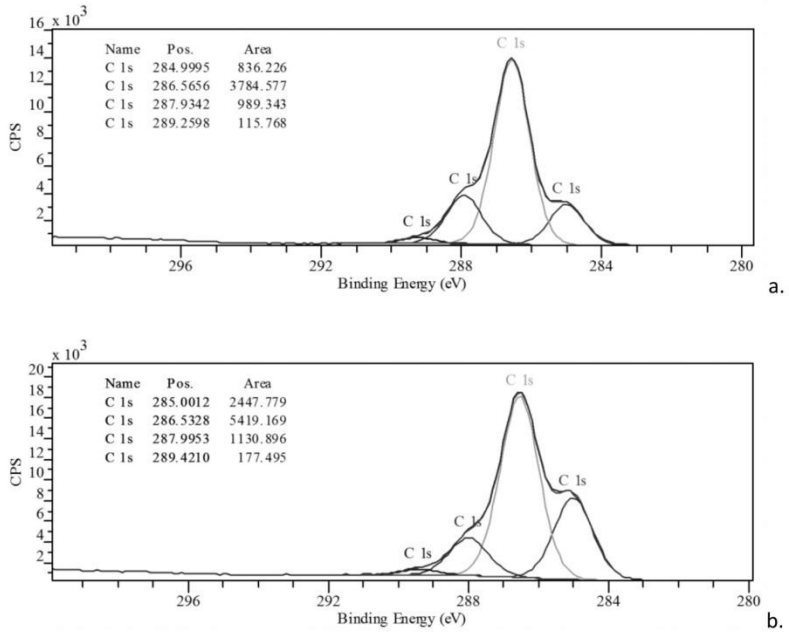


Fig. S13 - C1s core level spectra of Bare (a) and (b) Trp-CD samples.

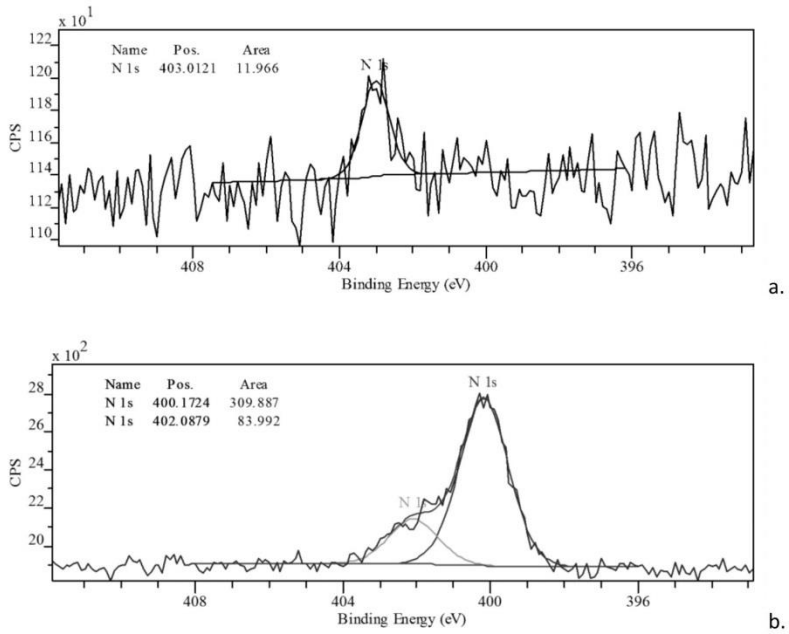


Fig. S14 – N1s core level spectra of Bare (a) and (b) Trp-CD samples.

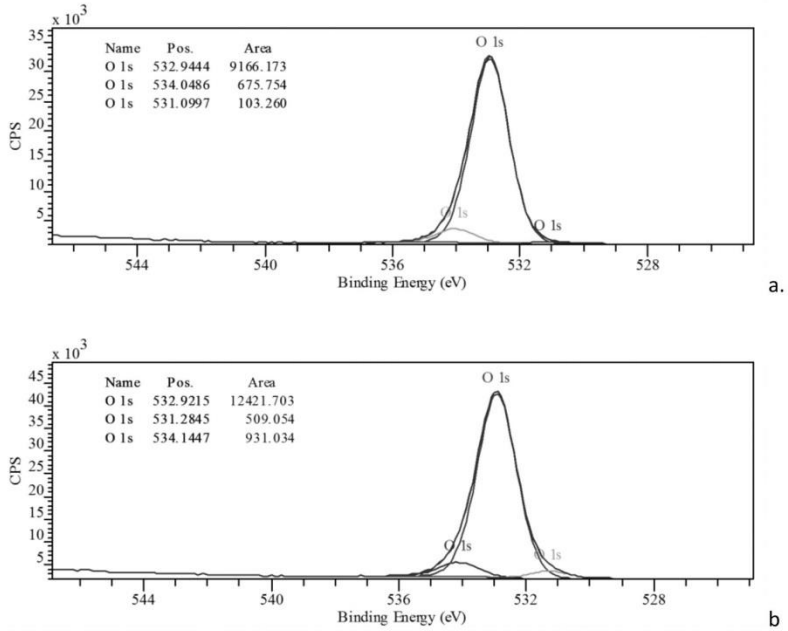


Fig. S15 – - O1s core level spectra of Bare (a) and (b) Trp-CD samples.

2.5 Particle size and shape analysis

In Table S14 and Fig. S16 presented the frequency particle size distribution for Bare-CD and Trp-CD obtained by DLS analysis.

Table S14 – Frequency particle size distribution of Bare and Trp-CD found by DLS.

	Particle size distribution (%)		
	10%	**50%**	**90%**
Bare-CD	5	8	167
Trp-CD	110	153	256

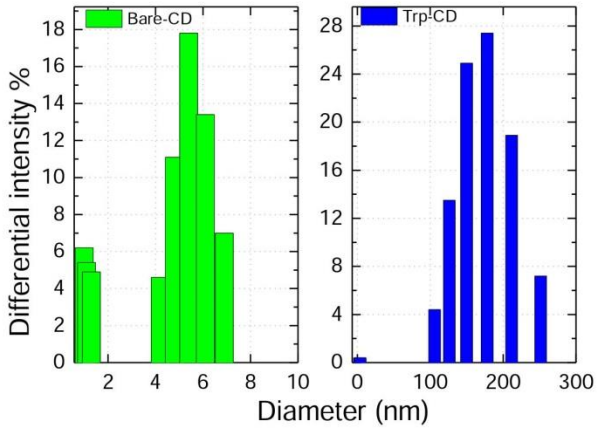


Fig. S16 – Frequency size distribution at 70% of Bare-CD and Trp-CD found by DLS.

3. Trp-CD sensing

3.1. $ONOO^-$ quantification

In Table S15 are presented the initial and final pH evaluated after $ONOO^-$ addition. The variation of the pH to basic by $ONOO^-$ addition is observed with water for $ONOO^-$ 5 μM and with buffer solution pH 7.4 for $ONOO^-$ 50 μM.

Table S15 – pH variation by addition of $ONOO^-$ standard solution in water and in a buffer solution pH 7.4.

	[$ONOO^-$] (μM)	pH	
		Initial	Final
Water	5	3.95	10.27
	10	3.99	10.66
	25	4.00	11.33
	50	4.02	11.67
	100	4.05	12.10
Phosphate buffer (pH 7.4)	5	7.07	7.13
	10	7.08	7.15
	25	7.08	7.28
	50	7.08	7.53
	100	7.08	9.15

In Fig. S17 are presented the linear fit found with at room temperature at the $ONOO^-$ range 0.5 - 25 and 0.5 - 50 μM.

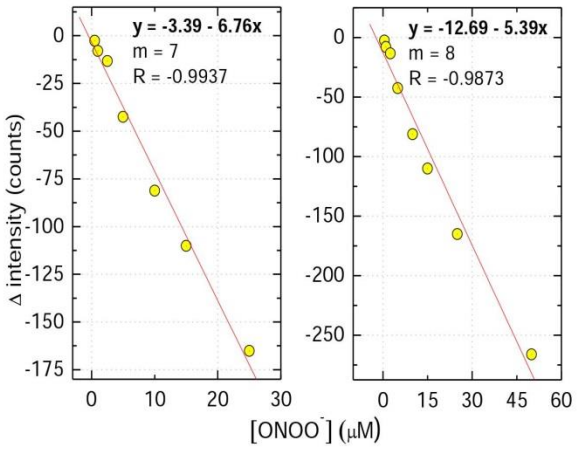


Fig. S17 – Linearity response of the Trp-CD by $ONOO^-$ addition at room temperature.

Equation S1 is the modified Stern-Volmer equation in order to calculate the fraction of the accessible tryptophan (f_a) to the iodide quenching. In Table S16 are presented the calculated f_a and the Stern-Volmer quenching constant (K_{SV}) of the accessible tryptophan to iodide.

Equation S1

$$\frac{F_0}{\Delta F} = \frac{1}{([Q] f_a K_{SV})} + \frac{1}{f_a}$$

Table S16 – Calculated accessible tryptophan fraction (f_a) and Stern-Volmer quenching constant (K_{SV}) of the accessible tryptophan to iodide at the different Trp-CD bands.

$\lambda_{Ex}/\lambda_{Em}$ (nm)	f_a	K_{SV} (M^{-1})
270/360	0.73	52.01
260/457	1.00	269.46
300/457	1.04	185.60
370/457	1.03	159.15

Chapter 9

Peroxynitrite and nitric oxide fluorescence sensing by ethylenediamine doped carbon dots

Eliana F. C. Simões, Joaquim C.G. Esteves da Silva, João M.M. Leitão
Sens. Actuator B-Chem. (2015) 220:1043–1049
doi:10.1016/j.snb.2015.06.072

CDs were prepared from different precursors and functionalized with different compounds. Besides Glc, was used as precursor citric acid (CA) in the CDs synthesis. In order to functionalize the CDs with amine groups, to the CDs synthesis from CA and Glc were added some amines such as ethylenediamine (EDA) and the 4, 7.10-Trioxo-1.13-tridecanediamina (TTDDA). For these CDs the QY obtained were for CDs prepared from 1 g Glc, 500 µL of TTDDA and 5 min microwave time of 1.53%, for CDs prepared from 1 g Glc, 500 µL of EDA and 5 min microwave time of 1.28%, CDs prepared from 1 g CA and of 500 µL TTDDA, 5 min microwave of 4.21% and CDs prepared from 1 g CA and EDA 500 µL, 5 min microwave time presented QY of 33.44%.

CDs prepared with 1 g of CA and 500µL EDA, 5 min in the microwave besides presented a high QY of 33.44% also showed sensibility towards NO and $ONOO^-$ by comparison with other ROS/RNS (H_2O_2, KO_2, NO and $ONOO^-$). Followed the study of detection of these two species at different pH values (4, 5, 6, 7 and 10) was made to evaluate the greater selectivity for each of these reactive species (NO and $OONO^-$). It was found that for NO was observed a higher quenching of fluorescence to pH 4, 6 and 7 values and that for $ONOO^-$ this fluorescence quenching was found at pH 6, 7 and 10 values. Observing the obtained results it was decided to study the response of the CDs at pH4 for NO and pH 7 and 10 for $ONOO^-$. Then the optimization of CDs synthesis conditions was made using experimental design methodologies, aiming the synthesis of CDs with high fluorescence intensity and also a greater fluorescence quenching

obtained by reaction with NO and $OONO^-$. Selective detection of NO and $ONOO^-$ at different pH values was performed using CDs synthesized under optimized conditions:

• m_{CA}= 2.5 g, V_{EDA} = 1000 µL, $t_{microwave}$ = 5 min, QY = 42%; NO detection at pH 4, sensibility - b = −2.1, linear range - 2.5 - 100 µM and r = 0.99.

• m_{CA} = 0.25 g, , V_{EDA} = 500 µL, $t_{microwave}$ = 5 min, QY = 40%; $ONOO^-$ detection at pH 10 and pH 7, sensibility - b = −41.6, linear range - 2.5 - 100 µM and r = 0.99.

The quantification was performed for each species using the CDs optimized synthesis conditions for NO at pH 4 and for $ONOO^-$ at pH 7 and 10 in standard solutions and in fortified serum samples.

These results were published in Sensors and Actuators B.

My personal contribution to this work includes the establishment of an initial objective and the bibliographic research of the state of the art related with the determination ROS/RNS applying these kinds of CDs, the protocols set up, the experimental execution and posterior data treatment. The microwave pyrolysis method used in the synthesis of the last CDs was also adopted for these CDs synthesis. Other precursors were tested for the CDs synthesis. In this study were added to the CDs synthesis different amines and was verified that the CDs synthetized with EDA provide CDs with higher QY and sensibility to ROS/RNS. The research, the microwave synthesis of the CDs testing different precursors, the characterization of the CDs and the study of the CDs behavior in presence of the different ROS/RNS was made with my contribution. The experiments were repeated several times in order to establish if the results were reproducible.

After the experimental part concluded the writing of the paper were made together with Professor João M. M. Leitão under the supervision of Professor Joaquim C.G. Esteves da Silva.

Sensors and Actuators B 220 (2015) 1043–1049

Contents lists available at ScienceDirect

Sensors and Actuators B: Chemical

journal homepage: www.elsevier.com/locate/snb

Peroxynitrite and nitric oxide fluorescence sensing by ethylenediamine doped carbon dots

Eliana F.C. Simões[a,b], Joaquim C.G. Esteves da Silva[b], João M.M. Leitão[a,*]

[a] CIQ-UP, Grupo de Ciências Biológicas e Bioanalíticas, Faculdade de Farmácia da Universidade de Coimbra, Pólo das Ciências da Saúde, 3000-548 Coimbra, Portugal
[b] CIQ-UP, Departamento de Química, Faculdade de Ciências da Universidade do Porto, R. Campo Alegre 687, 4169-007 Porto, Portugal

ARTICLE INFO

Article history:
Received 19 January 2015
Received in revised form 12 June 2015
Accepted 17 June 2015
Available online 24 June 2015

Keywords:
Carbon dots
Peroxynitrite
Nitric oxide
Sensing
Fluorescence quenching

ABSTRACT

The selective fluorescence sensing of nitric oxide (NO) and peroxynitrite anion ($ONOO^-$) in the presence of the principal reactive oxygen and nitrogen species (ROS/RNS) was achieved by fluorescence quenching through the pH variation of microwave synthesized fluorescent carbon dots (CDs) prepared from citric acid (CA) and ethylenediamine (EDA). The highest NO and $ONOO^-$ sensitivity, with the lowest sensitivity to the principal ROS/RNS, was demonstrated respectively at pH 4 and 10. The optimum synthesis and sensing conditions of CDs were obtained by multivariate full factorial experimental design methodologies: for NO, at pH 4, 2.5 g of CA and 1000 μL of EDA diluted in 15 mL of water exposed for 5 min to a microwave radiation of 700 W; for $ONOO^-$, at pH 7, 10–0.25 g of CA and 500 μL of EDA diluted in 15 mL of water exposed for 5 min to a microwave radiation of 700 W. In these optimized conditions the synthesized CDs have a quantum yield about 40%. The quantification of NO at pH 4 and of $ONOO^-$ at pH 7 and 10 were done in standard and in fortified serum solutions. Also the quantification of NO and of $ONOO^-$ in standard solutions was performed in the presence respectively of $ONOO^-$ and NO.

© 2015 Elsevier B.V. All rights reserved.

1. Introduction

Carbon dots (CDs) are luminescent carbon nanoparticles usually with dimensions less than 10 nm suspending in water or in other solvents. They have attractive analytical properties such as water solubility, high quantum yield fluorescence, high biocompatibility and good photostability [1–5]. CDs are a nontoxic and biocompatible alternative to the classic semiconductors quantum dots (QDs) nanoparticles that could be synthesized by different synthesis methodologies using different carbon precursors [6].

Microwave assisted synthesis is an efficient, rapid, simple and green methodology now frequently used for CDs synthesis. Since the first microwave CDs synthesis from glucose and poly(ethylene glycol) (PEG-200) [7], several other precursors had been used: glucose/poly(acrylatesodium) [8], carbohydrates/inorganic salts [9], glycerol/phosphate [9], glycerol/4,7,10-trioxa-1,13-tridecanediamine [10], citric acid (CA)/1,2-ethylenediamine (EDA) [11], CA/amines [12], phytic acid/EDA [13], poloxamer [14], triammonium citrate/soluble phosphate [15], chitosan [16] and dopamine [17]. Depending on the synthesis conditions and for the precursors used, CDs with different dimensions and quantum yields can be obtained [7–17]. CDs microwave synthesized from CA and EDA were used for bioimaging [12] and iodide detection [11] with a reported quantum yield (Φ) respectively of 30.2 and 43.8%.

Reactive oxygen (ROS) and nitrogen (RNS) species are usually implicated in several physiological and pathological processes acting as a signalling molecule, but they also could induce cell damage [18,19]. Two of the more important ROS/RNS are the nitric oxide (NO) and the peroxynitrite anion ($ONOO^-$). Due to their role, the analytical methodologies for their detection and/or quantification, based in different analytical methodologies, are of great relevance [20,21]. Fluorescent detection of $ONOO^-$ by nanoparticles was done by quenching methods based in thiol-capped CdTe or CdTe/ZnS quantum dots (QD) [22] and in tryptophan doped CDs [23]. Fluorescent detection of NO by nanoparticles was also done by some quenching methods based in carboxymethyl chitosan CdTe [24], in chitosan CdSe [25,26], in polymethacrylate CdSe/ZnS [27] and in triethanolamine CdSe QDs [28], by a turn on method based in iron(III) dithiocarbamates CdSe/ZnS QDs [29] and by a fluorescence resonance energy transfer (FRET) ratiometric method based in phenylenediamine-containing naphthalimide functionalized CDs synthesized from CA and EDA [30].

Due to the reported high quantum yield of the CDs synthesized from CA and EDA, these precursors were chosen in order to assess

* Corresponding author. Tel.: +351 239 488 465.
E-mail address: jleitao@ff.uc.pt (J.M.M. Leitão).

http://dx.doi.org/10.1016/j.snb.2015.06.072
0925-4005/© 2015 Elsevier B.V. All rights reserved.

the NO and $ONOO^-$ fluorescence sensing capability of the corresponding CDs. In this paper we present the optimization of the microwave synthesis of CDs from CA and EDA in order to the $ONOO^-$ and NO selective fluorescence sensing with the higher sensitivity at different pH values. This synthesis was optimized by multivariate full factorial experimental design methodologies. The synthesized CDs show a relatively high quantum yield. The sensibility to the NO and $ONOO^-$ at different pH were verified and their quantification ability was evaluated in standard solutions and in fortified serum samples.

2. Experimental

2.1. Reagents

Citric acid (CA), 1,2-ethylenediamine (EDA), hydrogen peroxide (H_2O_2), potassium superoxide (KO_2), sodium nitrite ($NaNO_2$), sodium nitrate ($NaNO_3$), ethylenediamine tetraacetic acid (EDTA) and potassium hydrogen phthalate analytical grade reagents were purchased from Sigma–Aldridch. Sodium hydroxide (NaOH), hydrogen chloride (HCl), sodium phosphate dibasic (Na_2HPO_4), monosodium phosphate (NaH_2PO_4), sodium carbonate (Na_2CO_3), sodium hydrogen carbonate ($NaHCO_3$) and ferrous sulphate ($FeSO_4$) analytical grade reagents were purchased from Merck, Darmstadt (Germany). Mili-Q water with resistivity of 18.2 MΩ cm at 25 °C was used in all experiments.

2.2. Solutions

The $ONOO^-$ standard solutions were prepared in a refrigerated beaker under constant stirring by mixing 100 mL of $NaNO_2$ 600 mM, 100 mL of H_2O_2 600 mM in HCl 0.6 M and 100 mL of NaOH 3.6 M. The solution will turn yellow indicating the formation of $ONOO^-$. The agitation is maintained until no O_2 is formed. Saturated standard NO solutions (1.9 mM) were prepared by bubbling NO gas in deoxygenated water (after bubbling argon for 15 min). The superoxide ($O_2^{\bullet -}$) standard solutions were prepared by rigorous weighing of KO_2, the H_2O_2 standard solutions by rigorous measurement of the required volume in deoxygenated water. Diluted standard solutions were prepared by rigorous dilution of the initial standard solutions for $ONOO^-$ in NaOH 0.1 M and for NO, $O_2^{\bullet -}$ and H_2O_2 in deoxygenated water. The hydroxyl radical ($HO^{\cdot}$) was generated in situ by the Fenton reaction by addition of a 5-fold excess of H_2O_2 to the EDTA–Fe(II) complex formed with different concentrations of $FeSO_4$.

The experiments were performed at different pH values. Phthalate buffer, phosphate buffer and carbonate buffer were respectively used for the experiments at pH 4, 7 and 10. Phosphate buffer was prepared through rigorous weighting of NaH_2PO_4 and Na_2HPO_4, phthalate buffer pH 4 was prepared through rigorous weighting of potassium hydrogen phthalate and carbonate buffer pH 10 was prepared through rigorous weighting of Na_2CO_3 and $NaHCO_3$ for the required volume of solution. With the three buffer solutions posterior addition of NaOH or HCl 0.1 M were added in order to adjust the pH. Also in order to the evaluation of the pH effect in the fluorescence intensity of the CDs the pH was adjusted with NaOH or HCl 0.1 M.

2.3. CDs synthesis

In order to establish the optimum conditions of CDs synthesis for the NO and $ONOO^-$ fluorescence sensing and attending to the performed experimental designs different masses of CA and volumes of EDA were diluted in 15 mL of water and posterior heated in a domestic microwave at the maximum power of 700 W at different heating times. Subsequently the solutions were leaving to cool and were dissolved in water. The obtained solutions were then centrifuged at 9000 rpm for 10 min in order to remove the suspended impurities and a volume of 30 mL were set with water.

2.3.1. Multivariate experimental design methodologies

Full factorial experimental design methodologies were used in order to establish the more adequate conditions to the CDs synthesis [31–33]. The full factorial experimental designs used were implemented with the Unscrambler® software version 7.51, Camo ASA, Norway.

In the performed full factorial experimental designs the significance of the main effects and the variable interactions were initially evaluated using Higher Orders Interactions Effects (HOIE) as comparison. As centre samples are used a curvature checking of the response is done by the evaluation of the significance of the curvature trough a curvature test of the main effects and the variable interactions designated as 'Center' test. The assessment of the significance was also done by the analysis of variance (ANOVA) through *F*-ratio and respective *p* value. The value of multiple linear regression coefficients ($R_{Multiple}$) of the response variables was also analysed.

2.4. Instrumentation

2.4.1. Spectrophotometric measurements

The absorbance and fluorescence spectra were acquired in a standard 1 cm fluorescence quartz cell and collected respectively in a Jasco V-530 UV-Visible spectrophotometer and in a Jasco FP-6200 spectrofluorimeter. The absorption spectra were obtained in a wavelength range from 250 to 650 nm with a 2 nm interval, slit widths 2 nm and wavelength scan rate medium; the fluorescence spectra were obtained in a wavelength range from 300 to 600 nm with a 1 nm interval, slit widths 5 nm, sensitivity response medium, response time fast and wavelength scan rate 1000 nm/min. Excitation emission matrices (EEM) were obtained in a wavelength range from 350 to 600 nm for emission and a range of 220–450 for excitation with a 1 nm interval; slit widths 5 nm, sensitivity response medium.

Fluorescence measurements were also made using a QE65000 charge-coupled detector (CCD), a 380 nm light emitting diode (LED), a sampling compartment (CUV-ALL-UV 4-way) and two 1.0 mm core diameter fibre optics (P1000-2-UV–VIS) from Ocean Optics. One of the fibres guides the light from the source to the sampling compartment and the other guide the emitted light to the detector. The reaction time profiles were obtained collecting the signal at the maximum emission wavelength of 496 nm every 10 s with an integration time of 300 ms.

The quantum yield (Φ) of the CD was evaluated comparing the integrated photoluminescence intensities and the absorbance values of the CD with the ones of the quinine sulphate reference.

$$\Phi = \Phi_R \times \frac{Grade}{Grade_R} \times \frac{\eta^2}{\eta_R^2}$$

In the equation Φ is the fluorescence quantum yield, *Grade* is the gradient from the plot of integrated fluorescence intensity vs. absorbance and η is the refractive index. The subscript *R* refers to reference fluorophore, quinine sulphate of known Φ. The literature Φ of the quinine sulphate is $\Phi = 0.54$ [34]. The η of the quinine sulphate in 0.1 M H_2SO_4 and of CD aqueous solutions used were $\eta = 1.33$.

Fourier transform infrared (FTIR) spectra were obtained by a Perkin Elmer FTIR Spectrum 400 in solid state with an attenuated total reflectance (ATR) accessory in a range of 4000–650 cm^{-1} with 16 accumulations and a resolution of 4 cm^{-1}.

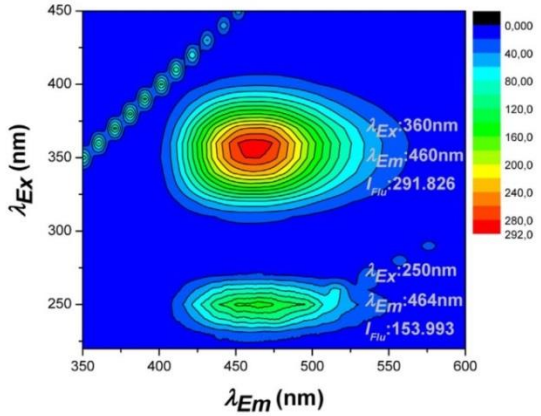


Fig. 1. Typical EEM of the synthetized CDs (m_{CA} = 1 g, V_{EDA} = 500 μL, t_{mic} = 5′).

2.4.2. Particle size measurements

The particle size and their frequency size distribution of the synthesized CDs in the optimum synthesis conditions was obtained by dynamic light scattering (DLS) in a Zetasizer Nano ZS, Malvern. The shape and size of these CDs were also evaluated by transmission electronic microscopy (TEM) analysis in a Fei Company Tecnai G2 20 S-Twin electronic microscopic.

3. Results and discussion

3.1. Preliminary assessment

Preliminary evaluations of the sensor were done with CDs obtained from a mass of CA (m_{CA}) of 1 g, a volume of EDA (V_{EDA}) of 500 μL diluted in 15 mL of water and exposed to a microwave radiation of 700 W during a microwave time (t_{mic}) of 5 min. The EEM of the CDs is shown in Fig. 1. The analysis of this EEM shows a main band with an excitation wavelength of 360 nm and a secondary one with an excitation wavelength of 250 nm and both with an emission wavelength of 460 nm.

The detection of the principal ROS/RNS by these CDs was done at the main fluorescence band for the three levels of concentrations (10, 50 and 100 μM). The results obtained shows that the presence of H_2O_2 and $O_2^{\cdot-}$ do not provoke a significant variation in the fluorescence intensity at the three levels of concentration and only the NO and $ONOO^-$ provoke quenching of fluorescence. Higher quenching, and consequently sensitivity, is observed for $ONOO^-$ (supplementary information).

Attending to these preliminary results, the quenching effect of NO and $ONOO^-$ was assessed at different pHs at the three levels of concentrations in order to checked the possibility of the selective detection of the NO and $ONOO^-$. The results obtained at the pHs 4, 5, 6, 7 and 10 are presented in Fig. 2. This figure shows a greater quenching effect by the NO at pH of 4, 6 and 7 and by the $ONOO^-$ at pH 6, 7 and 10. A different response was observed at pH 4 with the selective quenching induced by the NO and, at pH 10, with the selective quenching induced by the $ONOO^-$. Considering these results, the selective sensing with a higher sensitivity of NO (pH 4) and of $ONOO^-$ (pH 10) could be expected. Also the selective fluorescence detection of $ONOO^-$ at pH 7 could be evaluated with different synthesis conditions attending to the higher quenching effect by this RNS in comparison with NO.

3.2. NO and $ONOO^-$ sensing

Taking into consideration the previous information, an experimental optimization design was done to improve the selectivity and sensibility of the CDs towards NO and $ONOO^-$ (supplementary information). The quenching induced by NO and $ONOO^-$ at the maximum fluorescence intensity were assessed at pH 4, 7 and 10. The results show that a different m_{CA} is needed for the selective sensing of NO at pH 4, and of $ONOO^-$ at pHs 7 and 10: a higher m_{CA} for the sensing of NO and $ONOO^-$ respectively at pH 4 and 10; and, a lower m_{CA} for the sensing $ONOO^-$ at pH 7.

A deeper assessment of the quenching effect by the NO and $ONOO^-$ at the three pHs with different synthesis conditions (supplementary information) allowed to established rigorously the more adequate synthesis conditions in order to achieve higher quenching of NO at pH 4 and of $ONOO^-$ at pH 7 and 10. At the chosen optimum conditions (Table 1), the obtained CDs respond linearly to the concentration of NO and $ONOO^-$. Fig. 3 shows typical CDs fluorescence quenching profiles.

The analysis of Table 1 shows that the greater sensitivity is observed for $ONOO^-$ at pH 10 and the lowest sensitivity for NO at pH 4.

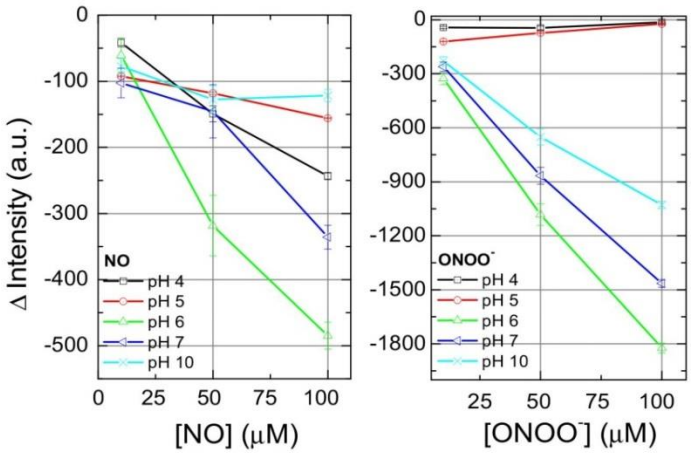


Fig. 2. Effect of the NO and $ONOO^-$ in the fluorescence of the synthetized CDs at a pH from 4 to 10 (m_{CA} = 1 g, V_{EDA} = 500 μL, t_{mic} = 5′).

Table 1
Evaluation of the NO and $ONOO^-$ fluorescence sensing capability of synthetized CDs with different synthesis conditions.*.

Synthesis conditions/Φ	NO		$ONOO^-$	
	pH 4	pH 7	pH 7	pH 10
m_{CA} = 0.25 g;	$a = -54.6 \pm 8.7$	–	$a = -315.4 \pm 116.5$	$a = -295.9 \pm 112.4$
V_{EDA} = 500 μL;	$b = -2.1 \pm 0.2$		$b = -29.3 \pm 2.5$	$b = -41.6 \pm 2.4$
t_{mic} = 5′/Φ = 39.7%	r = 0.9904		r = 0.9860	r = 0.9935
	5.0–100.0 μM		2.5–100.0 μM	2.5–100.0 μM
	m = 5		m = 6	m = 6
m_{CA} = 1 g;	$a = -66.6 \pm 8.9$	$a = -111.5 \pm 18.6$	$a = -289.9 \pm 104.0$	$a = -291.2 \pm 89.2$
V_{EDA} = 500 μL;	$b = -1.2 \pm 0.1$	$b = -4.2 \pm 0.7$	$b = -23.7 \pm 2.0$	$b = -33.3 \pm 1.9$
t_{mic} = 5′/Φ = 38.0%	r = 0.9988	r = 0.9891	r = 0.9881	r = 0.9936
	2.5–200.0 μM	2.5–50.0 μM	2.5–100.0 μM	2.5–100.0 μM
	m = 6	m = 5	m = 5	m = 6
m_{CA} = 2.5 g;	$a = -81.4 \pm 7.9$	$a = -108.1 \pm 29.2$	$a = -168.3 \pm 75.8$	$a = -266.5 \pm 77.2$
V_{EDA} = 1000 μL;	$b = -2.1 \pm 0.2$	$b = -3.5 \pm 0.2$	$b = -25.6 \pm 1.6$	$b = -33.7 \pm 1.6$
t_{mic} = 5′/Φ = 41.6%	r = 0.9923	r = 0.9934	r = 0.9921	r = 0.9953
	2.5–100.0 μM	2.5–200.0 μM	2.5–100.0 μM	2.5–100.0 μM
	m = 5	m = 6	m = 6	m = 6
m_{CA} = 2.5 g;	$a = -86.7 \pm 5.6$	$a = -73.3 \pm 3.2$	$a = -200.9 \pm 109.3$	$a = -218.6 \pm 54.8$
V_{EDA} = 1000 μL;	$b = -1.5 \pm 0.1$	$b = -3.9 \pm 0.1$	$b = -22.3 \pm 2.1$	$b = -29.8 \pm 1.2$
t_{mic} = 10′/Φ = 33.5%	r = 0.9981	r = 0.9996	r = 0.9867	r = 0.9970
	2.5–200.0 μM	2.5–100.0 μM	2.5–100.0 μM	2.5–100 μM
	m = 5	m = 5	m = 6	m = 5

* – linear fit not possible; Φ – quantum yield; a – intercept, b – slope; the ± term in a and b is the standard deviation respectively of the intercept and the slope; r – linear correlation coefficient; m – number of calibration points.

(i) For the selective detection of NO at pH 4, and considering the sensitivity obtained ($b = -2.1$), linear range (2.5–100 μM), greater Φ (42%) and the already high r (0.99), the selected synthesis conditions for the evaluation of the quantification capability of NO at pH 4 were m_{CA} = 2.5 g, V_{EDA} = 1000 μL, t_{mic} = 5′.
(ii) For the selective detection of $ONOO^-$ at pH 10, and considering the greater sensitivity obtained ($b = -41.6$), an already great linear range (2.5–100 μM), the already high r (0.99) associated to a great Φ (40%), the selected synthesis conditions for the evaluation of the quantification capability of $ONOO^-$ at pH 10 were m_{CA} = 0.25 g, V_{EDA} = 500 μL, t_{mic} = 5′. Also at pH 7 it is possible the selective fluorescence detection of the $ONOO^-$ with synthesized CDs with m_{CA} = 0.25 g, V_{EDA} = 500 μL, t_{mic} = 5′.

The fluorescence quenching effect of NO, $ONOO^-$, H_2O_2, $O_2^{\cdot-}$, $HO^{\cdot}$, NO_2^- and NO_3^- in the synthesized CDs at the selected conditions for the sensing of NO at pH 4 and of $ONOO^-$ at pH 7 and 10 was assessed (Fig. 4). The selective response in the presence of the H_2O_2 and $O_2^{\cdot-}$ was confirmed. Except for the $HO^{\cdot}$, in the sensing of NO at pH 4, where a similar response was found for the NO and the $HO^{\cdot}$, all the others results confirm the good selective response of NO at pH 4 and of $ONOO^-$ at pH 7 and 10. In comparison to the other evaluations at pH 7 and for the $HO^{\cdot}$ at this pH, also a slightly higher response, similar to the obtained for the $HO^{\bullet}$ at pH 4, was observed. For the $ONOO^-$ at pH 7, and when compared with the response of $HO^{\cdot}$, a response approximately 4× higher was obtained. The observed behaviour of $HO^{\cdot}$ is due to the greatest oxidant power of the $HO^{\cdot}$ However, it is important to stress, in what concern to the significance the possible interference of $HO^{\cdot}$, the rather low half-live of $HO^{\cdot}$ (10^{-9} s) when compared to the other ROS/RNS namely the NO (1–10 s) and $ONOO^-$ (0.05–1 s) [19]. The effect of the pH in the fluorescence intensity of the main band of CDs has no significant variation (supplementary information).

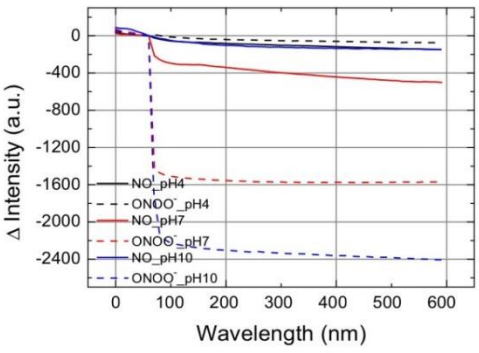


Fig. 3. Fluorescence profiles of CDs by addition of NO and $ONOO^-$ at pH 4, 7 and 10 (m_{CA} = 0.25 g, V_{EDA} = 500 μL, t_{mic} = 5′). (For interpretation of the references to color in this figure legend, the reader is referred to the web version of this article.)

3.3. CDs characterization

The characterization of the obtained CDs in the optimized conditions was performed. The size of the CDs in solution by DLS (supplementary information), their shape by TEM (Fig. 5) and the FTIR spectra of the CDs (Fig. 6) were obtained. DLS shows that the majority of the synthesized CDs nanoparticles have a size smaller than 10 nm. Taking into consideration the main DLS peak it was found an average size of 1.0 nm (m_{CA} = 0.25 g, V_{EDA} = 500 μL, t_{mic} = 5′) and of 4.8 nm (m_{CA} = 2.5 g, V_{EDA} = 500 μL, t_{mic} = 5′). The TEM images confirm the size found by DLS, mostly below 10 nm, and shows that a similar spherical or quasi-spherical shape was found for both synthesized CDs.

Quite different FTIR spectra were obtained for the two synthesized CDs in the optimized conditions which is due to the different CA and EDA content used in their synthesis. Beside a more complex spectrum for the synthesized CDs with a higher CA and EDA, namely at a wavenumbers lower than 1800 cm^{-1}, different wavenumbers were found for some of the principal common bands of the two spectra. The great difference was observed for the broad and strong band due to the —OH and —NH. For the CDs with a higher CA and EDA this band is shifted to a higher wavenumber. Small differences were found for the weak band of the —CH, the sharp band of —CN and one of the —NH bands. Attending to the resolution of the spectra no difference was fond for the second sharp band of —NH at 1546

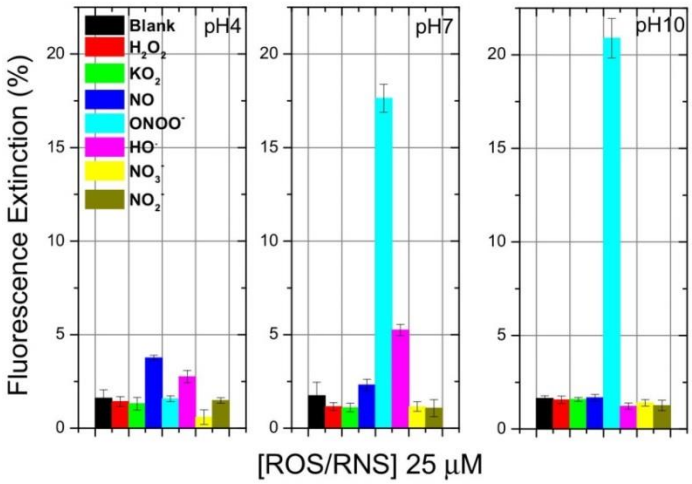


Fig. 4. Fluorescence quenching effect of NO, $ONOO^-$, H_2O_2, $O_2^{\cdot-}$, $HO^{\cdot}$, NO_2^- and NO_3^- 25 µM in the fluorescence of the synthetized CDs in the selected conditions at pH 4 (m_{CA} = 2.5 g, V_{EDA} = 1000 µL, t_{mic} = 5′) and at pH 7 and 10 (m_{CA} = 0.25 g, V_{EDA} = 500 µL, t_{mic} = 5′). (For interpretation of the references to color in this figure legend, the reader is referred to the web version of this article.)

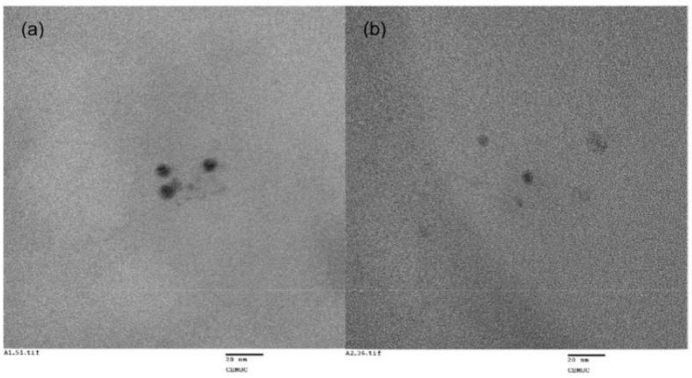


Fig. 5. TEM images of the synthetized CDs in the selected conditions. [(a) m_{CA} = 0.25 g, V_{EDA} = 500 µL, t_{mic} = 5′; (b) m_{CA} = 2.5 g, V_{EDA} = 1000 µL, t_{mic} = 5′].

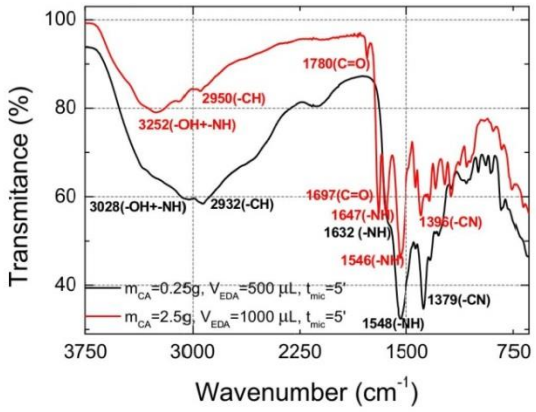


Fig. 6. FTIR spectra of the synthetized CDs in the selected conditions. (m_{CA} = 0.25 g, V_{EDA} = 500 µL, t_{mic} = 5′; m_{CA} = 2.5 g, V_{EDA} = 1000 µL, t_{mic} = 5′).

and 1548 cm^{-1}. For the CDs with lower CA and EDA a —NH band appears as a small shoulder of the other —NH band. New bands are also found for the CDs with a higher CA and EDA that could be assigned to the C=O of a carboxylic acid at 1780 cm^{-1} and of an amide at 1697 cm^{-1}. Also for this CDs, in the fingerprint region (1080–1360 cm^{-1}), a great number of bands are now clearly evident that could be mainly assigned to —CO and/or —CN with different bond energies.

3.4. NO and $ONOO^-$ quantification

The quantification capability was evaluated for the synthesized CDs in the selected conditions for NO at pH 4 and for $ONOO^-$ at pH 7 and 10. The calibration of NO (pH 4) and $ONOO^-$ (pH 7 and 10) was done with two determinations at each calibration point used. Also attending to the linear range found, the evaluation was done in standard solutions and in fortified serum samples at three levels of concentrations (10, 25 and 50 µM). Due to experimental limitations in the fortification by NO of the serum samples the quantification capability in fortified serum samples of NO was only done at the level of concentration of 10 µM. Beside this assessment, the

Table 2
Quantification of NO at pH 4 and of $ONOO^-$ at pH 7 and 10 in standard solutions and in fortified serum samples.*.

$[NO]$ (μM) pH 4	CDs (m_{CA} = 2.5 g, V_{EDA} = 1000 μL, t_{mic} = 5′)				
	Standard solutions				Fortified serum sample (100×)
Expected	10	25	50	25/[$ONOO^-$] = 25 μM	10
Estimated	8.5 ± 2.8	28.2 ± 2.7	46.2 ± 2.6	27.6 ± 2.7	9.7 ± 2.8
Recovery (%)	85.4	112.6	92.4	110.5	96.6
$y = bx + a$ [$\Delta I = f([NO])$]					
a = −47.5; s_a = 3.6					
b = −2.5; s_b = 0.1					
$s_{y/x}$ = 6.2; r = 0.9980					
m = 4; 10–100 μM, LOD = 4.6 μM					

$[ONOO^-]$ (μM) pH 7	CDs (m_{CA} = 0.25 g, V_{EDA} = 500 μL, t_{mic} = 5′)						
	Standard solutions				Fortified serum sample (100×)		
Expected	10	25	50	25/[NO] = 25 μM	10	25	50
Estimated	10.4 ± 5.8	28.9 ± 5.7	57.4 ± 5.8	27.9 ± 5.7	12.4 ± 5.8	31.0 ± 5.7	64.5 ± 5.8
Recovery (%)	104.5	115.8	114.7	111.5	123.9	123.9	128.9
$y = bx + a$ [$\Delta I = f([ONOO^-])$]							
a = −309.9; s_a = 79.2							
b = −31.1; s_b = 1.5							
$s_{y/x}$ = 168.9; r = 0.9904							
m = 5; 5–100 μM, LOD = 2.7 μM							

$[ONOO^-]$ (μM) pH 10	CDs (m_{CA} = 0.25 g, V_{EDA} = 500 μL, t_{mic} = 5′)						
	Standard solutions				Fortified serum sample (100×)		
Expected	10	25	50	25/[NO] = 25 μM	10	25	50
Estimated	8.7 ± 5.5	28.2 ± 5.3	57.5 ± 5.4	27.6 ± 5.3	8.7 ± 5.5	27.5 ± 5.3	54.6 ± 5.4
Recovery (%)	87.0	112.7	114.9	110.6	87.2	109.9	109.2
$y = bx + a$ [$\Delta I = f([ONOO^-])$]							
a = −272.4; s_a = 95.8							
b = −40.2; s_b = 1.9							
$s_{y/x}$ = 204.5; r = 0.9915							
m = 5; 5–100 μM, LOD = 2.0 μM							

*The ± term is the interpolated standard deviation (s_{xi}); a – intercept; s_a – intercept standard deviation; b – slope; s_b – slope standard deviation; $s_{y/x}$ – standard deviation of residuals; r – linear correlation coefficient; m – number of calibration points; LOD – limit of detection evaluated through the s of five determinations of a blank.

quantification capability of NO at pH 4 in the presence of $ONOO^-$ and of $ONOO^-$ at pH 7 and 10 in the presence of NO were done in standard solutions at a concentration of 25 μM. The results obtained are presented in Table 2.

A highest sensitivity with a generally higher error associated to the estimative of concentration was found for the quantification of $ONOO^-$ at pH 7 and 10. Associated to the high sensitivity in the $ONOO^-$ quantification a lowest limit of detection (LOD) was found for the $ONOO^-$ at pH 7 (2.7 μM) and 10 (2.0 μM) in comparison to the found for the NO at pH 4 (4.6 μM). The LOD found is generally higher than the obtained by other electrochemical sensors [20,21]. Nevertheless, and in comparison to the obtained by almost all of the already developed NO and $ONOO^-$ fluorescence nanoparticles optical sensors, a comparable LOD was observed [22–30]. Generally good quantifications results were found for the two RNS in the assays with the standard solutions and fortified serum samples. The lowest results were obtained for the NO at pH 4 and for the $ONOO^-$ at pH 10 at the level of concentration of 10 μM respectively with the standard solution and with the standard solution and fortified serum sample. The highest results were found for the quantification of $ONOO^-$ at pH 7 in fortified serum samples at the three levels of concentrations. Similar results to the obtained with a standard solution 25 μM were found in the quantification of NO and $ONOO^-$ 25 μM in the presence respectively of NO and $ONOO^-$ 25 μM.

4. Conclusions

The selective fluorescence sensing of NO at pH 4 and of $ONOO^-$ at pH 7 and 10 by ethylenediamine doped carbon dots microwave synthesized from citric acid was established. The selective fluorescence sensing was evaluated through the assessment of the quenching by the NO and $ONOO^-$ at different pHs of the fluorescence of ethylenediamine doped carbon dots, obtained with different synthesis conditions. A greater sensitivity was found for the determination of $ONOO^-$ at pH 7 and 10 and a lower sensitivity for the determination of NO at pH 4. Only for the selective fluorescence sensing NO at pH 4 a strong interference of $HO\cdot$ was observed although, taking into consideration the rather low lifetime of this radical, it should not constitute an interference problem. Generally good quantification results for NO at pH 4 and for $ONOO^-$ at pH 7 and 10 were obtained. Similar results were found for the quantification of NO at pH 4 and of $ONOO^-$ at pH 7 and 10 in the absence and in the presence respectively of $ONOO^-$ and NO. At the levels of concentrations evaluated generally good quantification results were found with the fortified serum samples.

Acknowledgments

A PhD grant SFRH/BD/81074/2011 to Eliana Simões from Fundação para a Ciência e Tecnologia (FCT, Lisbon) is acknowledged. The use of FTIR from UCQFarma, Pharmacy Faculty of the University of Coimbra and the TEM analyses from Nanomaterials and Micromanufacturing group of Centre for Mechanical Engineering of the University of Coimbra (CEMUC) are acknowledged.

Appendix A. Supplementary data

Supplementary data associated with this article can be found, in the online version, at http://dx.doi.org/10.1016/j.snb.2015.06.072

References

[1] J.C.G. Esteves da Silva, H.M.R. Gonçalves, Analytical and bioanalytical applications of carbon dots, Trends Anal. Chem. 30 (2011) 1327–1336.
[2] Y. Zhang, H. Goncalves, J.C.G. Esteves da Silva, C.D. Geddes, Metal-enhanced photoluminescence from carbon nanodots, Chem. Commun. 47 (2011) 5313–5315.
[3] H. Gonçalves, J.G. Esteves da Silva, Fluorescent carbon dots capped with PEG200 and mercaptosuccinic acid, J. Fluoresc. 20 (2010) 1023–1028.
[4] J.M.M. Leitão, H. Gonçalves, J.C.G.E. da Silva, Parallel factor analysis of EEM of the fluorescence of carbon dots nanoparticles, J. Chemom. 24 (2010) 655–664.
[5] M. Algarra, M. Perez-Martin, M. Cifuentes-Rueda, J. Jimenez-Jimenez, J.C.G. Esteves da Silva, T.J. Bandosz, et al., Carbon dots obtained using hydrothermal treatment of formaldehyde. Cell imaging in vitro, Nanoscale 6 (2014) 9071–9077.
[6] Y. Zhi, L. Zhaohui, X. Minghan, M. Yujie, Z. Jing, S. Yanjie, et al., Controllable synthesis of fluorescent carbon dots and their detection application as nanoprobes, Nano-Micro Lett. 5 (2013) 247–259.
[7] H. Zhu, X. Wang, Y. Li, Z. Wang, F. Yang, X. Yang, Microwave synthesis of fluorescent carbon nanoparticles with electrochemiluminescence properties, Chem. Commun. 34 (2009) 5118–5120.
[8] Q. Liu, S. Xu, C. Niu, M. Li, D. He, Z. Lu, et al., Distinguish cancer cells based on targeting turn-on fluorescence imaging by folate functionalized green emitting carbon dots, Biosens. Bioelectron. 64 (2015) 119–125.
[9] X. Wang, K. Qu, B. Xu, J. Ren, X. Qu, Microwave assisted one-step green synthesis of cell-permeable multicolor photoluminescent carbon dots without surface passivation reagents, J. Mater. Chem. 21 (2011) 2445–2450.
[10] C. Liu, P. Zhang, F. Tian, W. Li, F. Li, W. Liu, One-step synthesis of surface passivated carbon nanodots by microwave assisted pyrolysis for enhanced multicolor photoluminescence and bioimaging, J. Mater. Chem. 21 (2011) 13163–13167.
[11] F. Du, F. Zeng, Y. Ming, S. Wu, Carbon dots-based fluorescent probes for sensitive and selective detection of iodide, Microchim. Acta 180 (2013) 453–460.
[12] X. Zhai, P. Zhang, C. Liu, T. Bai, W. Li, L. Dai, et al., Highly luminescent carbon nanodots by microwave-assisted pyrolysis, Chem. Commun. 48 (2012) 7955–7957.
[13] W. Wang, Y. Li, L. Cheng, Z. Cao, W. Liu, Water-soluble and phosphorus-containing carbon dots with strong green fluorescence for cell labeling, J. Mater. Chem. B 2 (2014) 46–48.
[14] S. Mitra, S. Chandra, T. Kundu, R. Banerjee, P. Pramanik, A. Goswami, Rapid microwave synthesis of fluorescent hydrophobic carbon dots, RSC Adv. 2 (2012) 12129–12131.
[15] J. Hou, J. Yan, Q. Zhao, Y. Li, H. Ding, L. Ding, A novel one-pot route for large-scale preparation of highly photoluminescent carbon quantum dots powders, Nanoscale 5 (2013) 9558–9561.
[16] D. Xiao, D. Yuan, H. He, J. Lu, Microwave-assisted one-step green synthesis of amino-functionalized fluorescent carbon nitride dots from chitosan, Luminescence 28 (2013) 612–615.
[17] K. Qu, J. Wang, J. Ren, X. Qu, Carbon dots prepared by hydrothermal treatment of dopamine as an effective fluorescent sensing platform for the label-free detection of iron(III) ions and dopamine, Chemistry 19 (2013) 7243–7249.
[18] M. Valko, D. Leibfritz, J. Moncol, M.T. Cronin, M. Mazur, J. Telser, Free radicals and antioxidants in normal physiological functions and human disease, Int. J. Biochem. Cell Biol. 39 (2007) 44–84.
[19] L. Bergendi, L. Beneš, Z. Ďuračková, M. Ferenčik, Chemistry, physiology and pathology of free radicals, Life Sci. 65 (1999) 1865–1874.
[20] S.F. Peteu, R. Boukherroub, S. Szunerits, Nitro-oxidative species in vivo biosensing: challenges and advances with focus on peroxynitrite quantification, Biosens. Bioelectron. 58 (2014) 359–373.
[21] E.M. Hetrick, M.H. Schoenfisch, Analytical chemistry of nitric oxide, Annu. Rev. Anal. Chem. 2 (2009) 409–433.
[22] O. Adegoke, T. Nyokong, Probing the sensitive and selective luminescent detection of peroxynitrite using thiol-capped CdTe and CdTe@ZnS quantum dots, J. Lumin. 134 (2013) 448–455.
[23] E.F.C. Simões, J.C.G.E. da Silva, J.M.M. Leitão, Carbon dots from tryptophan doped glucose for peroxynitrite sensing, Anal. Chim. Acta 852 (2014) 174–180.
[24] L. Tan, A. Wan, H. Li, Q. Lu, Novel quantum dots–carboxymethyl chitosan nanocomposite nitric oxide donors capable of detecting release of nitric oxide in situ, Acta Biomater. 8 (2012) 3744–3753.
[25] L. Tan, A. Wan, H. Li, H. Zhang, Q. Lu, Biocompatible quantum dots–chitosan nanocomposites for fluorescence detection of nitric oxide, Mater. Chem. Phys. 134 (2012) 562–566.
[26] E.F. Simoes, J.M. Leitao, J.C. Esteves da Silva, NO fluorescence quantification by chitosan CdSe quantum dots nanocomposites, J. Fluoresc. 24 (2013) 639–648.
[27] V. Fabregat, M.A. Izquierdo, M.I. Burguete, F. Galindo, S.V. Luis, Quantum dot–polymethacrylate composites for the analysis of NO_x by fluorescence spectroscopy, Inorg. Chim. Acta 381 (2012) 212–217.
[28] X.Q. Yan, Z.B. Shang, Z. Zhang, Y. Wang, W.J. Jin, Fluorescence sensing of nitric oxide in aqueous solution by triethanolamine-modified CdSe quantum dots, Luminescence 24 (2009) 255–259.
[29] S. Wang, M.-Y. Han, D. Huang, Nitric oxide switches on the photoluminescence of molecularly engineered quantum dots, J. Am. Chem. Soc. 131 (2009) 11692–11694.
[30] C. Yu, Y. Wu, F. Zeng, S. Wu, A fluorescent ratiometric nanosensor for detecting NO in aqueous media and imaging exogenous and endogenous NO in live cells, J. Mater. Chem. B 1 (2013) 4152–4159.
[31] M.A. Bezerra, R.E. Santelli, E.P. Oliveira, L.S. Villar, L.A. Escaleira, Response surface methodology (RSM) as a tool for optimization in analytical chemistry, Talanta 76 (2008) 965–977.
[32] T. Lundstedt, E. Seifert, L. Abramo, B. Thelin, Å. Nyström, J. Pettersen, et al., Experimental design and optimization, Chemometr. Intell. Lab. 42 (1998) 3–40.
[33] J.M. Leitao, J.C. Esteves da Silva, Factorial analysis optimization of a Diltiazem kinetic spectrophotometric quantification method, Anal. Chim. Acta 609 (2008) 1–12.
[34] J.R. Lakowicz, Principles of Fluorescence Spectroscopy, Springer, New York, 2006, pp. 54–55.

Biographies

Eliana F.C. Simões finished her B.Sc. in Food Chemistry and Biochemistry and M.Sc. in Analytical Chemistry in the Chemistry Department of the University of Aveiro, Portugal. The master's degree research work was based in the development of a fibre optical sensor for monitoring frying oils degraded by frying procedures. Currently she is a PhD student in the third year of her doctoral programme at the Faculty of Sciences of the University of Porto, Portugal (FCUP). The focus of her research programme is the development of optical fluorescent nanoparticles sensors for the quantification of ROS/RNS namely the NO, $ONOO^-$, H_2O_2 and $O_2^{\bullet-}$.

Joaquim C.G. Esteves da Silva obtained his B.Sc., M.Sc. and Ph.D. in chemistry from the Faculty of Sciences of the University of Porto (FCUP), Portugal, where he worked on chemometric methodologies to environmental inorganic systems. Currently, he is an associate professor in the chemistry and biochemistry department of the FCUP where he teaches inorganic, environment, forensic, bioanalytical and chemometric courses. Current main research interests are the development of fluorescent nanomaterials and experimental and theoretical studies of chemiluminescent and bioluminescent systems. Also is focusing his R&D efforts on the development of biomedical, environmental and industrial innovative products.

João M.M. Leitão obtained his B.Sc. in Pharmaceutical Sciences and is Ph.D. in Pharmaceutical Chemistry at the Faculty of Pharmacy of the University of Coimbra, Portugal (FFUC). His M.Sc. in Chemical Quality Control was obtained at the Faculty of Sciences of the University of Coimbra, Portugal. His research work in order to obtain the M.Sc. and the Ph.D. was based in the development of analytical methodologies for the quantification of selected analytes respectively in environmental and pharmaceutical samples. A great focus is done in the analytical validation and in the development of the analytical methodologies with the appeal of chemometric multivariate experimental design and calibration methodologies. Currently is an assistant professor in the FFUC where he teaches Analytical Instrumental Methods of Analyses at the Integrated Master in Pharmaceutical Sciences and Bioanalytical Sciences courses. His current research work focus on the development of luminescent optical sensors namely based in fluorescent nanoparticles with the appeal of chemometric methodologies.

Peroxynitrite and nitric oxide fluorescence sensing by ethylenediamine doped carbon dots

Eliana F. C. Simões[a], João M.M. Leitão[a] and Joaquim C.G. Esteves da Silva [b,*]

[a] CIQ-UP, Grupo de Ciências Biológicas e Bioanalíticas, Faculdade de Farmácia da Universidade de Coimbra, Pólo das Ciências da Saúde, 3000-548 Coimbra, Portugal

[b] CIQ-UP, Departamento de Química, Faculdade de Ciências da Universidade do Porto, R. Campo Alegre 687, 4169-007 Porto, Portugal

Supplementary information

1. CD synthesis optimization

1.1 Full factorial experimental design

The CDs synthesis optimization through the microwave treatment of aqueous solutions of CA and EDA was done by full factorial experimental design methodologies in order to define the best conditions for the fluorescence sensing of NO and $ONOO^-$ at pH 4, 7 and 10. In Table S1 are presented the design variables and the levels evaluated in the CDs synthesis optimization by full factorial experimental designs.

Table S1 – Levels of design variables under investigation in the full factorial experimental designs used for the optimization of the CD synthesis conditions.

Design variables	Abbreviation	Cube Levels		Central level
		low	high	
Screening experimental design				
Mass of Citric Acid (g)	m_{CA}	0.2	3	1.6
Volume of EDA (µL)	V_{EDA}	200	800	500
Microwave time (min)	t_{mic}	2	10	6
Advanced experimental design at lowers M_{CA} (pH 7 and 10)				
Mass of Citric Acid (g)	m_{CA}	0.1	0.9	0.5
Volume of EDA (µL)	V_{EDA}	500	1000	750
Microwave time (min)	t_{mic}	5	15	10
Advanced experimental design at highers M_{CA} (pH 4)				
Mass of Citric Acid (g)	m_{CA}	1	5	3
Volume of EDA (µL)	V_{EDA}	500	1000	750
Microwave time (min)	t_{mic}	5	15	10

The main objective is to obtain CDs with the highest quantum yield associated to a higher NO and $ONOO^-$ fluorescence quenching effect. The responses variables evaluated are the fluorescence intensity (I_{Flu}) and the CDs fluorescence quenching by the NO and $ONOO^-$ 50 μM at pH 4, 7 and 10. In order to optimize these response variables a screening followed by an advanced full factorial experimental design of the factors mass of CA (m_{CA}), volume of EDA (V_{EDA}) and microwave time (t_{mic}) was done. For the full factorial experimental designs three continuous experimental design variables, each one with two levels, without repetitions, three center samples and two response variables were evaluated. A total of eleven experiences were done for each full factorial experimental design.

1.1.1 Screening experimental design

In Table S2 are presented the results obtained by the HOIE and CENTER tests. By the analysis of the results found it´s possible to see that by the HOIE test only at pH 10 the microwave time (t_{mic}) induces a significant increase of the quenching effect of the NO and at the same pH the t_{mic} and the mass of citric acid (m_{CA}) induces respectively a significant increase and decrease of the quenching effect of the $ONOO^-$. By the center test the more relevant is the significant positive curvature found for the fluorescence intensity (I_{Flu}) with all the main effects and interactions and a statistically significant negative curvature for the fluorescence quenching by the $ONOO^-$at pH 7 with the t_{mic}.

Table S2 – HOIE and CENTER tests results obtained in the screening full factorial experimental design used for the optimization of the CD synthesis conditions.*

Design variables	Fluorescence intensity		Fluorescence quenching (NO)						Fluorescence quenching (ONOO-)					
			pH4		pH7		pH10		pH4		pH7		pH10	
	HOIE	Center	HOIE	Center	HOIE	Center	HOIE	Center	HOIE	Center	HOIE	Center	HOIE	Center
m_{CA}	NS	+	NS	NS	NS	NS	NS	NS	NS	NS	NS	NS	+	NS
V_{EDA}	NS	+	NS	+	NS	NS	NS	NS	NS	NS	NS	NS	NS	NS
t_{mic}	NS	+	NS	+	NS	-	-	NS	NS	NS	NS	-	-	NS
$m_{CA} \times V_{EDA}$	NS	+	NS	NS	NS	-	NS	NS	NS	NS	NS	NS	NS	NS
$m_{CA} \times t_{mic}$	NS	+	NS	NS	NS	NS	NS	NS	NS	NS	NS	+	+	NS
$V_{EDA} \times t_{mic}$	NS	+	NS	NS	NS	NS	NS	NS	NS	NS	NS	NS	NS	NS

* NS – Statistically non-significant main effect, interaction or curvature, +, ++, +++ - Statistically significant positive main effect, interaction or curvature; -, --, --- - Statistically significant negative main effect, interaction or curvature.

The ANOVA results found for this experimental design are presented in Table S3. By the global evaluation of the linear and interactions models estimated by ANOVA for the variables of response, in the levels of the experimental design variables evaluated, it's possible to see that a global statistically non-significant model, a $R_{Multiple}$ from 0.5 to 0.7 and a statistically significant lack of fit were generally found. The exceptions were

obtained for the fluorescence quenching by the $ONOO^-$ at pH 10 with a $R_{Multiple}$ of 0.9 and statistically non-significant lack of fit and for the fluorescence quenching by the NO at pH 10 and $ONOO^-$ at pH 4 and 10 with a statistically non-significant lack of fit. These generally results found are according to the fact that the main effects and the variable interactions are all statistically non-significant. Even so better results were found with the ANOVA main effects linear and interaction models in comparison with the estimated ANOVA main effects linear models (data not presented).

A statistically non-significant variation for all the response variables were obtained with all the experimental design variables and interactions in the levels of the experimental design variables evaluated. Even so some generally conclusions could be obtained from the values of the estimated beta regression (b) coefficients. All the experimental design variables induces an increase of the I_{Flu}. A higher V_{EDA} and t_{mic} is favorable for a higher fluorescence quenching effect by NO and $ONOO^-$ at pH 4, 7 and 10. For the m_{CA} were obtained for NO and $ONOO^-$ a different effect in the fluorescence quenching at pH 4 and 7 and a similar result at pH 10. Indeed at pH 4 and 7 a higher m_{CA} is favorable for a higher fluorescence quenching effect by the NO and for a lower fluorescence quenching effect by the $ONOO^-$. At pH 10 a lower m_{CA} is favorable for the quenching effect by both species.

From the results obtained it´s clear that a different m_{CA} could be favourable for the selective fluorescence sensing based on the quenching effect of both species. A higher m_{CA} is favorable for a higher fluorescence quenching effect by the NO and a lower m_{CA} is favorable for a higher fluorescence quenching effect by the $ONOO^-$ at pH 4 and 7. Also attending to the greater fluorescence quenching effect by the $ONOO^-$ at pH 10, where a similar trend in effect of the m_{CA} in the quenching effect it's evaluated for both species, the selective fluorescence sensing of the $ONOO^-$ by the increase of m_{CA} at this pH could be evaluated in order to the selective fluorescence sensing of the $ONOO^-$.

Table S3 - ANOVA of the CDs fluorescent intensity ($\lambda_{exc.}$ = 380 nm/$\lambda_{emi.}$ = 470 nm) and of the fluorescence quenching by NO and $ONOO^-$ 50 μM at pH 4, 7 and 10 obtained by the full factorial experimental design for the CD synthesis.*

	Fluorescence Intensity		**Fluorescence quenching (NO)**						**Fluorescence quenching ($ONOO^-$)**					
			pH4		**pH7**		**pH10**		**pH4**		**pH7**		**pH10**	
	F-ratio (p-value)	**b**	**F-ratio (p-value)**	**b**	**F-ratio (p-value)**	**b**	**F-ratio (p-value)**	**b**	**F-ratio (p-value)**	**b**	**F-ratio (p-value)**	**b**	**F-ratio (p-value)**	**b**
Model	0.258 (0.931)	---	0.350 (0.879)	---	0.292 (0.913)	---	0.212 (0.954)	---	0.743 (0.646)	---	0.421 (0.835)	---	2.350 (0.214)	---
Lack of fit	238.439 (0.004)	---	80.899 (0.012)	---	97.528 (0.010)	---	0.784 (0.561)	---	0.649 (0.607)	---	51.335 (0.019)	---	2.248 (0.308)	---
$R_{multiple}$	0.528	---	0.586	---	0.726	---	0.491	---	0.726	---	0.622	---	0.883	---
	Factors													
Intercept	3.673 (0.128)	227.06	5.762 (0.074)	-112.23	6.042 (0.070)	-186.59	3.931 (0.118)	-48.41	8.505 (0.043)	-41.145	8.405 (0.044)	-545.31	16.447 (0.015)	-613.90
m_{CA}	0.192 (0.684)	43.53	0.118 (0.748)	-13.46	3.569×10^{-3} (0.955)	-3.80	0.185 (0.689)	8.80	0.201 (0.677)	5.295	0.248 (0.645)	78.46	3.681 (0.127)	243.25
V_{EDA}	0.286 (0.621)	0.25	0.390 (0.567)	-0.11	0.253 (0.641)	-0.15	1.911×10^{-2} (0.898)	-1.32×10^{-2}	0.152 (0.717)	-2.147×10^{-2}	0.141 (0.726)	-0.28	0.115 (0.751)	-0.20
t_{mic}	0.363 (0.579)	20.93	0.823 (0.416)	-12.43	0.981 (0.378)	-22.04	0.762 (0.432)	-6.25	1.009 (0.372)	-4.154	1.110 (0.352)	-58.08	5.733 (0.075)	-106.25
$m_{CA} \times V_{EDA}$	0.259 (0.638)	56.51	0.468 (0.531)	-30.02	0.328 (0.597)	-40.79	2.081×10^{-2} (0.892)	-3.30	0.295 (0.616)	-7.194	0.244 (0.647)	-87.08	7.168×10^{-2} (0.802)	-38.02
$m_{CA} \times t_{mic}$	0.180 (0.693)	47.18	4.482×10^{-2} (0.843)	-9.29	8.964×10^{-4} (0.977)	2.13	0.279 (0.625)	12.09	2.450 (0.193)	20.714	0.784 (0.426)	156.19	4.481 (0.102)	300.61
$V_{EDA} \times t_{mic}$	0.269 (0.632)	57.60	0.253 (0.641)	-22.05	0.186 (0.688)	-30.71	2.978×10^{-2} (0.959)	-1.25	0.352 (0.585)	7.856	9.558×10^{-5} (0.993)	1.73	1.975×10^{-2} (0.895)	-19.96

* $R_{multiple}$ – Multiple correlation, F-ratio – Fisher ratio; p-value - probability value (p) for a 5 % significance level; b – beta-regression coefficient; Main – main effects; Int. – interactions effects.

1.1.2 Advanced experimental design

Taking in consideration the previous conclusions by the screening full factorial experimental design performed, the fact that a different m_{CA} could be favourable for the selective fluorescence sensing and the fact that a high V_{EDA} and t_{mic} it's advantageous for a higher fluorescence quenching effect by both species at the three pHs, two more full factorial experimental designs were done. In order to evaluate preferentially the selective fluorescence sensing of $ONOO^-$ at pH 7 and 10 and of NO at pH 4 one experimental design was performed at pH 7 and 10 with lowers m_{CA} and the other was done at pH 4 with highers m_{CA}. Both full factorial experimental designs were performed with highers V_{EDA} and t_{mic} (Table S1).

Lower m_{CA}

In Table S4 are presented the results obtained by the HOIE and CENTER tests. By the generally overview of the results found it´s possible to see that by the HOIE test only the m_{CA} induces a significant increase of the fluorescence intensity. As for the screening full factorial experimental design, the more relevant found by the center test, is the statistically significant positive curvature found for the I_{Flu} with all the main effects and interactions and a statistically negative curvature for the fluorescence quenching effect by the $ONOO^-$ with the m_{CA} and t_{mic} at pH 7 and 10.

Table S4 – HOIE and CENTER tests results obtained in the optimization full factorial experimental design used for the optimization of the CD synthesis conditions at lower m_{CA}.*

Design variables	Fluorescence intensity		Fluorescence quenching (NO)				Fluorescence quenching (ONÕO-)			
			pH7		pH10		pH7		pH10	
	HOIE	Center	HOIE	Center	HOIE	Center	HOIE	Center	HOIE	Center
m_{CA}	+	++	NS	NS	NS	NS	NS	+	NS	-
V_{EDA}	NS	+	NS	NS	NS	NS	NS	NS	NS	NS
t_{mic}	NS	+	NS	NS	NS	NS	NS	NS	NS	-
$m_{CA} \times V_{EDA}$	NS	+	NS	NS	NS	NS	NS	++	NS	+
$m_{CA} \times t_{mic}$	NS	+	NS	++	NS	NS	NS	+++	NS	++
$V_{EDA} \times t_{mic}$	NS	+	NS	++	NS	NS	NS	++	NS	+

* See footnote of Table S2.

The ANOVA results found for this experimental design are presented in Table S5. By the global evaluation of the linear and interactions models estimated by ANOVA for the variables of response, in the levels of the experimental design variables evaluated, it's possible to see that a global statistically significant model with a high $R_{Multiple}$ of 0.99 and a statistically non-significant lack of fit was now found for the I_{Flu}.

Statistically non-significant models for the fluorescence quenching by the NO and and $ONOO^-$ with a statistically significant lack of fit, except for the fluorescence quenching by NO at pH 10, and a lower multiple correlation (0.6 - 0.7) for NO and a higher multiple correlation (0.9) for $ONOO^-$ were found at the two evaluated pHs. As for the found with the screening full factorial experimental design better results were found with the ANOVA main effects linear and interaction models in comparison with the estimated ANOVA main effects linear models (data not presented).

Table S5 - ANOVA of the CDs fluorescent intensity ($\lambda_{exc.}$ = 380 nm/$\lambda_{emi.}$ = 470 nm) and of the fluorescence quenching by NO and $ONOO^-$ 50 µM at pH 7 and 10 obtained by the full factorial experimental design for the CD synthesis.*

	Fluorescence Intensity		Fluorescence quenching (NO)				Fluorescence quenching ($ONOO^-$)			
			pH7		pH10		pH7		pH10	
	F-ratio (p-value)	b	F-ratio (p-value)	b	F-ratio (p-value)	b	F-ratio (p-value)	b	F-ratio (p-value)	b
Model	36.032 (0.002)	---	0.590 (0.732)	---	0.336 (0.887)	---	0.3672 (0.114)	---	1.999 (0.262)	---
Lack of fit	1.825 (0.354)	---	189.886 (0.005)	---	3.316 (0.731)	---	359.344 (0.003)	---	78.893 (0.012)	---
$R_{multiple}$	0.991	---	0.685	---	0.579	---	0.920	---	0.866	---
Factors										
Intercept	341.667 (0.0001)	231.81	13.107 (0.022)	-125.74	7.315 (0.054)	-56.90	154.895 (0.0002)	-702.82	89.197 (0.0007)	-1.17×10^3
m_{CA}	204.125 (0.0001)	525.25	3.578×10^{-2} (0.859)	-19.26	5.061×10^{-3} (0.947)	4.38	0.128 (0.738)	59.31	0.538 (0.504)	-265.18
V_{EDA}	1.843×10^{-2} (0.899)	-7.99×10^{3}	2.461×10^{-2} (0.883)	-2.56×10^{-2}	0.721 (0.444)	8.38×10^{-2}	4.252×10^{-4} (0.984)	5.46×10^{-3}	2.838×10^{-2} (0.874)	9.75×10^{-2}
t_{mic}	2.900 (0.164)	-5.01	4.675×10^{-2} (0.839)	-1.76	6.563×10^{-2} (0.810)	-1.26	8.416×10^{-2} (0.786)	-3.84	1.058 (0.362)	-29.76
$m_{CA}\times V_{EDA}$	0.120 (0.746)	-4.08	2.635×10^{-2} (0.879)	5.29	0.726 (0.442)	16.81	4.445 (0.103)	111.69	0.702 (0.449)	96.96
$m_{CA}\times t_{mic}$	8.887 (0.041)	-35.07	1.064 (0.360)	33.61	0.363 (0.579)	11.88	15.727 (0.017)	210.08	9.078 (0.039)	348.67
$V_{EDA}\times t_{mic}$	0.138 (0.729)	4.37	2.343 (0.201)	49.87	0.163 (0.731)	-7.28	1.646 (0.269)	67.97	0.586 (0.487)	88.60

* see footnote of table S3.

As we could expected, due to the found with the HOIE test, a statistically significant variation was now found by ANOVA for the I_{Flu} with the m_{CA} inducing a significant increase of the I_{Flu}. Beside this, also a statistically significant negative and a positive interaction between m_{CA} and t_{mic} respectively for the I_{Flu} and for the fluorescence quenching effect by the $ONOO^-$ at the two evaluated pHs were now found. By the analysis of the *b* coefficients for the I_{Flu} beside the statistically significant increase for the I_{Flu} with the m_{CA} a statistically non-significant decrease of the I_{Flu} was obtained for the V_{EDA} and t_{mic}. A different effect of the m_{CA} in the quenching effect by the NO and the $ONOO^-$ at each of the evaluated pHs was found. As for the obtained with the screening full factorial experimental design at pH 7 a higher m_{CA} is favorable for a higher fluorescence quenching effect by the NO and for a lower fluorescence

quenching effect by the $ONOO^-$. At pH 10 a different result was now obtained. Indeed contrary to the previous found, where at pH 10 a lower m_{CA} were favorable for the quenching effect by both species, now at pH 10 a higher m_{CA} is favorable for a higher fluorescence quenching effect by the $ONOO^-$ and for a lower fluorescence quenching effect by the NO. As the obtained in the previous screening full factorial experimental design for the other two main effects the same effect in the fluorescence quenching was found for both species at the evaluated pHs. Even so now, contrary to the previous found, the V_{EDA} induces a decrease and the t_{mic} still induces an increase of the quenching effect by the NO and $ONOO^-$ at pH 7 and 10.

So attending to these results, and for the sensitive and selective fluorescence sensing of the $ONOO^-$ at pH 7 and 10, a higher m_{CA} are favorable in order to a high I_{Flu}, at pH 7 a lower and at pH 10 a higher m_{CA} are more favourable for a greater quenching effect by this RNS and for the selective fluorescence sensing of the $ONOO^-$ at each of the evaluated pHs. For the NO, and beside the same positive effect of a higher m_{CA} in the I_{Flu}, at pH 7 a higher and at pH 10 a lower m_{CA} are more favourable for a greater quenching effect by this RNS. Also considering the non-statistically significant decrease by the V_{EDA} and t_{mic} for the I_{Flu}, with the statistically significant positive curvature found with all the main effects and interactions, and the statistically non-significant decrease by the V_{EDA} of the fluorescence quenching effect by the $ONOO^-$ at the two evaluated pHs and for NO at pH 7 it seems that the range of levels of these variables it´s already adequate on order to their sensitive fluorescence quenching.

Higher m_{CA}

In Table S6 are presented the results obtained by the HOIE and CENTER tests.

Table S6 – HOIE and CENTER tests results obtained in the optimization full factorial experimental design used for the optimization of the CD synthesis conditions at higher m_{CA}.*

Design variables	Fluorescence intensity		Fluorescence quenching (NO) pH4		Fluorescence quenching (ONÕO-) pH4	
	HOIE	Center	HOIE	Center	HOIE	Center
m_{CA}	NS	NS	NS	NS	NS	NS
V_{EDA}	NS	NS	NS	--	NS	NS
t_{mic}	NS	NS	NS	+	NS	NS
$m_{CA}\times V_{EDA}$	NS	NS	NS	-	NS	NS
$m_{CA}\times t_{mic}$	NS	NS	NS	NS	NS	NS
$V_{EDA}\times t_{mic}$	NS	NS	NS	+	NS	NS

* See footnote of Table S2.

By the generally overview of the results found by the HOIE and CENTER tests it´s possible to see that by the HOIE test a statistically non-significant variation were obtained for all the response variables and interactions in the levels of the experimental design variables evaluated. By the center test the more relevant is for the fluorescence quenching effect by the NO at the evaluated pH a statistically significant positive curvature for the t_{mic} and a statistically negative curvature with the V_{EDA}.

The ANOVA results found for this experimental design are presented in Table S7. By the global evaluation of the linear and interactions models estimated by ANOVA for the variables of response, in the levels of the experimental design variables evaluated, it's possible to see that were found a generally global statistically non-significant model, a statistically non-significant lack of fit, except for the fluorescence quenching effect by NO at pH 4, and a $R_{Multiple}$ of 0.6 for the I_{Flu} and of 0.8 for fluorescence quenching effect by NO and $ONOO^-$ at pH 4. As for the found with the other full factorial experimental design better results were also found with the ANOVA main effects linear and interaction models in comparison with the estimated ANOVA main effects linear models (data not presented).

Table S7 - ANOVA of the CDs fluorescent intensity ($\lambda_{exc.}$ = 380 nm/$\lambda_{emi.}$ = 470 nm) and of the fluorescence quenching by NO and $ONOO^-$ 50 µM at pH 4 obtained by the full factorial experimental design for the CD synthesis.*

	Fluorescence Intensity		**Fluorescence quenching (NO) pH4**		**Fluorescence quenching ($ONOO^-$) pH4**	
	F-ratio (p-value)	**b**	**F-ratio (p-value)**	**b**	**F-ratio (p-value)**	**b**
Model	0.338 (0.886)	---	1.156 (0.465)	---	0.959 (0.542)	---
Lack of fit	10.812 (0.085)	---	77.454 (0.013)	---	7.053×10^{-2} (0.934)	---
$R_{multiple}$	0.580	---	0.796	---	0.786	---
Factors						
Intercept	13.983 (0.020)	488.90	26.503 (0.007)	-158.73	4.390 (0.104)	-72.20
m_{CA}	1.134 (0.347)	-81.62	2.259×10^{-2} (0.888)	-2.72	1.658 (0.267)	-26.01
V_{EDA}	4.091×10^{-2} (0.850)	0.12	4.075 (0.114)	-0.29	1.287 (0.320)	-0.18
t_{mic}	0.263 (0.635)	-15.72	0.592 (0.485)	5.56	1.076 (0.358)	8.38
$m_{CA}\times V_{EDA}$	0.497 (0.520)	86.44	0.884 (0.400)	-27.19	1.655 (0.268)	-41.59
$m_{CA}\times t_{mic}$	8.164×10^{-2} (0.789)	35.04	5.080×10^{-2} (0.843)	-6.52	3.015×10^{-3} (0.789)	-1.78
$V_{EDA}\times t_{mic}$	1.284×10^{-2} (0.915)	-13.90	1.311 (0.316)	33.11	7.606×10^{-2} (0.796)	8.92

* see footnote of table S3.

As the found with the HOIE test also a statistically non-significant variation was now found by ANOVA for the I_{Flu} and quenching effect by NO and $ONOO^-$ at pH 4 with all the variables and interactions. Even so by analysis of the b coefficients a higher m_{CA} and t_{mic} induces a decrease and a higher V_{EDA} a decrease of the I_{Flu}. Similar results were found for the fluorescence quenching effect by the two RNS at the evaluated pH with the three design variables evaluated. Indeed a higher m_{CA} and V_{EDA} are favourable and a higher t_{mic} are not favourable for the fluorescence quenching effect by NO and $ONOO^-$ at pH 4. As for the found with the screening full factorial experimental design at pH 4 a higher m_{CA} is favorable for a higher fluorescence quenching effect by the NO but now, contrary to the previous found, a higher m_{CA} is also favorable for a higher fluorescence quenching effect by the $ONOO^-$.

So attending to these results, and for the sensitive and selective fluorescence sensing of the NO at pH 4, a higher m_{CA} are less favorable in order to a high I_{Flu} and more favourable for a greater quenching effect by this RNS. Also a higher m_{CA} it's favourable for the selective fluorescence sensing of the $ONOO^-$ at this pH. Considering the statistically non-significant decrease by the m_{CA} and t_{mic} for the I_{Flu} and the statistically non-significant decrease by the t_{mic} of the fluorescence quenching effect by the two RNS at the evaluated pH it seems that the range of levels of these variables it´s already adequate in order to a sensitive fluorescence quenching.

1.2. NO and $ONOO^-$ quenching evaluation

Attending to the results found in the experimental design optimization and in order to a deeper evaluation of the quenching effect of NO and $ONOO^-$ at pH 4, 7 and 10 CDs were synthetized in the following conditions: **1)** m_{CA} = 0.25 g, V_{EDA} = 500 µL, t_{mic} = 5'; **2)** m_{CA} = 0.25 g, V_{EDA} = 500 µL, t_{mic} = 10'; **3)** m_{CA} = 0.25 g, V_{EDA} = 1000 µL, t_{mic} = 5'; **4)** m_{CA} = 0.25 g, V_{EDA} = 1000 µL, t_{mic} = 10'; **5)** m_{CA} = 1 g, V_{EDA} = 500 µL, t_{mic} = 5'; **6)** m_{CA} = 1 g, V_{EDA} = 500 µL, t_{mic} = 10'; **7)** m_{CA} = 1 g, V_{EDA} = 1000 µL, t_{mic} = 5'; **8)** m_{CA} = 1 g, V_{EDA} = 1000 µL, t_{mic} = 10'; **9)** m_{CA} = 2.5 g, V_{EDA} = 500 µL, t_{mic} = 5'; **10)** m_{CA} = 2.5 g, V_{EDA} = 500 µL, t_{mic} = 10'; **11)** m_{CA} = 2.5 g, V_{EDA} = 1000 µL, t_{mic} = 5'; **12)** m_{CA} = 2.5 g, V_{EDA} = 1000 µL, t_{mic} = 10'; **13)** m_{CA} = 5 g, V_{EDA} = 500 µL, t_{mic} = 5'; **14)** m_{CA} = 5 g, V_{EDA} = 500 µL, t_{mic} = 10'; **15)** m_{CA} = 5 g, V_{EDA} = 1000 µL, t_{mic} = 5'; **16)** m_{CA} = 5 g, V_{EDA} = 1000 µL, t_{mic} = 10'.

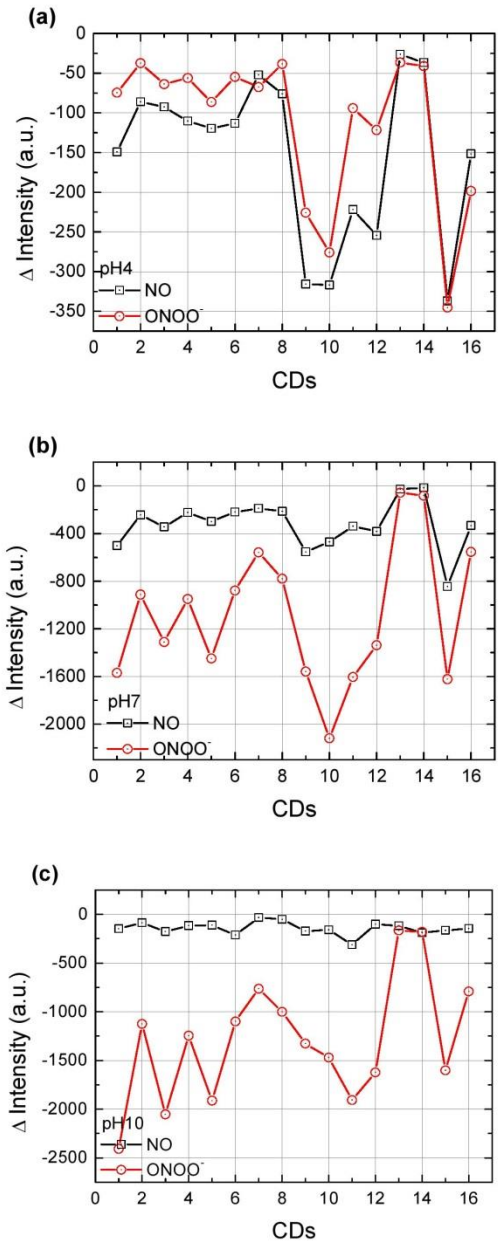


Fig. S1 – Quenching effect of NO and $ONOO^-$ 50 μM at pH 4 a), 7 b) and 10 c) in the fluorescence of synthetized CDs with different synthesis conditions.

In Fig. S1 are presented the results obtained by the evaluation fluorescence quenching by NO and $ONOO^-$ 50 μM at pH 4, 7 and 10 in the fluorescence of CDs synthetized in the previous indicated conditions [**1)** to **16)**]. By the analysis of the Fig. S1 a greater quenching is observed with $ONOO^-$ at pH 7 and 10 in comparison with that found with NO at pH 4 and 7. It's possible to see that a generally lowest difference of the quenching effect by NO and $ONOO^-$ for the three evaluated pHs were obtained for the synthetized CDs with m_{CA} = 5 g and that a greater quenching effect at pH 4 and 7 it's found for the synthetized CDs with m_{CA} = 2.5 g and at pH 10 with m_{CA} = 0.25 g.

2. NO and $ONOO^-$ sensing

In Fig. S2 is presented the response of the principal ROS/RNS in water at initially synthesis conditions (m_{CA} = 1 g, V_{EDA} = 500 µL, t_{mic} = 5') and in Fig. S3 is presented the response of the principal ROS/RNS with synthetized CDs in the selected conditions (m_{CA} = 2.5 g, V_{EDA} = 500 µL, t_{mic} = 5' at pH 4 and m_{CA} = 0.25 g, V_{EDA} = 500 µL, t_{mic} = 5'at pH 7 and 10).

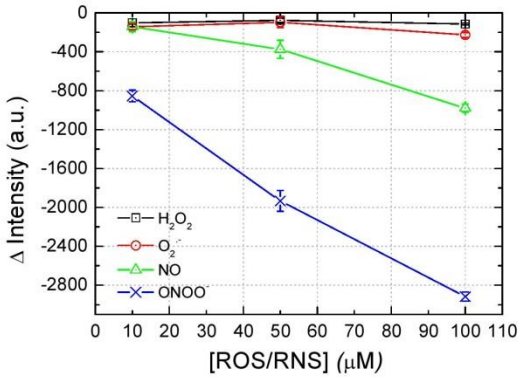


Fig S2 - Effect of the principal ROS/RNS in the fluorescence of the synthetized CDs in water (m_{CA} = 1 g, V_{EDA} = 500 µL, t_{mic} = 5').

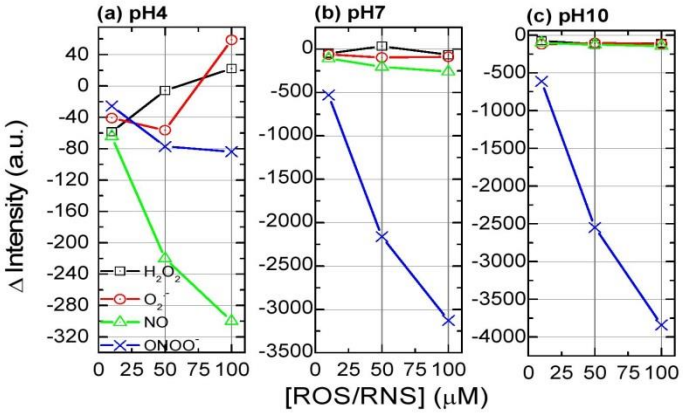


Fig S3 - Effect of the principal ROS/RNS in the fluorescence of the synthetized CDs [(a) m_{CA} = 2.5 g, V_{EDA} = 1000 µL, t_{mic} = 5' at pH 4; (b) and (c) m_{CA} = 0.25 g, V_{EDA} = 500 µL, t_{mic} = 5' at pH 7 and 10].

The effect of the pH in the maximum fluorescence intensity of the main band of the synthetized CDs in the optimized conditions are shown in Fig. S4.

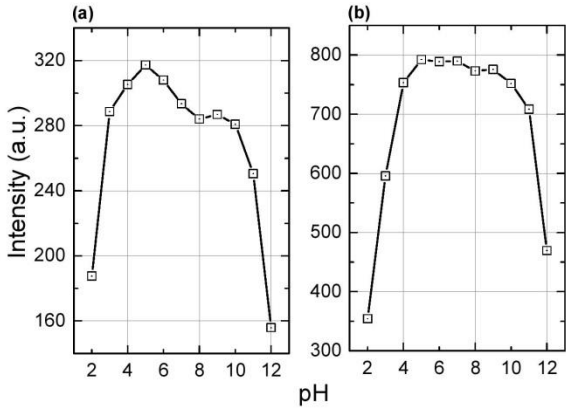


Fig. S4 – Typical fluorescence intensity variation of the synthesised CDs with the pH [(a) m_{CA} = 0. 25 g, V_{EDA} = 500 μL, t_{mic} = 5'; (b) m_{CA} = 2.5 g, V_{EDA} = 1000 μL, t_{mic} = 5'].

3. Particle size measurement

Are presented in Table S8 the average size and in Fig. S5 the size distribution obtained for the synthetized CDs in the selected conditions.

Table S8 – Average size of the synthetized CDs
[(a) m_{CA} = 0.25 g, V_{EDA} = 500 µL, t_{mic} = 5'; (b) m_{CA} = 2.5 g, V_{EDA} = 1000 µL, t_{mic} = 5'].

Size distribution	Average size (nm)	Standard deviation (nm)	Percentage (%)
(a) m_{CA} = 0.25 g, V_{EDA} = 500 µL, t_{mic} = 5'	1.0	0.3	94.4
	37.5	6.1	5.6
(b) m_{CA} = 2.5 g, V_{EDA} = 1000 µL, t_{mic} = 5'	4.8	2.7	82.8
	751.0	508.0	17.2

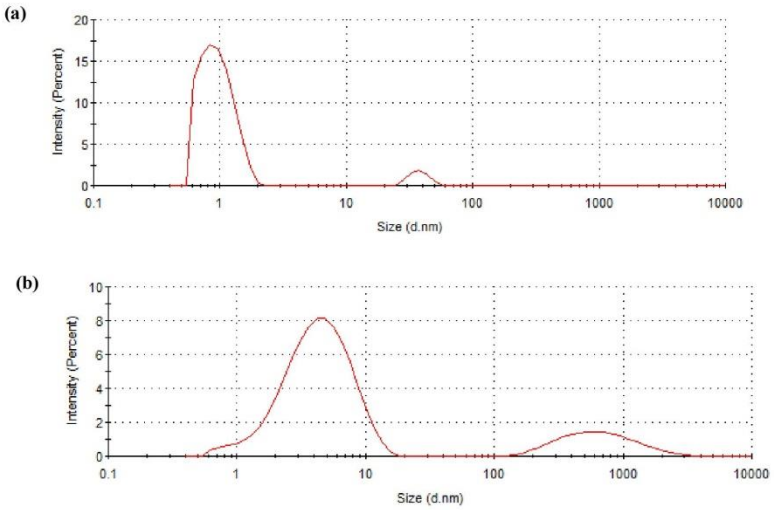


Fig. S5 – Size distribution of synthetized CDs
[(a) m_{CA} = 0.25 g, V_{EDA} = 500 µL, t_{mic} = 5'; (b) m_{CA} = 2.5 g, V_{EDA} = 1000 µL, t_{mic} = 5'].

Chapter 10

Carbon dots prepared from citric acid and urea as fluorescent probes for hypochlorite and peroxynitrite

Eliana F. C. Simões, João M.M. Leitão, Joaquim C.G. Esteves da Silva
MICROCHIMICA ACTA (2016)
doi: 10.1007/s00604-016-1807-6

CDs were also prepared using the same method of synthesis through microwave pyrolysis by adding urea (UR) to the synthesis and using as carbon precursor Glc, ascorbic acid (AA) or CA. It was observed that in the synthesis using UR and Glc none CDs were formed, for CDs prepared from UR and AA was obtained a QY of 2.45% and for CD prepared from UR and AC was obtained a QY of 12%. Then the study of the influence of ROS/RNS in these CDs was made. No relevant results were obtained with the addition of ROS/RNS to CDs prepared from AA and UR. However, for the CDs prepared from CA and UR was verified a change in the fluorescence intensity with the addition of some ROS/RNS. So, the CDs synthesis conditions were established by varying the amounts of CA and UR. For each of the synthesized CDs was made the characterization (excitation/emission matrix, QY) and evaluation of its response to ROS/RNS to three concentration levels at different pH values. Was observed sensitivity of CDs relatively to $ONOO^-$ at pH 9 using CDs synthetized with 0.5 or 1 g of CA and 3 g of UR and sensibility to ClO^- at pH4 with CDs constituted for 1 g of CA and 1 g of UR. Measurements in standard samples and in fortified serum samples were made. This work was published in Microchimica Acta.

My personal contribution to this work includes the establishment of an initial objective and the bibliographic research of the state of the art related with the determination ROS/RNS applying CDs similar to the synthetized, the protocols set up, the experimental execution and posterior data treatment. The CDs synthesis was also made using the microwave pyrolysis method. Other precursors were tested for the CDs synthesis. My personal contribution to this work includes after the research, the

microwave synthesis of the CDs testing different precursors (Glc, AA, UR, CA), the characterization of the CDs and the study of the CDs behavior in presence of the different ROS/RNS. The experiments were repeated several times in order to establish if the results were reproducible.

After the experimental part concluded the writing of the paper were made together with Professor João M.M. Leitão under the supervision of Professor Joaquim C. G. Esteves da Silva.

Microchim Acta
DOI 10.1007/s00604-016-1807-6

ORIGINAL PAPER

Carbon dots prepared from citric acid and urea as fluorescent probes for hypochlorite and peroxynitrite

Eliana F. C. Simões[1,2] · João M. M. Leitão[1] · Joaquim C. G. Esteves da Silva[2,3]

Received: 26 November 2015 / Accepted: 23 February 2016
© Springer-Verlag Wien 2016

Abstract Carbon dots (CDs) were prepared from citric acid and urea, and their fluorescence was found to be quenched by hypochlorite and peroxynitrite. Microwave based synthesis gives CDs with excitation/emission wavelength-dependent quantum yields (8 % at 400/520 nm; 10 % at 360/451 nm; 12 % at 350/420 nm). Quenching of fluorescence depends on pH values, and response is most selective and sensitive to hypochlorite at pH 4, and to peroxynitrite at pH 9. The lower detection limits are 0.5 and 1.5 μM, respectively. The method was successfully applied to quantify hypochlorite and peroxynitrite in standard solutions and in spiked dilute serum samples.

Keywords Carbon dots · Microwave synthesis · Reactive oxygen species · Reactive nitrogen species · Fluorescence · Quenching

Electronic supplementary material The online version of this article (doi:10.1007/s00604-016-1807-6) contains supplementary material, which is available to authorized users.

✉ João M. M. Leitão
jleitao@ff.uc.pt

[1] Centro de investigação em química da Universidade do Porto (CIQ-UP), Faculdade de Farmácia da Universidade de Coimbra, Pólo das Ciências da Saúde, 3000-548 Coimbra, Portugal

[2] Centro de investigação em química da Universidade do Porto (CIQ-UP), Departamento de Química e Bioquímica, Faculdade de Ciências da Universidade do Porto, R. Campo Alegre 687, 4169-007 Porto, Portugal

[3] Centro de investigação em química da Universidade do Porto (CIQ-UP), Departamento de Geociências, Ambiente e Ordenamento do Território, Faculdade de Ciências da Universidade do Porto, R. Campo Alegre 687, 4169-007 Porto, Portugal

Published online: 10 March 2016

Introduction

Carbon dots (CDs) [1] display features such as tunable fluorescence, water solubility, photo- and physico-chemical stability, biocompatibility and low toxicity. This makes them attractive materials for use in fluorescent sensors [2]. Different top-down and bottom-up methods of synthesis have been described for their synthesis [2–6]. The microwave and hydrothermal bottom-up methods have become to be of the most used methods of CDs synthesis [3, 4]. In comparison with the hydrothermal method, the microwave synthesis is a facile, rapid, green, low cost method of synthesis that also yield CDs with a relatively high quantum yield (Φ) [3]. In these CDs synthesis several precursors and other compounds for doping, passivated or functionalized the obtained CDs have been used originating CDs with different reactivity and fluorescent properties [2–4].

One of the most used precursors for the microwave synthesis is the citric acid [7–18]. Most of the citric acid synthesized CDs were doped with an amine as the 1,2-ethylenediamine (EDA) [7, 8, 10–12], diethylamine (DEA) [12], 1,4-butanediamine (BDA) [12], trimethylamine (TEA) [12] and poly(ethylenemine) (PEI) [9]. With these amine doped CDs, a Φ between 4 and 8 % for most of the amines [12], 30 % for PEI [9] and 30 [10, 12], 42.8 [7] or 43.8 % [8] for EDA doped CDs were obtained, with a maximum fluorescence intensity at an excitation wavelength (λ_{EX}) and an emission wavelength (λ_{EM}) respectively between 350 and 360 and 448–460 nm [3, 7, 8, 12]. Beside these amines, also urea, with a high nitrogen content, was used for doping microwave prepared CDs from citric acid yielding urea doped CDs with a Φ between 8 and 15 % and a maximum fluorescence intensity with a green emission around 520 nm after an excitation around 420 nm [15–18]. One of these synthesized CDs were also doped with

boron [15] and with other a nanocomposites, with zeolitic imidazolate framework-8 nanoparticles (ZIF8) [16]. By microwave synthesis, urea was also used for doping CDs obtained from calcium citrate [19], trisodium citrate [20] and glucose [21]. In the majority of the urea doped CDs synthesis from citric acid, and except for the boron doped CDs, a mass of citric acid (m_{CA}) and urea (m_{UR}) of 1 g [15] and 3 g [16–18] were used. These synthesized urea doped CDs were used as a ink [18] and evaluated as a multiple fluorescence ratiometric sensor of temperature, pH and Fe^{3+} [17].

Hypochlorite (ClO^-) and peroxynitrite ($ONOO^-$) belong to the reactive oxygen (ROS) and nitrogen species (RNS). These species are a group of endogenous substances with a particularly importance in several physiological and pathological process [22, 23]. The development of sensitive and selective sensors is an increased demand in order to their possible in vivo detection and/or quantification [24]. Beside the electrochemical sensors [25], fluorescent optical sensors [24, 26, 27], essentially based in organic fluorophores, have been established with that finally purpose. Due to their own characteristics some effort has been made in order to develop fluorescent nanoparticle sensors for ROS/RNS detection [28, 29]. Mostly of the already developed ROS/RNS fluorescent nanoparticle sensors are based in semiconductors quantum dots (QDs) [29]. However, due to the QDs chemical constituents, some issues arise due to their inherent toxicity. Some fluorescent nanoparticle sensors were based in potentially non-toxic CDs nanoparticles for hydrogen peroxide (H_2O_2) [30–34], nitric oxide (NO) [11, 35], $ONOO^-$ [35, 36], ClO^- [37–39], superoxide ($O_2^{\cdot-}$) [40] and hydroxyl radical ($HO^{\cdot}$) [31] detection and/or quantification.

CDs synthesized with different quantities of citric acid and urea by a simple one step microwave method was used for fluorescence quantification of ClO^- and $ONOO^-$. The detection at different pH values and the fluorescence selective quantification capability were verified in standard solutions and in spiked serum samples.

Experimental

Reagents

Citric acid, urea, hydrogen peroxide (H_2O_2), hydrogen chloride (HCl), potassium superoxide (KO_2), sodium hypochlorite 3.5 % (NaClO), sodium nitrite ($NaNO_2$), sodium nitrate ($NaNO_3$), sodium chloride (NaCl), potassium chloride (KCl), ethylenediamine tetraacetic acid (EDTA), iron(II) sulphate ($FeSO_4.7H_2O$), iron(III) nitrate [$Fe_3(NO_3)_3.9H_2O$], magnesium chloride ($MgCl_2.6H_2O$), copper(II) sulphate ($CuSO_4.5H_2O$), sodium phosphate dibasic (Na_2HPO_4), monosodium phosphate (NaH_2PO_4), sodium carbonate (Na_2CO_3), sodium hydrogen carbonate (NaHCO3), potassium hydrogen phthalate analytical, sodium hydroxide (NaOH), analytical grade reagents were used. Milli-Q water with a resistivity 18 MΩ.cm at 25 °C was used in all the work.

Solutions

The solutions of ROS/RNS species were prepared according to described standard procedures. Saturated NO solutions (1.9 mM) were prepared by bubbling NO in deoxygenated water, after bubbling argon for 15 min. Standard solutions were prepared in deoxygenated water. The $ONOO^-$ standard solutions were prepared in a refrigerated beaker under constant stirring by mixing 100 mL of $NaNO_2$ 600 mM, 100 mL of H_2O_2 600 mM in HCl 0.6 M and 100 mL of NaOH 3.6 M. The solution will turn yellow indicating the formation of $ONOO^-$. The agitation is maintained until no O_2 is formed. The solutions of H_2O_2, KO_2, NaClO, $NaNO_3$, $NaNO_2$ were prepared in water. Deoxygenated water was used for the preparation of H_2O_2, NaClO and KO_2 solutions. The hydroxyl ($HO^{\cdot}$) was generated in situ by the Fenton reaction by addition of a 5 fold excess of H_2O_2 to the EDTA-Fe(II) complex formed with different concentrations of $FeSO_4$. Serum ClO^- or $ONOO^-$ spiked sample solutions were done respectively in deoxygenated water or NaOH 0.1 M by dilution to the desired concentrations.

Phthalate buffer, phosphate buffer and carbonate buffer were respectively used for the experiments at pH 4, 7 and 9. Phosphate buffer was prepared through NaH_2PO_4 and Na_2HPO_4, phthalate buffer pH 4 was prepared through potassium hydrogen phthalate and carbonate buffer pH 10 was prepared through Na_2CO_3 and NaHCO3 weighting for the required volume of solution. Also solutions of HCl and NaOH 0.1 M were prepared in order to evaluate the influence of pH in the CD fluorescence and in order to adjust the pH of the prepared buffer solutions for the required pH.

Microwave CDs synthesis

As reported in the literature, the m_{CA} and m_{UR} were adjusted to a mass between 1 g and 3 g in the microwave synthesis of the CDs. A microwave oven with a maximum radiation power of 700 W was used. Identical conditions (i.e., a water volume of 15 mL, a microwave power of 700 W and a heating time of 5 min) were used in all syntheses. The resulting CDs were left to cool, diluted with water and then centrifuged at 9000 rpm for 10 min in order to eliminate suspended impurities. Finally, the volume of the CDs suspension was adjusted to 30 mL with water.

Quenching fluorescence evaluations

The ClO^- and $ONOO^-$ fluorescence detection, quantification and interference studies were made in a standard 1 cm

fluorescence quartz cell for a final volume of 2.5 mL by additions of the required volumes of the initially solutions for the desired final concentrations to 2 mL of the CDs suspension and adjustment of the final volume with water. These fluorescence evaluations were performed using a QE65000 charge-coupled detector, a 380 nm light emitting diode (LED), a sampling compartment (CUV-ALL-UV 4-way) and two 1.0 mm core diameter fiber optics (P1000-2-UV–VIS) from Ocean Optics. One of the fibers guides the light from the source to the sampling compartment and the other guide the emitted light to the detector. The reaction time profiles were obtained collecting the signal at the maximum emission wavelength, every 10 s with an integration time of 300 ms. A difference between the initial and the final fluorescence intensity measured after 10 min the addition of the ROS/RNS (intensity variation) were used in all the work.

Quantum yield

The quantum yield (Φ) was calculated comparing the integrated photoluminescence intensities and the absorbance values of the synthesized CDs with the ones of the quinine sulfate.

$$\Phi = \Phi_R \times \frac{Grad}{Grad_R} \times \frac{\eta^2}{\eta_R^2}$$

In the equation Φ is the fluorescence quantum yield, *Grad* is the gradient from the plot of integrated fluorescence intensity vs. absorbance and η is the refractive index. The subscripts R refer to reference fluorophore, quinine sulfate of known quantum yield. The Φ of the quinine sulfate is $\Phi = 0.54$ [41]. The η of the quinine sulfate in 0.1 M H_2SO_4 and of nanocomposites water solutions used were $\eta = 1.33$.

Instrumentation

Absorbance and fluorescence spectra were obtained in a standard 1 cm fluorescence quartz cell and collected respectively in a Jasco V-530 UV-Visible spectrophotometer and in a Jasco FP-6200 spectrofluorometer. The absorption spectra were obtained in a wavelength range from 250 to 650 nm with a 2 nm interval, slit widths 2 nm and wavelength scan rate medium; the Fluorescence spectra were obtained in a wavelength range from 300 to 700 nm with a 1 nm interval, slit widths 5 nm, sensitivity response medium, response time fast and wavelength scan rate 1000 nm/min. Fourier transform infrared (FTIR) spectra were obtained by a Perkin Elmer FTIR Spectrum 400 in solid state with an attenuated total reflectance (ATR) accessory in a range of 4000 to 650 cm^{-1} with 16 accumulations and a resolution of 4 cm^{-1}. The particle size, size distribution and shape of the CDs were evaluated by transmission electronic microscopy (TEM) in a FEI Company Tecnai G2 20 S-Twin electronic microscopic.

Results

ClO^- and $ONOO^-$ detection

CDs with different composition and potentially different fluorescent characteristics will be used in this study in order to verify the more sensitive and selective ClO^- and $ONOO^-$ fluorescence detection. A more sensitive and selective response with the majority of the prepared CDs were observed at pH 4 for the ClO^- and at pH 9 for the $ONOO^-$ (Fig. S1). The main ROS/RNS considered as interferences in the determination of ClO^- at pH 4 is the $HO^{\cdot}$ and of $ONOO^-$ at pH 9 is the NO. Also for almost all the CDs a more sensitive, but less selective response, was obtained at pH 7 for the $ONOO^-$ and ClO^-. At this pH the CDs also are also sensitive to NO and $HO^{\cdot}$ The lowest sensitivity was found with the CDs prepared with a m_{CA} of 3 g and a m_{UR} of 0.5 g at the three pHs.

For the $HO^{\cdot}$ at pH 9, and with almost all of the CDs, after an initially quenching effect by addition of Fe^{2+} in order to generate the $HO^{\cdot}$, there is a fluorescence enhancement with some of the prepared CDs at pH 9. This result is probably due to the reaction of Fe^{2+} with H_2O_2, which leaves to the formation of $HO^{\cdot}$ by the Fenton reaction and consequent consumption of

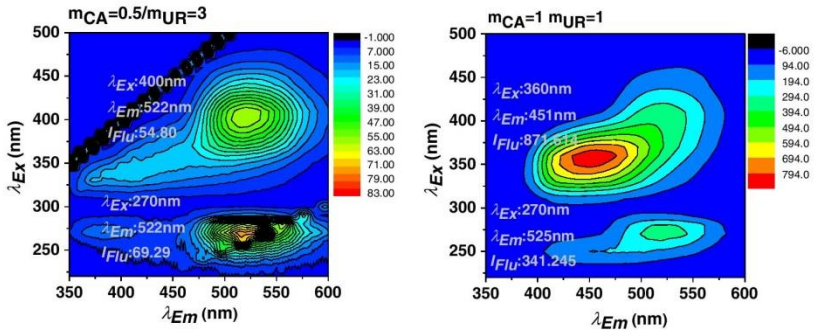


Fig. 1 Typical Excitation Emission Matrices (EEM) of selected CDs [m_{CA} (g)/m_{UR} (g)]

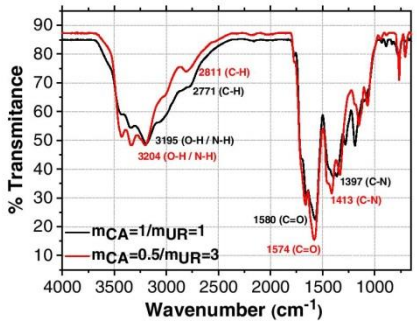


Fig. 2 FTIR spectra of selected CDs [m_{CA} (g)/m_{UR} (g)]

Fe^{2+}, or by possible light scattering due to the formation of ferric hydroxides at this pH. These CDs are probably sensitive to the $HO^{\cdot}$ at pH 9.

Considering the more sensitive response and the good selectivity for ClO^- at pH 4 and for $ONOO^-$ at pH 9, with the CDs prepared respectively with m_{CA} = 1 g/m_{UR} = 3 g and m_{CA} = 1 g/m_{UR} = 1 g, these CDs were chosen in order to evaluated their sensitivity and selectivity in their determination.

An evaluation of the fluorescence detection capability of the selected CDs to the ClO^- at pH 4 and to the $ONOO^-$ at pH 9 in a range of concentrations from 2.5 to 200 μM was done. The same evaluation was also performed for the $HO^{\cdot}$ at pH 4 and for the NO at pH 9. Similar prepared CDs with similar characteristics, higher content of urea (m_{CA} = 0.5 g/m_{UR} = 3 g) and a similar content of the two compounds (m_{CA} = 3 g/m_{UR} = 3 g), were also used for comparison. The results shows the linear fit parameters found in the more adequate concentration range (Table S1).

By the analysis of the slope of the linear fit obtained it is possible to see that the greatest sensitivity is found for ClO^- at pH 4 with the CDs prepared with a m_{CA} = 0.5 g/m_{UR} = 3 g and for $ONOO^-$ at pH 9 with a m_{CA} = 1 g/m_{UR} = 1 g. Also, for the ClO^- at pH 4, a close sensitivity is found with the prepared CDs with a m_{CA} = 1 g/m_{UR} = 3 g. For the $HO^{\cdot}$ at pH 4 the lowest sensitivity was observed with the prepared CDs with a m_{CA} = 1 g/m_{UR} = 1 g and for the NO at pH 9 with m_{CA} = 0.5 g/m_{UR} = 3 g. In comparison with the sensitivity found for the $HO^{\cdot}$ at pH 4 and for the NO at pH 9 a five times difference was obtained respectively for the ClO^- and for the $ONOO^-$. The lowest differences (4 ×) were found for the ClO^- at pH 4 and $ONOO^-$ at pH 9 with the CDs prepared with the same content of citric acid and urea. The greatest difference (29 ×) was found for the $ONOO^-$ at pH 9, in comparison with the found for NO at pH 9, for the CDs prepared with a m_{CA} = 0.5 g/m_{UR} = 3 g. It is also possible to observe that a similar linear correlation coefficient and a different linear range were obtained for all the evaluations with the ClO^- at pH 4 and with the $ONOO^-$ at pH 9.

This assessment allows to conclude that the more sensitive and selective CDs were the following: for the ClO^- at pH 4, are the CDs prepared with a m_{CA} = 0.5 g/m_{UR} = 3 g; and, for the $ONOO^-$ at pH 9, are the ones prepared with a m_{CA} = 1 g/m_{UR} = 1 g. The characterization of these CDs and the quantification capability of ClO^- at pH 4 and of $ONOO^-$ at pH 9 for these two selected CDs will be now assessed.

Characterization of carbon dots (CDs)

The characterization of the CDs prepared in the selected synthesis conditions was done by fluorescence, FTIR and TEM analysis. In order to comparison, the same analysis was also done for the CDs in the other synthesis conditions initially evaluated and an overall discussion was performed.

Figure 1 presents the fluorescence excitation-emission matrices of the CDs prepared in the selected conditions. In supplementary information, beside the fluorescence excitation-emission matrices of the CDs prepared in other synthesis

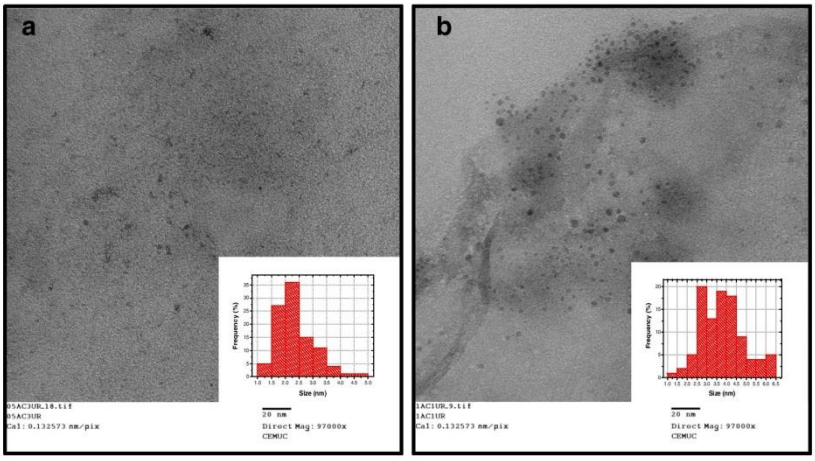


Fig. 3 Images and particle size distribution obtained by TEM analysis of selected CDs [**a** m_{CA} = 0.5 g, m_{UR} = 3.0 g; **b** m_{CA} = 1.0 g, m_{UR} = 1.0 g]

Table 1 Evaluation of the ClO^- quantification capability at pH 4 of selected CDs [m_{CA} (g)/m_{UR} (g)]

[ClO^-] (μM)	Standard solutions			Spiked serum sample (100 ×)		
CDs (m_{CA} = 0.5/m_{UR} = 3)						
Expected	**10**	**25**	**50**	**10**	**25**	**50**
Estimated	10.1 ± 22.6	26.8 ± 22.1	44.2 ± 21.8	9.7 ± 22.6	25.0 ± 22.1	45.3 ± 21.7
Recovery(%)	101.2	107.4	88.5	96.6	99.9	90.6
CDs (m_{CA} = 1/m_{UR} = 1)						
Expected	**10**	**25**	**50**	**10**	**25**	**50**
Estimated	8.5 ± 7.6	23.0 ± 7.5	53.6 ± 9.6	5.4 ± 7.8	9.2 ± 7.6	13.8 ± 7.5
Recovery(%)	85.6	92.0	107.3	54.5	36.8	27.5

The numbers in bold are the expected concentrations of the standard and spiked serum sample solutions. The ± term is the interpolated standard deviation (s_{xi})

conditions (Fig. S2), also contains the main fluorescence features (Table S2) as well the normalized absorbance excitation and emission fluorescence spectra (Fig. S3) of all CDs samples.

A greater maximum excitation and emission wavelength were found for the CDs in the selected synthesis conditions with a greater content of urea. The overall analysis of the fluorescence excitation-emission matrices shows that the synthesized CDs have fluorescence characteristics highly dependent of the m_{CA} and a m_{UR} used for their synthesis. Increasing m_{UR} and m_{CA} results in higher and lower, respectively, λ_{EX}, λ_{EM} and Φ for the principal fluorescence band. These different fluorescence characteristics are also revealed by the analysis of their absorbance spectra where two bands are observed (334 and 408 nm) for the CDs prepared with a higher content of urea and with 3 g of urea and citric acid. The band at 408 nm is less evident for the prepared CDs with 1 g of citric acid and urea and only one band at 336–338 nm with a small shoulder around 400–404 nm is found for the prepared CDs with a higher content of citric acid.

An evaluation of the influence of the pH and ionic strength in the fluorescence of these CDs and of their fluorescence stability was done in order to evaluate the better conditions for the ClO^- and $ONOO^-$ fluorescence detection (supplementary information).

Depending of the CDs a different influence of the ionic strength and pH is evaluated (Fig. S4 and S5). A reduced influence of the ionic strength in the fluorescence was observed for the CDs prepared in the selected conditions. Also the great stability for these CDs between a pH 4 and 9 suggests this pH range for fluorescence detection. A greater effect of the pH and ionic strength is observed for the CDs prepared with a greater content of citric acid and lowest content of urea. The CDs, prepared with 0.5 g of urea, are more sensitive to the pH with a great increase of the fluorescence intensity until a pH 7 and posterior decrease at a pH above 7.

The more photo-stable prepared CDs are the ones with a higher content of urea followed by the ones with same content of citric acid and urea and the less stable are the ones with a higher content of citric acid (Fig. S6). Also a good stability, evaluated by the variation of the fluorescence intensity for a long time in the dark, was observed for the CDs prepared with a higher content of urea and a worse stability were found with the ones with a higher content of citric acid and with the same content of citric acid and urea (Table S3).

The FTIR spectra of the selected CDs are presented in Fig. 2. The FTIR spectra of the CDs prepared in other synthesis conditions and a summary of the wavenumbers of the principal IR bands of all CDs samples are presented in supplementary information (Fig. S7 and Table S4).

Major differences are observed between the FTIR spectra of the prepared CDs with a higher content of urea or with the

Table 2 Evaluation of the $ONOO^-$ quantification capability at pH 9 of selected CDs

[$ONOO^-$] (μM)	Standard solutions			Spiked serum sample (100 ×)		
CDs (m_{CA} = 0.5/m_{UR} = 3)						
Expected	**10**	**25**	**50**	**10**	**25**	**50**
Estimated	10.0 ± 3.4	26.1 ± 3.4	51.8 ± 4.2	6.5 ± 3.5	22.7 ± 3.4	41,3 ± 3.8
Recovery(%)	100.5	104.4	103.6	65.1	91.0	82.5
CDs (m_{CA} = 1 g,/m_{UR} = 1)						
Expected	**10**	**25**	**50**	**10**	**25**	**50**
Estimated	9.3 ± 3.4	22.9 ± 3.3	49.0 ± 3.4	8.8 ± 3.4	22.3 ± 3.3	43.5 ± 3.3
Recovery(%)	93.4	91.5	98.0	79.8	89.1	87.0

See the footnote of Table 1

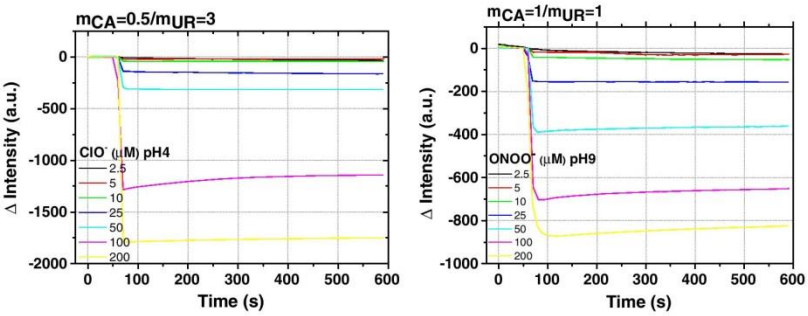


Fig. 4 Typical fluorescence time profiles of selected CDs by addition of ClO^- at pH 4 and of $ONOO^-$ at pH 9 [m_{CA} (g)/m_{UR} (g)]

same quantity of the two compounds and the ones with a higher content of citric acid. Slightly different wavenumbers are found for the broad and strong bands due to the –OH/–NH above 3000 cm^{-1}, for the sharp bands due to the C = O between 1500 and 2000 cm^{-1} and for the sharp bands due to the –CO, –CN and –CH between 1000 and 1500 cm^{-1}.

In Fig. 3 are presented the TEM images and the particle size distribution evaluated by TEM analysis of CDs prepared in the selected synthesis conditions. The TEM images with the particle size distribution of the other prepared CDs and the shape and particle size found by TEM analysis of all the CDs are also presented in supplementary information (Fig. S8 and Table S5).

A similar spherical or quasi spherical shape was observed by TEM for the CDs in the selected synthesis conditions. For a number of 100 nanoparticles an average particle size of 2.3 and 3.8 nm and a standard deviation of 0.7 and 1.1 were evaluated respectively for the synthesized CDs with a m_{CA} = 0.5 g, m_{UR} = 3 g and with a m_{CA} = 1.0 g, m_{UR} = 1.0 g. A more homogeneous particle size distribution was found for the ones prepared with m_{CA} = 0.5 g and a m_{UR} = 3 g. A slightly different average particle size with a similar shape was found with the other CDs. The lowest particle size was found for the prepared CDs with m_{CA} = 0.5 g and a m_{UR} = 3 g and the highest particle size (average particle size 8.1 nm, standard deviation 2.7) was found for the prepared CDs with a m_{CA} and a m_{UR} of 3 g.

ClO^- and $ONOO^-$ quantification

The quantification capability of ClO^- at pH 4 and of $ONOO^-$ at pH 9 by the CDs prepared with a m_{CA} = 0.5 g/m_{UR} = 3 g and with a m_{CA} = 1 g/m_{UR} = 1 g were evaluated in standard and in spiked serum sample solutions. The results found are presented in Tables 1 and 2. In supplementary information are also presented the linear fit parameters obtained (Table S6).

For the ClO^- better quantification results were found for the CDs prepared with a m_{CA} = 0.5 g/m_{UR} = 3 g. Good recoveries were obtained with the standard solutions with both CDs. Lowest recoveries were found in the evaluation of spiked serum samples for the prepared CDs with a m_{CA} = 1 g/m_{UR} = 1 g. In comparison, with the prepared CDs with a m_{CA} = 1 g/m_{UR} = 1 g, were now found for the CDs with a m_{CA} = 0.5 g/m_{UR} = 3 g the same linear correlation coefficient (r = −0.996), a similar slope (b = −9), a larger linear range (5–200 μM) and a higher limit of detection (2.0 μM). The lowest limit of detection (0.5 μM) is obtained with the CDs prepared with a m_{CA} = 1 g/m_{UR} = 1 g.

For the $ONOO^-$ better quantification results were observed for the CDs prepared with a m_{CA} = 1 g/m_{UR} = 1 g. Good recoveries were obtained with the standard solutions and spiked serum samples with both CDs. Slightly worst estimates were obtained with the spiked serum samples for the prepared CDs with a m_{CA} = 0.5 g/m_{UR} = 3 g. For the CDs prepared with a m_{CA} = 1 g/m_{UR} = 1 g, and considering the obtained with the CDs with a m_{CA} = 0.5 g/m_{UR} = 3 g, a higher linear correlation

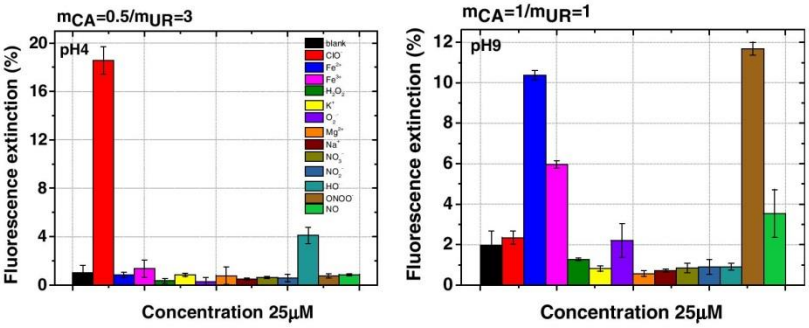


Fig. 5 Fluorescence quenching effect obtained by addition of ROS/RNS or ionic species to the selected CDs [m_{CA} = 0.5 g /m_{UR} = 3 g for ClO^- at pH 4 and m_{CA} = 1 g /m_{UR} = 1 g for $ONOO^-$ at pH 9]

(r = −0.9997), a higher slope (b = −8), a larger linear range (2.5–100 μM) and a lower limit of detection (1.5 μM) were found.

In Fig. 4 are presented typical fluorescence quenching time profiles of the CDs prepared with a m_{CA} = 0.5 g/m_{UR} = 3 g and with a m_{CA} = 1 g/m_{UR} = 1 g by addition respectively of ClO^- at pH 4 and of $ONOO^-$ at pH 9.

Similar fluorescence quenching time profiles are obtained at pH 4 by addition of ClO^- and at pH 9 by addition of $ONOO^-$ respectively to prepared CDs with a m_{CA} = 0.5 g/m_{UR} = 3 g and with a m_{CA} = 1 g/m_{UR} = 1 g. A fast fluorescence intensity decrease followed by a constant intensity was observed - a small increase was observed for higher ClO^- and $ONOO^-$ concentrations.

The fluorescence quenching mechanism is probably due to a pH dependent redox reaction between the ClO^- or $ONOO^-$ and the CDs surface oxygen and nitrogen functionalities and dangling bonds. Indeed, the fluorescence of CD are markedly affected by the surface chemistry and the oxidation of surface functionalities modified those properties [42]. Both ClO- and ONOO- are strong oxidant species, whose oxidation reaction extent depends on the protonation state of the reagents. In this work the results showed that this reaction is more favourable for the ClO- at pH 4 and for the ONOO- at pH 9.

Considering the previous results obtained and previous related Fe^{3+} detection by synthesized CDs with a m_{CA} = 3 g/m_{UR} = 3 g [17], an evaluation of the selectivity with the selected CDs for the ROS/RNS, Fe^{2+}, Fe^{3+} and some other common ionic species was performed. The results obtained are presented in Fig. 5 and in supplementary information (Fig. S9).

The analysis of Fig. 5 and Fig. S9 shows that both evaluated CDs are sensitive to the pair Fe^{2+}/Fe^{3+} at pH 9. The more selective response to the $HO^{\cdot}$ at pH 4 and to the NO at pH 9 were found respectively with the CDs prepared with a m_{CA} = 1 g/m_{UR} = 1 g and with a m_{CA} = 0.5 g/m_{UR} = 3 g. Also at pH 9 a higher response to the $ONOO^-$ in comparison to the obtained with the Fe^{3+} is found with both CDs and for the for the pair Fe^{2+} and Fe^{3+} with the CDs prepared with a m_{CA} = 1 g/m_{UR} = 1 g. This analysis shows a good selectivity for the ClO^- and $ONOO^-$ with both synthesized CDs at the two pHs.

Table 3 shows the comparison of the sensor characteristics of the current methodology with published reports using CDs for the quantification of ClO^- and of $ONOO^-$.

The sensing characteristics of the CDs described in this paper are globally similar to others described in the literature, with the exception of the worse limit of detection for ClO^-. However, this limitation is due to use of a low power source. A posterior evaluation with a more powerful radiation source using a standard spectrofluorimeter shows a global improvement of the figures of merit of the present sensor based CD (Table S7).

Table 3 Comparison of ClO^- and $ONOO^-$ quantification by the selected CDs with the quantification by CDs used in previous literature reports

CDs		Fluorescence detection			Figures of merit			Ref.
Precursor/Synthesis	Φ (%)	pH	λ_{Ex} (nm)	λ_{EM} (nm)	LR (μM)	LOD (μM)	Sensitivity (a.u./μM^{-1})	Selectivity (possible interferents)	
ClO^-									
—	—	7.4	360	448	0.03–15	0.001	—	Good(TBO$^{\cdot}$, Fe^{2+}, $HO^{\cdot}$)	[37]
SU,PA/Microwave	14.2	5.0	410	512	0.2–2	0.015	n.p.	Good (MnO_4^-)	[38]
Pepper /Autoclave	19.3	8.0	360 (780)	460	0.1–10/10–300	0.05/0.06	12×10^{-3}/2.4×10^{-3}	Good[a]	[39]
CA,UR /Microwave	7.5	4.0	400	522	5–200/2.5–50	2.0/0.5	8.7	Good (Fe^{3+}, $HO^{\cdot}$)/Good (Fe^{3+})	Our work
$ONOO^-$									
CA,EDA /Microwave	39.7	7/10	360	460	5–100/5–100	2.7/2.0	31.1/40.2	Good [$HO^{\cdot}$(pH 7)]	[35]
GL,TRY /Microwave	12.4	7.4	370	486	5–25	1.5	3.25	Good[a]	[36]
CA,UR/Microwave	10.2	9.0	360	451	2.5–50/2.5–100	2.9/1.5	7.5	Good (Fe^{2+}, Fe^{3+}, NO)/Good (Fe^{2+}, Fe^{3+}, HO)	Our work

Φ Quantum yield, λ_{EM} Emission wavelength at maximum fluorescence intensity, *LR* Linear range. The value presented in brackets is the calculated ratio between the highest and the lowest concentration of the evaluated linear range; *LOD* Limit of detection, — not possible to see, *n.p.* not presented, *TBO* tert-butoxy radical, *SU* Sucrose, *PA* Phosphoric acid, *AC* Autoclave, *CA* Citric acid, *UR* Urea, *EDA* 1,2-ethylenediamine, *GL* Glucose, *TRY* Tryptophan

[a] In ref. [36] only ionic species and in ref. [33] only ROS/RNS were evaluated

Conclusions

CDs with different citric acid and urea content were obtained and were used for the quantification of ClO^- at pH 4 and of $ONOO^-$ at pH 9 through a fluorescence quenching mechanism. A less sensitive and selective detection of the ClO^- and $ONOO^-$ was evaluated with these CDs at pH 7. Good quantification results were found with the standard and the spiked dilute serum samples. The better quantification results with greater sensitivity and selectivity were found for the ClO^- at pH 4 with a m_{CA} = 0.5 g/m_{UR} = 3 g and for the $ONOO^-$ at pH 9 with a m_{CA} = 1 g/m_{UR} = 1 g. The quantification of ClO^- and $ONOO^-$ it's also possible with each of these two CDs, prepared with the same synthesis conditions, only through the pH variation.

Acknowledgments A PhD grant SFRH/BD/81074/2011 to Eliana Simões and financial support, project PTDC/QEQQAN/5955/2014, from Fundação para a Ciência e Tecnologia (FCT, Lisbon) are acknowledged. The use of FTIR from UCQFarma, Pharmacy Faculty of the University of Coimbra and the TEM analyses from Nanomaterials and Micromanufacturing group of Centre for Mechanical Engineering of the University of Coimbra (CEMUC) are also acknowledged.

Compliance with ethical standards The author(s) declare that they have no competing interests.

References

1. Xu X, Ray R, Gu Y, Ploehn HJ, Gearheart L, Raker K, Scrivens WA (2004) Electrophoretic analysis and purification of fluorescent single-walled carbon nanotube fragments. J Am Chem Soc 126(40):12736–12737. doi:10.1021/ja040082h
2. Zuo P, Lu X, Sun Z, Guo Y, He H (2016) A review on syntheses, properties, characterization and bioanalytical applications of fluorescent carbon dots. Microchimica Acta 183:519–542. doi:10.1007/s00604-015-1705-3
3. Yang Z, Li Z, Xu M, Ma Y, Zhang J, Su Y, Gao F, Wei H, Zhang L (2013) Controllable synthesis of fluorescent carbon dots and their detection application as nanoprobes. Nano-Micro Lett 5(4):247–259. doi:10.1007/BF03353756
4. Lim SY, Shen W, Gao Z (2015) Carbon quantum dots and their applications. Chem Soc Rev 44(1):362–381. doi:10.1039/C4CS00269E
5. Ma N, Jiang W, Li T, Zhang Z, Qi H, Yang M (2014) Fluorescence aggregation assay for the protein biomarker mucin 1 using carbon dot-labeled antibodies and aptamers. Microchim Acta 182(1–2):443–447. doi:10.1007/s00604-014-1386-3
6. Kang W, Ding Y, Zhou H, Liao Q, Yang X, Yang Y, Jiang J, Yang M (2014) Monitoring the activity and inhibition of alkaline phosphatase via quenching and restoration of the fluorescence of carbon dots. Microchim Acta 182(5–6):1161–1167. doi:10.1007/s00604-014-1439-7
7. Hu Q, Paau MC, Zhang Y, Chan W, Gong X, Zhang L, Choi MM (2013) Capillary electrophoretic study of amine/carboxylic acid-functionalized carbon nanodots. J Chromatogr A 1304:234–240. doi:10.1016/j.chroma.2013.07.035
8. Du F, Zeng F, Ming Y, Wu S (2013) Carbon dots-based fluorescent probes for sensitive and selective detection of iodide. Microchim Acta 180(5–6):453–460. doi:10.1007/s00604-013-0954-2
9. Salinas-Castillo A, Ariza-Avidad M, Pritz C, Camprubi-Robles M, Fernandez B, Ruedas-Rama MJ, Megia-Fernandez A, Lapresta-Fernandez A, Santoyo-Gonzalez F, Schrott-Fischer A, Capitan-Vallvey LF (2013) Carbon dots for copper detection with down and upconversion fluorescent properties as excitation sources. Chem Commun 49(11):1103–1105. doi:10.1039/c2cc36450f
10. Hou X, Zeng F, Du F, Wu S (2013) Carbon-dot-based fluorescent turn-on sensor for selectively detecting sulfide anions in totally aqueous media and imaging inside live cells. Nanotechnology 24(33):335502. doi:10.1088/0957-4484/24/33/335502
11. Yu C, Wu Y, Zeng F, Wu S (2013) A fluorescent ratiometric nanosensor for detecting NO in aqueous media and imaging exogenous and endogenous NO in live cells. J Mater Chem B 1(33):4152. doi:10.1039/c3tb20686f
12. Zhai X, Zhang P, Liu C, Bai T, Li W, Dai L, Liu W (2012) Highly luminescent carbon nanodots by microwave-assisted pyrolysis. Chem Commun 48(64):7955–7957. doi:10.1039/c2cc33869f
13. Milosavljevic V, Moulick A, Kopel P, Adam V, Kizek R (2014) Microwave preparation of carbon quantum dots with different surface modification. J Metallomics Nanotechnol 3:16–22
14. Wang Q, Zhang C, Shen G, Liu H, Fu H, Cui D (2014) Fluorescent carbon dots as an efficient siRNA nanocarrier for its interference therapy in gastric cancer cells. J Nanobiotechnol 12(1):58. doi:10.1186/s12951-014-0058-0
15. Bourlinos AB, Trivizas G, Karakassides MA, Baikousi M, Kouloumpis A, Gournis D, Bakandritsos A, Hola K, Kozak O, Zboril R, Papagiannouli I, Aloukos P, Couris S (2015) Green and simple route toward boron doped carbon dots with significantly enhanced non-linear optical properties. Carbon 83:173–179. doi:10.1016/j.carbon.2014.11.032
16. He L, Wang T, An J, Li X, Zhang L, Li L, Li G, Wu X, Su Z, Wang C (2014) Carbon nanodots@zeolitic imidazolate framework-8 nanoparticles for simultaneous pH-responsive drug delivery and fluorescence imaging. CrystEngComm 16(16):3259–3263. doi:10.1039/C3CE42506A
17. Qu S, Chen H, Zheng X, Cao J, Liu X (2013) Ratiometric fluorescent nanosensor based on water soluble carbon nanodots with multiple sensing capacities. Nanoscale 5(12):5514–5518. doi:10.1039/C3NR00619K
18. Qu S, Wang X, Lu Q, Liu X, Wang L (2012) A biocompatible fluorescent ink based on Water-soluble luminescent carbon nanodots. Angew Chem Int Ed 51(49):12215–12218. doi:10.1002/anie.201206791
19. Xu M, He G, Li Z, He F, Gao F, Su Y, Zhang L, Yang Z, Zhang Y (2014) A green heterogeneous synthesis of N-doped carbon dots and their photoluminescence applications in solid and aqueous states. Nanoscale 6(17):10307–10315. doi:10.1039/C4NR02792B
20. Stefanakis D, Philippidis A, Sygellou L, Filippidis G, Ghanotakis D, Anglos D (2014) Synthesis of fluorescent carbon dots by a microwave heating process: structural characterization and cell imaging applications. J Nanoparticle Res 16(10):1–10. doi:10.1007/s11051-014-2646-1
21. Dey S, Chithaiah P, Belawadi S, Biswas K, Rao CNR (2014) New methods of synthesis and varied properties of carbon quantum dots with high nitrogen content. J Mater Res 29(03):383–391. doi:10.1557/jmr.2013.295
22. Valko M, Leibfritz D, Moncol J, Cronin MT, Mazur M, Telser J (2007) Free radicals and antioxidants in normal physiological functions and human disease. Int J Biochem Cell Biol 39(1):44–84. doi:10.1016/j.biocel.2006.07.001
23. Bergendi L, Beneš L, Ďuračková Z, Ferenčik M (1999) Chemistry, physiology and pathology of free radicals. Life Sci 65(18–19):1865–1874. doi:10.1016/S0024-3205(99)00439-7
24. Tarpey MM, Wink DA, Grisham MB (2004) Methods for detection of reactive metabolites of oxygen and nitrogen: in vitro and in vivo

considerations. Am J Physiol Regul Integr Comp Physiol 286(3): R431–R444. doi:10.1152/ajpregu.00361.2003
25. Borgmann S (2009) Electrochemical quantification of reactive oxygen and nitrogen: challenges and opportunities. Anal Bioanal Chem 394(1):95–105. doi:10.1007/s00216-009-2692-1
26. Kalyanaraman B, Darley-Usmar V, Davies KJ, Dennery PA, Forman HJ, Grisham MB, Mann GE, Moore K, Roberts LJ 2nd, Ischiropoulos H (2012) Measuring reactive oxygen and nitrogen species with fluorescent probes: challenges and limitations. Free Radic Biol Med 52(1):1–6. doi:10.1016/j.freeradbiomed.2011.09.030
27. Schäferling M, Grögel DBM, Schreml S (2011) Luminescent probes for detection and imaging of hydrogen peroxide. Microchim Acta 174(1–2):1–18. doi:10.1007/s00604-011-0606-3
28. Uusitalo LM, Hempel N (2012) Recent advances in Intracellular and In vivo ROS Sensing: focus on nanoparticle and nanotube applications. Int J Mol Sci 13(9):10660–10679. doi:10.3390/ijms130910660
29. Adegoke O, Forbes PB (2015) Challenges and advances in quantum dot fluorescent probes to detect reactive oxygen and nitrogen species: a review. Anal Chim Acta 862:1–13. doi:10.1016/j.aca.2014.08.036
30. Shan X, Chai L, Ma J, Qian Z, Chen J, Feng H (2014) B-doped carbon quantum dots as a sensitive fluorescence probe for hydrogen peroxide and glucose detection. Analyst 139(10):2322–2325. doi:10.1039/c3an02222f
31. Song Y, Zhu S, Xiang S, Zhao X, Zhang J, Zhang H, Fu Y, Yang B (2014) Investigation into the fluorescence quenching behaviors and applications of carbon dots. Nanoscale 6(9):4676–4682. doi:10.1039/c4nr00029c
32. Wu G, Zeng F, Yu C, Wu S, Li W (2014) A ratiometric fluorescent nanoprobe for H2O2 sensing and in vivo detection of drug-induced oxidative damage to the digestive system. J Mater Chem B 2(48): 8528–8537. doi:10.1039/C4TB01432D
33. Du F, Min Y, Zeng F, Yu C, Wu S (2014) A targeted and FRET-based ratiometric fluorescent nanoprobe for imaging mitochondrial hydrogen peroxide in living cells. Small 10(5):964–972. doi:10.1002/smll.201302036
34. Yeh TY, Wang CI, Chang HT (2013) Photoluminescent C-dots@RGO for sensitive detection of hydrogen peroxide and glucose. Talanta 115:718–723. doi:10.1016/j.talanta.2013.06.035
35. Simões EFC, Esteves da Silva JCG, Leitão JMM (2015) Peroxynitrite and nitric oxide fluorescence sensing by ethylenediamine doped carbon dots. Sensors Actuators B Chem 220:1043–1049. doi:10.1016/j.snb.2015.06.072
36. Simoes EF, da Silva JC, Leitao JM (2014) Carbon dots from tryptophan doped glucose for peroxynitrite sensing. Anal Chim Acta 852:174–180. doi:10.1016/j.aca.2014.08.050
37. Wang D, Xu H, Zheng B, Li Y, Liu M, Du J, Xiao D (2015) N-doped carbon dots with high sensitivity and selectivity for hypochlorous acid detection and its application in water. Anal Methods 7(12):5311–5317. doi:10.1039/C5AY00944H
38. Huang Z, Lin F, Hu M, Li C, Xu T, Chen C, Guo X (2014) Carbon dots with tunable emission, controllable size and their application for sensing hypochlorous acid. J Lumin 151:100–105. doi:10.1016/j.jlumin.2014.02.013
39. Yin B, Deng J, Peng X, Long Q, Zhao J, Lu Q, Chen Q, Li H, Tang H, Zhang Y, Yao S (2013) Green synthesis of carbon dots with down- and up-conversion fluorescent properties for sensitive detection of hypochlorite with a dual-readout assay. Analyst 138(21): 6551–6557. doi:10.1039/c3an01003a
40. Gao X, Ding C, Zhu A, Tian Y (2014) Carbon-dot-based ratiometric fluorescent probe for imaging and biosensing of superoxide anion in live cells. Anal Chem 86(14):7071–7078. doi:10.1021/ac501499y
41. Lakowicz JR (2006) Principles of fluorescence spectroscopy. Springer, New York, pp. 54–55
42. Ding H, Yu S-B, Wei J-S, Xiong H-M (2016) Full-color light-emitting carbon dots with a surface-state-controlled luminescence mechanism. ACS Nano 10(1):484–491. doi:10.1021/acsnano.5b05406

Carbon dots prepared from citric acid and urea as fluorescent probes for hypochlorite and peroxynitrite

Eliana F. C. Simões[a,b], João M.M. Leitão [a,*] and Joaquim C.G. Esteves da Silva [b]

[a,*] Centro de investigação em química da Universidade do Porto (CIQ-UP), Faculdade de Farmácia da Universidade de Coimbra, Pólo das Ciências da Saúde, 3000-548 Coimbra, Portugal

[b] Centro de investigação em química da Universidade do Porto (CIQ-UP), Departamento de Química, Faculdade de Ciências da Universidade do Porto, R. Campo Alegre 687, 4169-007 Porto, Portugal

Supplementary information

1. ClO^- and $ONOO^-$ detection

In Fig. S1 are presented the results obtained by the assessment of the response of the CDs prepared in all the evaluated experimental conditions at three concentrations levels of ClO^-, $ONOO^-$, H_2O_2, $O_2^{\cdot-}$, NO, and $HO^{\cdot}$ at pHs 4, 7 and 9.

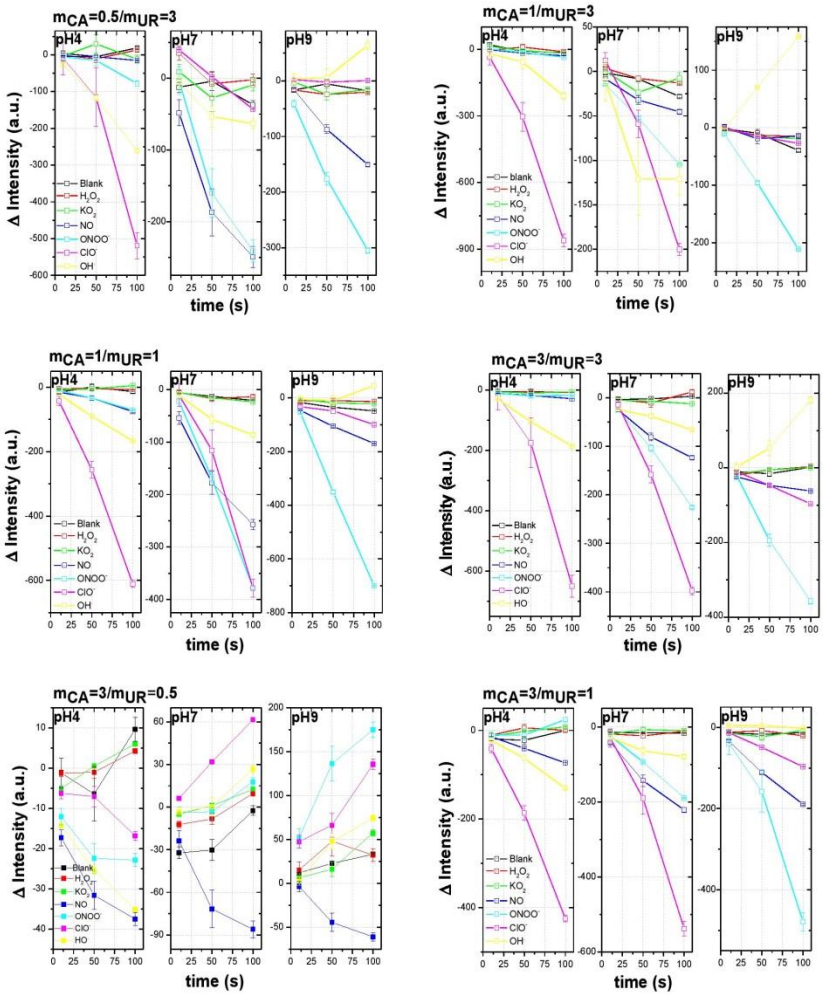


Fig. S1 – Fluorescence ClO^-, $ONOO^-$, H_2O_2, $O_2^{\cdot-}$, NO, and $HO^{\cdot}$ detection assessment of the CDs prepared in all the evaluated synthesis conditions [m_{CA} (g)/m_{UR} (g)].

In Table S1 are presented the linear fit parameters found in the more adequate concentration range of ClO^- and $HO^\cdot$ at pH 4 and of $ONOO^-$ and NO at pH 9 with the CDs prepared in the selected synthesis conditions.

Table S1 – Evaluation of ClO^- and $HO^\cdot$ (pH 4) and of $ONOO^-$ and NO (pH 9) fluorescence sensing capability of the CDs prepared in the selected synthesis conditions.*

m_{CA} (g), m_{UR} (g) / Φ	pH4		pH9	
	ClO^-	**$HO^\cdot$**	**$ONOO^-$**	**NO**
m_{CA} = 0.5, m_{UR} = 3 / Φ = 7.5 %	a = 12.3 ± 32.7 b = -12.4 ± 0.7 r = -0.9938 5 – 100 µM m = 5	a = 7.9 ± 8.3 b = -2.7 ± 0.2 r = -0.9947 5 – 100 µM m = 5	a = -14.4 ± 8.5 b = -2.9 ± 0.2 r = -0.9953 2.5 – 100 µM m = 6	a = -3.9 ± 1.4 b = -0.1 ± 0.01 r = 0.9793 10 – 200 µM m = 5
m_{CA} = 1, m_{UR} = 3 / Φ = 7.7 %	a = 159.5 ± 56.2 b = -10.8 ± 1.0 r = -0.9919 10 – 100 µM m = 4	a = 4.4 ± 4.5 b = -2.3 ± 0.1 r = -0.9979 5 – 100 µM m = 5	a = 13.9 ± 4.5 b = -2.3 ± 0.1 r = -0.9988 10 – 100 µM m = 4	a = 1.1 ± 3.8 b = -0.5 ± 0.04 r = -0.9902 10 – 200 µM m = 5
m_{CA} = 1, m_{UR} = 1 / Φ = 10.2 %	a = 35.1 ± 18.9 b = -6.9 ± 0.4 r = -0.9932 2.5 – 100 µM m = 6	a = -4.4 ± 3.3 b = -1.3 ± 0.04 r = -0.9977 2.5 – 200 µM m = 7	a = 3.5± 13.8 b = -6.7 ± 0.3 r = -0.9936 5 – 100 µM m = 5	a = -20.9 ± 5.6 b = -1.3 ± 0.1 r = -0.9960 5 – 200 µM m = 6
m_{CA} = 3, m_{UR} = 3 / Φ = 10.8 %	a = 119.7 ± 61.9 b = -7.8 ± 1.1 r = -0.9817 10 – 100 µM m = 4	**a** = 3.7 ± 8.7 **b** = -1.9 ± 0.1 r = -0.9817 10 – 200 µM m = 6	a = 16.2 ± 7.9 b = -3.8 ± 0.2 r = -0.9903 2.5 – 100 µM m = 6	a = -9.1 ± 2.1 b = -1.0 ± 0.04 r = -0.9957 2.5 – 100 µM m = 6

* Φ – Quantum yield; a – Intercept; b – Slope; The ± term in a and b is the standard deviation respectively of the intercept and the slope; r – Linear correlation coefficient; m – Number of calibration points.

2. CDs characterization

2.1 UV-Vis/Fluorescence

In Fig. S2 are presented the fluorescence excitation-emission matrices of the synthesized CDs in the indicated synthesis conditions. In Table S2 Are presented the principal fluorescence characteristics and in Fig. S3 the absorbance, excitation and emission normalized spectra of the CDs prepared in all the evaluated synthesis conditions.

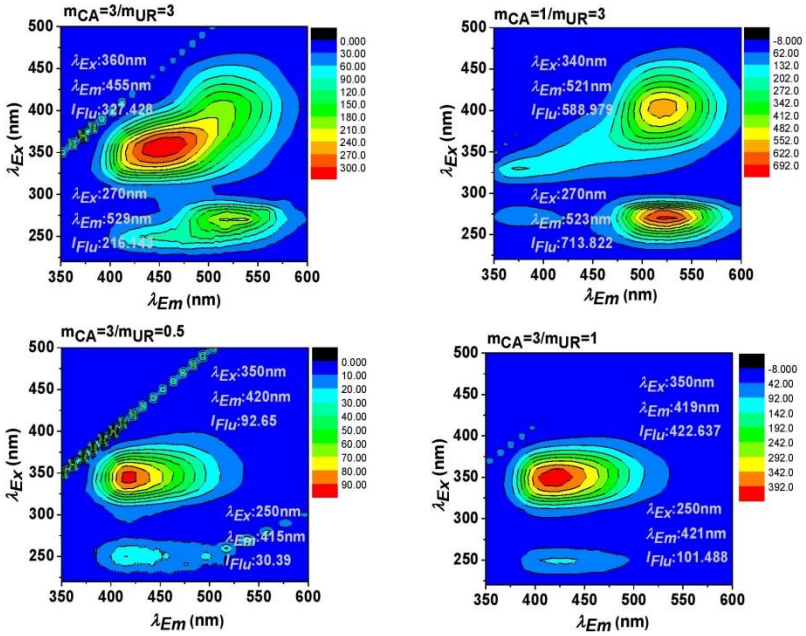


Fig. S2 – Typical Excitation Emission Matrices (EEM) of the prepared CDs in the indicated synthesis conditions [m_{CA} (g)/m_{UR} (g)].

Table S2 – Resume of the fluorescence characteristics of the CDs prepared in all the evaluated synthesis conditions.*

CDs [m_{CA} (g)/m_{UR} (g)]	Φ (%)	Fluorescence bands	
		Main [λ_{EX} (nm) /λ_{EM} (nm)]	Secondary [λ_{EX} (nm) /λ_{EM} (nm)]
m_{CA} = 0.5/m_{UR} = 3	7.5	**400 / 522**	**270 / 522**
m_{CA} = 1/m_{UR} = 3	7.7	400 / 521	270 / 523
m_{CA} = 1/m_{UR} = 1	10.2	**360 / 451 (400 / 535)**	**270 / 525**
m_{CA} = 3/m_{UR} = 3	10.8	360 / 453 (410 / 529)	270 / 516
m_{CA} = 3/m_{UR} = 0.5	12.2	350 / 420	250 / 415
m_{CA} = 3/m_{UR} = 1	12.1	350 / 419	250 / 421

* Φ – Quantum yield; λ_{EX} – Excitation wavelength at maximum fluorescence intensity; λ_{EM} – Emission wavelength at maximum fluorescence intensity; In brackets are the λ_{EX} and λ_{EM} at the maximum fluorescence intensity of the band nearest the main band.

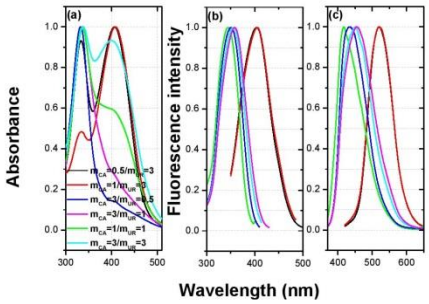


Fig. S3 – Normalized absorbance (a), excitation (b) and emission (c) spectra of the CDs prepared in all the evaluated synthesis conditions [m_{CA} (g)/m_{UR} (g)].

2.1.1 Effect of pH and ionic strength

In Fig. S4 and Fig. S5 are presented respectively the influence of the pH and of the ionic strength in the fluorescence intensity of CDs prepared in all the evaluated synthesis conditions.

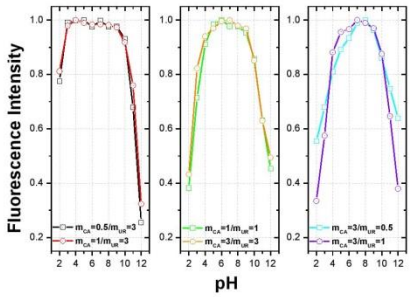


Fig. S4 – Normalized fluorescence intensity variation profiles with the pH of the CDs in all the evaluated synthesis conditions [m_{CA} (g)/m_{UR} (g)].

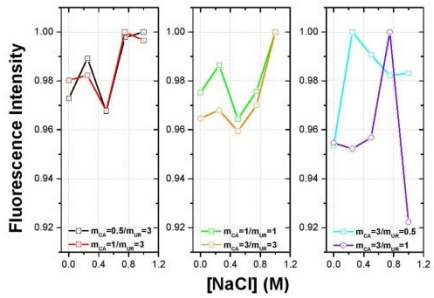


Fig. S5 – Normalized fluorescence intensity variation profiles with the ionic strength of the CDs in all the evaluated synthesis conditions [m_{CA} (g)/m_{UR} (g)].

2.1.2 Stability

In Fig. S6 is presented an evaluation of the photostability at the maximum fluorescence intensity of the principal band and in Table S3 the results found by an evaluation of the fluorescence stability with the time of the CDs prepared in all the evaluated synthesis conditions.

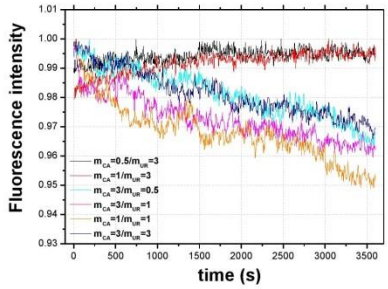


Fig. S6 – Normalized fluorescence intensity variation profiles with the time of the CDs fluorescence in all the evaluated synthesis conditions [m_{CA} (g)/m_{UR} (g)].

Table S3 – Fluorescence intensity variation at maximum fluorescence intensity of the CDs with the time prepared in all the evaluated synthesis conditions.

CDs [m_{CA} (g)/m_{UR} (g)]	Fluorescence intensity		
	Initial	Final (Elapsed time)	Variation (%)
m_{CA} = 0.5/m_{UR} = 3	54.8	49.9 (2 months)	-4.9 (9.0 %)
m_{CA} = 1/m_{UR} = 3	589.0	550.6 (2.5 months)	-38.4 (6.5 %)
m_{CA} = 1/m_{UR} = 1	871.6	515.2 (2.5 months)	-356.4 (41 %)
m_{CA} = 3/m_{UR} = 3	283.2	204.5 (2 months)	-78.7 (27.8 %)
m_{CA} = 3/m_{UR} = 0.5	92.7	78.8 (2.5 months)	-13.8 (14.9 %)
m_{CA} = 3/m_{UR} = 1	422.6	73.9 (2.5 months)	-348.8 (82.5 %)

2.2 FTIR

In Fig. S7 are presented the FTIR spectra of CA, UR and of the CDs prepared in the indicated synthesis conditions and in Table S4 the wavenumbers of the principal FTIR infrared bands found by analysis of the CDs prepared in all the evaluated synthesis conditions.

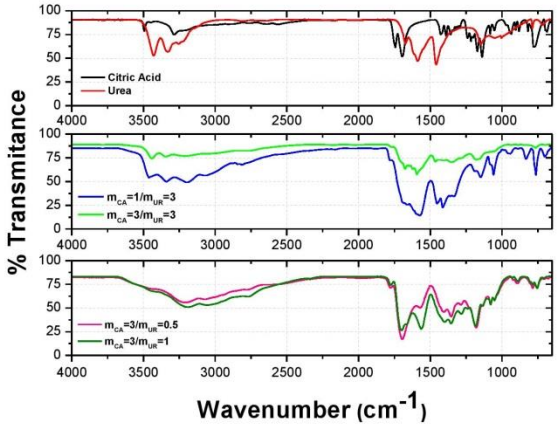


Fig. S7 – FTIR spectra of the CDs in the indicated synthesis conditions [m_{CA} (g)/m_{UR} (g)].

Table S4 – Principal FTIR infrared bands of the CDs prepared in all the evaluated synthesis conditions.*

CDs [m_{CA} (g)/m_{UR} (g)]	FTIR bands (cm^{-1})			
	O–H / N–H (3500 – 3000 cm^{-1})	**C–H (3000 – 2500 cm^{-1})**	**C=O / N-H (2000 – 1500 cm^{-1})**	**C–O / C–N / C–H (1500 – 1000 cm^{-1})**
m_{CA} = 0.5/m_{UR} = 3	3429, 3336, **3204**, 3003 (SH)	2811	1767 (SH), 1665, **1580**	**1413**, 1333, 1161, 1069
m_{CA} = 1/m_{UR} = 3	3461, 3341, **3197**, 3073 (SH)	2813	1779 (SH), 1660, **1575**	1452, **1413**, 1149, 1059
m_{CA} = 1/m_{UR} = 1	3442, 3342, **3195**, 3043 (SH)	2771	1768, 1651, **1574**	**1397**, 1362, 1281, 1181, 1098 (SH)
m_{CA} = 3/m_{UR} = 3	3441, 3347, **3211**, 3028 (SH)	2770	1774 (SH), 1676, 1622, **1590**	1464, 1410, **1354**, 1285 (SH), 1179
m_{CA} = 3/m_{UR} = 0.5	3457 (SH), **3210**, 3075	2763	1776, **1695**, 1571	1405, **1354**, 1286, 1180, 1079
m_{CA} = 3/m_{UR} = 1	3442 (SH), **3192**, 3058	2771	1776, **1704**, 1563	1400, **1354**, 1283, 1184, 1079

* For each infrared FTIR bands the wavenumbers in bold are the ones with greater transmittance; SH – shoulder.

2.3 Particle size and shape analysis

In Fig. S8 are presented the TEM images of the CDs prepared in the indicated synthesis conditions and in Table S5 are presented the results found by TEM analysis of the CDs prepared in all the evaluated synthesis conditions.

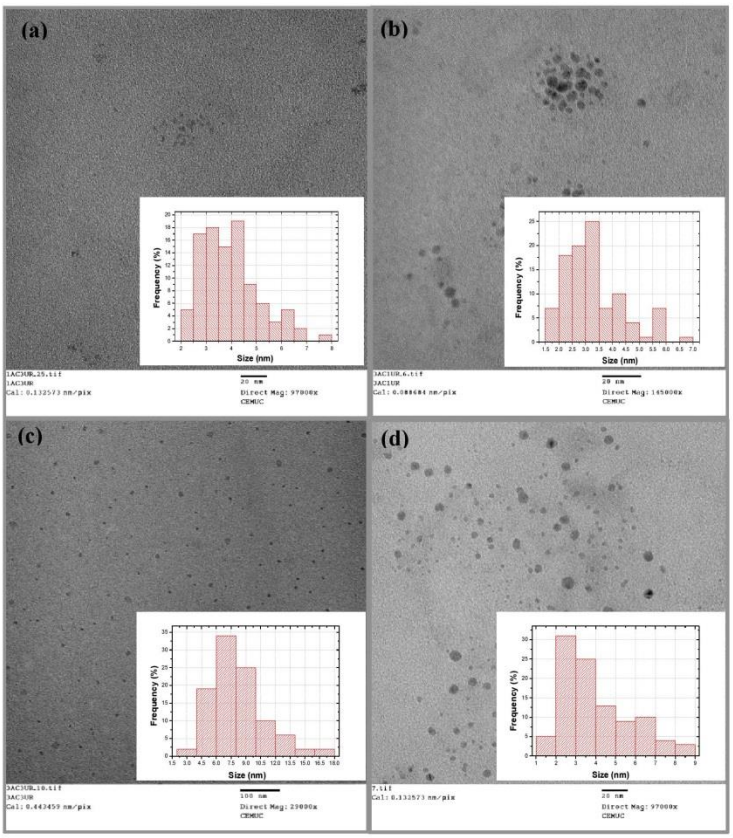


Fig. S8 – TEM images of the CDs prepared in the indicated synthesis conditions [(a) m_{CA} = 1.0 g, m_{UR} = 3.0 g; (b) m_{CA} = 3.0 g, m_{UR} = 1.0 g; (c) m_{CA} = 3.0 g, m_{UR} = 3.0 g; (d) m_{CA} = 3.0 g, m_{UR} = 0.5 g].

Table S5 – Shape and particle size found by TEM analysis of the CDs prepared in all the evaluated synthesis conditions.

CDs [m_{CA} (g)/m_{UR} (g)]	Shape	Particle size					
		n	$\bar{x}$	σ	Minimum	Maximum	Sum
m_{CA} = 0.5/m_{UR} = 3	Spherical / Quasi spherical	100	2.32	0.68	1.11	4.50	232.12
m_{CA} = 1/m_{UR} = 3	Spherical / Quasi spherical	100	4.02	1.14	2.08	3.87	402.42
m_{CA} = 1/m_{UR} = 1	Spherical / Quasi spherical	100	3.78	1.07	1.35	6.31	377.50
m_{CA} = 3/m_{UR} = 3	Spherical / Quasi spherical	100	8.13	2.66	3.56	7.55	813.13
m_{CA} = 3/m_{UR} = 0.5	Spherical / Quasi spherical	100	4.00	1.69	1.34	3.45	400.33
m_{CA} = 3/m_{UR} = 1	Spherical / Quasi spherical	100	3.30	1.08	1.71	3.10	329.82

3. ClO^- and $ONOO^-$ quantification

In Table S6 are presented the linear fit parameters, linear range and limit of detection found by addition of ClO^- and $ONOO^-$ to the selected CDs at pH 4 and 9 and in Fig. S9 the results obtained by the evaluation of the selectivity with the selected CDs for the ClO^-, $ONOO^-$, H_2O_2, $O_2^{\cdot-}$, NO, $HO^\cdot$, Fe^{2+}, Fe^{3+}, NO_3^-, NO_2^- and some other common ionic species.

Table S6 – Linear fit parameters found by addition of ClO^- at pH 4 and of $ONOO^-$ at pH 9 to the selected CDs.

ClO^- (pH 4)	**$ONOO^-$ (pH 9)**
CDs (m_{CA} = 0.5/m_{UR}= 3)	
$y = bx + a$ [$\Delta I = f([ClO^-])$]	**$y = bx + a$ [$\Delta I = f([ONOO^-])$]**
a = 71.0; s_a= 35.5	a =-5.7 ; s_a=2.2
b =-8.7; s_b=0.4	b =-3.5; s_b= 0.1
$s_{y/x}$=62.9; r = -0.9963	$s_{y/x}$=3.4; r = -0.9991
m =6 ; 5 - 200 µM, **LOD** = 2.0 µM	m = 5; 2.5 - 50 µM, **LOD** = 2.9 µM
CDs (m_{CA} = 1/m_{UR}= 1)	
a =-27.7 ; s_a=12.8	a =16.9 ; s_a=4.6
b =-9.2; s_b= 0.5	b =-7.5; s_b= 0.1
$s_{y/x}$=19.7; r = -0.9956	$s_{y/x}$=8.3; r = -0.9997
m = 5; 2.5 - 50 µM, **LOD** = 0.5 µM	m = 6; 2.5 - 100 µM, **LOD** = 1.5 µM

* a - Intercept; s_a - Intercept standard deviation; b - Slope; s_b - Slope standard deviation; $s_{y/x}$ - Standard deviation of residuals; r - Linear correlation coefficient; m - Number of calibration points; LOD – Limit of detection evaluated through the s of five determinations of a blank.

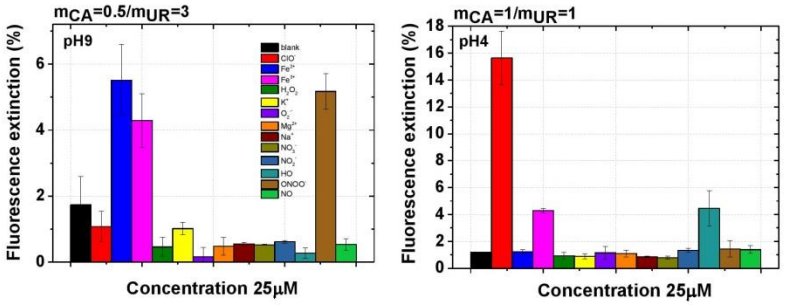


Fig. S9 – Fluorescence quenching effect obtained by addition of ClO^-, $ONOO^-$, H_2O_2, $O_2^{\cdot-}$, NO, $HO^\cdot$ and some ionic species to the selected CDs [m_{CA} = 0.5 g /m_{UR} = 3 g for $ONOO^-$ at pH 9 and m_{CA} = 1 g /m_{UR} = 1 g for ClO^- at pH 4].

In Table S7 are also presented a comparison of the linear fit parameters and limit of detection found with different instrumental conditions (more powerful LED and standard spectrofluorimeter) in a lowest and higher linear range by addition of ClO^- and $ONOO^-$ to the selected CDs at pH 4 and 9. Also a comparison of the limit of detection evaluated through the signal to noise ratio and through the standard deviation of the blank is presented.

Table S7 – Linear fit parameters and limit of detection found by addition of ClO^- at pH 4 and of $ONOO^-$ at pH 9 to the selected CDs.

CDs (m_{CA} = 0.5/m_{UR}= 3), **ClO^- (pH 4)**				
Instrumental conditions	**Linear range (µM)**	**$y = bx + a$ / r**	**$LOD_{S/N}$ (µM)**	**LOD_{blank} (µM)**
LED (385 nm)	0.1 -5	y= -1057.5x+74.1 / -0.9967	0.03	0.12
	2.5 - 100	y= -430.1+242.0 / -0.9964	---	0.28
Standard spectrofluorimeter	0.1 -5	y= -35.5x+7.4 / -0.9970	0.08	0.16
	2.5 - 50	y= -10.9x-10.2 / -0.9932	---	0.52
CDs (m_{CA} = 1/m_{UR}= 1), **$ONOO^-$ (pH 9)**				
LED (385 nm)	0.5 -5	y= -321.0x-2592.3 / -0.9903	0.01	0.56
	2.5 100	y= -197.0-2713.4 / -0.9993	---	0.92
Standard spectrofluorimeter	0.1 -5	y= -13.2x+7.2 / -0.9983	0.23	1.45
	2.5 - 50	y= -9.5x+5.1 / -0.9996	---	2.02

* *a* - Intercept; *b* - Slope; *r* - Linear correlation coefficient; $LOD_{S/N}$ – Limit of detection evaluated through the signal to noise ratio; LOD_{blank} – Limit of detection evaluated through the *s* of five determinations of a blank.

Chapter 11

Sulphur and nitrogen co-doped carbon dots sensors for nitric oxide fluorescence quantification

Eliana F. C. Simões, João M.M. Leitão, Joaquim C.G. Esteves da Silva
Analytica Chimica Acta. (2016)

The synthesis of sulphur and nitrogen co-doped CDs (S,N-CDs) were also studied. These CDs were prepared using the same method of synthesis by microwave pyrolysis. In this case, in order to dope the CDs with sulphur, to the precursors already used in previous CDs synthesis were added also sodium thiosulfate (ST). Different masses of ST varying from 0 to 3 g were tested. The characterization of the synthetized CDs with different masses was made. Each of the synthesized CDs were characterized (excitation/emission matrix, QY) and is response to ROS/RNS were evaluated with three concentration levels at different pH values. The higher QY of 6.5% was observed for the S,N-CDs prepared with 3 g of ST.

Relatively to the study of the influence of ROS/RNS in these CDs was observed that S,N-CDs respond with great sensibility and selectively to NO. A strong quenching effect in a linear response range from 1 to 25 μM with a sensitivity of 16 μM^{-1} and a detection limit of 0.3 μM was observed. The NO quantification capability was done in standard and in fortified serum solutions with good results. Relatively to the interference study only the Fe^{2+} and Fe^{3+} ionic species causes a small interference in the NO quantification.

This work was submitted for Analytica Chimica Acta.

My personal contribution to this work includes the establishment of an initial objective and the bibliographic research of the state of the art related with the determination ROS/RNS applying CDs similar to the synthetized, the protocols set up, the experimental execution and posterior data treatment. The CDs synthesis was also made using the microwave pyrolysis method. In this CDs synthesis was a Sulphur precursor: the ST. My personal contribution to this work includes after the research, the

microwave synthesis of the CDs testing the addition of a Sulphur precursor, the characterization of the CDs and the study of the CDs behavior in presence of the different ROS/RNS. The experiments were repeated several times in order to establish if the results were reproducible.

After the experimental part concluded the writing of the paper were made together with Professor João M. M. Leitão under the supervision of Professor Joaquim C. G. Esteves da Silva.

ARTICLE IN PRESS

Analytica Chimica Acta xxx (2017) 1–6

Contents lists available at ScienceDirect

Analytica Chimica Acta

journal homepage: www.elsevier.com/locate/aca

Sulfur and nitrogen co-doped carbon dots sensors for nitric oxide fluorescence quantification

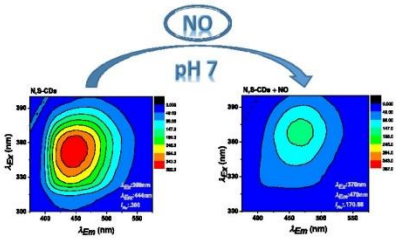
Eliana F.C. Simões [a, b], João M.M. Leitão [a, *], Joaquim C.G. Esteves da Silva [b]

[a] Centro de Investigação em Química da Universidade do Porto (CIQ-UP), Faculdade de Farmácia da Universidade de Coimbra, Pólo das Ciências da Saúde, 3000-548 Coimbra, Portugal
[b] Centro de Investigação em Química da Universidade do Porto (CIQ-UP), Departamento de Geociências, Ambiente e Ordenamento do Território, Faculdade de Ciências da Universidade do Porto, R. Campo Alegre 687, 4169-007 Porto, Portugal

HIGHLIGHTS

- S,N co-doped CDs were microwave synthetized from citric acid, urea and sodium thiosulfate.
- The NO fluorescence sensing was evaluated at pH 7.
- The selective and sensitive detection of NO at pH 7 was achieved.
- Good NO quantification results in serum samples were obtained.

GRAPHICAL ABSTRACT



ARTICLE INFO

Article history:
Received 17 October 2016
Received in revised form
11 November 2016
Accepted 5 January 2017
Available online xxx

Keywords:
Carbon dots
Citric acid
Urea
Sodium thiosulfate
Nitric oxide
Fluorescence quenching
pH 7

ABSTRACT

Microwave synthetized sulfur and nitrogen co-doped carbon dots responded selectively to nitric oxide (NO) at pH 7. Citric acid, urea and sodium thiosulfate in the proportion of 1:1:3 were used respectively as carbon, nitrogen and sulfur sources in the carbon dots microwave synthesis. For this synthesis, the three compounds were diluted in 15 mL of water and exposed for 5 min to a microwave radiation of 700 W. It is observed that the main factor contributing to the increased sensitivity and selectivity response to NO at pH 7 is the sodium thiosulfate used as sulfur source. A linear response range from 1 to 25 μM with a sensitivity of 16 μM^{-1} and a detection limit of 0.3 μM were obtained. The NO quantification capability was assessed in standard and in fortified serum solutions.

© 2017 Elsevier B.V. All rights reserved.

1. Introduction

Reactive Oxygen (ROS) and Nitrogen Species (RNS) are typically involved in numerous physiological and pathological processes acting as signaling molecules [1]. The nitric oxide (NO), one of most studied ROS/RNS, it is a free radical that plays as a physiological messenger and as effector in mammalian cells. It has a vital role in vascular and neuronal signal transduction, bioenergetics, immunity and cell death regulation. However at high concentrations it can be injurious to cells and can be associated with some diseases [2–5].

* Corresponding author.
E-mail address: jleitao@ff.uc.pt (J.M.M. Leitão).

http://dx.doi.org/10.1016/j.aca.2017.01.007
0003-2670/© 2017 Elsevier B.V. All rights reserved.

Please cite this article in press as: E.F.C. Simões, et al., Sulfur and nitrogen co-doped carbon dots sensors for nitric oxide fluorescence quantification, Analytica Chimica Acta (2017), http://dx.doi.org/10.1016/j.aca.2017.01.007

Sensors based in nanoparticles (NPs) have attracted much attention due their own specific characteristics [6]. Recently some sensors based in NPs have been developed for the NO detection [7–24]. NO optical nanosensors based in NPs as gold NPs (AuNPs), carbon nanotubes (CNT) and quantum dots (QDs) were developed. Two AuNPs optical sensors to NO detection based on immobilization of AuNPs onto a fiber optic were reported [7,8]. CNT were used in optical sensors with potential for NO sensing [9,10]. The NO detection using QDs is usually based on fluorescence quenching of QDs by NO. TEA modified CdSe-QDs were quenched with NO [11]. QDs with chitosan (CS) were used as NO sensors [12,13]. A CdSe-QDs sensor stabilized by CS and mercaptosuccinic acid was showed by Simões et al. [14]. A sensor synthetized by adsorption of CdSe/ZnS-QDs on polymethacrylate was presented [15]. An optical fiber sensor based on CdSe-QDs using cellulose as NO sensitive membrane was developed [16]. CdSe functionalized with trivalent porphirin were used in NO sensing [17]. Modified hyperbranched polyether nanospheres and QDs were reported in NO detection [18]. The detection based on the degradation of the polymethyl methacrylate molecule (PMMA) by NO in CdS-PMMA nanocomposites was presented [19]. Ferric dithiocarbamate compounds were used in the QDs functionalization for NO sensors [20,21]. Organogel–CdSe/ZnS QDs hybrid materials showed fluorescence sensitivity towards NO [22]. CdSe/ZnS-QDs coordinated with dirhodium complex were presented [23]. A QDs system capable of releasing NO and meanwhile detecting the NO release under conditions similar to physiological environment based on the fluorescence quenching by NO was presented [24].

The carbon Dots (CDs), the nanoparticles focus of the present work, had become to be a priority for the scientific research due to their non-toxicity and biocompatible properties [25]. Furthermore CDs also can be functionalized and conjugated with various compounds and therefore could be used in several analytical and bioanalytical applications [26]. A great number of methods for the CDs synthesis have proposed in last years. One of the most used method of synthesis is the microwave synthesis due to the fact that it is a rapid and simple method of CDs synthesis [27]. Different kind of precursors like carbohydrates, chitosan, citric acid (CA), amines and others can be used in CDs production [28,29]. Many CDs were microwave synthetized having as precursors CA combined with different amines [30–32]. Also the CDs can be doped to increase their quantum yield (Φ), to provide sensibility and selectivity as sensor to adjust their compositions and structures. Some works presented the CDs microwave synthesis from CA as carbon source and urea (UR) as nitrogen source [33–35].

Doping CDs with heteroatoms (e.g., oxygen, nitrogen, phosphor, boron or sulfur) allows adjusting their compositions and structures and is one way of tuning their electronic and optical properties [36]. Generally the quantum yield of the doped CDs is higher than the Φ of the non-doped CDs. Nitrogen doping CDs is a well established procedure [37,38]. More recently sulfur and nitrogen co-doped CDs prepared from various precursors have been reported [39–45]. The synergistic effect of the various dopants allows the synthesis of CDs with different characteristics and can have diverse applications [46]. The sulfur and nitrogen co-doped CDs commonly exhibit higher catalytic activity to the oxygen reduction reaction compared with the nitrogen doped CDs through a cooperative effect [36,47]. The co-doped sulfur atoms can help to enhance the effect of nitrogen doping through this cooperative effect. For the sulfur and nitrogen co-doped CDs, the sulfur atoms seems to be able to eliminate the O states and enhance the N states [48].

Two applications of CDs as NO nanoprobe were discussed [49,50]. In one of the works the ratiometric sensing of NO based in CDs through the fluorescence resonance energy transfer (FRET) process was assessed [49]. More recently, a NO sensor based in CDs microwave synthesized from CA and EDA showed selective fluorescence sensing of NO and $ONOO^-$ in the presence of the main ROS/RNS. A greater sensitivity was obtained for the determination of $ONOO^-$ at pH 7 and 10 and a lower sensitivity for the determination of NO at pH 4 [50].

In this work a selective and sensitive sensor to NO detection and quantification at pH 7 based on microwave synthetized CDs prepared from CA, UR and sodium thiosulfate (ST) was developed. The fluorescence response of the synthetized CDs relatively to NO in the presence of other ROS/RNS and the NO quantification capability in standard and in fortified serum solutions were evaluated.

2. Experimental

2.1. Reagents

Citric Acid (CA), urea (UR), sodium thiosulfate (ST), hydrogen peroxide (H_2O_2), hydrogen chloride (HCl), potassium superoxide (KO_2), sodium hypochlorite 3.5% (NaClO), sodium nitrite ($NaNO_2$), sodium nitrate ($NaNO_3$), sodium chloride (NaCl), potassium chloride (KCl), ethylenediamine tetraacetic acid (EDTA), iron(II) sulfate ($FeSO_4 \cdot 7H_2O$), iron(III) nitrate [$Fe_3(NO_3)_3 \cdot 9H_2O$], magnesium chloride ($MgCl_2 \cdot 6H_2O$), copper(II) sulfate ($CuSO_4 \cdot 5H_2O$), sodium phosphate dibasic (Na_2HPO_4), monosodium phosphate (NaH_2PO_4), sodium hydroxide (NaOH) analytical grade reagents and Mili-Q water with a resistivity 18 MΩ cm at 25 °C were used in all the work.

2.2. Solutions

Saturated NO solutions (1.9 mM) were prepared by bubbling argon for 15 min in water and follow bubbling NO another 15 min. $ONOO^-$ solutions were prepared in a refrigerated beaker under constant stirring by mixing 100 mL of $NaNO_2$ 600 mM, 100 mL of H_2O_2 600 mM in HCl 0.6 M and 100 mL of NaOH 3.6 M. The solution will turn yellow indicating the formation of $ONOO^-$. The agitation is maintained until no O_2 is formed. The hydroxyl ($HO^\cdot$) was generated in situ by the Fenton reaction by addition of a 5 fold excess of H_2O_2 to the EDTA-Fe(II) complex formed with different concentrations of $FeSO_4$. Serum fortified sample solutions were done respectively in water by rigorous dilution to the desired concentrations. The solutions of H_2O_2, KO_2, NaClO, $NaNO_3$, $NaNO_2$ were prepared in water.

All the experiences were made at pH 7. The phosphate buffer 0.01 M (pH 7) used was prepared through weighting the required mass of NaH_2PO_4 and Na_2HPO_4. Solutions of HCl and NaOH 0.1 M were also prepared in order to adjust the pH of the phosphate buffer solution and in order to evaluate the influence of pH in the CDs fluorescence.

2.3. Instrumentation

The fluorescence sensing evaluations were made using a QE65000 charge-coupled detector, a 380 nm light emitting diode (LED), a sampling compartment (CUV-ALL-UV 4-way) and two 1.0 mm core diameter fiber optics (P1000-2-UV–VIS) from Ocean Optics. One of the fibers guides the light from the source to the sampling compartment and the other guide the emitted light to the detector. The reaction time profiles were obtained collecting the signal at the maximum emission wavelength, every 10 s with an integration time of 300 ms. A difference between the initial and the final fluorescence intensity measured after 10 min the addition of the ROS/RNS (intensity variation) were used in all the work.

The absorbance and fluorescence spectra were obtained in a standard 1 cm fluorescence quartz cell and collected respectively in a Jasco V-530 UV–Visible spectrophotometer and in a Jasco FP-

Please cite this article in press as: E.F.C. Simões, et al., Sulfur and nitrogen co-doped carbon dots sensors for nitric oxide fluorescence quantification, Analytica Chimica Acta (2017), http://dx.doi.org/10.1016/j.aca.2017.01.007

ARTICLE IN PRESS

6200 spectrofluorimeter. The absorption spectra were obtained in a wavelength range from 250 to 650 nm with a 2 nm interval, slit widths 2 nm and wavelength scan rate medium; the Fluorescence spectra were obtained in a wavelength range from 300 to 700 nm with a 1 nm interval, slit widths 5 nm, sensitivity response medium, response time fast and wavelength scan rate 1000 nm/min Fourier transform infrared (FTIR) spectra were obtained by a Perkin Elmer FTIR Spectrum 400 in solid state with an attenuated total reflectance (ATR) accessory in a range of 4000 to 650 cm^{-1} with 16 accumulations and a resolution of 4 cm^{-1}. The particle size, size distribution and shape of the synthetized CDs were evaluated by transmission electronic microscopy (TEM) in a FEI Company Tecnai G2 20 S-Twin electronic microscopic.

2.4. CDs synthesis

Attending to previous published work a mass of citric acid (m_{CA}) and a mass of urea (m_{UR}) of 1 g with the same synthesis conditions were used for all the CDs synthesis [35]. In these CDs synthesis, and beside 1 g of these two compounds, a different mass of sodium thiosulfate (m_{ST}) from 0.5 to 3 g was also used. For the CDs microwave synthesis a domestic microwave with a maximum radiation potency of 700 w was used. A volume of water of 15 mL, a microwave radiation potency of 700 w and a microwave time 5 min were used in all the synthesis. The synthesized CDs were leaving to cool, diluted with water and posterior centrifuged at 9000 rpm during 10 min in order to eliminated suspended impurities. A final of 30 mL were posterior set with water.

2.5. ROS/RNS evaluations

The more adequate CDs dilution in phosphate buffer 0.01 M was assessed by the evaluation of successive dilutions of CDs solution in order to obtain a higher fluorescence intensity. For the selected synthetized CDs, a 20 × dilution was chosen. The ROS/RNS addition, in the required concentration to the more adequate CDs dilution, was done in a cuvette with a Hamilton® syringe with permanent agitation while the fluorescence signal is continuously monitored for a period of 10 min.

2.6. Quantum yield

The Φ of the synthetized CDs were calculated comparing the integrated photoluminescence intensities and the absorbance values of the synthesized CDs with the ones of the quinine sulfate.

$$\Phi = \Phi_R \times \frac{Grad}{Grad_R} \times \frac{\eta^2}{\eta_R^2}$$

In the equation Φ is the fluorescence quantum yield, Grad is the gradient from the plot of integrated fluorescence intensity vs. absorbance and η is the refractive index. The subscripts R refer to reference fluorophore, quinine sulfate of known quantum yield. The Φ of the quinine sulfate is $\Phi = 0.54$ [38]. The η of the quinine sulfate in 0.1 M H_2SO_4 and of nanocomposites water solutions used were $\eta = 1.33$.

3. Results

3.1. Preliminary evaluations

It was previously observed that the CDs synthetized without ST show non-selectivity towards NO at pH 7 [35]. Consequently, in order to optimized the effect of ST in the increased sensitivity and selectivity of the response of the CDs towards NO a first set of formulations were prepared constituted by: $m_{CA} = 1$ g, $m_{UR} = 1$ g and m_{ST} of 0.5, 1, 2 and 3 g. The evaluation of the response of these CDs with the main ROS/RNS (NO, $ONOO^-$, ClO^-, $HO^•$, H_2O_2 and $O_2^{•-}$) was initially made at the concentrations 10, 50 and 100 μM (Fig. 1 and Fig. S1).

Higher selectivity to NO was now observed with the synthetized CDs with different quantities of ST and the highest was found for CDs synthesized with $m_{ST} = 0.5$ g and 3 g. CDs synthetized with $m_{ST} = 1$ g also respond to $ONOO^-$ and $HO^•$ and the CDs synthetized with $m_{ST} = 2$ g also respond to $ONOO^-$. Also CDs synthesized with a $m_{ST} = 3$ g show the greater sensitivity to NO (Fig. 1 and Fig. S1). Attending to these preliminary results the synthetized CDs with a $m_{CA} = 1$ g, $m_{UR} = 1$ g and $m_{ST} = 3$ g will be considered for the NO sensitivity and selectivity quantification at pH 7.

3.2. CDs characterization

The characterization of the synthetized CDs with a $m_{CA} = 1$ g, $m_{UR} = 1$ g and $m_{ST} = 3$ g will be achieved by fluorescence, FTIR and TEM analysis. A sample of CDs synthesized without ST and with a $m_{ST} = 0.5$, 1 and 2 g was also analysed for comparative purposes. In Fig. 2 is presented the fluorescence excitation-emission matrices (EEM) of the synthetized CDs with a $m_{CA} = 1$ g, $m_{UR} = 1$ g and a $m_{ST} = 3$ g. (Fig. S2 show the EEM for CD without ST); the normalized absorbance, excitation and emission spectra (Fig. S3) and, for easier comparison, a table with the main fluorescence features (Table S1) of the all the synthetized CDs.

In comparison with the CDs without ST a decrease of the excitation, emission wavelength and of the Φ are evaluated with the CDs with ST. Relatively similar fluorescence characteristics are observed for the CDs with different quantities of ST. For all the CDs with different quantities of ST a similar excitation wavelength of 350 nm and a slightly decrease of the emission wavelength from 451 nm to 440 nm with the synthetized CDs with the increase of ST it's found. Relatively to the others synthetized CDs with ST the greater Φ it's evaluated with the synthetized CDs with an $m_{ST} = 3$ g. A similar excitation and emission and a slightly different absorbance spectra were found with the synthetized CDs without ST and with different quantities of ST.

The normalized fluorescence intensity variation with the pH and ionic strength of the CDs with a $m_{ST} = 3$ g is also shown in supplementary information (Fig. S4). The fluorescence intensity of the synthetized CDs with a $m_{CA} = 1$ g, $m_{UR} = 1$ g and a $m_{ST} = 3$ g is marked influenced by the pH with an increase from 2 to 6. A higher

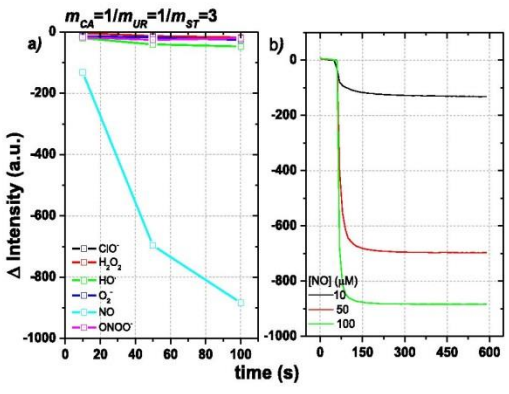


Fig. 1. NO, $ONOO^-$, ClO^-, $HO^•$, H_2O_2 and $O_2^{•-}$ fluorescence response evaluation a) and NO time profile b) at 10, 50 and 100 μM concentrations.

Please cite this article in press as: E.F.C. Simões, et al., Sulfur and nitrogen co-doped carbon dots sensors for nitric oxide fluorescence quantification, Analytica Chimica Acta (2017), http://dx.doi.org/10.1016/j.aca.2017.01.007

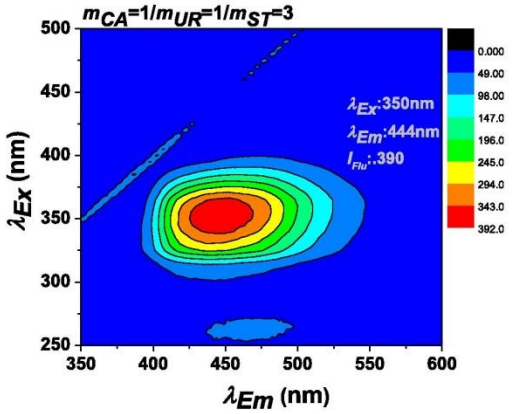


Fig. 2. EEM of the synthetized CDs.

fluorescence intensity stability is observed above pH 6. The fluorescence intensity does not change with the ionic strength.

The FTIR spectra of the CDs without ST and with a $m_{ST} = 3$ g are presented in Fig. 3. FTIR spectra of CDs with other contents of ST and of the three precursors are shown in Fig. S5 (Table S2).

Fig. 3 shows that different spectra were found with the CDs without and with ST. The main differences of the spectra are the strong broad band due to the −OH/−NH shifted from 3347 to 3191 cm^{-1}, the existence of two new weakens sharp bands at 2068 and 2179 cm^{-1} respectively due to a −C≡C and −C≡N, the strong sharp band to the −C=N/−C=O shifted from 1568/1615 to 1579/1663 cm^{-1}, the disappearance of a weaker sharp band at 1189 cm^{-1} due to −C−O and two new strong sharp band at 995 and 1112 cm^{-1} respectively due to a −S−O and −C−S. In comparison with the synthetized CDs with others quantities of ST a more similar spectrum was found with a $m_{ST} = 2$ g and the more different with a $m_{ST} = 0.5$ g.

The size and shape of the synthetized CDs with a $m_{ST} = 3$ g was evaluated by TEM analysis (Fig. 4). For these CDs a size of 1 and up to 4 nm is observed with a spherical or almost spherical shape. The statistical evaluation of the size distribution considering a sample of 100 nanoparticles shows: $\bar{x} = 2.49$ nm ($\sigma = 0.57$).

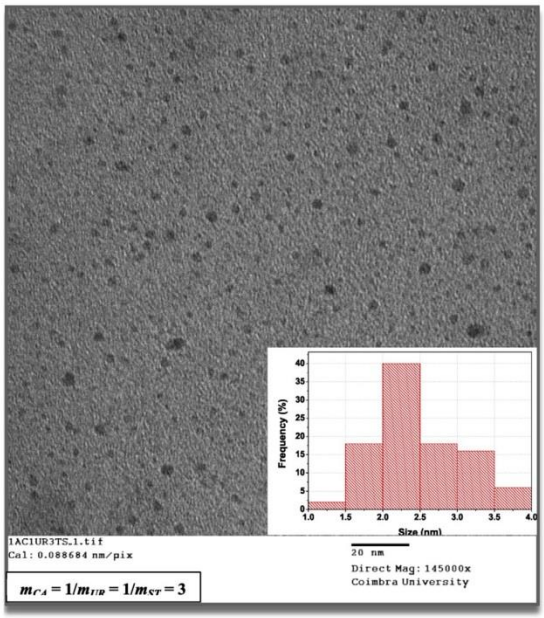


Fig. 4. TEM images of the synthetized CDs.

3.3. Quantification capability

In order to assess the quantification capability of the NO by the CDs, the quenching effect, the recovery of NO in standard and fortified serum samples solutions and the selectivity were evaluated. In Fig. 5 is presented the fluorescence time profiles and the fluorescence quenching effect found by addition to the synthetized CDs with a $m_{CA} = 1$ g, $m_{UR} = 1$ g and $m_{ST} = 3$ g of NO at concentrations from 1 to 200 μM.

Similar fluorescence time profiles were obtained at different NO concentrations. A strong quenching was verified by addition of NO concentrations from 1 to 200 μM. It is possible to observe an initially linear variation with a deviation of linearity at higher NO

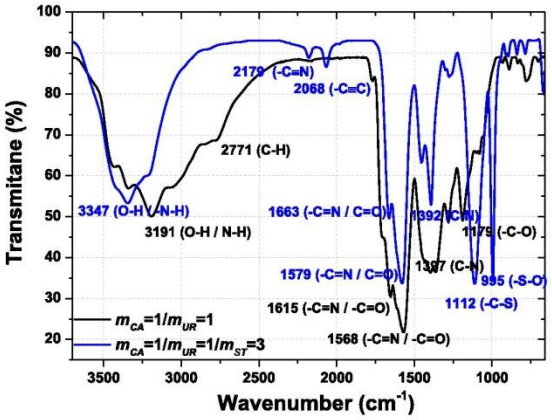


Fig. 3. FTIR spectra of the synthetized CDs with and without ST.

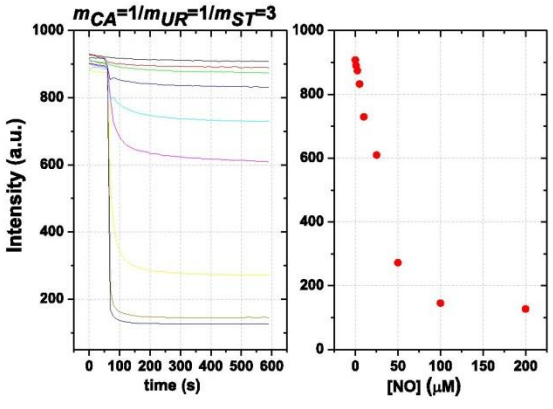


Fig. 5. Fluorescence time profiles and quenching effect found by addition of NO concentrations from 1 to 200 μM.

Please cite this article in press as: E.F.C. Simões, et al., Sulfur and nitrogen co-doped carbon dots sensors for nitric oxide fluorescence quantification, Analytica Chimica Acta (2017), http://dx.doi.org/10.1016/j.aca.2017.01.007

Table 1
NO quantification results in standard solutions and in spiked serum samples found in the linear range from 1 to 25 μM.

CDs ($m_{CA} = 1/m_{UR} = 1/m_{ST} = 3$)						
$y = bx + a$			$\boldsymbol{b} = -16.0 \pm 0.6$; $\boldsymbol{a} = 1.9 \pm 7.2$; $\boldsymbol{m} = 5$ $\boldsymbol{s_{y/x}} = 11.5$; $\boldsymbol{r} = -0.9980$ **LR** −1−25 μM; **LD** = 0.3 μM			
[NO] (μM)	Standard solutions			Spiked serum samples (100×)		
Expected	**2.5**	**5**	**10**	**2.5**	**5**	**10**
Estimated	2.5 ± 2.6	5.0 ± 2.5	10.5 ± 2.5	2.9 ± 2.6	5.0 ± 2.5	9.5 ± 2.5
Recovery (%)	101.6	100.4	104.8	115.6	99.5	95.6

* a - Intercept; s_a - Intercept standard deviation; b - Slope; s_b - Slope standard deviation; $s_{y/x}$ - Standard deviation of residuals; r - Linear correlation coefficient; m - Number of calibration points; LR – Linear range; LD – Limit of detection evaluated through the s of five determinations of a blank.

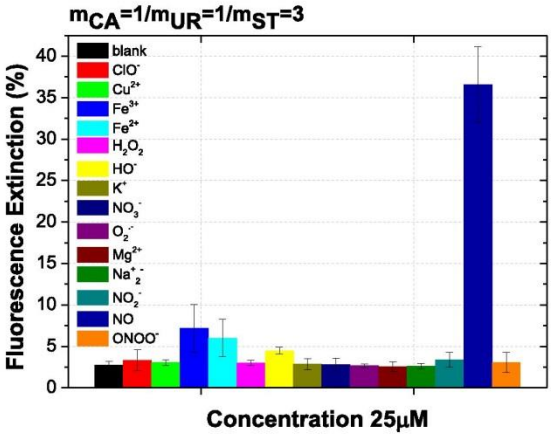


Fig. 6. Fluorescence quenching effect obtained by addition of ROS/RNS or ionic species.

concentrations. In supplementary information are presented the Stern-Volmer behaviour at two temperatures and the effect of KI in the fluorescence intensity. A linear behaviour described by the Stern-Volmer is verified by addition of NO concentration from 1 to 25 μM (Fig. S7). The evaluation of the Stern-Volmer behaviour at two temperatures and the calculation of the fraction of the accessible groups to iodide confirm that a dynamic quenching is not responsible for the decrease of fluorescence. Indeed, by increasing the temperature a decrease of this constant was observed. Besides, the addition of KI do not shows the expected variation in a dynamic quenching and do not allows the calculation of the fraction of the accessible groups to the iodide quenching. A static quenching mechanism is more probable due to the oxidation of S groups or even N groups due to the already described enhancement of N –states in CDs by a sulfur and nitrogen co-doping effect obtained by addition of sodium thiosulfate as precursor.

Attending the results of the NO addition from 1 to 200 μM to the CDs $m_{CA} = 1$ g, $m_{UR} = 1$ g and $m_{ST} = 3$ g (Fig. 5) the linearity of the ΔI ($I - I_0$) in function of concentration was evaluated at two linear ranges from 1 to 25 μM and 1–50 μM. In supplementary information are presented the results found (Fig. S8). The more adequate linear concentration range is obtained in the concentration range from 1 to 25 μM. A linear decrease in the fluorescence of the synthetized CDs $m_{CA} = 1$ g, $m_{UR} = 1$ g and $m_{ST} = 3$ g was observed with a sensitivity of 16 and a detection limit of 0.3 μM.

In the more adequate linear range were obtained good quantification results with recoveries near 100% in the analysis of the standard and spiked serum samples at the levels of concentration evaluated (Table 1).

The interference study was done with the main ROS/RNS and ionic species by addition of a concentration of 25 μM to the synthetized CDs $m_{CA} = 1$ g, $m_{UR} = 1$ g and $m_{ST} = 3$ g (Fig. 6). A great selectivity was observed with these synthetized CDs. Only a small interference of Fe^{3+}, Fe^{2+} and $HO^{\cdot}$, maybe due to the excess of Fe^{2+} needed to the formation of $HO^{\cdot}$, was evaluated.

Table 2 resumes the methods of synthesis, fluorescence characteristics and principal figures of merit of the already developed CDs based sensors for NO detection.

As already discussed in the introduction, up to the authors knowledge, only two papers report the use if CDs as NO sensors [49,50]. In one of them, CDs were synthesized from CA and EDA, and in the other, phenylenediamine-containing naphthalimide functionalized CDs synthetized from CA and EDA, were developed respectively as a quenching and a FRET ratiometric NO sensor. In the first one the quantification capability and in the second one the fluorescence imaging of NO were evaluated respectively at pH 4 and 7. Comparing the features of the CDs studied in this paper with other samples, a good selectivity, high sensitivity and a lower limit of detection are observed.

4. Conclusions

Sulfur and nitrogen co-doped CDs allow the NO quantification with great sensitivity and selectivity. A strong fluorescence quenching effect was verified by addition of NO to sulfur and nitrogen co-doped synthetized CDs with a $m_{CA} = 1$ g, $m_{UR} = 1$ g and a $m_{ST} = 3$ g. The great increase in the NO sensitivity and selectivity detection is due to the effect of sodium thiosulfate by sulfur co-doping nitrogen CDs that alters the intrinsic characteristics of the nitrogen doping effect.

Good quantification results were assessed in standard solutions and in spiked serum samples. Only the Fe^{2+} and Fe^{3+} ionic specie causes a small interference in the NO quantification. The evaluated analytical methodology for NO quantification shows a linear

Table 2
Comparison of NO detection by the synthetized CDs with the indicated by other CDs used in previous literature reports.[a]

CDs		Fluorescence detection			Figures of merit				Ref.
Prec./Synt./Funct.	Φ (%)	pH	λ_{EX} (nm)	λ_{EM} (nm)	LR (μM)	LOD (μM)	Sensitivity (a.u./μM^{-1})	Selectivity (possible interferents)	
CA,EDA/MW/–	42	4	360	460	10–100	4.6	2.5	Good ($HO^{\cdot}$)[b]	[50]
CA,EDA/MW/NPH	n.p.	7.4	370	455/535	n.p.	0.003	n.p.	Good[b]	[49]
CA,UR,ST/MW/–	7	7.4	350	444	1–25	0.3	16	Good (Fe^{2+}, Fe^{3+})	Our work

[a] Prec. – Synthesis precursors; Synt. – Method of synthesis; Funct. - Functionalization; Φ – Quantum yield; λ_{EX} – Excitation wavelength at maximum fluorescence intensity λ_{EM} – Emission wavelength at maximum fluorescence intensity; LR - Linear range; LOD – Limit of detection; n.p. – not presented; CA – Citric acid; EDA – 1,2-ethylenediamine; MW – Microwave synthesis; NPH - naphthalimide with an *o*-phenylenediamine group; UR – Urea; ST – Sodium thiosulfate.

[b] In these refs. the ionic species were not evaluated. In ref. $ONOO^-$, H_2O_2, $O_2^{\bullet -}$, $HO^{\bullet}$, NO_3^- and NO_2^- and in ref. H_2O_2, HClO, $^1O_2$, $HO^{\bullet}$, NO_3^-, NO_2^- and ascorbic acid were the evaluated compounds.

Please cite this article in press as: E.F.C. Simões, et al., Sulfur and nitrogen co-doped carbon dots sensors for nitric oxide fluorescence quantification, Analytica Chimica Acta (2017), http://dx.doi.org/10.1016/j.aca.2017.01.007

response in a range from 1 to 25 μM with a sensitivity of 16 μM^{-1} and a detection limit of 0.3 μM.

Acknowledgments

A PhD grant SFRH/BD/81074/2011 to Eliana Simões and financial support, project PTDC/QEQQAN/5955/2014, from Fundação para a Ciência e a Tecnologia (FCT, Lisbon) are acknowledged. The use of FTIR from UCQFarma, Pharmacy Faculty of the University of Coimbra and the TEM analyses from Nanomaterials and Micro-manufacturing group of Centre for Mechanical Engineering of the University of Coimbra (CEMUC) are also acknowledged.

Appendix A. Supplementary data

Supplementary data related to this article can be found at http://dx.doi.org/10.1016/j.aca.2017.01.007.

References

[1] M. Valko, et al., Free radicals and antioxidants in normal physiological functions and human disease, Int. J. Biochem. Cell Biol. 39 (1) (2007) 44–84.
[2] E.M. Hetrick, M.H. Schoenfisch, Analytical chemistry of nitric oxide, Annu. Rev. Anal. Chem. 2 (2009) 409–433.
[3] D. Yao, A.G. Vlessidis, N.P. Evmiridis, Determination of nitric oxide in biological samples, Microchim. Acta 147 (1–2) (2004).
[4] S. Paolo, Nitric Oxide in Human Health and Disease, eLS, John Wiley & Sons, 2013.
[5] L. Bergendi, et al., Chemistry, physiology and pathology of free radicals, Life Sci. 65 (18–19) (1999) 1865–1874.
[6] X. Luo, et al., Application of nanoparticles in electrochemical sensors and biosensors, Electroanalysis 18 (4) (2006) 319–326.
[7] S.L. Barker, R. Kopelman, Development and cellular applications of fiber optic nitric oxide sensors based on a gold-adsorbed fluorophore, Anal. Chem. 70 (23) (1998) 4902–4906.
[8] S.L. Barker, et al., Ratiometric and fluorescence-lifetime-based biosensors incorporating cytochrome c' and the detection of extra- and intracellular macrophage nitric oxide, Anal. Chem. 71 (9) (1999) 1767–1772.
[9] J.-H. Kim, et al., The rational design of nitric oxide selectivity in single-walled carbon nanotube near-infrared fluorescence sensors for biological detection, Nat. Chem. 1 (6) (2009) 473–481.
[10] N.M. Iverson, M.S. Strano, G.N. Wogan, In vivo delivery of nitric oxide-sensing, single-walled carbon nanotubes, Curr. Protoc. Chem. Biol. 7 (2015) 93–102, http://dx.doi.org/10.1002/9780470559277.ch140196.
[11] X.Q. Yan, et al., Fluorescence sensing of nitric oxide in aqueous solution by triethanolamine-modified CdSe quantum dots, Luminescence 24 (4) (2009) 255–259.
[12] L. Tan, et al., Novel quantum dots-carboxymethyl chitosan nanocomposite nitric oxide donors capable of detecting release of nitric oxide in situ, Acta Biomater. 8 (10) (2012) 3744–3753.
[13] L. Tan, et al., Biocompatible quantum dots–chitosan nanocomposites for fluorescence detection of nitric oxide, Mater Chem. Phys. 134 (2–3) (2012) 562–566.
[14] E.F. Simoes, J.M. Leitao, J.C. Esteves da Silva, NO fluorescence quantification by chitosan CdSe quantum dots nanocomposites, J. Fluoresc. 24 (2014) 639–648.
[15] V. Fabregat, et al., Quantum dot–polymethacrylate composites for the analysis of NOx by fluorescence spectroscopy, Inorg. Chim. Acta 381 (2012) 212–217.
[16] L. Ding, et al., A sensitive optic fiber sensor based on CdSe QDs fluorophore for nitric oxide detection, Sens. Actuators B Chem. 185 (2013) 70–76.
[17] A. Ivanisevic, et al., Photoluminescent properties of cadmium selenide in contact with solutions and films of Metalloporphyrins: nitric oxide sensing and evidence for the aversion of an analyte to a buried Semiconductor–Film interface, J. Am. Chem. Soc. 122 (15) (2000) 3731–3738.
[18] S. Liu, et al., Hyperbranched polyether hybrid nanospheres with CdSe quantum dots incorporated for selective detection of nitric oxide, Mater. Lett. 123 (2014) 104–106.
[19] L. Ding, et al., Synthesis and characterization of a novel nitric oxide fluorescent probe CdS-PMMA nanocomposite via in-situ bulk polymerization, Mater. Sci. Eng. C 35 (2014) 29–35.
[20] J. Sun, et al., Fluorescence turn-on detection of gaseous nitric oxide using ferric dithiocarbamate complex functionalized quantum dots, Anal. Chem. 86 (12) (2014) 5628–5632.
[21] S. Wang, M.-Y. Han, D. Huang, Nitric oxide switches on the photoluminescence of molecularly engineered quantum dots, J. Am. Chem. Soc. 131 (33) (2009) 11692–11694.
[22] P.D. Wadhavane, et al., Organogel–quantum dots hybrid materials displaying fluorescence sensitivity and structural stability towards nitric oxide, Soft Matter 8 (16) (2012) 4373.
[23] E. Koo, J.-C. Lee, A turn-on fluorescent probe for detecting nitric oxide in aqueous media, J. Nanomater. 2014 (2014) 210.
[24] L. Tan, A. Wan, H. Li, Quantum dots-poly(N-isopropylacrylamide) hybrid nanogel diazeniumdiolates as donors and real-time probes of nitric oxide, Mater Chem. Phys. 138 (2–3) (2013) 956–962.
[25] Y. Wang, A. Hu, Carbon quantum dots: synthesis, properties and applications, J. Mater. Chem. C 2 (34) (2014) 6921–6939.
[26] J.C.G. Esteves da Silva, H.M.R. Gonçalves, Analytical and bioanalytical applications of carbon dots, Trends Anal. Chem. TrAC 30 (8) (2011) 1327–1336.
[27] H. Zhu, et al., Microwave synthesis of fluorescent carbon nanoparticles with electrochemiluminescence properties, Chem. Commun. 34 (2009) 5118–5120.
[28] E.F.C. Simões, J.C.G.E. da Silva, J.M.M. Leitão, Carbon dots from tryptophan doped glucose for peroxynitrite sensing, Anal. Chim. Acta. 852 (2014) 174–180.
[29] Z. Yang, et al., Controllable synthesis of fluorescent carbon dots and their detection application as nanoprobes, Nano Micro Lett. 5 (4) (2013) 247–259.
[30] F. Du, et al., Carbon dots-based fluorescent probes for sensitive and selective detection of iodide, Microchim. Acta 180 (5) (2013) 453–460.
[31] X. Zhai, et al., Highly luminescent carbon nanodots by microwave-assisted pyrolysis, Chem. Commun. 48 (64) (2012) 7955–7957.
[32] A. Salinas-Castillo, et al., Carbon dots for copper detection with down and upconversion fluorescent properties as excitation sources, Chem. Commun. 49 (11) (2013) 1103–1105.
[33] S. Qu, et al., A biocompatible fluorescent ink based on water-soluble luminescent carbon nanodots, Angew. Chem. Int. Ed. 51 (49) (2012) 12215–12218.
[34] A.B. Bourlinos, et al., Green and simple route toward boron doped carbon dots with significantly enhanced non-linear optical properties, Carbon 83 (2015) 173–179.
[35] E.F.C. Simões, J.M.M. Leitão, J.C.G.E. da Silva, Carbon dots prepared from citric acid and urea as fluorescent probes for hypochlorite and peroxynitrite, Microchim. Acta 183 (5) (2016) 1769–1777.
[36] Y. Park, et al., Improving the functionality of carbon nanodots: doping and surface functionalization, J. Mater. Chem. A 4 (30) (2016) 11582–11603.
[37] C. Zheng, X. An, J. Gong, Novel pH sensitive N-doped carbon dots with both long fluorescence lifetime and high quantum yield, RSC Adv. 5 (41) (2015) 32319–32322.
[38] J. Liao, Z. Cheng, L. Zhou, Nitrogen-doping enhanced fluorescent carbon dots: green synthesis and their applications for bioimaging and label-free detection of Au3+ ions, ACS Sustain. Chem. Eng. 4 (2016) 3053–3061.
[39] L. Li, B. Yu, T. You, Nitrogen and sulfur co-doped carbon dots for highly selective and sensitive detection of Hg (II) ions, Biosens. Bioelectron. 74 (2015) 263–269.
[40] Y. Wang, S.-H. Kim, L. Feng, Highly luminescent N, S-Co-doped carbon dots and their direct use as mercury (II) sensor, Anal. Chim. Acta 890 (2015) 134–142.
[41] W. Lu, et al., Comparative study for N and S doped carbon dots: synthesis, characterization and applications for Fe3+ probe and cellular imaging, Anal. Chim. Acta. 898 (2015) 116–127.
[42] Y. Guo, et al., Carbon dots doped with nitrogen and sulfur and loaded with copper(II) as a "turn-on" fluorescent probe for cystein, glutathione and homocysteine, Microchim. Acta 183 (4) (2016) 1409–1416.
[43] Q. Xu, et al., Preparation of highly photoluminescent sulfur-doped carbon dots for Fe(iii) detection, J. Mater. Chem. A 3 (2) (2015) 542–546.
[44] M. Xue, et al., Nitrogen and sulfur co-doped carbon dots: a facile and green fluorescence probe for free chlorine, Sens. Actuators B Chem. 219 (2015) 50–56.
[45] D. Sun, et al., Hair fiber as a precursor for synthesizing of sulfur- and nitrogen-co-doped carbon dots with tunable luminescence properties, Carbon 64 (2013) 424–434.
[46] C.J. Reckmeier, et al., Luminescent colloidal carbon dots: optical properties and effects of doping [Invited], Opt. Express 24 (2) (2016) A312–A340.
[47] H. Ding, J.-S. Wei, H.-M. Xiong, Nitrogen and sulfur co-doped carbon dots with strong blue luminescence, Nanoscale 6 (22) (2014) 13817–13823.
[48] Y. Dong, et al., Carbon-based dots co-doped with nitrogen and sulfur for high quantum yield and excitation-independent emission, Angew. Chem. Int. Ed. Engl. 52 (30) (2013) 7800–7804.
[49] C. Yu, et al., A fluorescent ratiometric nanosensor for detecting NO in aqueous media and imaging exogenous and endogenous NO in live cells, J. Mater. Chem. B 1 (33) (2013) 4152.
[50] E.F.C. Simões, J.C.G. Esteves da Silva, J.M.M. Leitão, Peroxynitrite and nitric oxide fluorescence sensing by ethylenediamine doped carbon dots, Sens. Actuators B Chem. 220 (2015) 1043–1049.

Please cite this article in press as: E.F.C. Simões, et al., Sulfur and nitrogen co-doped carbon dots sensors for nitric oxide fluorescence quantification, Analytica Chimica Acta (2017), http://dx.doi.org/10.1016/j.aca.2017.01.007

Sulphur and nitrogen co-doped carbon dots for nitric oxide fluorescence quantification

Eliana F. C. Simões[a,b], João M.M. Leitão [a,*] and Joaquim C.G. Esteves da Silva [b]

[a,*] Centro de investigação em química da Universidade do Porto (CIQ-UP), Faculdade de Farmácia da Universidade de Coimbra, Pólo das Ciências da Saúde, 3000-548 Coimbra, Portugal

[b] Centro de investigação em química da Universidade do Porto (CIQ-UP), Departamento de Química, Faculdade de Ciências da Universidade do Porto, R. Campo Alegre 687, 4169-007 Porto, Portugal

Supplementary information

1. ROS/RNS evaluation

In Fig. S1 are presented the results obtained by the assessment of the response of the synthesized CDs with 1g of CA and UR with a mass of 0.5, 1 and 2 g of ST at three concentrations levels of ClO^-, $ONOO^-$, H_2O_2, $O_2^{\cdot-}$, NO, and $HO^\cdot$ at pHs 7. In this figure is also presented typical fluorescence quenching time profiles of the previous indicated CDs by addition of NO.

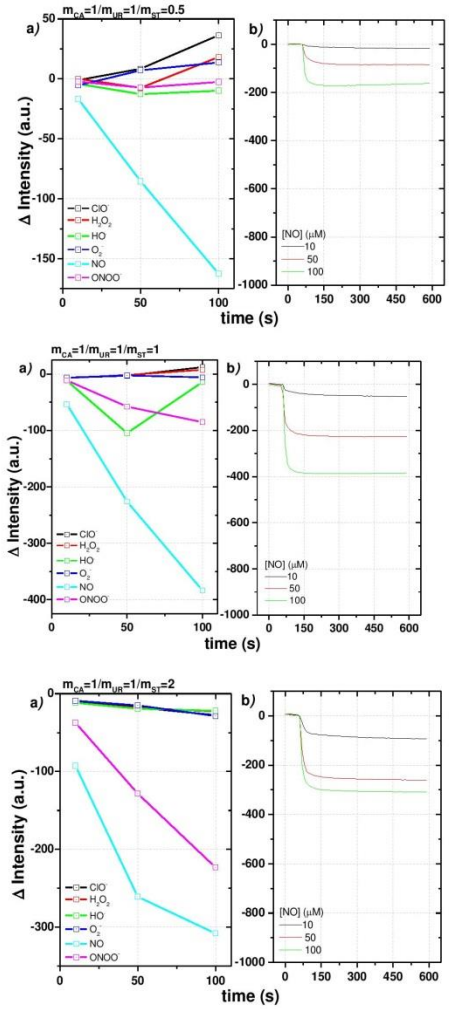


Fig. S1 – NO, $ONOO^-$, ClO^-, $HO^\cdot$, H_2O_2 and $O_2^{\cdot-}$ fluorescence response evaluation a) and NO time profile b) at 10, 50 and 100 µM concentrations.

2. CDs characterization

2.1 UV-Vis/Fluorescence

In Fig. S2 are presented the fluorescence excitation-emission matrices (EEM) of the synthetized CDs with m_{CA} = 1g, m_{UR} = 1 g and m_{ST} = 0.5, 1 and 2 g of ST.

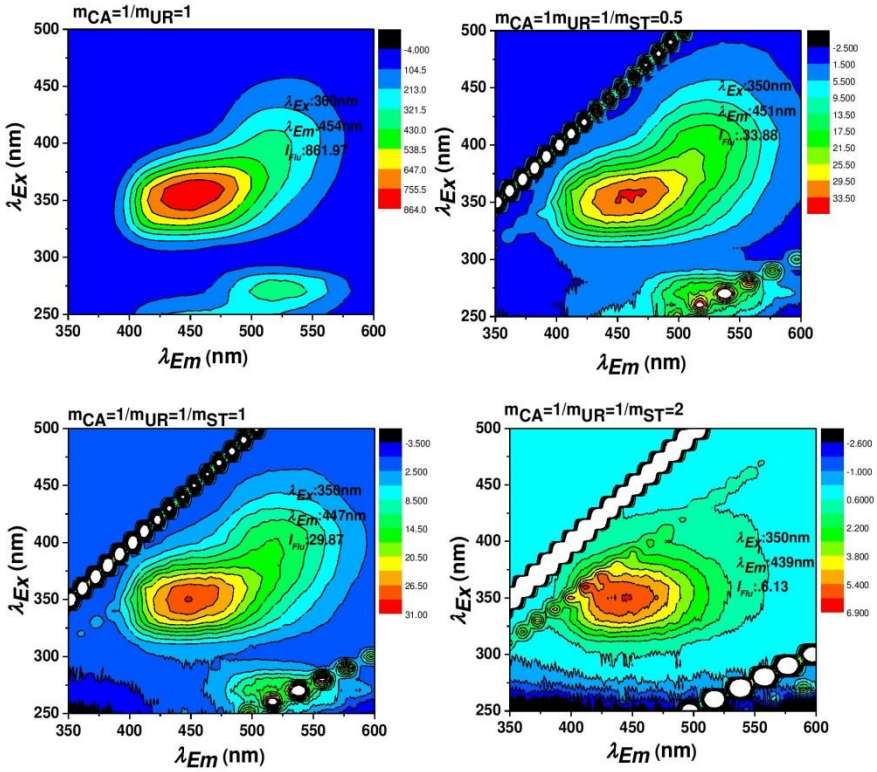


Fig. S2 – Typical EEM of the synthetized CDs.

In Fig. S3 the absorbance, excitation and emission normalized spectra of the synthetized CDs with 1g of CA and UR without ST and with a mass of 0.5, 1, 2 and 3 g of ST.

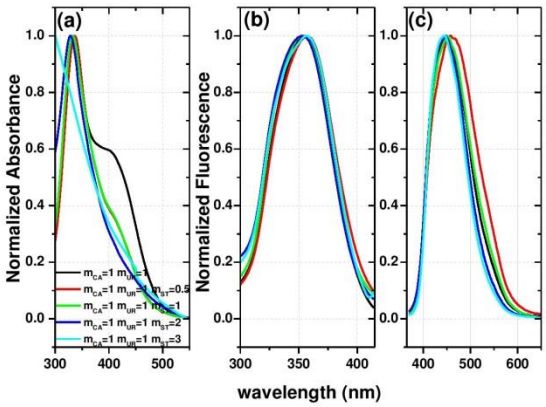


Fig. S3 – Normalized absorbance (a), excitation (b) and emission (c) spectra of the synthetized CDs.

In Table S1 are presented the principal fluorescence characteristics of the synthetized CDs with m_{CA} = 1g, m_{UR} = 1 g, without ST and with m_{ST} = 0.5, 1, 2 and 3 g of ST.

Table S1 – Resume of the fluorescence characteristics of the CDs prepared in all the evaluated synthesis conditions.*

CDs m_{CA}=1 g/m_{UR}=1 g	Φ (%)	Fluorescence detection	
m_{ST} (g)		λ_{Ex} (nm)	λ_{EM} (nm)
0	10.80	360	454
0.5	4.07	350	451
1	4.88	350	447
2	3.06	350	439
3	6.49	350	440

* Φ – Quantum yield; λ_{EX} – Excitation wavelength at maximum fluorescence intensity; λ_{EM} – Emission wavelength at maximum fluorescence intensity.

In Fig. S4 are presented the influence of the pH (a) and of the ionic strength (b) in the fluorescence intensity at the maximum fluorescence intensity of the synthetized CDs with m_{CA} = 1g, m_{UR} = 1 g and m_{ST} = 3 g.

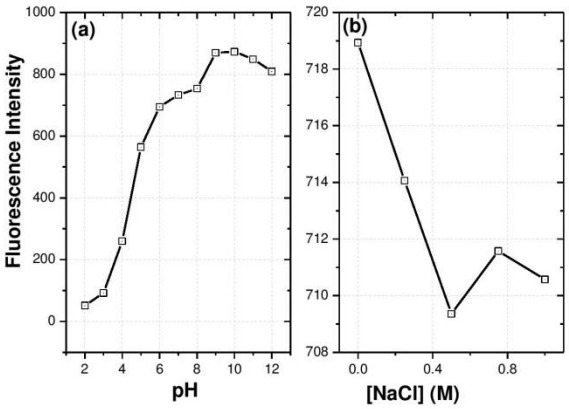


Fig. S4 – Normalized fluorescence intensity variation profiles with the pH (a) and with the ionic strength (b) of synthetized CDs with m_{CA} = 1g, m_{UR} = 1 g and m_{ST} = 3 g.

2.2 FTIR

In Fig. S5 are presented the FTIR spectra of the synthetized CDs with m_{CA} = 1g, m_{UR} = 1 g and m_{ST} = 0.5, 1 and 2 g of ST. The FTIR spectra of CA, UR and ST are presented for comparison.

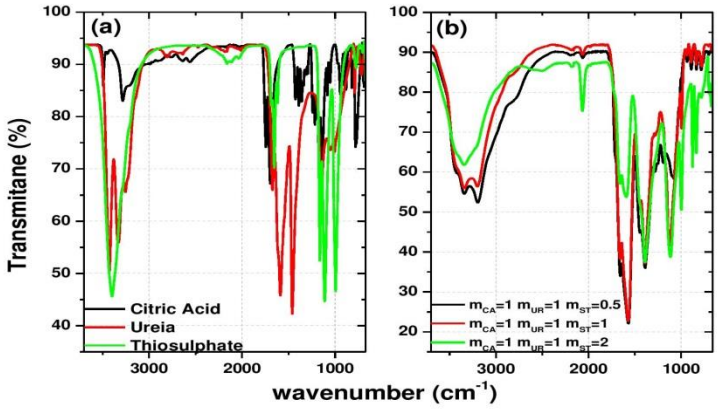


Fig. S5 – FTIR spectra of citric acid, urea and sodium thiosulfate (a) and of the synthetized CDs m_{CA} = 1g, m_{UR} = 1 g and m_{ST} = 0.5, 1, and 2 g of ST (b).

In Table S2 the wavenumbers of the principal FTIR infrared bands found by analysis of synthetized CDs with m_{CA} = 1g, m_{UR} = 1 g without ST and with m_{ST} = 0.5, 1, 2 and 3 g of ST.

Table S2 – Principal FTIR infrared bands of the synthetized CDs with m_{CA} = 1g, m_{UR} = 1 g without ST and with a m_{ST} = 0.5, 1, 2 and 3 g and of citric acid, urea and sodium thiosulfate.*

CDs m_{CA}=1 g/m_{UR}=1 g	FTIR bands (cm^{-1})					
m_{ST} (g)	O–H / N–H (3500–3000 cm^{-1})	C–H (2500–3000 cm^{-1})	C≡C/C≡N (2000–2500 cm^{-1})	C=C/C=N/C=O (1500–2000 cm^{-1})	S–O/C–S/C=S (1000–1500 cm^{-1})	C–C/C–N/C–O (1000–1500 cm^{-1})
0	3075/3191/3340 /3426	2786	---	1568/1615	---	1189/1281/1396
0.5	3196/3342	2789	2063/2161	1569/1657	1080	11931388/1445
1	3199/3343	2791	2061/2185	1574/1660	995/1131	1390/1446
2	3195/3345	---	2065/2164	1591/1661	998/1116	1389
3	3208/3347	---	2068/2179	1579/1663	995/1112	1276/1392/1455
Citric acid	3213/3284/3494	2562/2638/2770	---	1697/1743	---	1138/1171/1216/1 239/1389/1426
Urea	3256/3330/3429	2638/2805	2012/2184	1588/1673	---	1049/1147/1459
Sodium thiosulfate	3400	---	2038/2114	1617/1654/1684	994/1112/1163	

* For each infrared FTIR bands the wavenumbers in bold are the ones with greater transmittance; SH – shoulder.

2.3 Fluorescence quenching

In Fig. S7 are presented the Stern-Volmer plots at 20 and 37 ºC of the synthetized CDs with m_{CA} = 1g, m_{UR} = 1 g and with a m_{ST} = 3 g.

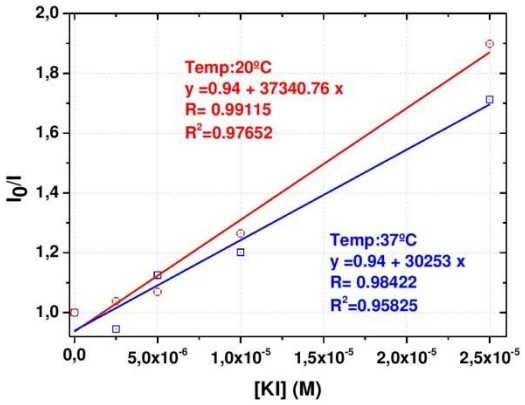


Fig. S7 – Stern-Volmer plots at two different temperatures of the synthetized CDs with m_{CA} = 1g, m_{UR} = 1 g and with a m_{ST} = 3 g.

The Equation S1 is the modified Stern-Volmer in order to calculate the fraction of the accessible groups (f_a) to the iodide quenching. In Table S4 are presented the f_a and the Stern-Volmer quenching constant (K_{SV}) of the accessible groups to iodide.

Equation S1

$$\frac{F_0}{\Delta F} = \frac{1}{([Q]f_a K_{SV})} + \frac{1}{f_a}$$

Table S4 – Calculated accessible tryptophan fraction (f_a) and Stern-Volmer quenching constant (K_{SV}) of the accessible tryptophan to iodide at the different Trp-CD bands.

$\lambda_{Ex}/\lambda_{Em}$ (nm)	f_a	K_{SV} (M^{-1})
370/457	0.0	1.50

2.4 Linear range evaluation

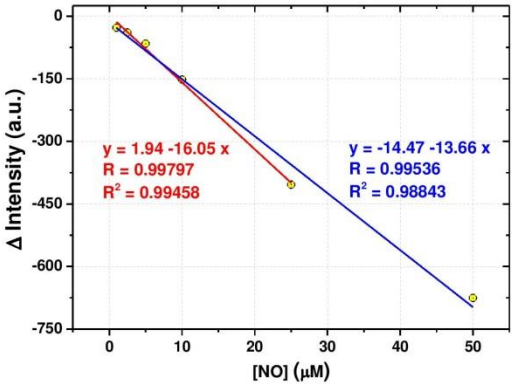


Fig. S8 – Linear fit obtained by addition of a NO concentration from 1 to 25 μM and 1 to 50 μM to the synthetized with m_{CA} = 1g, m_{UR} = 1 g and with a m_{ST} = 3 g.

Conclusions and future perspectives

Conclusions

The final objective of this work is the development of luminescent fiber-optic sensor based on NPs for the detection of ROS and RNS in biological systems with the potential for *in vivo* determinations.

The luminescent sensing of ROS/RNS was reported in a variety of works using different kinds of fluorophores as lanthanide complexes, QDs and CDs. In the beginning of this work, although not be the principal objective of this thesis, the detection of ROS/RNS using fluorophores of pharmaceutical origin namely lanthanide complexes was made. The NO detection was performed using lanthanide complexes constituted by europium (III) and different kind of tetracyclines. These Eu:Tc complexes are selective to NO in presence of H_2O_2.

After this work the research in the luminescent sensing of NPs is evaluated. The use of NPs has been extensively researched in the last years due to their distinctive properties. In this work two different kinds of NPs (CDs and QDs) were synthetized, but was given particular attention to CDs. Due to their biocompatible and non-toxic characteristics CDs have been preferred relatively to QDs. The methods of synthesis of the CDs have been studied and optimized. Sometimes, optimization experimental design methods were applied, in order to evaluate all the factors that interview in the synthesis conditions and with the objective of stablish the better synthesis conditions. After the synthesis of each new CDs their spectroscopic characterization (UV-Vis, fluorescence and FTIR spectra) and size characterization were evaluated.

The ROS/RNS detection and quantification is very difficult because these species are be very reactive, generally are presents in low concentrations and have short lifetimes. The development of systems for detection and quantification of ROS/RNS is of fundamental importance, since these species are present in many physiological processes and appear frequently related to some diseases. In this work were prepared standard solutions of these species to be subsequently added to the luminescent systems (europium: tetracycline) and synthesized NPs. After each

different NPs synthesis the evaluation of the effect of the addition of each of the different ROS/RNS was made. If the synthetized CDs present some sensibility to any of the ROS/RNS would be subsequently the optimization of the response to the respective responsive reactive specie.

Synthetized QDs were applied in the detection of ROS/RNS. The NO quantification was achieved with selectivity relatively to the other ROS/RNS using QD CdSe-CS-MSA nanocomposites.

Relatively to CDs, their synthesis was initially made using only as unique precursor the carbohydrate Glc and then was attempted the functionalization with different compounds in order to enhance their QY and with the objective of to become the CDs sensible to the ROS/RNS. Different precursors were studied. For the CDs synthesis were used as precursors Glc, CA, amino acids (tryptophan, cysteine phenylalanine), amines (EDA, TTDDA) and inorganic salts (sodium hidrogenophosphate, sodium tiosulphate). Some of the results obtained were not conclusive but successfully results, as the $ONOO^-$ sensing using Trp doped Glc CDs, the $ONOO^-$ and NO sensing by EDA doped CDs, the $ONOO^-$ and ClO^- sensing using CDs prepared from CA and UR and the detection of NO using co doped sulphur CDs were presented in international journals.

Relatively to the immobilization of CDs in a fiber optic, there was no time to complete this part of the investigation and what will be made in the future, in the next part of the investigation work.

After four years, it can be concluded that the work was successfully developed in accordance with the program of doctoral project. CDs and QDs were synthesized and their response to ROS/RNS was studied. The results of the work prepared over these years were presented in the form of panel and oral communications as well as having already been published in international journals.

Future Perspectives

Methods that allow the detection and quantification of ROS/RNS in real time and in biological systems are very useful.

NPs based sensors had special interest and are of critical importance. Such NPs are small enough to enter almost all areas of the body, including cells and

organelles, potentially leading to new approaches in nanomedicine. Expecting to-making more efficient and less invasive methods is the objective of the recent studies. The immobilization of the CDs and other kind of nanoparticle in an optical fiber could be an efficient method based for the sensing of ROS/RNS *in vivo*.

In future works, studies would be made in order to allow an efficient immobilization of the CDs at the end of an optical fiber using the layer by layer immobilization technique. Also the sensing using the CDs immobilized in an optical fiber will be studied.

After this immobilization process is completed the studies in biological matrices and further *in vivo* determinations will be made.